DE CONING, ESTELLE

ISENTROPIC ANALYSIS AS A FORECASTING TOOL IN SOUTH AFRICA

MSc UP 1997

ISENTROPIC ANALYSIS AS A FORECASTING TOOL IN SOUTH AFRICA

Estelle de Coning

A dissertation submitted in partial fulfilment of
the requirements for the degree for

MASTER OF SCIENCE (METEOROLOGY)

in the

FACULTY OF ENGINEERING

UNIVERSITY OF PRETORIA

January 1997

DISSERTATION SUMMARY
ISENTROPIC ANALYSIS AS A FORECASTING TOOL IN SOUTH AFRICA

Estelle de Coning

Supervisor: Prof. J. van Heerden
Co-supervisor: Eugene Poolman
Department: Civil Engineering
University: University of Pretoria
Degree: Master of Science (Meteorology)

Keywords: numerical models, Eta model, isentropic levels, adiabatic conditions, sloping surface, three dimensional, topography, vertical motion, tropical air mass, heavy rain

Forecasting short term changes in weather is and will remain a very important but also very difficult task. In order to provide a weather forecaster with the best possible tools to make an accurate weather forecast, it was decided to research the possibility of isentropic analysis methods for South African circumstances.

This study introduces the basic concepts of isentropic analysis and the way to interpret variables on isentropic surfaces.

Three case studies are presented where significant weather systems influenced the country's weather. In two of the cases heavy rainfall and flooding occurred and in the last case widespread moderate falls were reported.

Results of these case studies prove to be very helpful in identifying rainfall areas as well as areas where heavier precipitation could be expected. Operational use of isentropic analysis is recommended.

SAMEVATTING VAN VERHANDELING
ISENTROPIC ANALYSIS AS A FORECASTING TOOL IN SOUTH AFRICA

Estelle de Coning

Leier : Prof. J. van Heerden
Mede-leier: Eugene Poolman
Departement: Siviele Ingenieurswese
Universiteit: Universiteit van Pretoria
Graad: Magister Scientiae (Weerkunde)

Sleutelwoorde: numerical models, Eta model, isentropic levels, adiabatic conditions, sloping surface, three dimensional, topography, vertical motion, tropical air mass, heavy rain

Kort termyn weervoorspelling is en sal altyd 'n baie belangrike en ingewikkelde aspek van ons lewe bly. Om die weervoorspeller toe te rus met die beste moontlik hulpmiddels om 'n akkuarte voorspelling te kan uitreik, is daar besluit om die moontlikhede van isentropiese analise te ondersoek vir Suid-Afrikaanse omstandighede.

Hierdie studie bespreek die basiese konsepte van isentropiese analise en verskaf ook metodes om die isentropiese veranderlikes te interpreteer.

Drie gevallestudies is gedoen op tye wanneer interessante weerstelsels die land se weer beïnvloed het. In twee van die gevalle het swaar reën en vloede voorgekom, terwyl die laaste geval wydverspreide, matige neerslae tot gevolg gehad het.

Resultate van hierdie gevallestudies het bewys dat isentropiese analise 'n goeie hulpmiddel kan wees om reënvalgebiede en gebiede waar swaarder neerslae verwag kan word, te voorspel. Operasionele ingebruikneming van isentropiese analises word aanbeveel.

ACKNOWLEDGEMENTS

I am indebted to Professor Forbes, associate professor in the Meteorology Department of the Pennsylvania State University for guiding my research and advising on the practical aspects in which he has farreaching experience.

I wish to thank Mrs Hilarie Riphagen for editing the text.

Stephan Stoddart was responsible for some of the graphics of synoptic charts.

Suzette Pienaar spent a great deal of time taking care of the text and format - I am very grateful to her.

I would also like to thank my husband and son for their support during the period of study.

To God Almighty - glory and praise for giving me talents, courage and opportunities !

TABLE OF CONTENTS

LIST OF TABLES

LIST OF FIGURES

CHAPTER 1

INTRODUCTION

1.1 South Africa's weather patterns

Current weather patterns influence people's lives to a great extent. Some people are only interested in the weather so that they know what to wear; others have to know what kind of harvest to expect. Weather forecasts also play an important role in the economic growth of our country, planning of sport events and warning of floods in case of torrential rains. The fact is that weather forms a part of our daily lives. Over the years people have developed skills in order to predict the weather of the next day or even the next year, and this knowledge is very important for government, the private sector and the general public.

The main feature of South Africa's topography (Figure 1.1) is the high plateau rising in all directions from about 1000m in the centre (over the Kalahari region) to a general level of about 1200 m in the great escarpment which in Lesotho reaches to over 3000 m. From the great escarpment there is a more or less abrupt fall to the coast (Schulze, 1984). As will become clear later in this study, these physical features play an important role in South Africa's weather.

South Africa is situated within a high pressure belt which is split in two by the continent to form the Indian Ocean High to the east and the Atlantic Ocean High to the west of the country (Schulze, 1984). These high pressure systems vary in intensity and position from one season to the next which, as will be seen later, has an important effect on South Africa's rainfall distribution. South Africa is almost entirely under the influence of the mid-latitude westerly circulation (to a lesser extent in the summer than in the winter) and it can be said that the weather changes in this country are largely dominated by perturbations in the Southern Hemisphere's westerly circulation which on the surface appear as a succession of cyclones or anticyclones moving around the coast or across South Africa from the west (Schulze, 1984).

Although forecasts for the short term have been improved over recent years, in certain

situations problems still arise which lead to incorrect forecasts. Van Heerden and Hurry (1987) summarize the difficulties experienced in day-to-day forecasting as follows :
- The movement of pressure systems from the west to the east over South Africa has the most profound effect on the day-to-day weather of the region. There is often a lack of information about certain components of the highly complex interactions in the atmosphere and it is thus difficult to predict the direction and speed of movement of pressure cells.

- Processes within a moving pressure cell cause changes within it; these changes may be gradual or rapid. Along with these changes goes the resulting weather, and forecasting the correct change at the correct time becomes difficult.

- Although meteorologists obtain information from a number of widely distributed sources, including ships at sea and satellites, the information often is still insufficient to give a clear picture of weather processes on a global scale. South Africa is also surrounded by oceans where observations are even more sparse or even absent which makes the situation even harder to handle.

1.2 Numerical weather prediction models in South Africa

Pressure tendency (as determined from pressure changes over a preceding 3- or 6-hour period) has long been used to provide information concerning the rate of displacement of pressure systems (Preston-Whyte and Tyson, 1988). Although this method is still used as a weather predictor for activities such as yachting, the pressure tendency alone is insufficient for prediction of complex weather systems.

During the 1950's numerical weather predictions were made by means of barotropic models. In these models divergence and changes in absolute vorticity of the wind field were estimated. Results from these models in combination with traditional subjective skills, brought about a significant improvement in forecasting ability in the short term (less than 3 days).

In the 1970's the earth's atmosphere was modelled by making use of the so-called primitive equations; i.e., equations derived from the conservation laws of physics. The

output of two British numerical weather prediction models, namely the European Centre for Medium-range Weather Forecasting (ECMWF) model and the Unified Model from Bracknell are available at the South African Weather Bureau (SAWB). Both of these models are based on numerical approximations of the primitive equations. The output of these two models available in South Africa is on a relatively coarse horizontal grid and only a few (mostly standard) levels in the vertical.

To eliminate the adverse computational effects of the topography and to simplify the lower boundary condition, the vertical coordinate of choice in many numerical models is the terrain-following coordinate, sigma, defined by Philips (1957) as pressure normalized by surface pressure.

$$\sigma = \frac{p - p_T}{p_{sfc} - p_T} \qquad (1)$$

Here p_{sfc} is the pressure at the surface of the model terrain and p_T is the constant pressure at the top of the model domain.

A version of the global, spectral medium-range prediction model of the National Centres for Environmental Prediction (NCEP) in the USA which is also currently being used at the SAWB (and there designated by GSM) is a sigma-coordinate model. The horizontal resolution of this model is 208 km with 28 levels in the vertical.

Recently the SAWB also implemented a regional model from NCEP, with a horizontal resolution of 80 km with 38 levels in the vertical. The vertical coordinate of this model (appropriately designated the Eta model) is eta (η), defined by Mesinger (1984) as

$$\eta = \sigma \eta_s \qquad (2)$$

where

$$\eta_s = \frac{p_{ref}(z_{sfc}) - p_T}{p_{ref}(0) - p_T} \qquad (3)$$

σ is as above, z_{sfc} is the height at the surface of the model terrain and p_{ref} is a reference pressure state independent of time for which the standard atmosphere is used.

Mesinger (1984) applied a different approach to the terrain-following methods used previously in defining the eta coordinate. In conjunction with the eta coordinate the model terrain is chosen so that it assumes a step-like appearance with tops of mountains coinciding with coordinate surfaces. Since eta-surfaces are very nearly horizontal, problems associated with steeply sloping coordinate surfaces are minimized. At the same time the coordinate preserves the simplified lower boundary condition of a terrain-following vertical coordinate (Treadon, 1993).

Researchers in South Africa are able to adapt both the GSM and Eta models for South African conditions such as topography or the parameters governing convective rainfall.

With the four above-mentioned models the SAWB has a good amount of guidance in hand to improve short-term weather forecasting. Mistakes are, however, still being made. For instance, tropical weather systems are usually not handled very well so that the prediction of the movement and development of tropical cyclones and tropical troughs or low pressure systems is often unreliable.

1.3 Isentropic analysis

All four models described above generate output on pressure levels. These charts are supplemented by manual analyses of surface and upper air data. This conventional method of depicting weather data, in use since the 1940's, has some disadvantages. Many a forecaster has experienced difficulty describing the transport of moisture from one pressure level to the next, because real atmospheric flow also has an upward or downward component not depicted on the quasi-horizontal pressure charts. One way of overcoming this problem is through isentropic analysis in which isentropic surface charts depict meteorological parameters on surfaces of constant potential temperature whose slope in many instances is identical to the upward or downward trajectories followed by the air. Potential temperature is defined as the temperature a parcel would have if it were transported without external energy gain or loss (adiabatically) to a pressure of 1000 hPa. By this definition an isentropic surface is also a surface of

constant energy and therefore a surface on which all dry adiabatic processes will take place (Anderson, 1984). Thus, though air parcels tend to move around, they remain on the sloping isentropic surface. Isentropic uplifting typically represents not only vertical motion but moisture advection as well, probably one of the greatest advantages of isentropic analyses (Moore, 1992).

Analysis of meteorological variables on isentropic levels has been implemented with considerable success at NCEP. This analysis supplements analyses on standard constant pressure levels. The basic concepts of isentropic analysis have been available since the 1940's. Early isentropic charts were derived from an array of less than 50 upper air stations. Data were sparse and analyses tended to be highly subjective (Anderson, 1984). Increased computer power in the seventies made it possible to calculate and display the usual meteorological variables on isentropic surfaces in a much shorter time and it became a reasonable option for routine forecasting. Thus isentropic fields have become a valuable additional tool for weather forecasters.

At the Conference on Isentropic Analysis and Forecasting which was held in March 1995 in Lancaster, Pennsylvania, Louis Uccellini stated: "*Given the advancements in the utilization of the isentropic framework, the question is no longer if the isentropic framework positively impacts analyses and forecasts; the question now is how to integrate this framework into the operational community at all levels of the forecast process*".

1.4 Aims of the study

The purpose of the present research is to develop an additional short term weather forecasting technique using isentropic analyses for South African circumstances.

To achieve this goal the research can be subdivided into the following steps :

The first step is a study of the whole concept of isentropic analysis and its advantages and disadvantages (see Chapter 2).

Chapter 3 describes the data and interpolation method as well as the way in which the

appropriate variables (such as static stability and adiabatic vertical motion) are calculated.

Chapter 4 shows how the data can be interpreted. Understanding the isentropic variables can be an initial problem since forecasters are used to interpretation of weather data on isobaric surfaces. Usually it takes some time to get used to the type of charts and the information available on them, but is not difficult, just different.

Three case studies, showing various weather circulation systems, will be analyzed isentropically and discussed in chapters 5, 6 and 7.

Chapter 8 contains conclusions and suggests areas for further research and application of this additional forecasting tool.

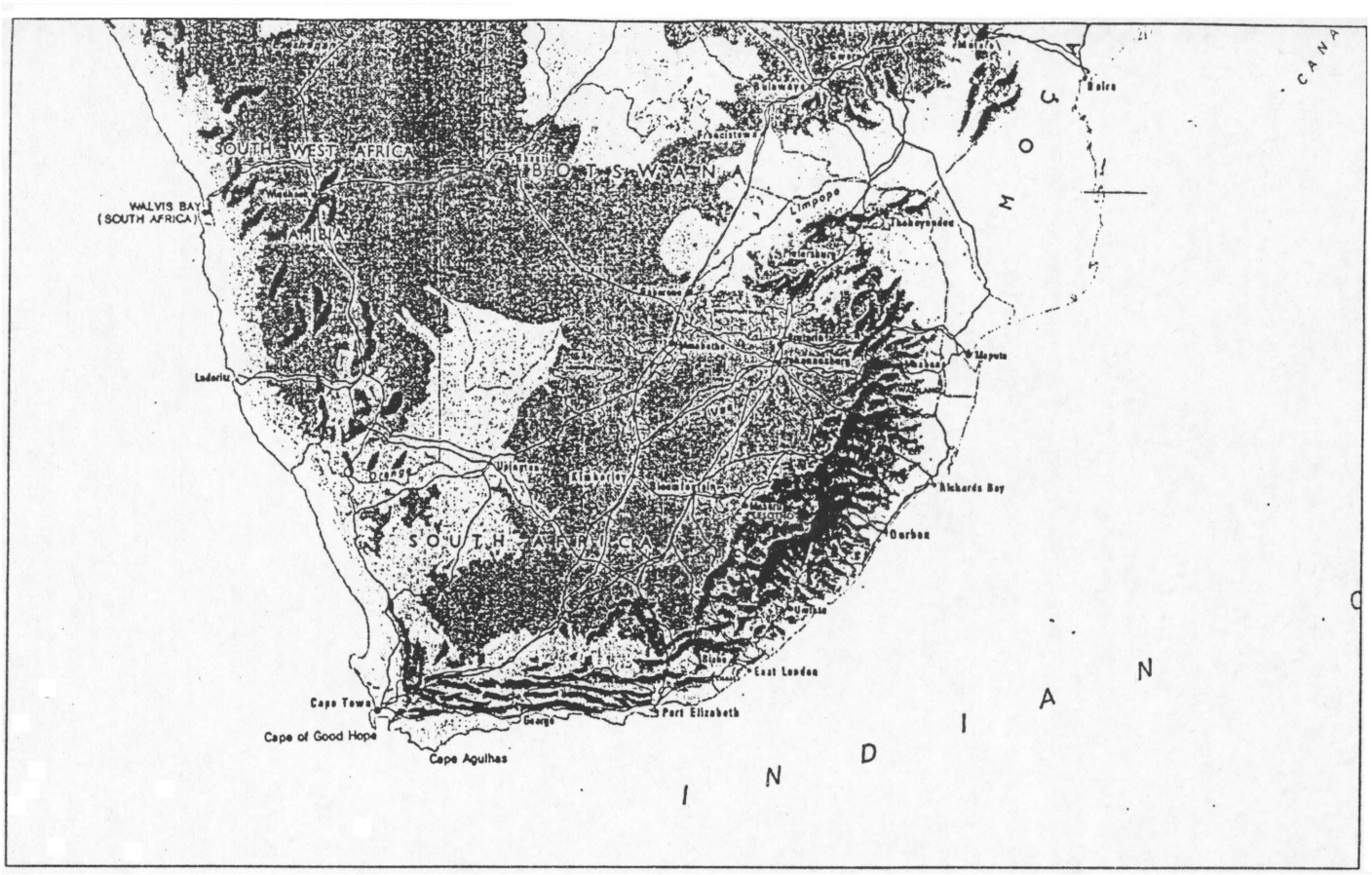

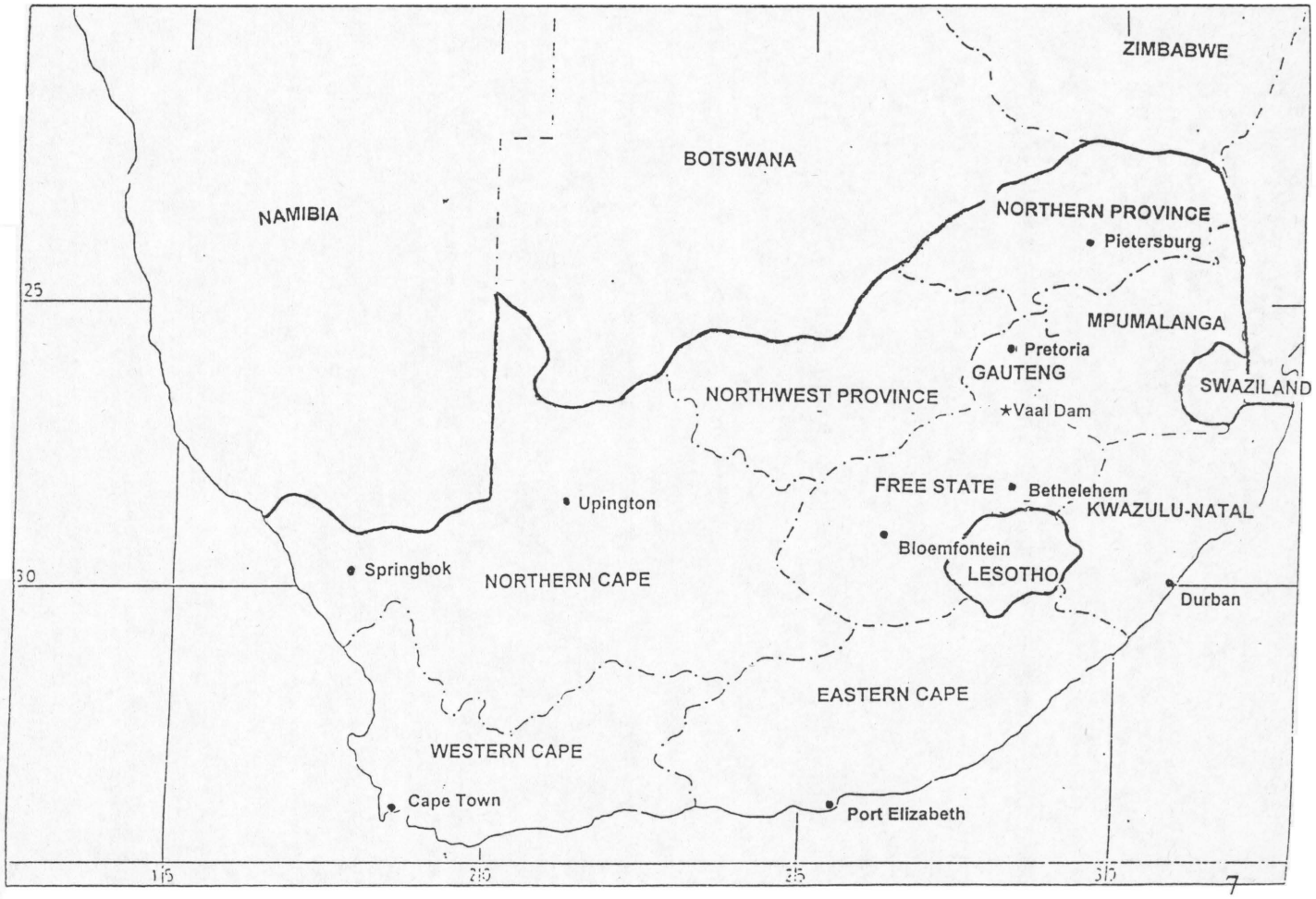

Fig. 1.1 South Africa's topography and Provinces

CHAPTER 2

AN INTRODUCTION TO ISENTROPIC ANALYSIS CONCEPTS

2.1 Definition of isentropic concepts

The first law of thermodynamics governs the changes that take place when a parcel of air in the atmosphere absorbs heat (energy). A parcel of air has internal energy made up of the kinetic energy of the molecules of the gas and the potential energy of the gas with reference to some origin (sea level). If a parcel is heated, its internal energy will increase as the molecular motion in the parcel becomes more vigorous. If at the same time the parcel is allowed to expand, then it performs work (Joule/sec=Watt) against the ambient environmental air. The amount of work (W) will depend on the volume expanded (dv) as well as the pressure (p) exerted by the surrounding air in such a way that W = pdv (Wallace and Hobbs, 1977).

The amount of heat added during the heating process (enthalpy), dH, must be equal to the sum of the increase in the internal energy of the parcel plus the work done against the environment. This is a statement of the first law of thermodynamics which, in its general form, can be expressed as :

heat added = change in internal energy + work done

In mathematical form it is expressed as :

$$dH = m\ C_v dT + pdv \qquad (1)$$

where C_v is the specific heat of air at constant volume, dT is the change in

temperature (Kelvin), p is the pressure of the parcel, m is the mass of the volume and dv is the change in volume of the parcel.

By dividing both sides of the equation by the mass of the volume and making use of the equation of state, namely :

$$p\ \alpha\ =\ RT \tag{2}$$

where R is the gas constant for dry air (287 J $kg^{-1}K^{-1}$), and α is the specific volume (V m^{-1}) it is more convenient, meteorologically, to write the first law of thermodynamics as

$$dh\ =\ C_p dT\ -\ \alpha\ dp \tag{3}$$

where C_p is the specific heat of air at constant pressure and dh is the change of heat per unit volume. In this form energy changes are related to pressure and temperature variations rather than to temperature and volume.

An adiabatic process is defined as a process where a parcel of air will experience no heat exchange (no heat loss or gain) with its environment. Therefore, for an adiabatic process :

$$dh\ =\ 0\ =\ C_p dT\ -\ \alpha\ dp \tag{4}$$

Substituting the equation of state, results in :

$$\frac{dT}{T}\ =\ \frac{R}{C_p}\frac{dp}{p} \tag{5}$$

Integration from some temperature T and pressure p to temperature θ at 1000 hPa Hess (1959), results in :

$$\theta = T(\frac{1000}{p})^{\kappa} \quad where\ \kappa = \frac{R}{C_p} \tag{6}$$

referred to as Poisson's equation for potential temperature. The potential temperature θ is physically defined as the temperature that a parcel of air would have if it were compressed (or expanded) adiabatically from its original pressure to 1000 hPa. The potential temperature is a conservative property for parcels of air under adiabatic conditions (no changes in heat due to processes such as radiation, mixing with environmental air and latent heating/evaporative cooling). These restrictions would seem to make the application of this thermodynamic variable very limited. However, diabatic heating and cooling processes are usually secondary in importance for temporal scales on the order of the synoptic (± one day). Hess (1959) also showed that the entropy ϕ of an air parcel is related to its potential temperature as :

$$\phi = C_p \ln\theta + constant \tag{7}$$

Therefore a parcel which ascends under dry adiabatic conditions conserves its potential temperature and also its entropy. A layer of air in which potential temperature is constant, is described as an equal entropy or isentropic layer. Entropy is defined as a measure of the disorder of a system and is expressed in units of J/kg. Operational meteorologists have little use for this rather mystical concept and aside from using the term isentropic, potential temperature is preferred as a variable rather than entropy.

Most of the following definitions are based on the work of Moore (1992), except when otherwise specified.

The lapse rate, γ, measures the rate of observed temperature change with height $\gamma=-(\partial T/\partial z)$. Involving the hydrostatic equation which prescribes the variation of pressure with height in the large scale atmosphere

$$\frac{\partial p}{\partial z} = -\rho g = -\frac{g}{\alpha} \qquad (8)$$

equation 8 can be used to determine the lapse rate of an adiabatic layer, Γ_d. This is referred to as the dry adiabatic lapse rate $\Gamma_d=g/c_p$ and equals to 0.0098°C/m. Except in thin heated layers near the surface and in other rare instances, $\gamma < \gamma_d$.

In the troposphere the atmosphere is, on the average, stable, thus according to Rogers and Yau (1989) :

$$-\frac{\partial T}{\partial z} \equiv \gamma_{envir} < 9.8°C\ km^{-1} \qquad (9)$$

where z refers to height. Typically $\gamma = 6.5°C\ km^{-1}$. Stability indicates a condition of equilibrium of an air parcel relative to the surrounding air. A state of stable equilibrium is said to exist when a parcel of air, uplifted by some outside force, tends to return to its original position on removal of the displacing force. In such an atmosphere the potential temperature can be shown to increase with height :

$$\frac{1}{\theta}\frac{\partial \theta}{\partial z} = \frac{(\Gamma_d - \gamma)}{T} \qquad (10)$$

In equation 10 Γ_d is the dry adiabatic lapse rate and γ is the actual or environmental lapse rate. Under stable conditions $\gamma < \Gamma_d$, so that $\partial\theta/\partial Z > 0$ and θ increases with height. If the lapse rate is neutral then $\gamma = \Gamma_d$ and $\partial\theta/\partial Z=0$, i.e. θ is constant with height. If $\gamma > \Gamma_d$ the lapse rate is superadiabatic and θ decreases with height. As Rossby and collaborators (1937) noted, the potential temperature increases equatorward at about the same rate as the dry bulb temperature. So the troposphere may be viewed as being composed of a number of isentropic layers which gradually descend from cold polar to warmer subtropical latitudes. As one ascends from the troposphere into the stable stratosphere isentropic surfaces become compacted with height. This attribute makes isentropic surfaces extremely valuable for resolving upper-level stable frontal zones in the presence of upper tropospheric wind maxima or jet streams. Thus, in a stably stratified atmosphere potential temperature can be an excellent vertical coordinate - especially as it increases progressively with height - thereby avoiding the difficulties of dealing with a vertical coordinate (like pressure) which decreases with height. Isentropic surfaces become far apart vertically or "ill-defined" in regions where the lapse rate is neutral or superadiabatic; i.e. $\partial\theta/\partial z \leq 0$. In the neutral case, when $\partial\theta/\partial z=0$, the isentropic surface is vertical, while in the super-adiabatic case it is folded. This is a serious deficiency of isentropic analysis because a vertical coordinate should change monotonically with height.

2.2 History of isentropic analysis

The principles of isentropic analysis came to the fore in the 1940's. Once a large number of upper-air observations became available, a wide ranging debate was launched on which vertical coordinate system would be best. Many researchers and

meteorologists favoured pressure as a vertical coordinate, while others wanted a geometric system. A few meteorologists like Rossby and Namias wanted to introduce isentropic coordinates. Rossby and collaborators (1937) stated *"it can hardly be doubted that the isentropic charts represent the true motion of air more faithfully by far than synoptic charts for any fixed level in the free atmosphere".*

Although isentropic coordinates were used by the US Weather Bureau in the late 1930's, the practice was later discontinued and a constant-pressure level scheme was adapted. Bleck (1973) and Wilson (1985) give a few reasons for this decision:

- Standardization took place during the second World War, and the aviation community required winds on constant pressure levels.

- Fast computers were not available at the time to perform the computations within operational time constraints.

- The Montgomery stream function (which is basically equivalent to height on a constant pressure surface in terms of its relationship to the geostrophic wind) is defined by Montgomery (1937) as :

$$M = \psi + C_p T_\theta \qquad \textbf{(11)}$$

where T_θ is the temperature at a specific isentropic level. This expression states that the streamfunction on an isentropic level is calculated by summation of enthalpy, ($C_p T_\theta$) and geopotential (ψ) at a specific isentropic level. At first M was computed by interpolating the two terms ψ ($=gz_\theta$ where z_θ is the height of the theta level) and $C_p T_\theta$ separately. Danielsen (1959) found that these two terms are related via the hydrostatic

equation in isentropic coordinates and therefore, computing the two terms independently resulted in errors of as much as 20% in their sum (Moore 1992). Danielsen (1959) subsequently corrected the Montgomery stream function computation.

The availability of computers in the seventies together with Danielsen's correction opened a whole new world of opportunities for meteorological analysis on isentropic levels.

Some examples of recent research work which used isentropic analysis techniques include :

1) Studies on the progress and development of a cut-off-low situation by means of vertical cross sections and potential vorticity through isentropic analysis (Mills and Boa-Jun, 1995)

2) An isentropic perspective on elevated thunderstorms associated with heavy rainfall (Market and Moore, 1995)

3) The utility of an isentropic perspective in documenting the development of upward vertical motion and moisture transport associated with a snowstorm (Nolan and Moore, 1995)

4) Operational application of isentropic analysis to the diagnoses of severe convective weather threat areas (Wilson, Siok and Marios, 1980)

5) Isentropic analysis in strong baroclinicity and flood-producing rains in Kentucky

(Kirkpatrick, 1992)

6) Research on intense cyclone development along the mid-Atlantic coast (known as the President's Day Storm) by using isentropic potential vorticity maps (Spaete, Johnson and Schaak, 1993).

7) Using isentropic potential vorticity and its advection to diagnose strong cyclogenetic developments (Kurz, 1994).

2.3 Advantages of isentropic analyses

The advantages of isentropic analysis have been described by various authors; a summary of the advantages include :

- As a first approximation the atmospheric motion is adiabatic (as much as it is geostrophic) and this motion is related to the configuration and origin of air streams (Carlson, 1991).

- Vertical motion can be shown explicitly on a quasi-horizontal isentropic chart (Carlson , 1991).

- Isentropic flow presents a truer picture of the three-dimensional air motion than isobaric surfaces and preserves the quasi-horizontal behaviour of the three-dimensional flow (Carlson, 1991). Parcel trajectories can be computed on isentropic levels. These trajectories have been shown to be true and highly correlated with the

four-dimensional flow associated with mid-latitude synoptic and even sub-synoptic-scale motions (Moore, 1992).

- For synoptic time scales, isentropic surfaces are similar to "material" surfaces. That means air parcels are thermodynamically bound to their isentropic surfaces in the absence of diabatic processes (Rossby et al., 1937).

- Since an isentropic surface can vary with pressure (and pressure is a function of height), "horizontal" flow along the surface includes the adiabatic component of the vertical motions dz/dt and dp/dt, one or the other of which would otherwise be derived as a separate velocity component in either Cartesian or isobaric coordinates. This factor allows for a more accurate determination of true atmospheric trajectories when these are represented on isentropic surfaces (Danielsen, 1961).

- A more coherent three-dimensional depiction of moisture transport is attained using isentropic maps rather than the standard 850 hPa or 700 hPa charts on which moisture patterns tend to be discontinuous and fragmentary (Oliver and Oliver 1951).

- Frontal discontinuities are virtually non-existent on isentropic surfaces since frontal zones (if not occluded) tend to run parallel to isentropic surfaces (Bleck 1973). This property of isentropic surfaces makes them extremely useful in diagnosing kinematic and dynamic variables, especially in baroclinic zones and because frontal width on constant pressure charts cannot usually be properly defined with synoptic scale data.

- The static stability of the atmosphere is easily computed. The vertical separation

between two adjacent isentropic levels is a measure of the atmosphere's stability. Also noteworthy is the fact that one measure of static stability is $\partial p/\partial \theta$, which can be related via the continuity equation in isentropic coordinates to divergence taking place in the layer. Divergence in the layer increases the static stability while convergence in the layer reduces the static stability (Moore, 1992). This aspect will be addressed in Chapter 4.

- The slope of an isentropic surface in the vertical is directly related to the thermal wind. A vertically sloping isentropic layer is indicative of a strong thermal contrast which is represented on the isentropic surface as a tight packing of isobars or isotherms. Thus, where isentropic surfaces tilt up or down significantly, one can diagnose a frontal zone and a substantial change in the wind velocity with height (Moore, 1992).

- Isentropic analysis can be used to distinguish between airstreams from different origins by making use of limiting streamlines on the pressure charts (Carlson, 1991).

2.4 Disadvantages of isentropic analyses

Although isentropic analysis has definite advantages, there are also a few problems:

- Motion in the atmosphere is not truly adiabatic, especially in the boundary layer and in the vicinity of strong vertical mixing or convection (Carlson, 1991). The continuity of isentropic analysis is disrupted significantly in the presence of strong diabatic processes (Namias 1940). This problem occurs where radiation, evaporation, condensation or convection carries energy into a parcel of air.

- Isentropic analysis becomes ill-defined where the atmospheric lapse rate is neutral or superadiabatic (Moore, 1992).

- In near-neutral lapse rate regions there is poor vertical resolution of the atmosphere (Moore, 1992).

- Choosing the proper isentropic surface to work with is not a trivial problem (Moore, 1992). It is important to choose a level which is not too close to the surface because isentropic surfaces tend to intersect the ground at steep angles which makes the analysis near the surface difficult and therefore suspect. Shallow nocturnal inversions can also cause problems.

- Isentropic analyses require a large number of computations which are only operationally feasible on computers. It is impractical for a weather forecaster or analyst to execute the calculations required for isentropic analysis manually. Fast supercomputers overcome this difficulty.

- Finally, there is the "inertia" problem, as Wilson (1985) put it; namely that weather forecasters still "think in pressure coordinates". A whole new approach is required to understand and interpret isentropic maps. Forecasters should familiarize themselves with isentropic analysis, since "*in many cases isentropic analyses should result in a better understanding of the atmosphere and better short range forecasts*" (Anderson, 1984) and weather systems and air flow are, after all, three dimensional.

2.5 Summary

In this chapter the basic definitions and concepts of isentropic analysis were discussed. Some of the advantages and disadvantages were highlighted. Although certain problems associated with isentropic analysis and the interpretation of variables on isentropic surfaces exist, the advantages far surpass the difficulties. Generally, the isentropic charts can be interpreted in a simple fashion; only rarely will more intricate factors complicate the analysis.

CHAPTER 3

DATA, INTERPOLATION SCHEME AND ISENTROPIC VARIABLES

3.1 Data

Isentropic analysis is usually started with data from upper-air soundings in the area of interest. In South Africa only ten upper-air stations perform upper-air soundings twice daily. This is insufficient to make a proper isentropic analysis over such a large area. Therefore, it was decided to make use of the Eta model to generate input data for isentropic analysis. The Eta model which is currently operational South Africa has 38 levels in the vertical and a horizontal resolution of 80 km. Output is available on a one degree grid zonally as well as meridionally. For a comprehensive description of the Eta model, the work of Mesinger, et al. (1988) is recommended. The Eta model thus provides a good (pseudo) data base to work with.

For isentropic analysis purposes every second eta-level is used so that 19 levels are available in the vertical.

3.2 Interpolation method

The variables from the Eta model are originally on eta-levels and thus the first step is to interpolate from eta to the relevant isentropic levels. For this study interpolation was done from 290K to 330K in a 5K step.

NCEP's Global Spectral Model uses sigma as a vertical coordinate and because sigma and eta are closely related, it was decided to use the Global Spectral Model's interpolation scheme and to adjust it for eta-levels. The Global Spectral Model interpolates sigma to theta assuming that the fields vary linearly in the vertical. Thus, the value of a variable, x, on any isentropic surface θ is calculated by :

$$x = x_{el} + \frac{\ln\theta - \ln\theta_{el}}{\ln\theta_{eu} - \ln\theta_{el}} [x_{eu} - x_{el}] \qquad (1)$$

where el indicates the eta-level immediately below and eu the eta-level immediately above the θ-surface at the particular location.

To express ln θ_{el} and lnθ_{eu} in terms of eta, we note that the equation for potential temperature is :

$$\theta = T\,(\frac{p_0}{p})^{\kappa} \qquad where \quad \kappa = \frac{R}{C_p} \qquad p_0 = 1000hPa \tag{2}$$

Taking the logs, results in :

$$\ln\theta = lnT + \kappa(lnp_0 - lnp) \tag{3}$$

Using equations 1, 2 and 3 of Chapter 1 and solving for p we have:

$$p = \frac{\eta}{\eta_s}\,(p_{sfc} - p_T) + p_T \tag{4}$$

with η, η_s, p_{sfc} and p_T as defined in that chapter.

Substituting this into equation 3 gives an expression for θ on eta-levels:

$$\ln\theta = lnT + \kappa(\ln p_0 - \ln[\frac{\eta}{\eta_s}(p_{sfc} - p_T) + p_T]) \tag{5}$$

Values of T and η at the appropriate eta-level are then substituted into (5) in order to compute the terms of (1). The p_T at the upper boundary was 50 hPa for the Eta model runs used in this study.

Typical variables which are interpolated in this way include: pressure, temperature, u-wind component, v-wind component, omega, specific humidity, moisture flux convergence and potential vorticity.

3.3 Calculating the relevant variables on isentropic surfaces

A number of variables are used to do an isentropic analysis. The following variables were used in this study:

a) Pressure (p)

The pressure on each isentropic level as interpolated from eta levels. Wind arrows or streamlines are usually plotted with pressure contours.

b) Condensation pressure (p_c)

Condensation pressure is defined as the pressure to which a parcel of unsaturated air must be elevated dry-adiabatically in order to reach saturation, i.e. the condensation level (Moore, 1992). Byers (1938) recommended that the condensation pressure should be used for isentropic analysis. He found that it can be expressed as:

$$p_c = p\left(\frac{T_c}{T}\right)^{\frac{mC_p}{R}} \qquad (6)$$

where T is the temperature at a point with pressure p ($>p_c$) on the isentropic surface; T_c is the temperature at p_c (isentropic-condensation temperature); m is the molecular weight of dry air; C_p is the specific heat at constant pressure and R is the universal gas constant.

The condensation level is defined as the level at which a parcel of moist air becomes saturated when it is displaced vertically and adiabatically. When an parcel is lifted the mixing ratio w of the air and its potential temperature θ remain constant, but the saturation mixing ratio w_s (which is a function of pressure and temperature) decreases with height. At the lifting condensation level it becomes equal to w (Wallace and Hobbs, 1977).

It is therefore sufficient to calculate w and w_s and to see where w_s=w. When that happens, the condensation level has been reached. Substituting the temperature at this point into equation 6 results in the condensation pressure.

The key advantage of condensation pressure over specific humidity q, is that condensation pressure represents moisture differences better at low values of

q.

Another variable, namely condensation difference, is also useful to present moisture values in isentropic analysis. This variable is computed by subtracting the value of condensation pressure from the corresponding pressure value. The smaller the value of the condensation difference, the closer to saturation a parcel is (Anderson, 1984).

c) Static stability ($\Delta p/\Delta\theta$) can be represented by:

$$\Delta p = p\ (\theta_u) - p\ (\theta_l) \qquad (7)$$

where *u* and *l* refer to upper theta and lower theta level respectively. Δp is always negative because pressure decreases with height as long as potential temperature increases with height, which is usually the case. Horizontal plots of this variable on an isentropic surface, using adjacent surfaces for computation, are "quick and dirty" estimates of stability and stability change (Moore, 1992). In this study θ_u and θ_l are taken 5 Kelvin apart.

d) Moisture advection/flux convergence

Considering moisture conservation, moisture advection is expressed mathematically as :

$$-\overline{V} \cdot \overline{\nabla} q \qquad (8)$$

Computation is done by :

$$-\frac{u}{r \cos \phi}\frac{\Delta q_x}{\Delta \lambda} - \frac{v}{r}\frac{\Delta q_y}{\Delta \phi} \qquad (9)$$

where Δq_x is the difference between two adjacent grid point values of condensation pressure along a latitude, Δq_y is the difference between two adjacent grid point values of condensation pressure along a longitude, r is the radius of the earth, $\Delta\lambda$ is the difference between two adjacent longitudes and $\Delta\phi$ is the difference between two adjacent latitudes in radials.

Moore (1992) defines moisture flux convergence on isentropic surfaces as:

$$-\overline{\nabla} \cdot q\,\overline{V} = -\overline{V} \cdot \overline{\nabla}\, q - q\,\overline{\nabla} \cdot \overline{V} \qquad (10)$$

Moisture flux convergence is an output variable of the Eta model's postprocessor.

e) Adiabatic vertical motion:

Analysis of wind **V** and pressure p on an isentropic surface can yield a direct, quantitative estimate of the vertical velocity (omega) simply from the expansion of the total derivative (dp/dt) where :

$$\omega = \frac{dp}{dt} = \left(\frac{\partial p}{\partial t}\right)_\theta + \overline{V} \cdot \overline{\nabla_\theta}\, p + \frac{d\theta}{dt}\frac{\partial p}{\partial \theta} \qquad (11)$$

The local pressure change (term 1) over a 12-hour period can be estimated at specific locations using successive pressure fields. The contribution due to horizontal advection of pressure (term 2) can be computed by the u, v and p fields for the specific time. The diabatic heating term (term 3) is important in regions of clouds and precipitation, but this term is difficult to calculate given the great uncertainty in estimating the magnitude of dθ/dt as well as the fact that the local pressure tendency term will usually act against the diabatic term. The near cancellation between the local pressure tendency and diabatic terms justifies the practise that the pressure advection term is a good approximation to omega. Thus, the "horizontal" flow along an isentropic surface can be viewed as implicitly including an adiabatic component of the vertical motion which is easy to compute at any given time (Uccellini, 1995). The adiabatic vertical motion is calculated by:

$$\omega_{adiab} \simeq \overline{V} \cdot \overline{\nabla_\theta}\, p \qquad (12)$$

In many instances the weather systems are travelling in essentially a non-varying "frozen" wave pattern. In such a case the local tendency ∂p/∂t can be

expressed in terms of a weather system travelling at a propagation velocity of **C** and thus:

$$\left(\frac{\partial p}{\partial t}\right)_\theta \simeq -\overline{C} \cdot \overline{\nabla_\theta p} \qquad (13)$$

Thus, another estimate of vertical velocity will be :

$$\omega_{adiabatic} \approx (\overline{V}-\overline{C}) \cdot \overline{\nabla_\theta P} \qquad (14)$$

where **C** is the motion vector of the synoptic scale system being examined (Carlson, 1991). The difference **(V-C)** yields the wind relative to the motion of the system being analyzed. The only difference between equation 12 and 14 is that equation 14 uses system-relative winds and equation 12 uses ground-relative winds. This difference can cause significantly different values for omega for faster moving systems. Because the wind at any given point contains a component equivalent to the system's wave speed (Holton, 1979) equation 14 should therefore provide more accurate values of the vertical motion (Gerard, 1995).

System-relative vertical motions tend also to be better correlated to satellite imagery than those obtained by assuming **C** zero (Moore, 1992). Calculating a value for **C** is not so easy. Following Moore (1992) and Gerard (1995) **C** can be estimated from the 12-hour displacement of absolute vorticity maxima (for anti-cyclones) or minima (for cyclones) in the southern hemisphere. The method of equation 14 may not yield accurate results for ω in areas distant from the influence of the cyclone or anti-cyclone since vertical motions there may be relative to an isentropic pattern having different velocity **C.**

In this study the absolute vorticity maxima were calculated for 0-hours and 12 hours and the relevant positions were used to see how the position of maximum absolute vorticity shifted. The x-component and the y-component of the movement were calculated by :

$$cu = \frac{\Delta x}{\Delta t} \qquad (15)$$

and

$$cv = \frac{\Delta y}{\Delta t} \qquad (16)$$

respectively. In this case $\Delta x = r \cos \phi \, d\lambda$ and $\Delta y = r \, d\phi$ where ϕ is latitude (in radials), λ is longitude (in radials), r is the radius of the earth and Δt is 12 hours. Equation 14 is then determined by :

$$(\overline{V} - \overline{C}) \cdot \overline{\nabla} p = \frac{(u - cu)}{r \cos \phi} \frac{\Delta p_x}{\Delta \lambda} + \frac{(v - cv)}{r} \frac{\Delta p_y}{\Delta \phi} \qquad (17)$$

where Δp_x is the difference between one grid point's pressure and the next in the x direction, Δp_y is the difference between one grid point's pressure and the next in the x direction, Δx is the difference between tow adjacent longitudes (in radials) and Δy is the difference between adjacent latitudes in radials.

3.4 Summary

In this chapter the data and methodology used to get to an isentropic analysis was explained. The Eta model's output is used as input to the eta-to-isentropic interpolation scheme. Variables which are frequently used in isentropic analyses were defined and derived. The software with which the calculations were done is included in the Annex.

CHAPTER 4

GRAPHICAL DEPICTION AND INTERPRETATION OF ISENTROPIC VARIABLES

4.1 Introduction

The interpretation of isentropic charts is discussed in great detail by Anderson (1984). The following ideas are based on his perceptions.

The quality of short range forecasts is closely related to the forecaster's understanding of the current state of the atmosphere in his forecast region. Data analysis produced on isentropic charts can provide a different view of weather systems and can enhance the forecaster's understanding of local weather conditions. Although isentropic charts are not a replacement for isobaric charts they can, with practice, supply an understanding of the state of the atmosphere that is hard to achieve using isobaric charts.

Isentropic charts depict meteorological parameters on a surface of constant potential temperature. According to the definition of potential temperature, an isentropic surface is also a surface of constant entropy and therefore a surface on which all adiabatic processes will take place.

4.2 Vertical cross-section charts

The first step in isentropic analysis is to choose the correct isentropic surface to work with. According to Moore (1992), care must be taken not to choose an isentropic level which reaches the ground. However, it is also important to go as close to the ground as possible in order to identify the moist or dry tongues associated with synoptic scale flow. In other words, the source of atmospheric moisture is at the surface of the earth.

An easy way to decide on which isentropic level to work is to look at a cross-section of the area where the most weather activity is suspected.

On such a chart (cross-sections were chosen along a latitude) the following variables

are depicted :

- topography of the area

- specific humidity

- horizontal component of the wind within the cross-section together with a scaled vertical velocity (omega)

On a vertical cross-section the isentrope closest to the ground, without intersecting it, can easily be identified. Vertical motion and the distribution of moisture can also be seen.

In order to choose the ideal isentropic surface to work with for a specific case study, it is best to look at a cross-section of the area where the relevant weather system has an effect (for example 30°S). Namias (1940) suggests the following low level isentropic surface ranges for individual seasons in North America :

Season	Low level potential temperature
Winter	290 - 295 K
Spring	295 - 300 K
Summer	310 - 315 K
Autumn	300 - 305 K

Table 4.1 Potential temperatures for each season in North America

Although this gives a good indication of the levels to choose for each season, it can differ from one area to the next. One or more (for lower and middle levels of the atmosphere) isentropic levels can be decided upon.

After selecting the appropriate isentropic level to work with, a closer look at the different variables for each isentropic level is possible.

4.3 The horizontal charts

Once the appropriate isentropic level(s) has been chosen, a number of charts can be drawn :

4.3.1 Pressure chart (hPa)

In general, the lower (higher) the pressure value on the isentropic surface, the higher (lower) the isentropic level occurs in the atmosphere. In this way, the pressure chart can be interpreted as showing ridges and valleys that make up the vertical displacement of the isentropic surface.

With the definition of isentropic surfaces, lines of equal pressure can have a few other interpretations as well :

a) Lines of equal pressure are also lines of equal temperature.
b) Along the lines of equal pressure, density is also equal.
c) Pressure lines are also rough indicators of constant height.
d) The temperature of the column below the isentrope is also indicated by the pressure lines; thus higher (lower) pressure values indicate higher (lower) temperatures in the column of air below. In this way isentropic analysis provides a way to identify cold and warm tongues of air in the atmosphere; warm tongues are indicated by ridges in the pressure field and cold tongues by valleys in the pressure field.

If winds are also plotted on a pressure chart, they can give an indication of both the horizontal and vertical movements. If the streamlines are flowing across the isobars from higher (lower) pressure to lower (higher) pressure, then as a first approximation based on equation 12 in chapter 3, there is upward (downward) motion. If the streamlines are flowing parallel to the isobars there is no vertical motion. Analyses of vertical velocity of this type are useful for forecasting cloudiness and stratiform precipitation in the winter and favourable areas for convection in the summer. The closer the streamline's crossing of the isobars is to perpendicular, and the greater the packing of the isobars, the greater the corresponding vertical motion.

If streamlines are either drawn in from the wind data or plotted, it is possible to draw

limiting streamlines in regions where the streamlines have a tight gradient. These limiting streamlines separate different airstreams and this can be used to identify air masses from different origins. A limiting streamline can coincide with edges of cloud bands on a satellite image and also indicate where development might take place.

4.3.2 *The moisture chart (hPa)*

Graphical depiction of condensation pressure on a chosen isentropic level indicates the distribution of the moisture content of the atmosphere. Just as regular pressure on the isentropic surface traces cold and warm tongues, the condensation pressure field traces moist and dry tongues (Moore, 1992). However, this variable contains effects of horizontal variations of both temperature and relative humidity, and it is therefore better to use condensation differences.

Anderson (1984) also notes that condensation pressure isobars can be useful in identifying frontal positions. A moist tongue, represented as a ridge of condensation pressure is usually present along or slightly ahead of a strong, mature cold front. As a cyclone occludes the moist tongue will typically branch into two tongues - one turning cyclonically to the northwest and the other anti-cyclonically to the north east in the northern hemisphere. The occlusion is usually found in the vicinity of the branching and Anderson found that this is also the area of heaviest precipitation.

If condensation difference is used, a difference of less than 100 hPa has been found to represent areas close to saturation. With a difference of less than 20 hPa essentially the air parcel is considered to be saturated (Anderson, 1984).

4.3.3 *Stability chart (hPa)*

Changes in pressure over a 5 Kelvin interval of 200 hPa or more are taken as significant. Static stability is a relative measure of instability which DOES NOT take moisture into account. It is a simple and quick estimate of the stability of the atmosphere. Following Moore (1992) what is also noteworthy is the fact that static stability is related (via the continuity equation in isentropic coordinates) to divergence/convergence taking place in the layer. The mass continuity equation in

isentropic coordinates is:

$$\frac{\partial}{\partial t}\left[\frac{\partial p}{\partial \theta}\right] = \overline{V} \cdot \overline{\nabla}\frac{\partial p}{\partial \theta} + \frac{d\,\theta}{dt}\frac{\partial}{\partial \theta}\left[\frac{\partial p}{\partial \theta}\right] = -\frac{\partial p}{\partial \theta}\overline{\nabla} \cdot \overline{V_\theta} - \frac{\partial p}{\partial \theta}\frac{\partial}{\partial \theta}\left[\frac{d\,\theta}{dt}\right] \quad (1)$$

Assuming that no diabatic effects are taken into account, the continuity equation can be written as :

$$\frac{\partial}{\partial t}\left[\frac{\partial p}{\partial \theta}\right] = -\overline{V} \cdot \overline{\nabla}\left[\frac{\partial p}{\partial \theta}\right] - \frac{\partial p}{\partial \theta}\left[\overline{\nabla} \cdot \overline{V}\right] \quad (2)$$

Since $\partial p/\partial\theta$ is always negative (for θ to be a valid coordinate) it flips the sign of the tendency term. If either the advection or the divergence term is negative it contributes to destabilization. Likewise, positive values indicate a tendency towards stabilization. Divergence in the layer acts to increase the stability (positive sign) while convergence acts to decrease stability (negative sign). An important fact to remember is that divergence/convergence is NOT uniquely related to vertical motion in an isentropic framework. In pressure coordinates vertical motion is directly related to the vertical profile of the horizontal divergence. Divergence or convergence in a layer affects the static stability by changing the amount of mass between consecutive isentropic surfaces: If a parcel of air in a layer between two isentropic levels flows from a stable to an unstable area, the column expands vertically and by mass continuity, there must be a horizontal convergence in the column.

4.3.4 Moisture advection chart (g kg^{-1} h^{-1})

Positive (negative) values indicate increasing (decreasing) moisture locally. Local increases or decreases through evaporation or condensation are neglected.

4.3.5 Moisture flux convergence chart (g kg^{-1}h^{-1})

This variable includes the advection of moisture and the effect of the divergence/convergence on the moisture field. In an isentropic framework this variable

not only measures the advection of moisture but also the increase (decrease) in moisture content that takes place with convergence (divergence). This is often useful in forecasting convection. Positive (negative) values indicate convergence (divergence) and often destabilization (stabilization).

4.3.6 Adiabatic vertical motion chart (microbar s^{-1})

Negative (positive) values indicate upward (downward) motion.

4.4 Summary

In this chapter various graphs which can be generated for isentropic analysis were listed and a brief idea of interpretation methods were given. Although a few rules can be made to understand the information given by charts on isentropic levels, practical experience is the best way of mastering the isentropic analysis knowledge.

The isentropic variables which are most commonly displayed are:

- Vertical cross section(s) in the area(s) where interesting weather is occurring to determine the isentropic level(s) to work with and to get an idea of moisture distribution and vertical motion.
- Pressure and wind charts to identify cold and warm tongues of air and draw limiting streamlines if possible to separate different air masses.
- Vertical adiabatic motion maps on lower and middle levels to shed some light on vertical motion (upward or downward).
- Condensation pressure difference chart(s) to recognize areas where the air is close to saturation.
- Moisture advection maps to see where moisture is increasing locally.
- Moisture flux convergence maps to see where moisture is accumulating and destabilization might occur.
- Static stability charts to gain some knowledge on areas where the air is relatively unstable and development might occur.

The following chapters will discuss case studies and the way in which isentropic analysis can contribute to interpretation of weather data.

CHAPTER 5

CASE STUDY IN JANUARY 1996

5.1 Introduction

During January 1996 extensive rain fell over South Africa. From Figure 5.1 it is clear that a large part of the country received between 100 and 200 percent of the average monthly rainfall. A few major rainfall events could be identified which contributed to the high rainfall figures for January. One of these cases was 24 - 29 January 1996. In this period heavy rain fell over the eastern parts of the country leading to local flooding in places. In Kwazulu/Natal Estcourt measured 114 mm on the 25th and Durban 101mm on the 26th.

5.2 Aims of the case study

The January heavy rainfall event will be analysed isentropically and compared with the real time observations. It will also be shown how isentropic analysis could have aided the weather forecaster in the decision of where and how much rain would fall.

5.3 Data used

The Central Forecasting Office (CFO) at the SAWB supplied a synoptic sequence of events for the week. The Climate Section of the SAWB supplied daily rainfall figures and reports of flooding. Satellite images were also used to get an indication of the cloudmass and the relevant weather systems. Data for the isentropic analysis were derived by the methods described in chapter 3 using the 12 hour forecast fields of the Eta model.

5.4 Synoptic sequence of events for 24 - 29 January 1996

Surface at 12:00 UT:

On the 24th (Figure 5.3) moist, tropical air was in circulation around a low pressure system over the interior and fairly general rain and thundershowers occurred over the

eastern half of the country. Heavy falls were reported in Gauteng, Mpumalanga and the Free State. A cold front passed south of the country causing some cloudy, cooler conditions with rain along the Cape south coast.

On the 25th (Figure 5.5) fairly general rain and thundershowers occurred over most of the country, except in the extreme west, due to a deep, tropical low pressure system over Botswana on the surface as well as in the upper-air. Heavy falls were again recorded at places in Gauteng, Mpumalanga and KwaZulu/Natal. A south-easterly flow maintained overcast weather along the south and east coasts where light rain fell.

With moist air in circulation around the coastal low pressure system near Durban and the deep, tropical low pressure system over Botswana, widespread rain fell over the eastern half of the country on the 26th (Figure 5.7). A cold front on the south coast caused cooler conditions and when the cold air later undercut the very humid , tropical air over KwaZulu/Natal and eastern Mpumalanga heavy falls resulted.

On the 27th (Figure 5.9) the cold front had moved to the eastern parts of the country with the Atlantic Ocean high pressure system ridging eastwards along the eastern coast behind it on the east coast where rain developed in the onshore flow. The passing of the cold front caused drying and cooling as polar air replaced the tropical air mass over the eastern parts of the country. Over the north-eastern parts moist tropical air was still in circulation and scattered thundershowers and rain remained.

The cold front passed over the eastern regions of the country to be situated over Zimbabwe on the 28th (Figure 5.11) with much cooler conditions behind it. The high pressure system east of the country maintained an onshore flow over KwaZulu/Natal, and Mpumalanga where cloudy conditions and light rain continued. An off-shore flow developed over the western and south-western coasts.

On the 29th (Figure 5.13) the rain producing systems were a thing of the past. Most of the country was under the influence of cooler, drier air. A trough was situated over the western interior and light falls were recorded in a narrow band over the northern Cape interior. The high pressure system south-east of the country together with the low pressure system in the southern Mozambique channel caused cloudy conditions over

the extreme north-eastern parts of the country where light falls still continued.

Upper-air at 12:00 UT:

On the 23rd a westerly upper-air trough started to develop west of the country, while an easterly tropical low was present over Botswana.

North-westerly winds with windspeeds of up to 50 knots were present over the southern and south-western parts of the country (associated with the westerly trough) on the 24th, while 20 knot north-easterlies were dominant in the north-east (in association with the upper-air low pressure system).

A strong westerly trough was present on the west coast on the 25th (Figure 5.14) while the tropical low pressure system and associated northerly to north-easterly winds was still present over the northern parts of the country.

On the 26th (Figure 5.15) the low pressure system strengthened and moved a little south-eastwards to 22S. The westerly trough was still situated over the south-western part of the country.

The tropical system played a major part in the heavy precipitation up to the 26th; after that the westerly upper-air trough combined forces with the tropical low to cause more widespread rain towards the end of the period over the eastern parts of the country.

On the 27th (not shown) the upper-air systems weakened and moved away to the east. A weak perturbation was still evident over the south-eastern parts of the country.

A westerly wind flow developed over the southern parts of the country on the 28th (not shown), while the previous system moved further eastwards.

Strong north-westerly winds of up to 50 knots were once again reported over the south-western parts of the country on the 29th (not shown) where the westerly trough was developing. A tropical low pressure system was present north-east of the country with associated south-easterly winds over the eastern parts of the country.

5.5 Satellite images at 12:00 UT

On the 24th (Figure 5.2) the sub-continent was almost covered by extensive convective cloud clusters in association with the tropical air in circulation over these parts. A tropical cyclone was situated south-east of Madagascar.

Figure 5.4 shows that the cloud amount associated with the tropical low pressure system was still increasing over the eastern and northern parts of the country on the 25th.

On the 26th (Figure 5.6) the upper air low pressure system (now centred over eastern Botswana) intensified. This resulted in enhanced convective cloud development along its eastern and southern flanks depicted by the cloudbands of Figure 5.6.

On the 27th (Figure 5.8) moisture advection by the ridging high pressure system reached the latitudes south of the upper-air low pressure system leading to enhanced cloud formation.

On the 28th (Figure 5.10) convective cloud development was suppressed when cooler and drier air reached southern Mozambique and Zimbabwe.

Figure 5.12 shows that the convective cloud fields were moving toward the north and east and clear skies were once again visible over the southern half of the country on the 29th.

5.6 Rainfall distribution and intensity

Rainfall data was only available for South Africa and consequently the rainfall distribution and isentropic analysis results will only be discussed for the South African region.

On the 24th (Figure 5.16) rain was reported over the entire country excluding the extreme western parts. Moderate (more than 25 mm) to heavy (more than 50 mm) falls were restricted to the eastern parts of the country (Free State, Northwest, Northern

Province, Mpumalanga and KwaZulu/Natal).

Rainfall distribution on the 25th (Figure 5.17) was similar to the 24th, but the moderate to heavy falls were concentrated in the Northern Province, Northern Cape and KwaZulu/Natal.

KwaZulu/Natal received rainfall in excess of 50 mm on the 26th (Figure 5.18), while only moderate falls were reported over the Northern Province. Due to faulty rainfall records (as explained below) an area south and south-east of Lesotho should also have been included in the rainfall figures, but was omitted.

The area of heavier precipitation shifted to the north-eastern parts of the country on the 27th (Figure 5.19), where falls of more than 50 mm were recorded. Drying was evident from the west with only light falls over the south-eastern parts of the country.

On the 28th (Figure 5.20) light falls (less than 25mm) were recorded over the eastern parts, with moderate falls over the northern extremes of the country.

The heavy rain had ended by the 29th (Figure 5.21) with light falls still occurring but none of the stations reported more than 25 mm.

A problem occurred with the rainfall data on the 28th: Rainfall was not reported over the weekend (26-28 January) and the total for the weekend was reported for the 28th without indicating that it was a figure for accumulated rainfall. This means that the rainfall reports for the 26th and 27th were thus not completely realistic and indications are that an area south-east and south of Lesotho received extensive falls on the 26th, much less on the 27th and less than 5 mm on the 28th. This means that an area of heavy precipitation should also be included on the rainfall map for the 26th south and south-east of Lesotho.

5.7 Eta model evaluation

The general surface (mean sea level pressure or MSLP) and upper-air (500 hPa) analyses patterns of 24 January were handled well by the Eta model, but the tropical

low pressure system which was present over Botswana on the surface, as well as in the upper air, was not shown on the Eta maps. The trough building west of the country was depicted by the 500 hPa analysis.

On the 25th the Eta model started to show signs of a low pressure system on the surface over Botswana but it was placed further northwards than observed. The upper-air low pressure system over Botswana was still not depicted on the 500 hPa analysis.

The upper-air low pressure system as well as the surface low pressure over Botswana was clearly visible on the MSLP and upper-air analyses on the 26th. The high pressure system which was beginning to ridge on the south coast was also present on the MSLP analysis.

The surface low pressure system on the 27th was positioned a little further northwards on the Eta MSLP charts than the observed position, but the upper-air trough on 20-25E was well positioned. The high pressure system ridging on the east coast behind the passing cold front could clearly be seen on he MSLP Eta analysis.

The Eta model evaluation on the 28th was very good, placing the upper-air and MSLP systems in the correct position.

5.8 Isentropic analysis results

5.8.1 ETA analysis date : 96012500 with a 12-hour forecast for 96012512

The strong inflow of moisture from the east and upward motion along the escarpment was evident on cross-sections, especially in the north (28S and 25S) (Figures 5.22 and 5.23). A deep layer with moisture content more than 6 g kg^{-1} was evident on all the cross-sections. The strong (6 cm s^{-1}) influx of moisture carried over the entire continent on 25S caused the rainfall area to extend further westwards (to 24E) than on the other cross-sections.

The heaviest precipitation (up to 110mm) occurred in areas where warmest (720 hPa)

air was present (Figure 5.24), together with moist and most saturated (60 hPa) air on 315 as well as 325K (Figures 5.25 and 5.26). Isentropic analysis is useful for separating airstreams from different origins by means of limiting streamlines. Limiting streamlines can be indicative of a front or a site for frontogenesis, but this is not always the case. If the limiting streamlines can be related to relative humidity, clouds, static stability, that relationship may continue farther out in the forecast. In this case limiting streamlines on the pressure chart in the centre of the country are separating dry and moist air masses and create a transition zone which corresponds well to the condensation difference patterns. Vertical adiabatic motion (VAM) on 315 K (close to the surface) indicated upward motion over the southern half of the country (Figure 5.27), with 8 microbar s^{-1} over the southern interior and 6 microbar s^{-1}south-east of Lesotho where falls in excess of 20 mm were recorded. VAM on 325K (more or less 550 hPa) was only negative (6 microbar s^{-1}) over the northern parts of the country (Figure 5.28). This is the area where falls of up to 100 mm were reported. Moisture advection was more pronounced on the south coast (up to 0.6 g kg^{-1} $hour^{-1}$), but values of up to 0.4 g $kg^{-1}hour^{-1}$ were present south-east of Lesotho and along 28E. Moisture flux convergence (Figure 5.29) also favoured the areas around Lesotho (0.6 g kg^{-1} $hour^{-1}$) as well as the western parts of Northwest where heavy falls occurred. Static stability values were no more than 120 hPa over any part of the country.

In spite of the fact that the Eta model did not analyse the tropical low pressure systems in the upper air or on the surface very well on this day, results of the isentropic analysis were nevertheless agreed well with the rainfall distribution and intensity.

5.8.2 *Eta analysis date : 96012600 with a 12-hour forecast for 96012612*

The strong inflow of moisture from the east was no longer evident on the southern vertical cross-sections but a layer of moisture (above 8 g kg^{-1}) was still present. The vertical component of the wind (cross isentropic) was much less than the previous day on 25S (not shown) and 23S (Figure 5.30), making isentropic analysis more useful.

The influx of cooler air ahead of the cold front could clearly be seen on the pressure chart (Fig. 5.31) showing values of less than 640 hPa over the western and southern coastal areas as well as the adjacent interior. Warmer (more than 720 hPa), moist air

was still in circulation over the interior. A general picture of the rainfall area could be derived from the condensation pressure chart on 315K (not shown) where values of more than 550 hPa were present. The condensation difference chart on 315K (Figure 5.32) with values of lower than 80 hPa and even 60 hPa indicated the area where heavier precipitation occurred. The condensation difference values on 325K (not shown) were similar to the values on 315K, also favouring the south-east coast and interior. Moisture advection (Figure 5.33) of more than 0.5 g kg^{-1} $hour^{-1}$ and flux convergence (0.4 g kg^{-1} $hour^{-1}$) patterns favoured the south-eastern parts of the country where moist air moved in behind a coastal low pressure system on the south-east coast. This coincides with the area of heavy precipitation. The moisture flux convergence chart (not shown) also favoured the area east and north-east of Lesotho as well as a part of Northwest Province which also tied in with areas of heavier precipitation. Strong VAM on 315K (Figure 5.34) could be seen over the south-western parts (20 microbar s^{-1}) ahead of the cold front, as well as behind the coastal low pressure system which advected cooler , moist air into the south-eastern parts of the country. Weaker VAM (2 microbar s^{-1}) could be seen over the southern and south-western interior on the 325K level (Figure 5.35) ahead of the westerly upper-air trough still present in that area. An area of upward motion on 325K was evident over the north-eastern parts of the country. This coincided with the heavier falls in that area caused by the presence of the upper-air low pressure system. Static stability values of more than 100 hPa were not found. With most of the relevant upper-air soundings over South Africa having general rain profiles rather than unstable, convective profiles, it is not surprising that the static stability values were low.

5.8.3 *Eta analysis date : 96012700 with a 12-hour forecast for 96012712*

With the wind direction changing to easterly again (due to the ridging of the high pressure system east of the country) the inflow of moisture from the east was more pronounced on all the vertical cross-sections. The moisture layer was significantly deeper on 25S and 23S (Figure 5.36) than on 30S and 28S. Strong upward motion could be seen along the escarpment making isentropic analyses in this area difficult.

The passage of the cold front to the eastern parts of the country could be seen on the pressure chart (Figure 5.37) where the cooler air (less than 640 hPa) spread into

Mpumalanga. Warmer air was still evident over the northern Cape and parts of Northwest. The strongest vertical adiabatic movement on 315K (Figure 5.38) was over the central and eastern parts where the convergence of the colder air from the south and the warmer air from the north caused frontal uplift. Parts of Gauteng and Northwest Province also showed some vertical movement where heavier falls occurred. The upper-air systems deepened compared to the previous day. The westerly trough moved somewhat eastwards to the central parts of the country and combined with the tropical low pressure system in the north. Although upward motion was evident over most of the country on 325K, significant VAM (up to 7 microbar s^{-1}) could be seen (Figure 5.39) over the central, southern and eastern parts of the country. The retreat of moisture to the northern parts could be seen on the condensation pressure chart (Figure 5.40) , with values of less than 600 hPa only north-east of a line stretching from the north-west to the south-east through Lesotho. Condensation difference values on 315K (Figure 5.41) and 325K (not shown) were similar, with values of less than 90 hPa again giving a good indication of the entire rainfall area, with preference to the eastern and northeastern parts (values lower than 60 hPa) where the heavier falls were recorded. Maximum moisture advection patterns shifted to the northern parts where values of up to 0.3 g $kg^{-1}hour^{-1}$ could be seen over the area north and north-west of Lesotho. Moisture flux convergence patterns on 315K (Figure 5.42) favoured the same area (up to 1.2 g kg^{-1} $hour^{-1}$) as well as a small area on the east coast on 29S. Static instability between 315 and 320K was evident (Figure 5.43) in a narrow band north-west of Lesotho where values between 120 and 160 hPa were given. This would probably have been the area were thundershowers occurred rather than rain. The rainfall area and the heavy rainfall regions could clearly be identified by means of the isentropic maps.

5.8.4 *Eta analysis date : 96012800 with a 12-hour forecast for 96012812*

Although an inflow of moisture from the east still existed on 25S (not shown) and 23S (Figure 5.44), definite drying was visible on 28S and 30S (not shown) which tied in with the off-shore flow developing on the south-east coast.

The southern, south-eastern and eastern parts of the country were under the influence of cooler, post-frontal air by this time (due to a high pressure system ridging on the east coast behind the cold front) and the warmer, tropical airmass was clearly displaced

by this cooler, maritime air. Much less moisture was available and the area closest to saturation (not exceeding 100 hPa) on 315K (Figure 5.45) as well as 325K (not shown) was small and included only the north-eastern parts of the country. Values of lower than 30 hPa were evident over the far north-eastern parts which coincided with the area where falls of more than 40 mm were recorded. Vertical adiabatic motion on 315K indicated only weak rising motion. In the upper-air a westerly wind system was again approaching the country and the wind flow on 500 hPa indicated a north-westerly to westerly flow over this region. Relatively strong vertical adiabatic motion on 325K (Figure 5.46) was thus indicated on the west coast , while lower values were evident over the southern interior. Values over the eastern parts were only slightly negative with a large area of sinking motion over the northern and north-western parts. On 325K condensation pressure values (not shown) of below 100 hPa were evident over the south-western parts where another upper-air trough was situated. Moisture flux convergence on 315K (Figure 5.47) indicated increasing accumulation of moisture over the north-eastern parts of the country coinciding with the rainfall area. Moisture advection and flux convergence patterns on 315K (not shown) both indicated an area over the western parts of increasing moisture accumulation ahead of an approaching cold front. Static stability values were below 120 hPa.

5.9 Conclusions

There were two source regions of surface moisture on the surface during this period:

a) Warm, continental, tropical air was advected from the north and north-east;
b) Moisture advection took place from the east as the high pressure system ridged in behind the cold front. The low pressure system which formed in the upper layers (700 and 500 hPa) enhanced the general rain situation and was nearly stationary for a relatively long time in the period. It later combined with the westerly upper-air trough to cause extensive falls over the eastern part of the country towards the end of the period.

Considering the isentropic analyses, it seems that orographic uplift and subsequent moisture flux convergence along the escarpment played key roles in the rain production. Upward vertical adiabatic motion over the interior on 315K and 325K was

characteristic of the period but weakened towards the 28th. Orographic lifting played an important role in the precipitation in the areas closest to the escarpment. Time and again the area where heavier precipitation occurred coincided with the area where the condensation pressure values were the highest, the condensation difference values were less than 100 hPa (and even as low as 30 hPa) and where moisture accumulation (convergence) took place. The presence of the warmer tropical air over the interior could clearly be seen as well as the passage of the cold front, when the cooler maritime air replaced the warmer, tropical air. In a situation where tropical air (close to saturation) was present over the interior, it is not expected that static instability would play a major role in the rain production, and this could be seen in the static stability values, which only showed values of 120-160 hPa on the western edge of the rainfall area near the upper-air trough. Even though the model did not handle the interior and upper-air troughs very well on the 25th, good indicators of the rainfall area was possible.

A problem with any model is its inability to have a completely realistic model topography: The Eta model is certainly one of the best models available with regard to modelling topography, South Africa's Drakensberg range remains a very difficult part of the country to represent in the model topography. This sometimes leads to unrealistic model results in the vicinity of the mountain range, especially over the eastern part of Mpumalanga where gradients are steep. To the best knowledge of the numerical modellers at the SAWB there are, however, no specific problems in this region.

The general rain pattern and even the areas of heavy precipitation could clearly be identified by the isentropic analyses. A combination of the condensation pressure, condensation difference, moisture advection and moisture flux convergence charts proved to be helpful in predicting the rainfall area. Although isentropic analysis does not solve every forecasting problem, it is an extremely useful tool provided the user understands the limitations of the technique.

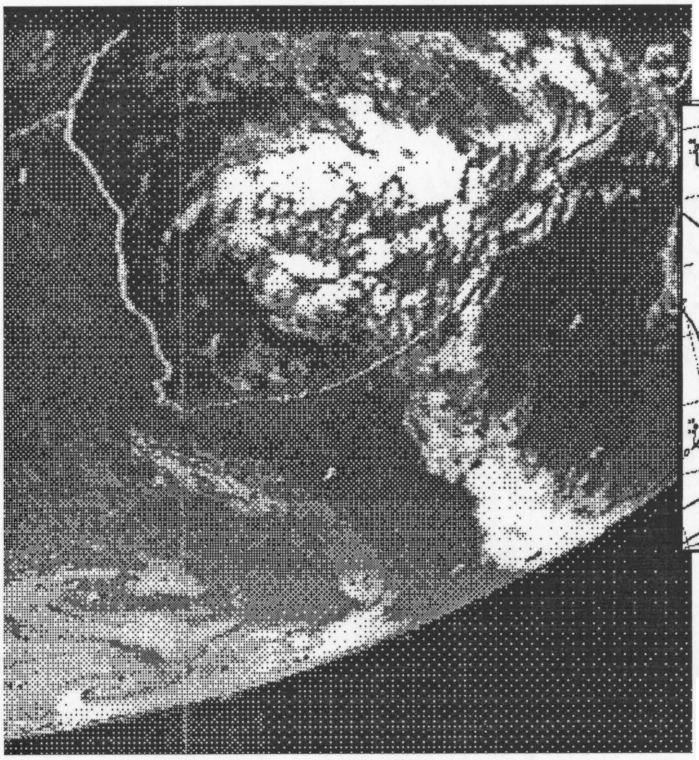

Figure 5.2 Meteosat IR image at 12:00 UT on 24 January 1996

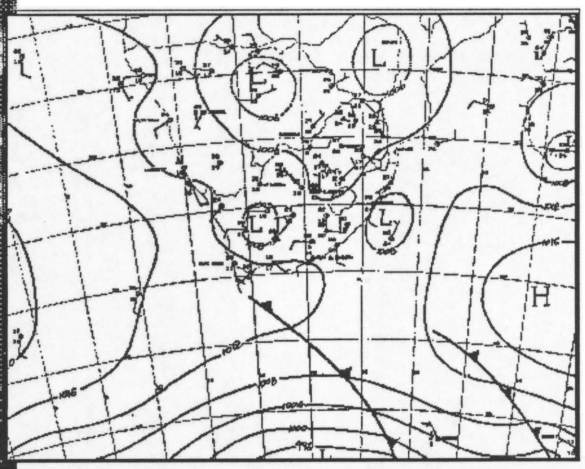

Figure 5.3 Surface pressure chart for 12:00 UT on 24 January 1996. Isobars are in hPa and spaced every 4 hPa. Over the interior pressures are hydrostatically converted to sea level.

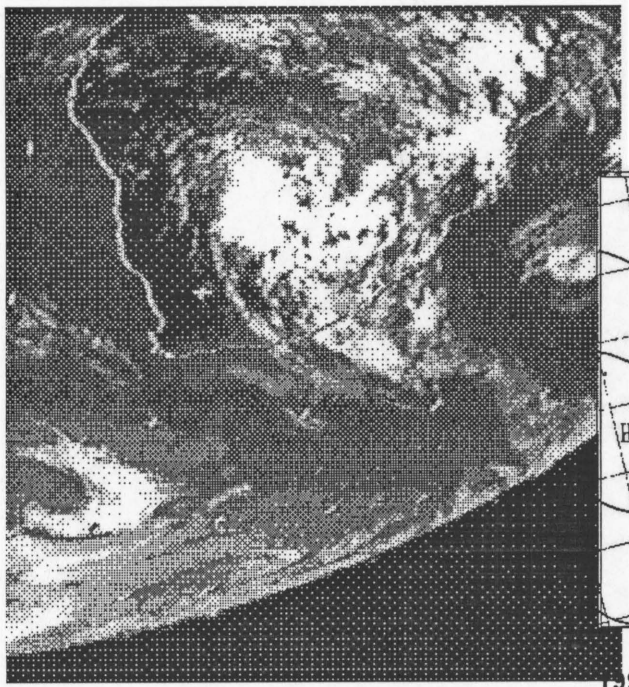

Figure 5.4 As Fig.5.2 but on 25 January 1996

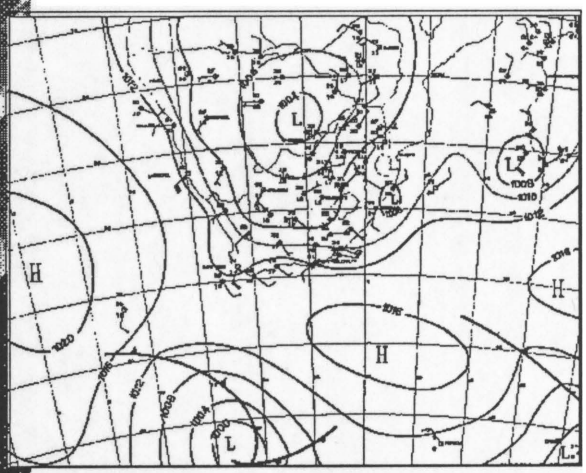

Figure 5.5 As Fig.5.3 but on 25 January 1996

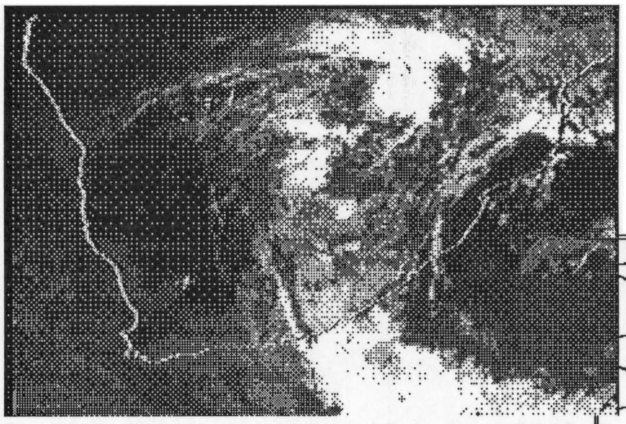

Figure 5.6 As Fig.5 2 but on 26 January 1996

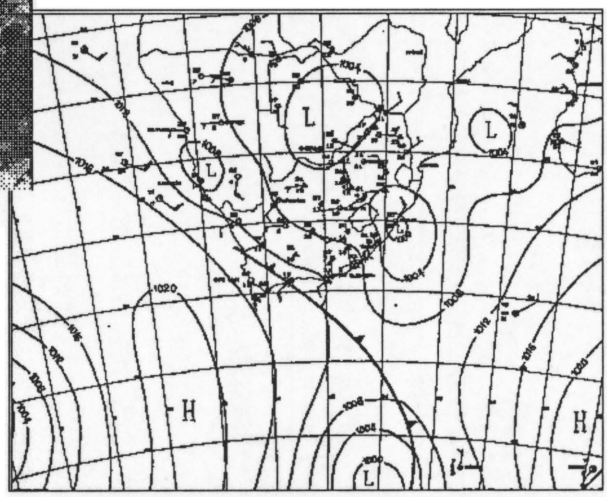

Figure 5.7 As Fig.5.3 but on 26 January 1996

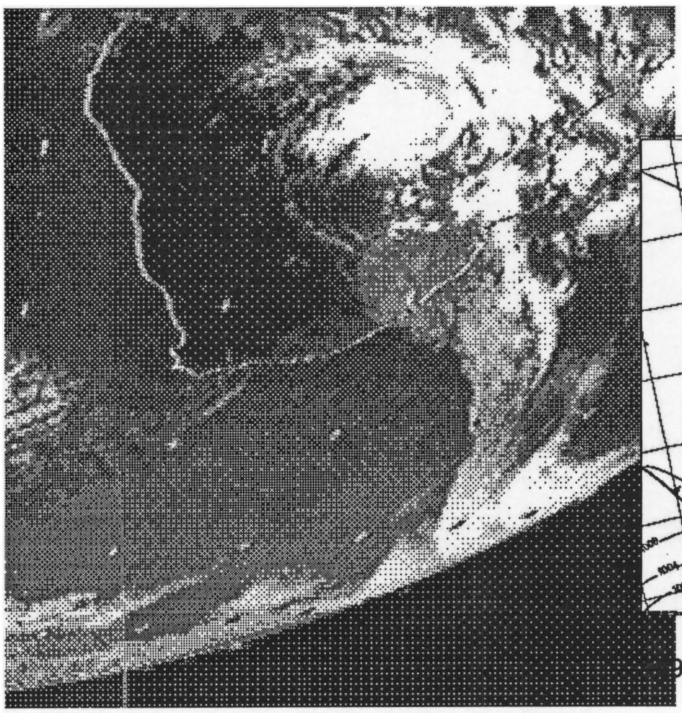

Figure 5.8 As Fig.5.2 but on 27 January 1996

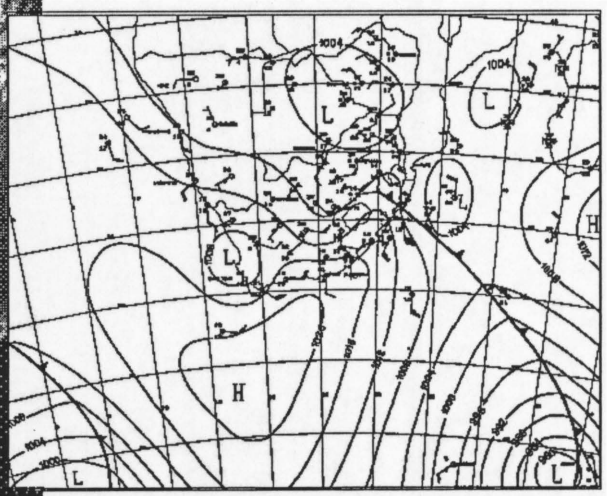

Figure 5.9 As Fig. 5.3 but on 27 January

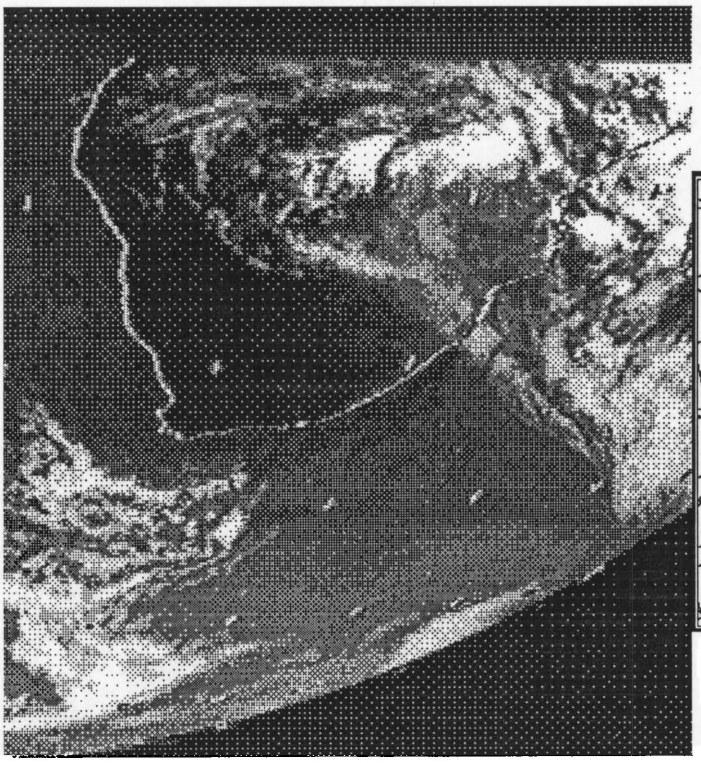

Figure 5.10 As Fig.5.2 but on 28 January 1996

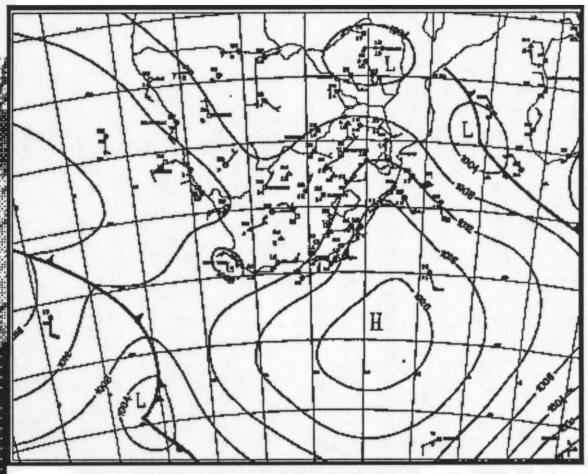

Figure 5.11 As Fig.5.3 but on 28 January 1996

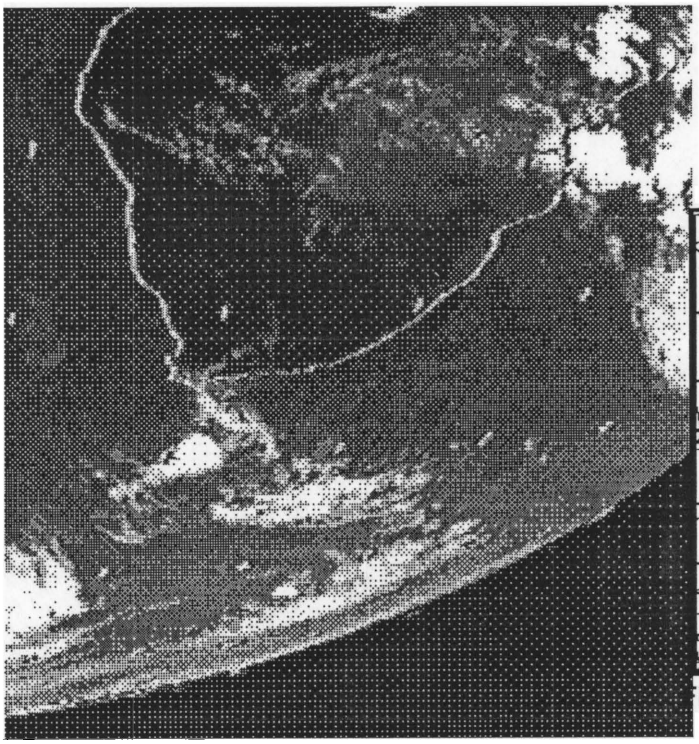

Figure 5.12 As Fig.5.2 but on 29 January 1996

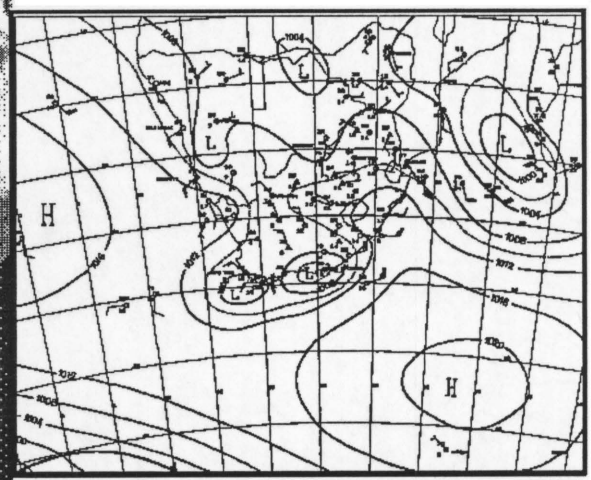

Figure 5.13 As Fig.5.3 but on 29 January 1996

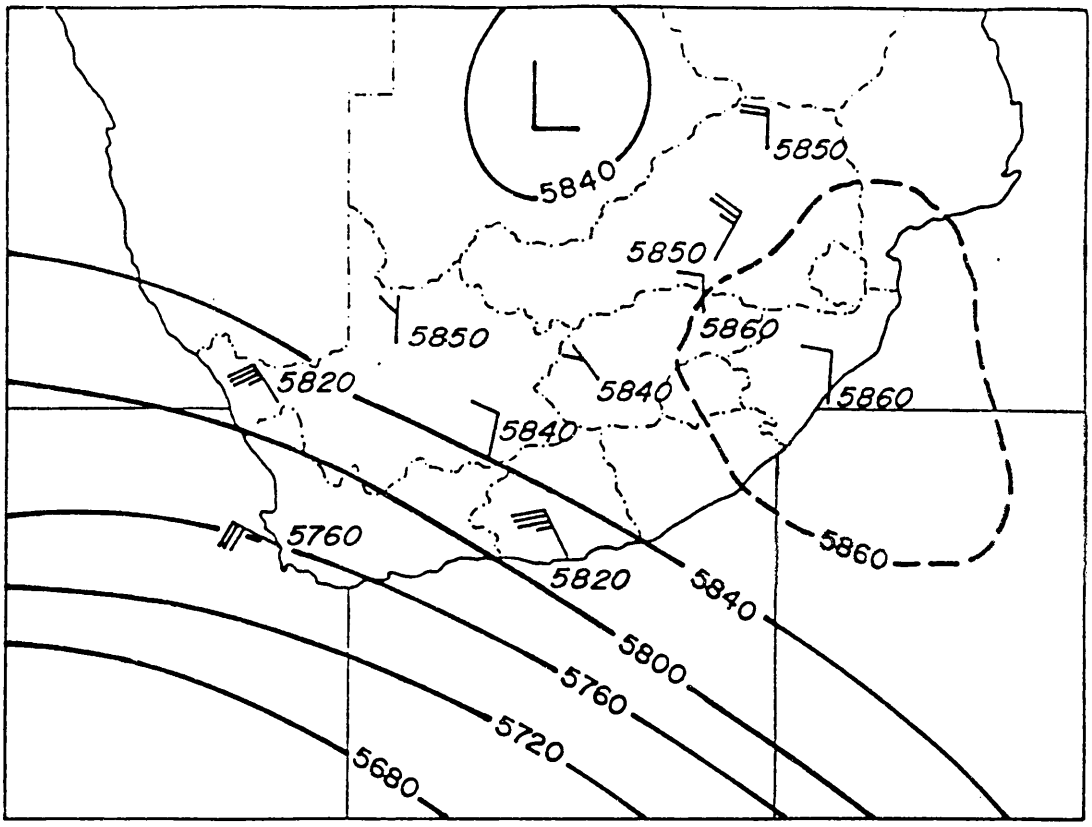

Fig. 5.14 500 hPa constant pressure map for 25 January 1996. Contours are in geopotential meters (gpm). Contour spacing is 40 gpm.

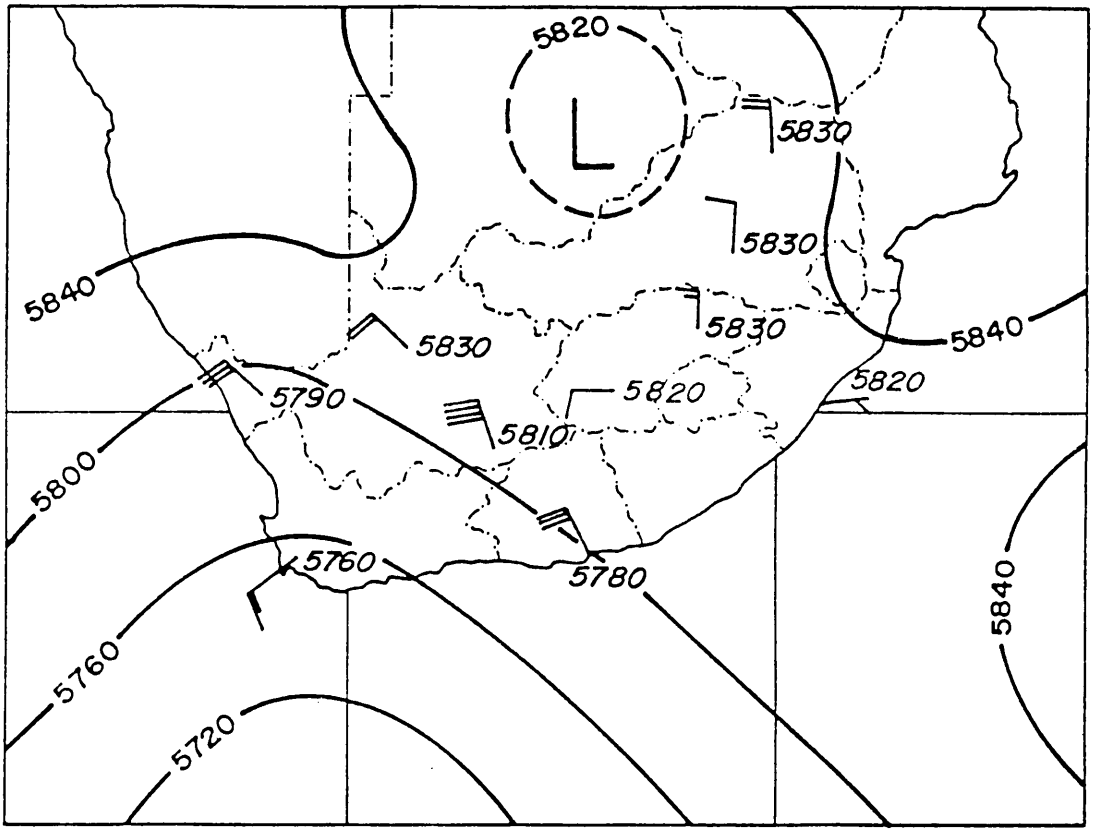

Fig. 5.15 As Fig. 5.14 but on 26 January 1996

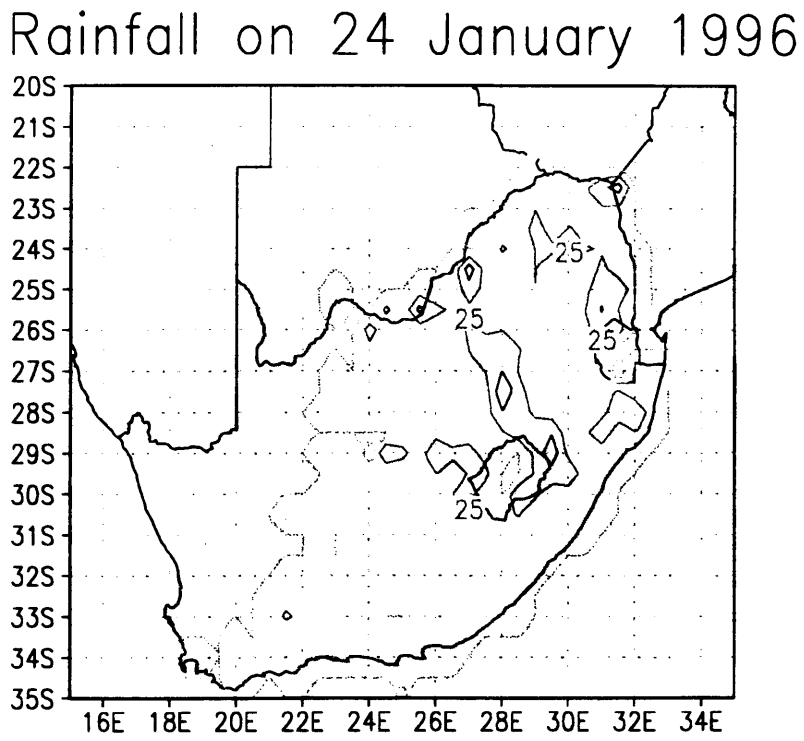

Fig. 5.16 Rainfall on 24 January 1996 in millimeters. Spacing is 25 mm.

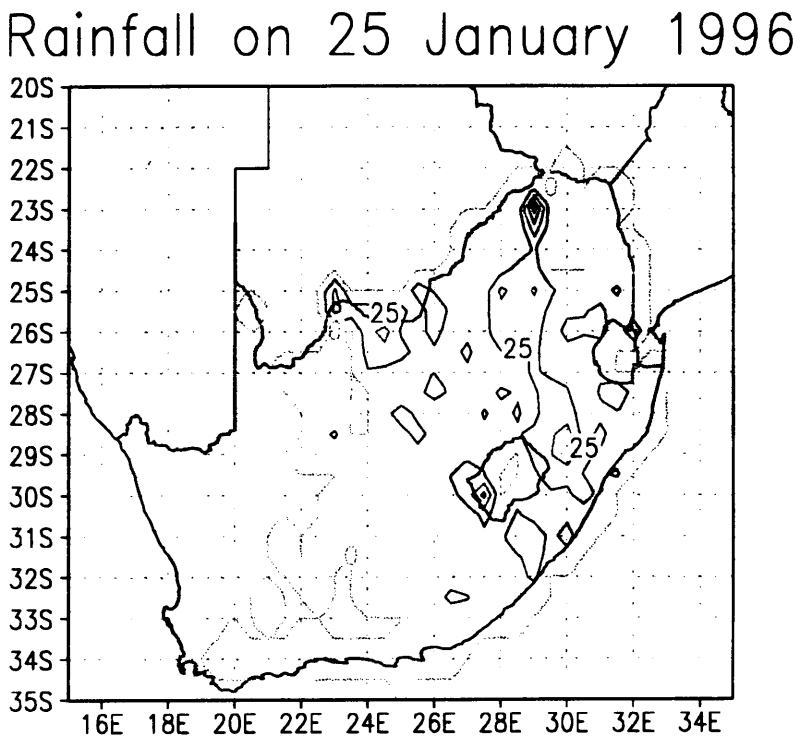

Fig. 5.17 As Fig. 5.16 but on 25 January 1996

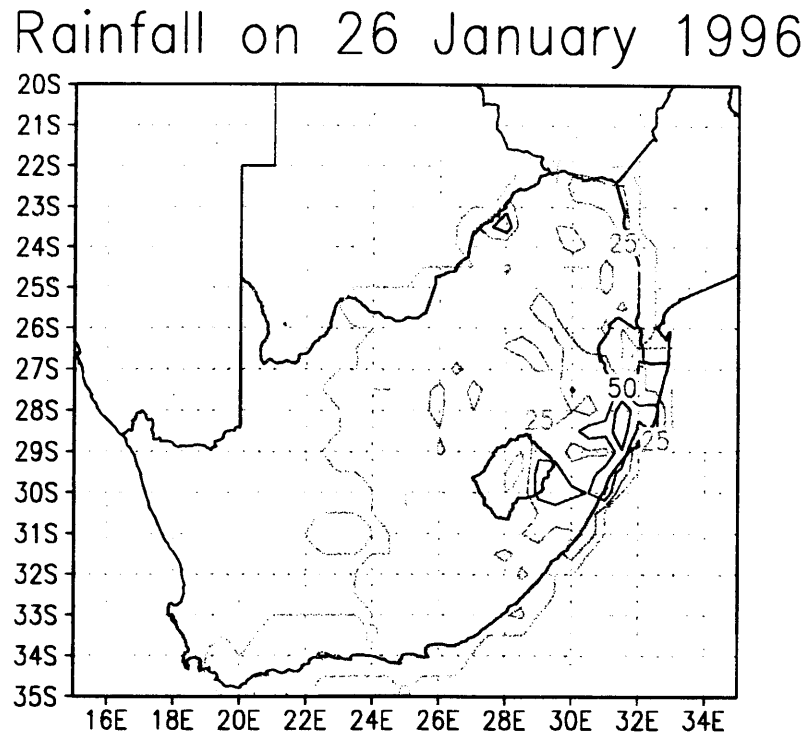

Fig. 5.18 As Fig. 5.16 but on 26 January 1996

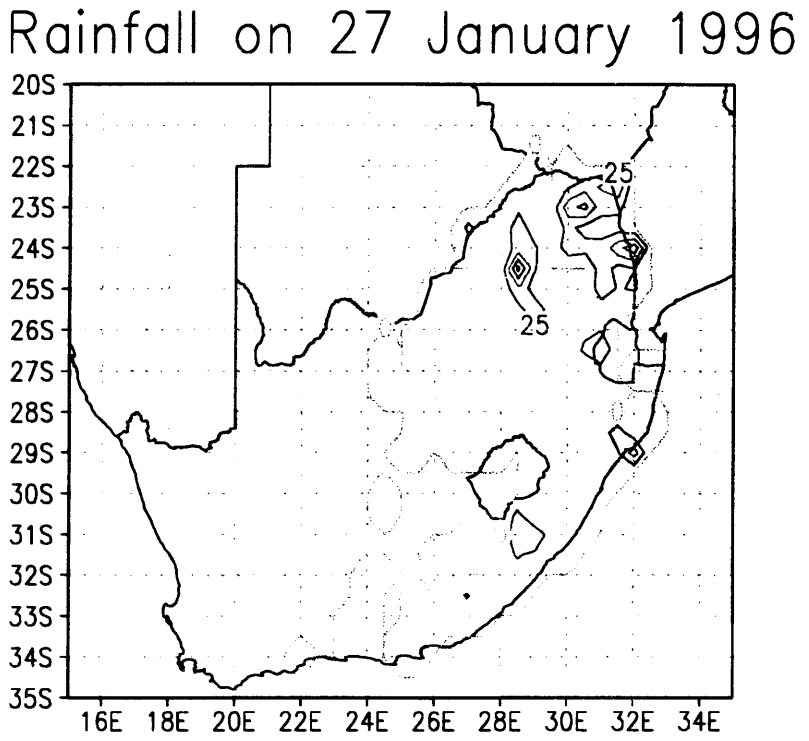

Fig. 5.19 As Fig. 5.16 but on 27 January 1996

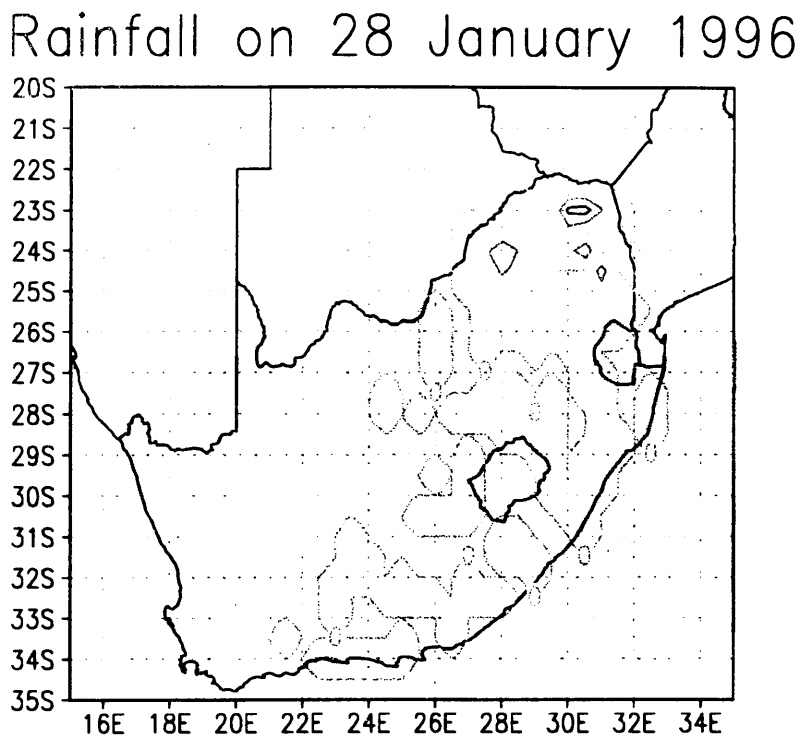

Fig. 5.20 As Fig. 5.16 but on 28 January 1996

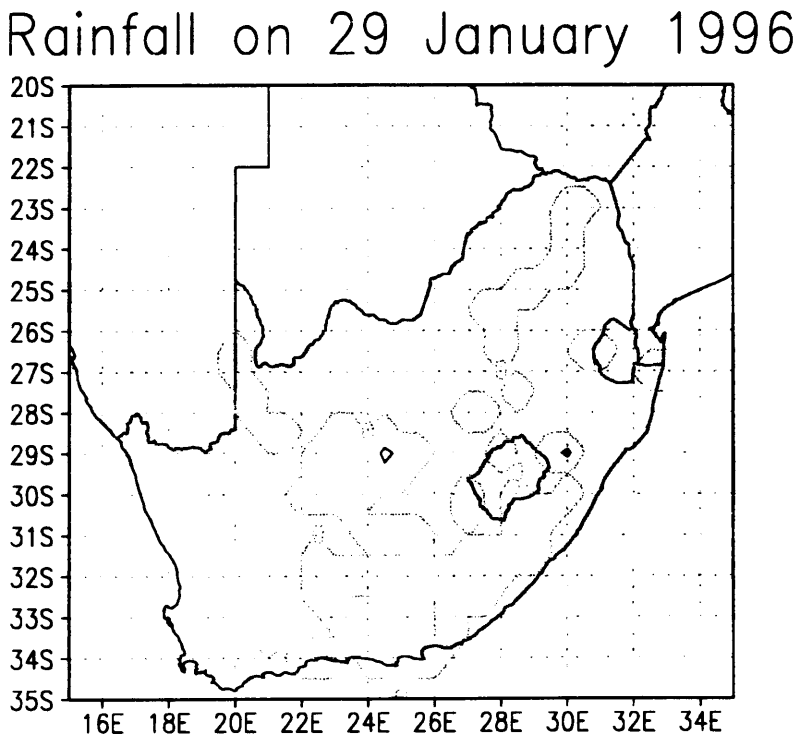

Fig. 5.21 As Fig. 5.16 but on 29 January 1996

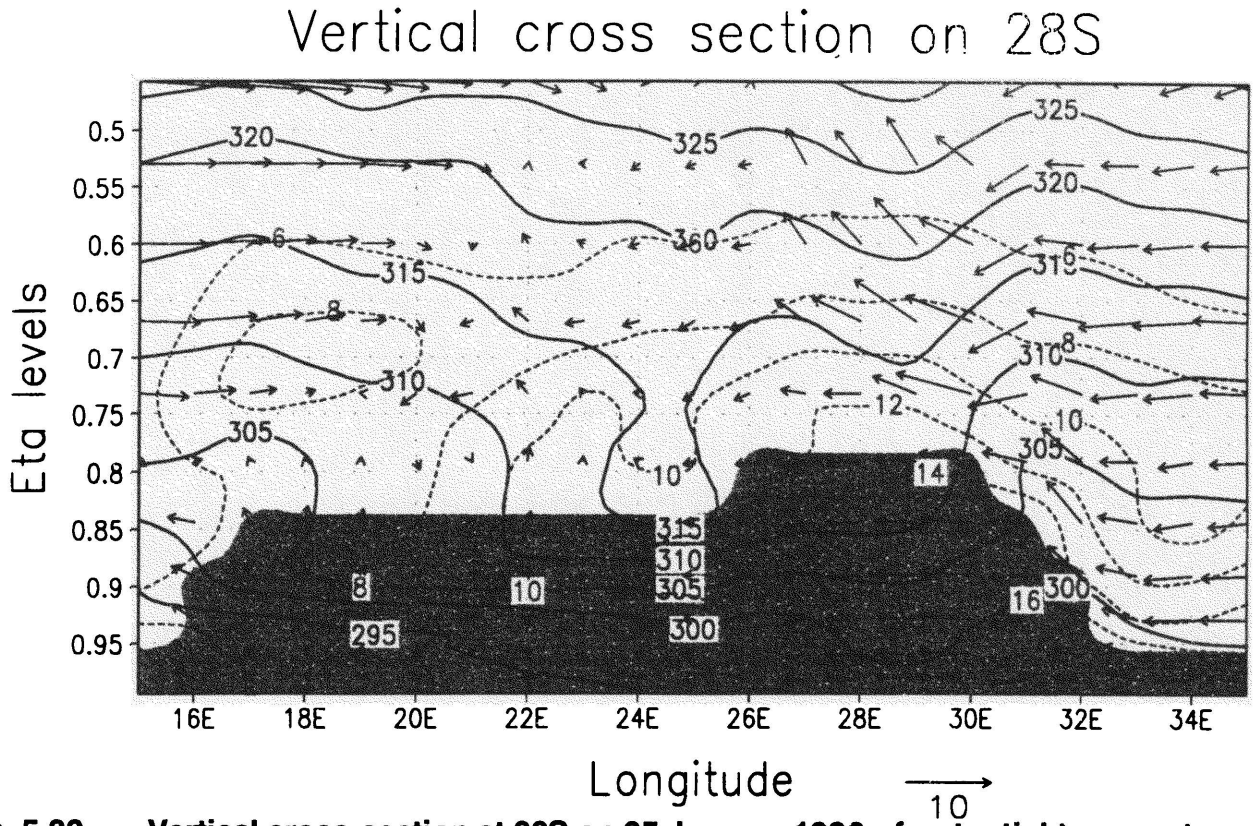

Fig. 5.22 **Vertical cross-section at 28S on 25 January 1996 of potential temperature in Kelvin (solid line), horizontal component of the wind in m s^{-1}, vertical component of the wind in cm s^{-1}, and specific humidity in g kg^{-1}(dotted line). Topography is indicated by the shaded area.**

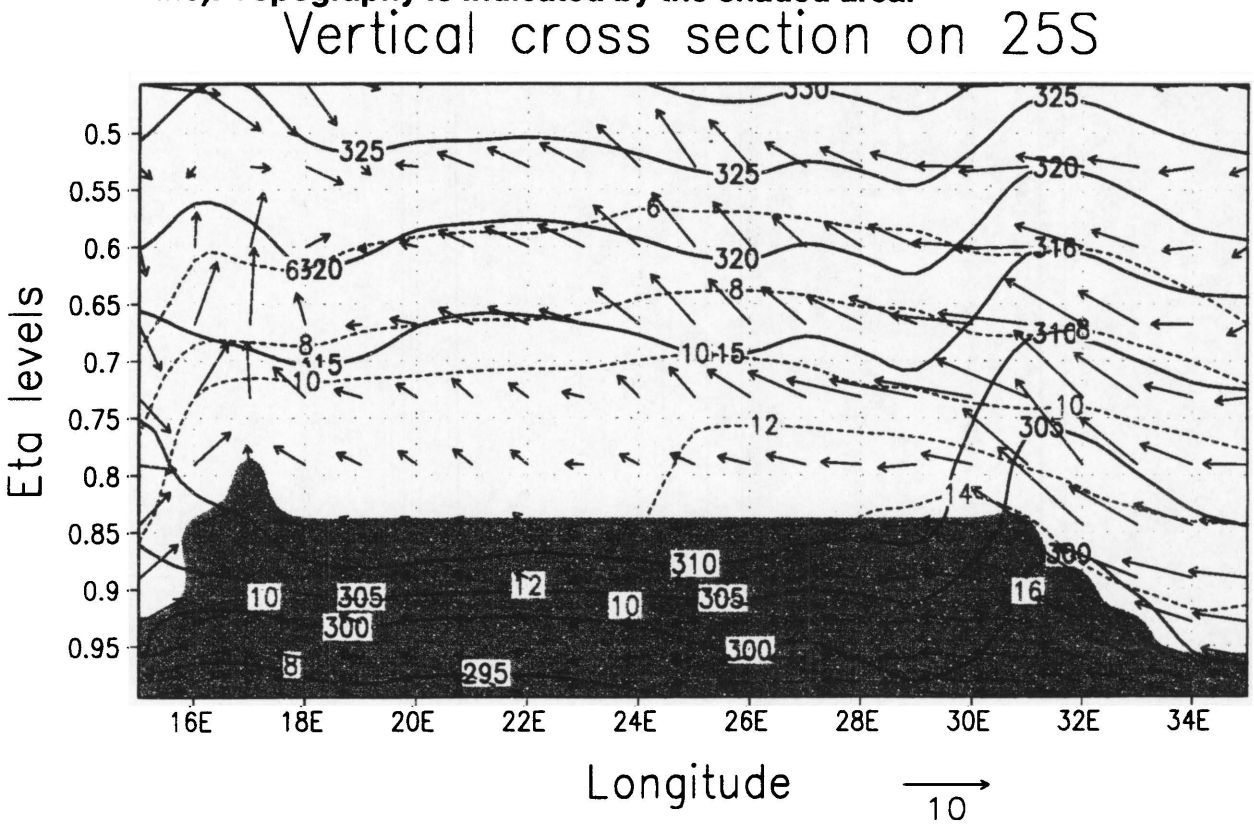

Fig. 5.23 **As Fig.5.22 but at 25S.**

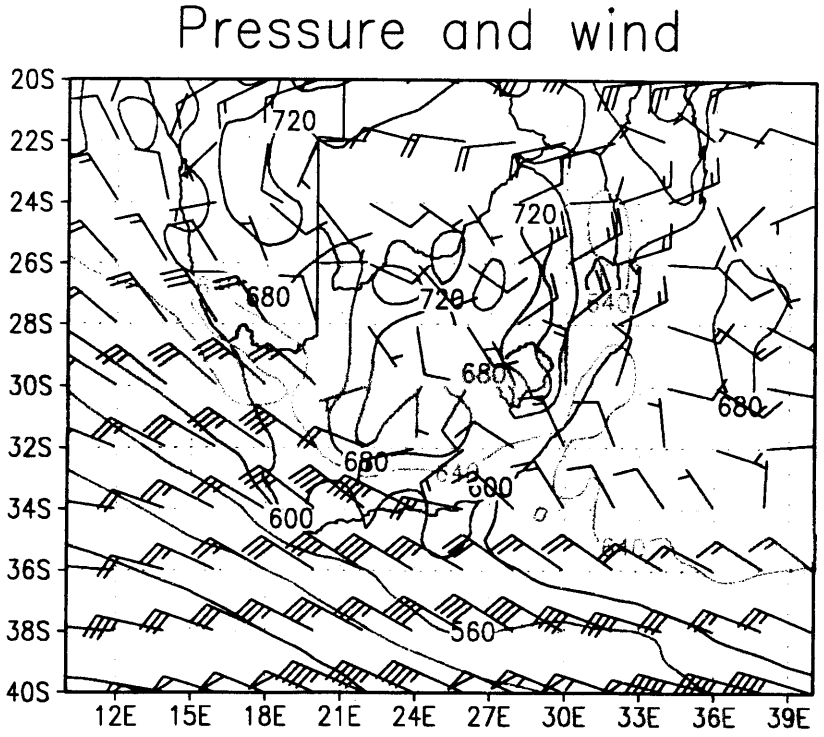

Fig. 5.24 Pressure (hPa) and windspeed (knots) on 315K on 25 January 1996

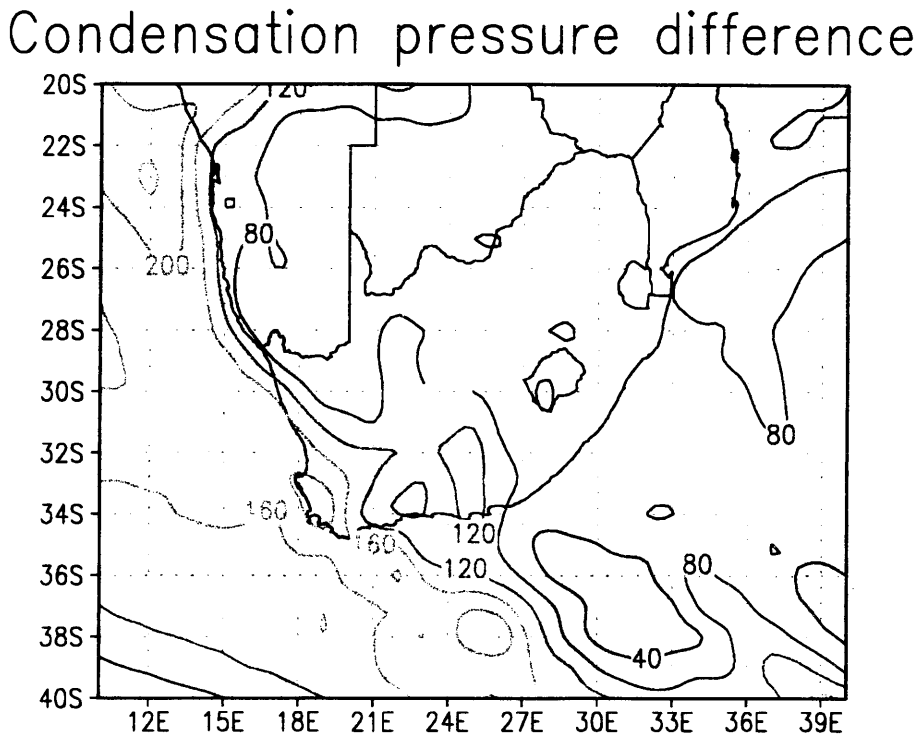

Fig. 5.25 Condensation pressure difference (hPa) on 315K on 25 January 1996

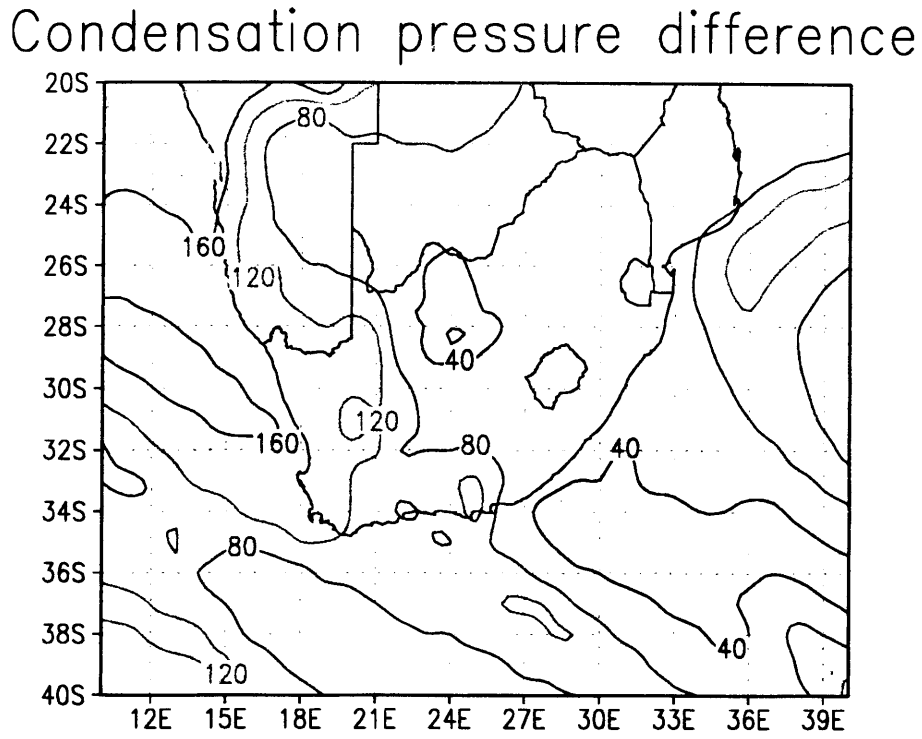

Fig. 5.26 Condensation pressure difference (hPa) on 325K on 25 January 1996

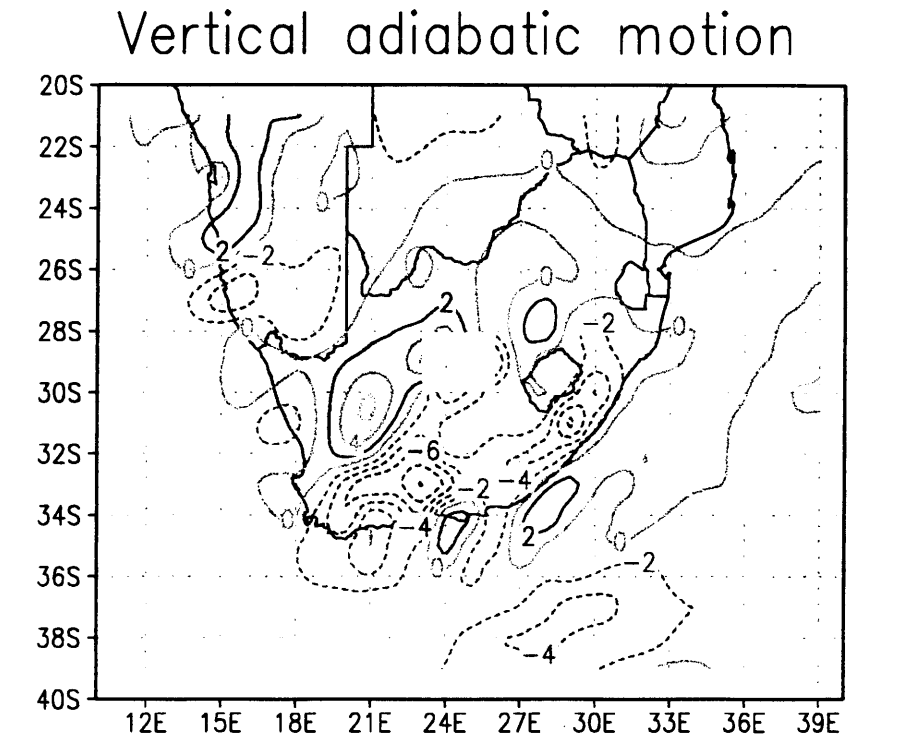

Fig. 5.27 Vertical adiabatic motion (microbar s^{-1}) on 315K on 25 January 1996

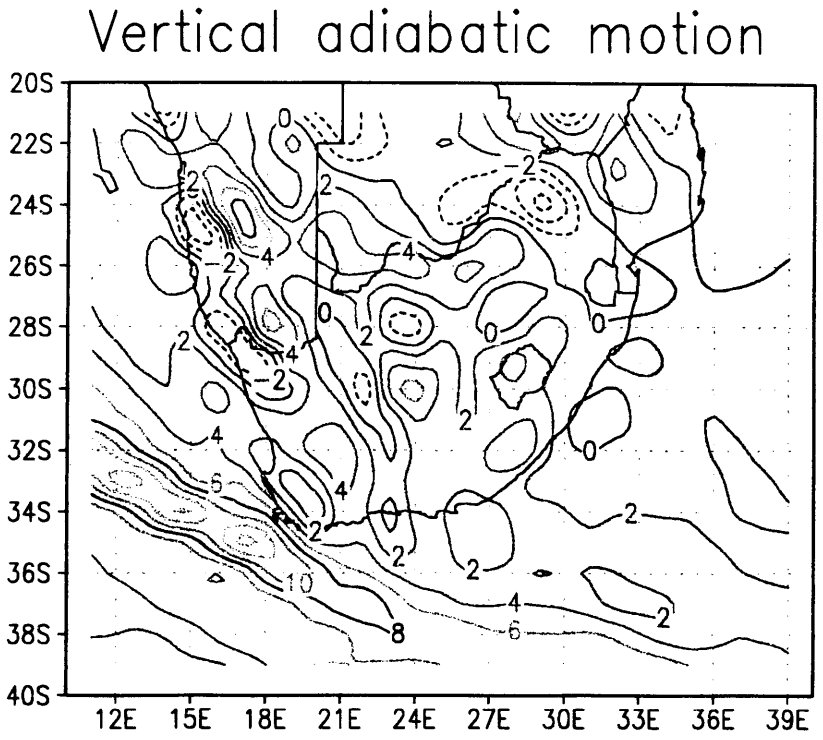

Fig. 5.28 Vertical adiabatic motion (microbar s^{-1}) on 325K on 25 January 1996

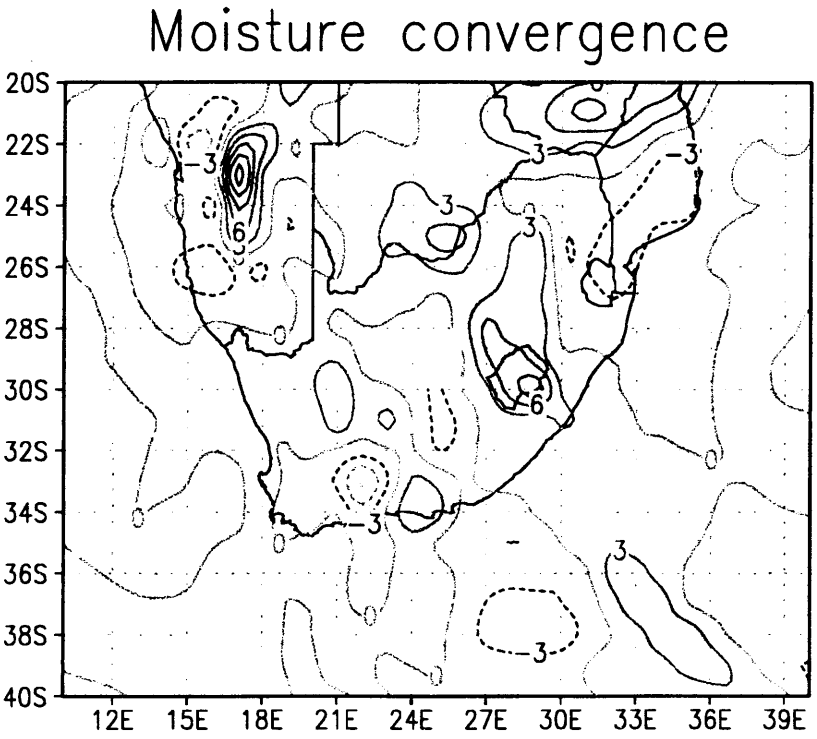

Fig. 5.29 Moisture convergence (g kg^{-1} h^{-1} X10) on 315K on 25 January 1996

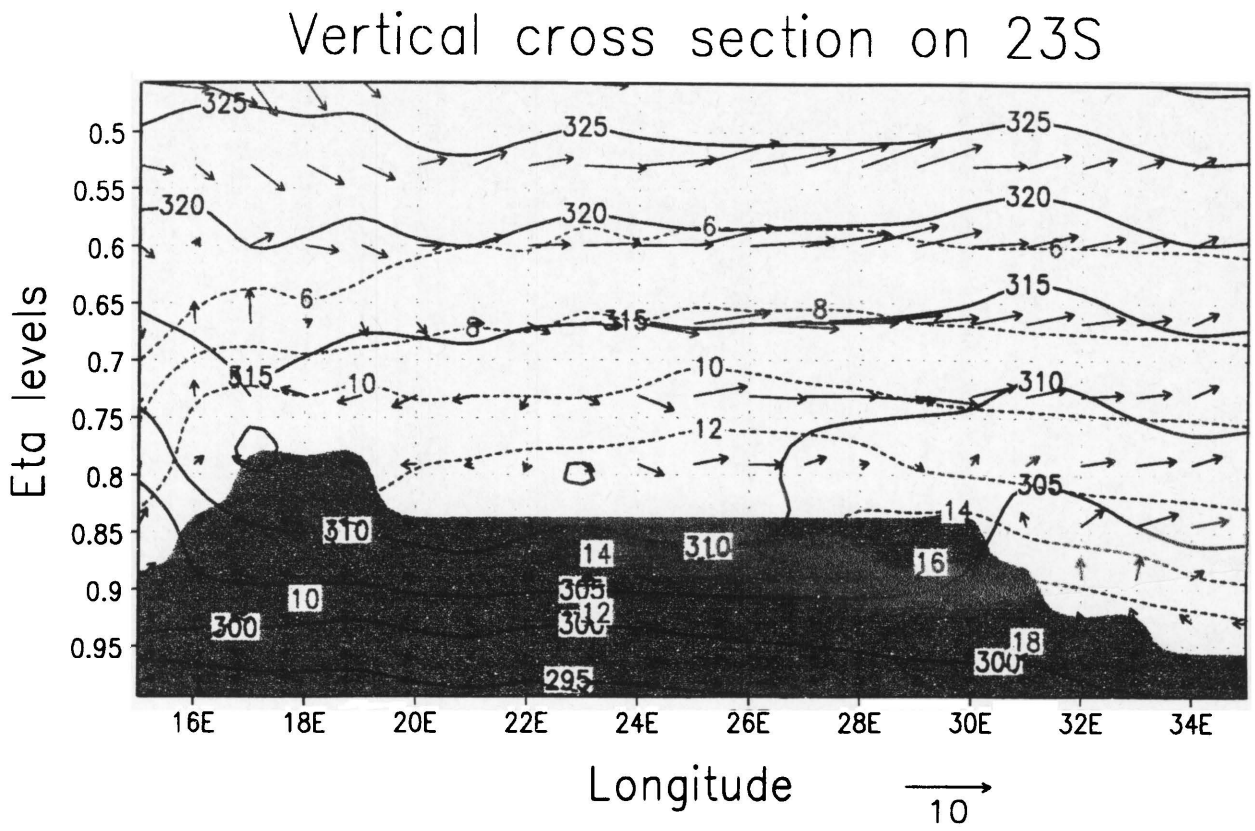

Fig. 5.30 As Fig. 5.22 but at 23S on 26 January 1996

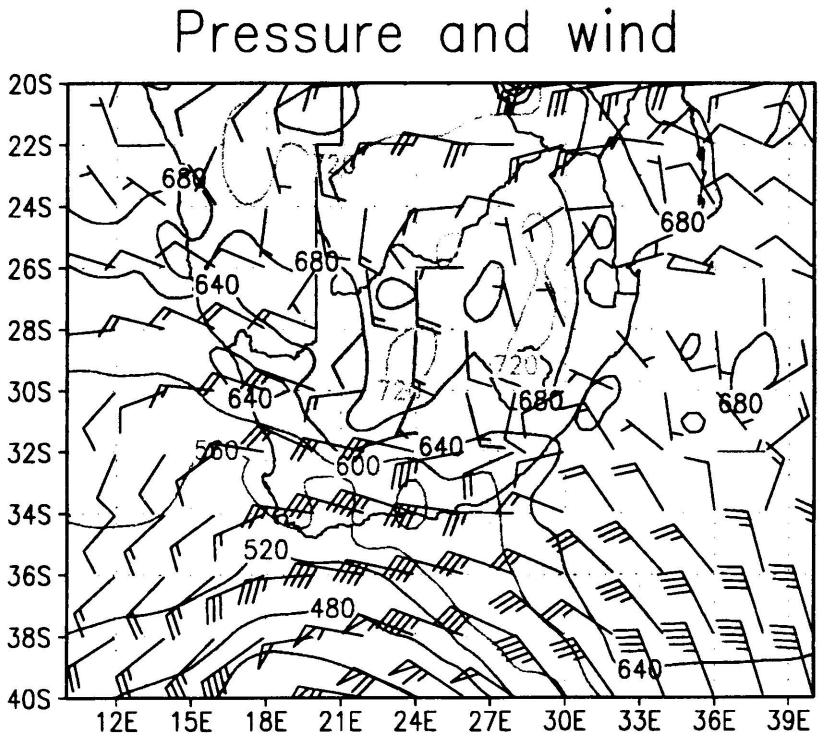

Fig. 5.31 As Fig. 5.24 but on 26 January 1996

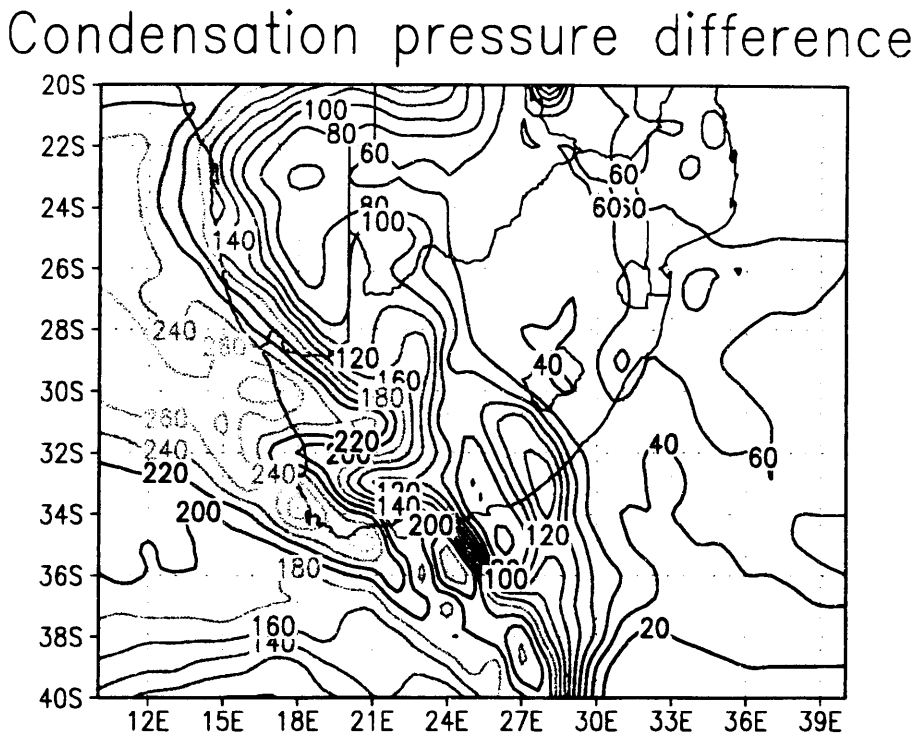

Fig. 5.32 Condensation pressure difference (hPa) on 315K on 26 January 1996

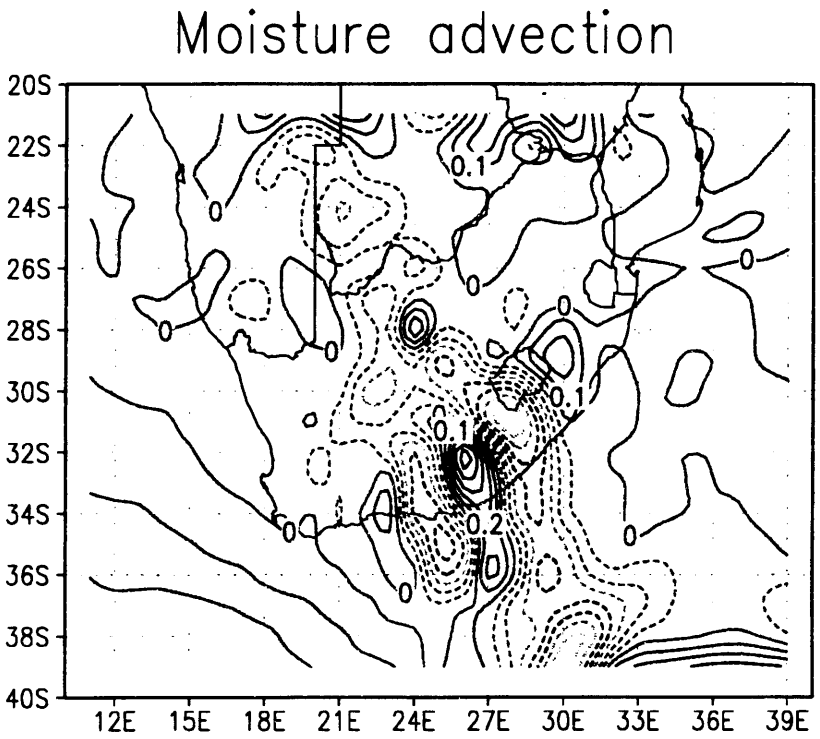

Fig. 5.33 Moisture advection (g kg^{-1} h^{-1}) on 315K on 26 January 1996

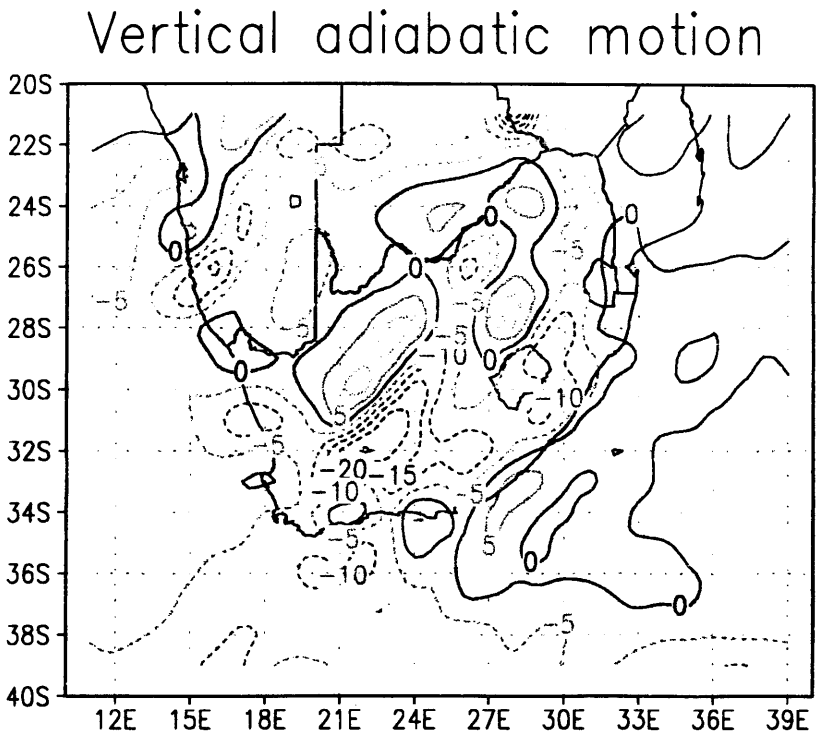

Fig. 5.34 Vertical adiabatic motion (microbar s^{-1}) on 315K on 26 January 1996

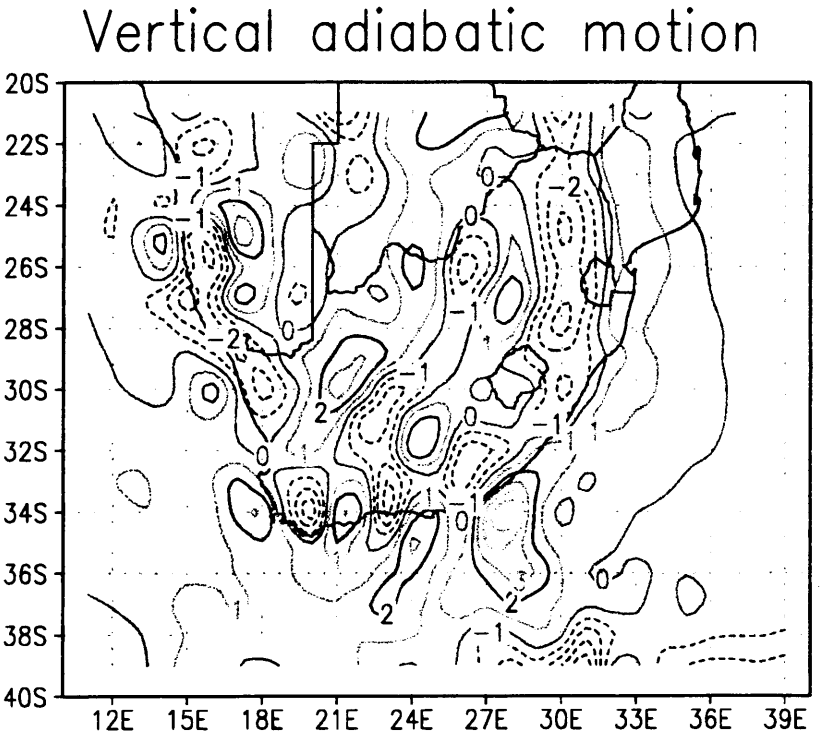

Fig. 5.35 Vertical adiabatic motion (microbar s^{-1}) on 325K on 26 January 1996

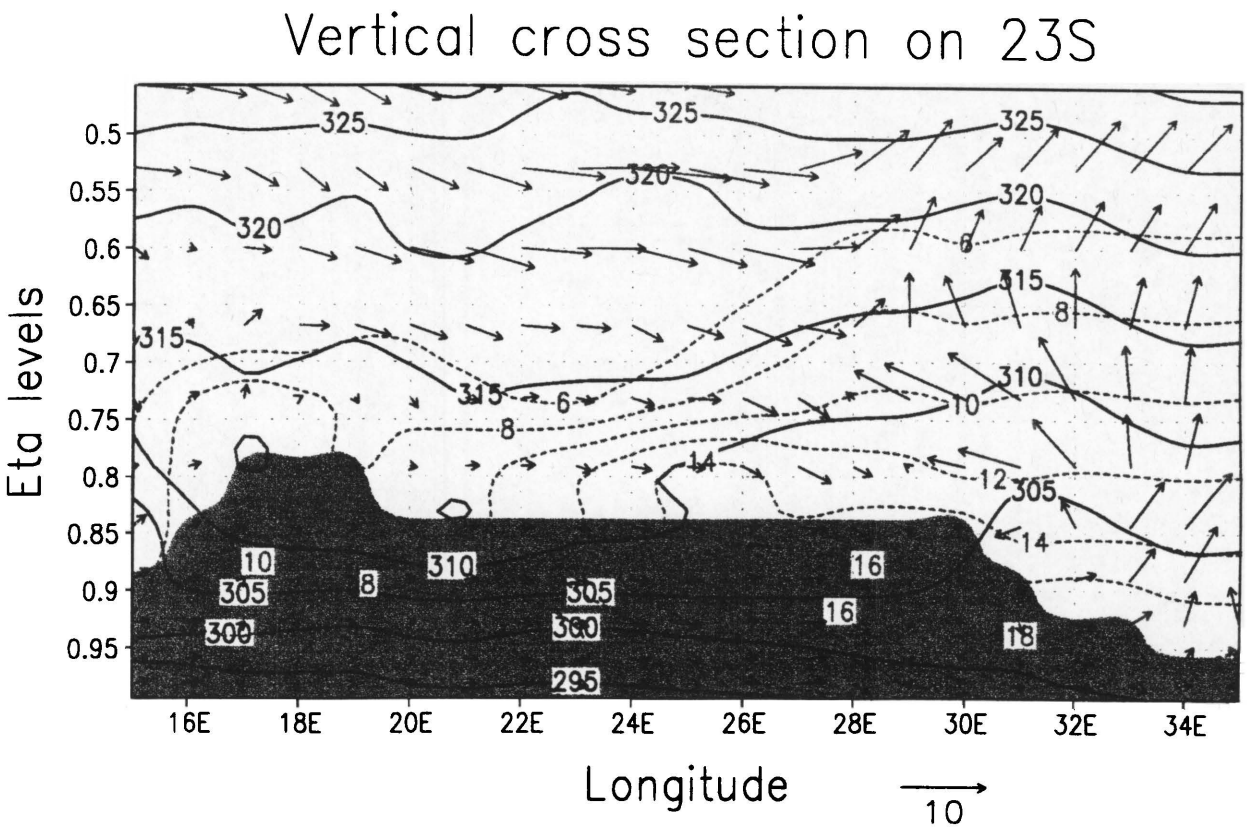

Fig. 5.36 As Fig. 5.22 but at 23S on 27 January 1996

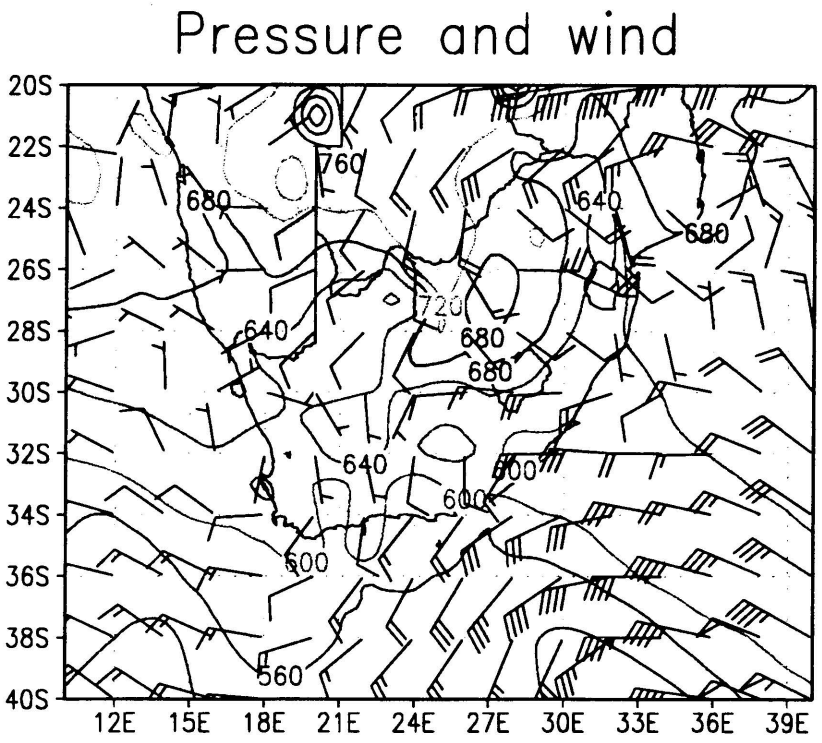

Fig. 5.37 As Fig. 5.24 but on 27 January 1996

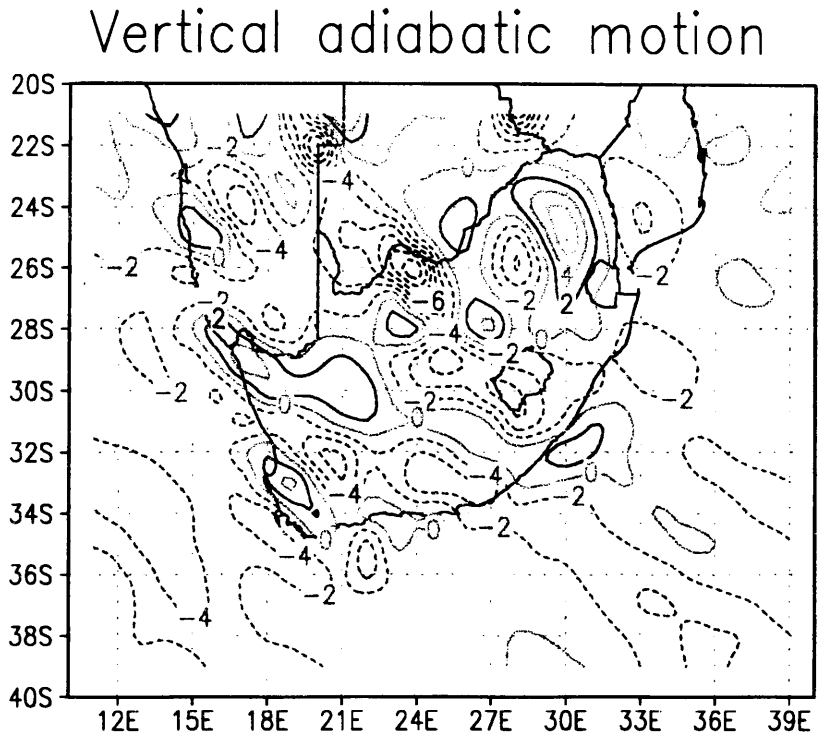

Fig. 5.38 Vertical adiabatic motion (microbar s^{-1}) on 315K on 27 January 1996

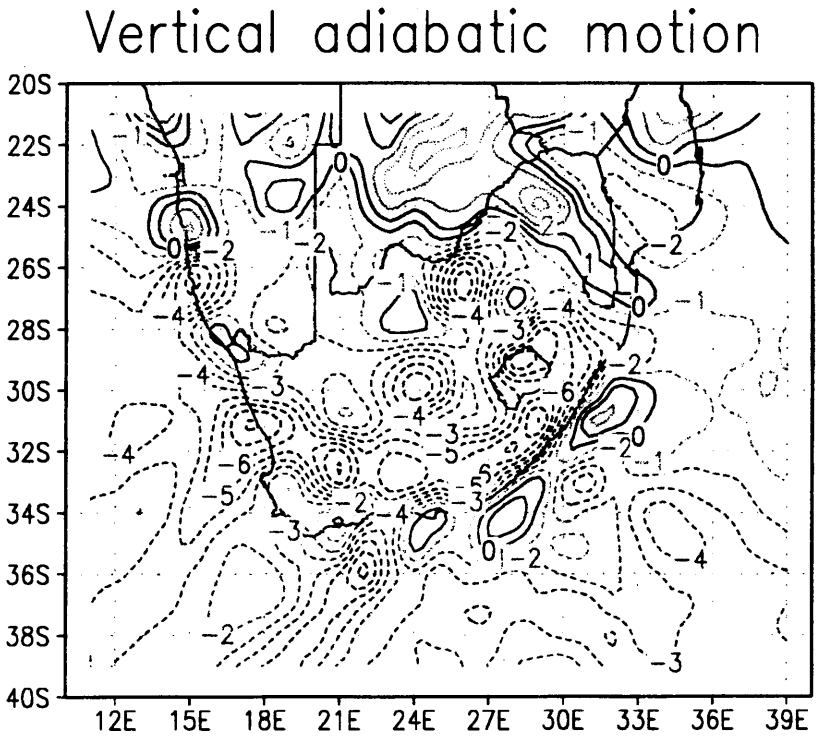

Fig. 5.39 Vertical adiabatic motion (microbar s^{-1}) on 325K on 27 January 1996

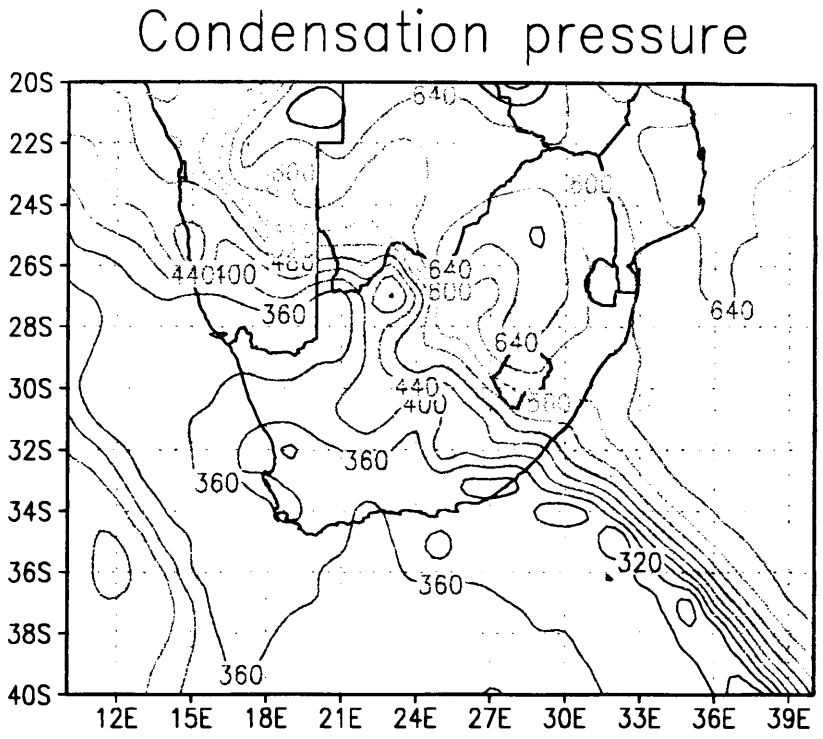

Fig. 5.40 Condensation pressure (hPa) on 315K on 27 January 1996

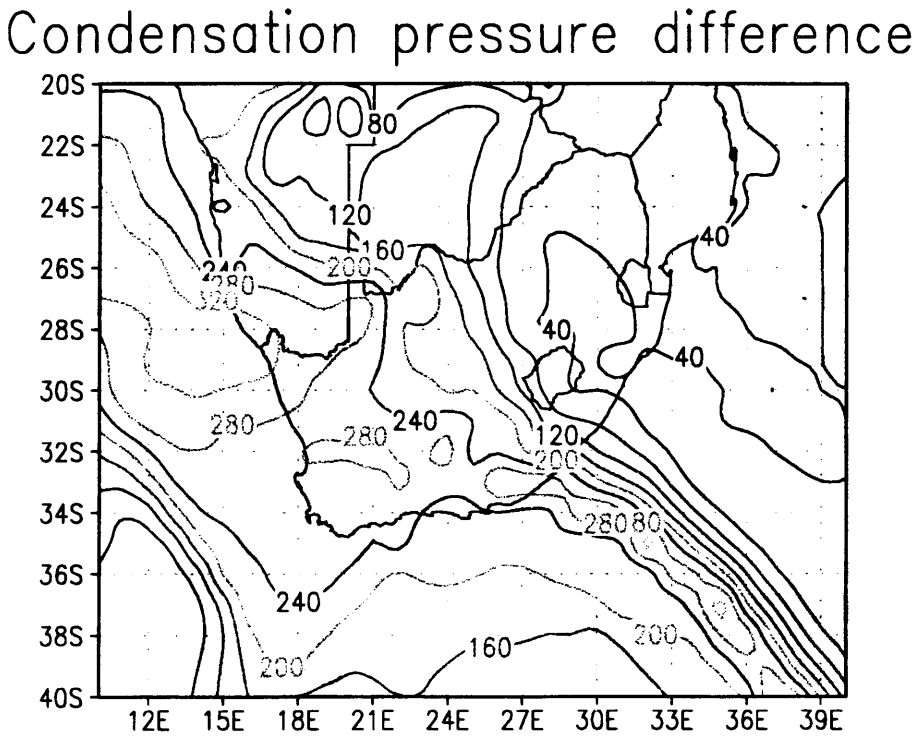

Fig. 5.41 Condensation pressure difference (hPa) on 315K on 27 January 1996

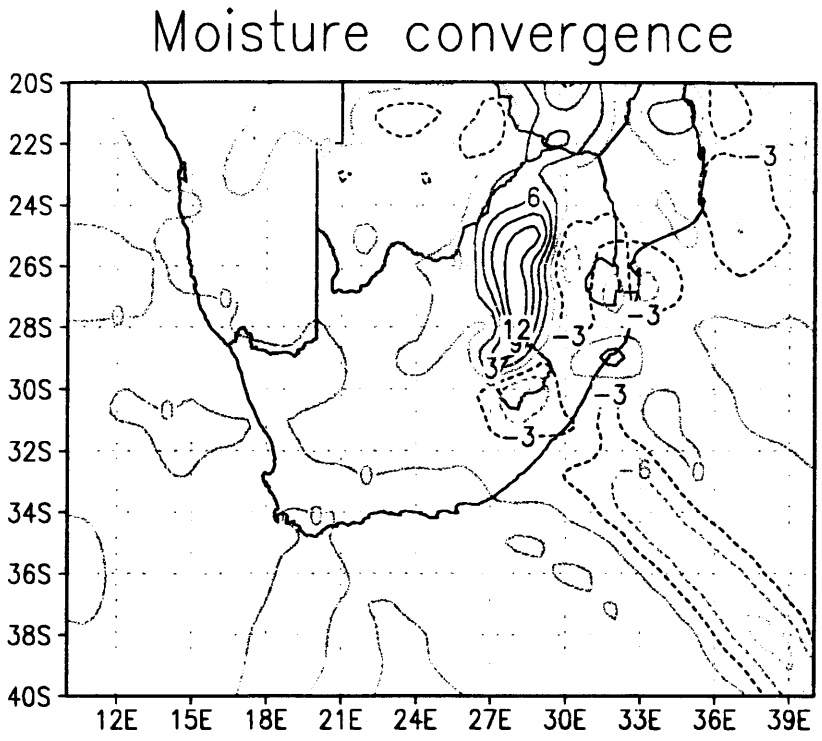

Fig. 5.42 Moisture convergence (g kg^{-1} h^{-1} X10) on 315K on 27 January 1996

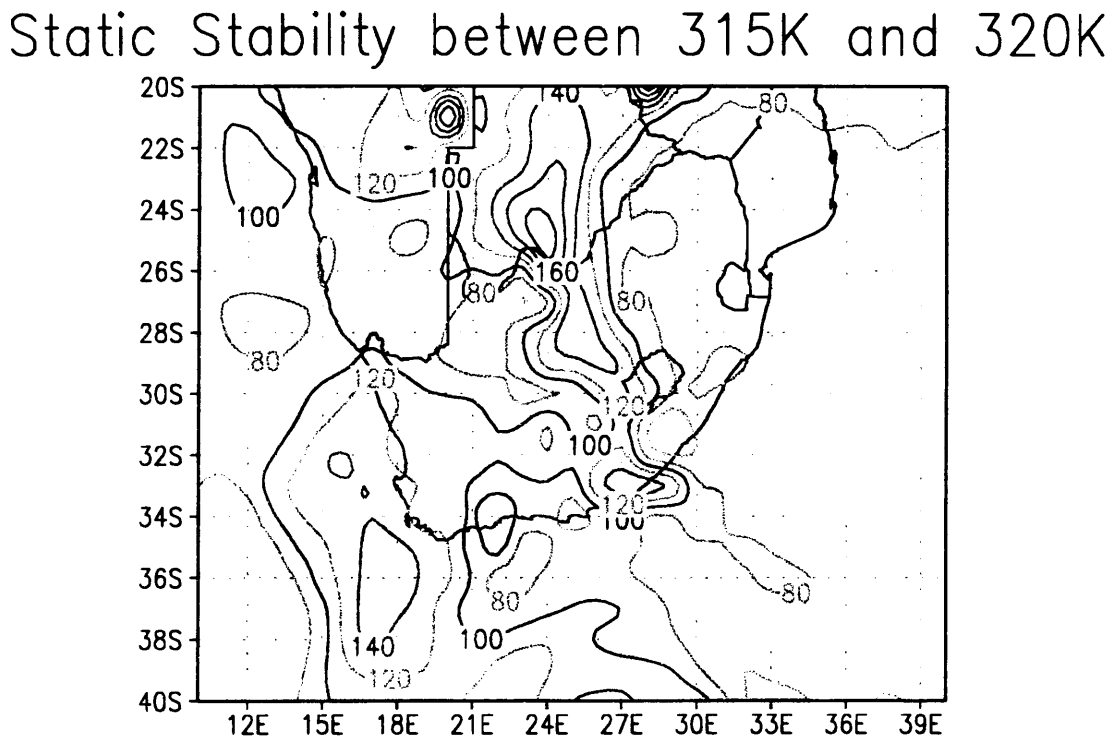

Fig. 5.43 Static stability (hPa) between 315 and 320K on 27 January 1996

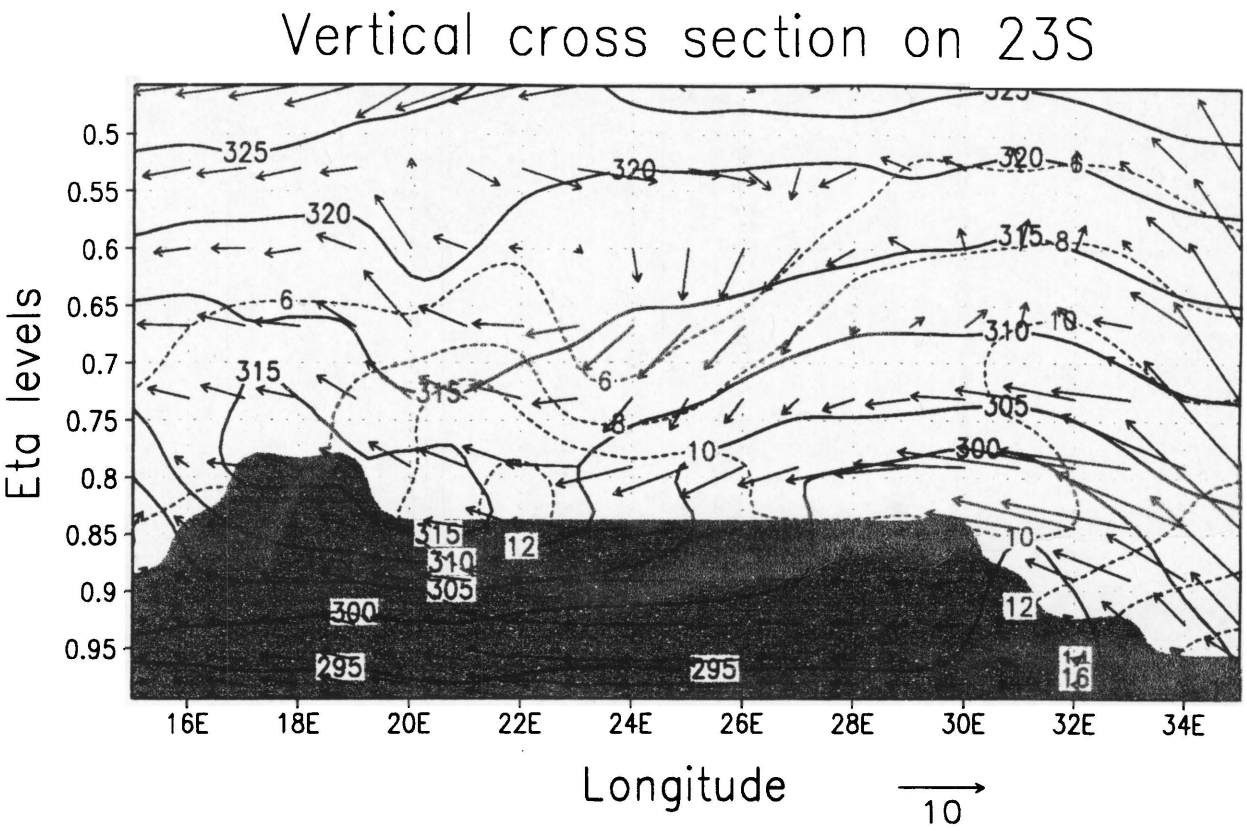

Fig. 5.44 **As Fig.5.22 but at 23S on 28 January 1996**

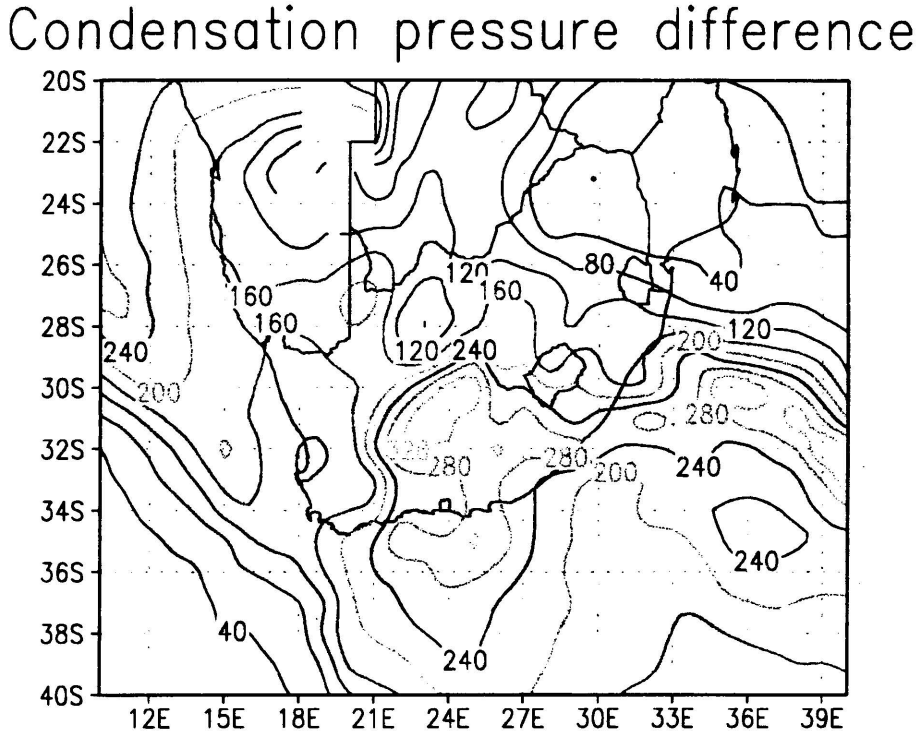

Fig. 5.45 **Condensation pressure difference (hPa) on 315K on 28 January 1996**

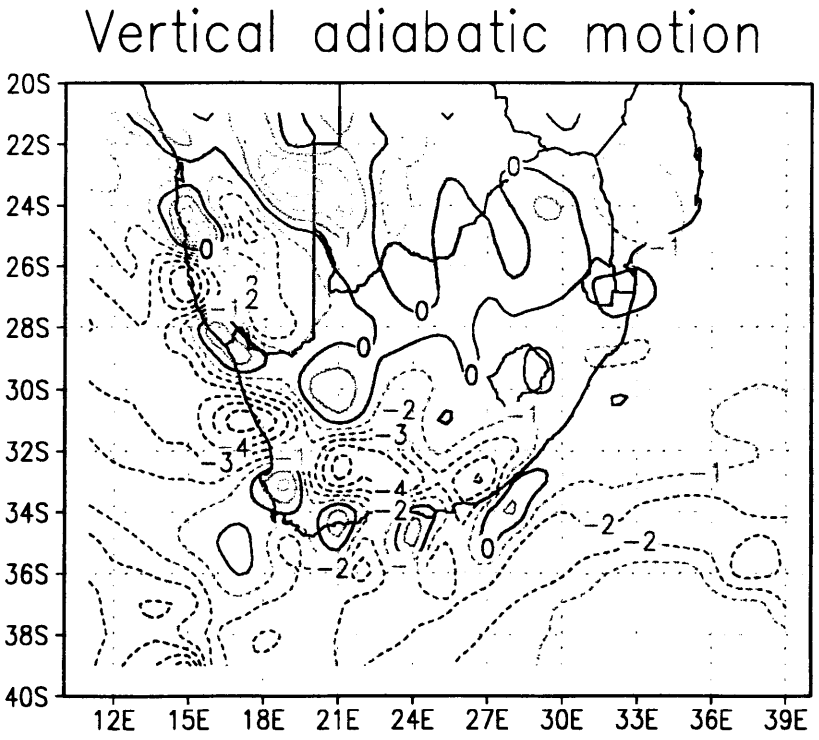

Fig. 5.46 Vertical adiabatic motion (microbar s^{-1}) on 325K on 28 January 1996

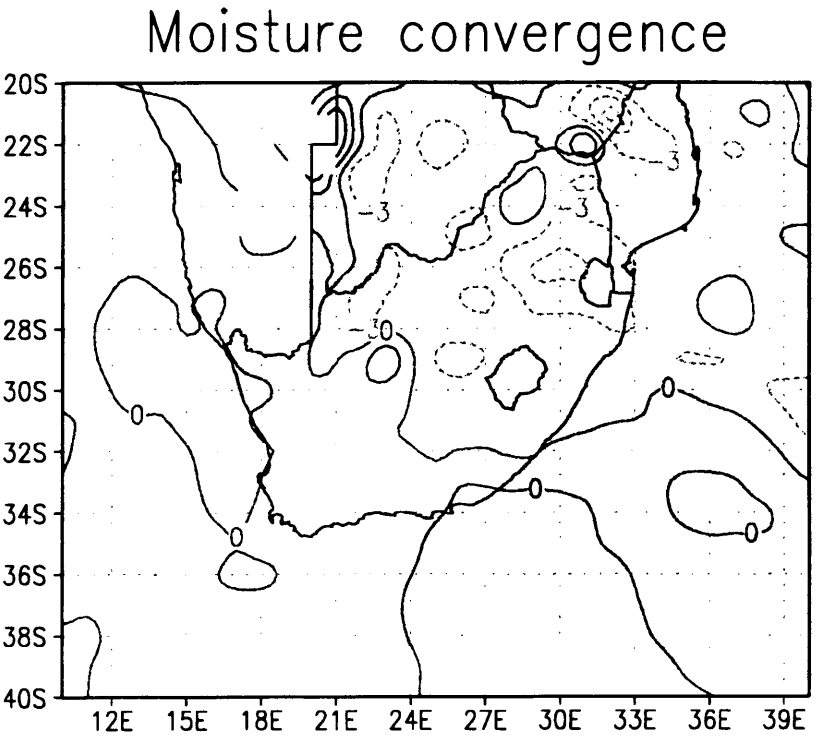

Fig. 5.47 Moisture convergence (g kg^{-1} h^{-1} X10) on 315K on 28 January 1996

CHAPTER 6

CASE STUDY IN FEBRUARY 1996

6.1 Introduction

Figure 6.1 shows the rainfall percentage of the normal for the month of February 1996. It is clear that a large part of the subcontinent had above normal rainfall. The eastern half of the country had rainfall in excess of 100 percent of the normal, while a large part in the north-east had more than 200 percent of the normal February rainfall. One of the heavy rainfall events which was identified in this month occurred from 12-17 February. Several places in Gauteng and the Free State recorded daily rainfall totals in excess of 50 mm on the 13th. In the Northern Province 102 mm fell at Messina on the 14th and in KwaZulu/Natal 124 mm at Sezela. Most rivers were in flood and serious damage was reported.

6.2 Aims of the case study

The February heavy rainfall event will be analysed isentropically and compared with the real time observations. Considerable differences between the February and the January heavy rainfall events exists. An effort will be made to note these differences and the way isentropic analysis handles them.

6.3 Data used

The Central Forecasting Office (CFO) at the SAWB supplied a synoptic sequence of events for the week 12 - 17 February 1996. The Climate Section of the SAWB supplied daily rainfall figures and reports of flooding. Satellite images were also used to get an indication of the cloud cover and relevant weather systems. Data for the isentropic analysis were derived by the methods described in Chapter 3 using the 12-hour forecast fields of the Eta model.

6.4 Synoptic sequence of events for 12 - 17 February 1996

Surface at 12:00 UT:

General rain fell over the north-eastern part of the country due to the deep, tropical low pressure system over Botswana on the 12th (Figure 6.3). Heavy falls occurred over the Northern Province and Mpumalanga. Widespread rain also occurred over the western Cape due to the passage of the cold front with falls of 20 mm and more over the south-western parts of the province.

The cold front moved in over the Western Cape on the 13th (Figure 6.5) with moderate falls which extended to the Eastern Cape. Widespread rain and thundershowers occurred over the eastern and central parts of the country in the area covered by tropical air in circulation east of the low pressure system(s) present over the central interior. Heavy falls were recorded in many places.

Moist, tropical air was still present over the north-eastern parts of the country on the 14th (Figure 6.7) and scattered thundershowers occurred here, while colder air and rainy conditions following the cold front were spreading in over the south-eastern region. Heavy falls fell along the KwaZulu/Natal coast (123 mm reported at Scottburgh) and places in Mpumalanga and the Northern Province (102 mm recorded at Messina). These falls were attributed to the undercutting of the tropical air by colder, post-frontal air. Very low minimum temperatures were recorded with the passage of the cold front and minimum temperature records for the month of February were broken at several places.

On the 15th (Figure 6.9) the ridging Atlantic Ocean high pressure system had moved rapidly south-eastwards extending a ridge from Marion Island towards the Cape south coast. This ridge maintained the circulation of humid air over the southern parts of the country. The moist, tropical air moved westwards over Zimbabwe and the Northern Province from the Mozambique Channel. Sunny conditions prevailed over the western parts.

It was cool over the south-eastern parts of the country on the 16th (Figure 6.11) in the wake of the cold front which passed over this region. Rain continued to fall over the eastern parts of the country, but was not as intense as the previous day. Fine and hot conditions persisted over the western part of the country. The interior trough was

displaced westwards by the high pressure system east of the country and the high pressure system over the eastern interior.

With moist air in circulation east of the trough over the eastern parts on the 17th (Figure 6.13), scattered thundershowers developed in the areas around the low with centre near Durban. Over the remainder of the country the air was drier and the weather mainly fine.

Upper air at 12:00 UT:

On the 12th a tropical low pressure system was present over Botswana (20S), while a westerly trough was building along 5E. A weak perturbation was present over the southern parts of the country on 29E.

A strong westerly wind system was developing on the west coast of the country on the 13th (Figure 6.14). Upper air winds were mainly from the north-west and the speeds were of the order of 40 to 60 knots. The tropical low pressure system had weakened considerably.

The upper-air trough had moved eastwards the central parts of the country (25E) on the 14th (Figure 6.15). Wind speeds over the western parts were 30 to 50 knots from a south-westerly direction, while the eastern parts still had north-westerly winds of 20 to 30 knots.

The upper-air trough developed into a cut-off low (COL) on the 15th (Figure 5.16) over the Free State. This low pressure system caused widespread rain on its flanks. Windspeeds were more or less 20 to 40 knots. A upper-air high pressure system was ridging on the west coast.

The upper-air system weakened and the low pressure system moved southwards on the 16th.

On the 17th the cut-off low weakened even further moving southwards, and only a trough remained on 27E.

6.5 Satellite images at 12:00 UT:

Figure 6.2 shows that a band of cloud stretched from the south-east north-westwards over the eastern parts of the country on the 12th. This was in association with the tropical air mass advected from the north. A cloud band associated with the approaching cold front could also be seen south-west of the country.

On the 13th (Figure 6.4) the cold front was over the south-western Cape and tropical moisture could still be seen east of the upper-air trough.

Figure 6.6 shows that the activity had extended even further to the east on the 14th where the cold front and the tropical air converged into a single cloud band. Thundershower development was evident over this area.

The cloud pattern development which took place from 12 - 14 February 1996 was described by Harrison (1986) and named as a tropical-temperate-trough. This system is a major rain-producing system in the South Africa region.

On the 15th (Figure 6.8) the upper-air trough had been cut off and the cloud band associated with this cut-off low is visible over the south-eastern parts of the country. East of there moisture was still evident and showers still occurred.

Low-level moisture was advected over the eastern parts of the country by the high pressure system on the 16th (Figure 6.10) and the upper-air system was present over the southern parts of the country.

On the 17th (Figure 6.12) the activity had decreased to a few thundershowers over the south-eastern parts due to the remnants of the upper-air system along 26E, while a great deal of moisture was still present in a thick cloud band over the Botswana region in association with deep, tropical convection.

In the summer months of the southern hemisphere a branch of the Intertropical Convergence Zone (ITCZ) stretches east-west along about 15°S (Leroux, 1983). Occasionally tropical lows or troughs extend southward from the ITCZ and often affect

the weather on the plateau to 25°S or even 30°S (Taljaard, 1995). In this case study this phenomena is clearly illustrated.

6.6 Rainfall distribution and intensity

Rainfall reports for Namibia were not available and consequently only the rainfall distribution and isentropic analysis results for South Africa will be discussed.

On the 12th (Figure 6.17) rain was reported over the southern and eastern parts of the country. Moderate (more than 25 mm) to heavy (more than 50 mm) falls were restricted to the eastern and north-eastern parts (Northwest, Northern Province and Mpumalanga).

Rainfall distribution on the 13th (Figure 6.18) included the southern, south-western and eastern half of the country. Heavier falls (more than 25mm) were reported in KwaZulu/Natal, Mpumalanga, Gauteng, Northwest and the Northern Province.

KwaZulu/Natal and the Northern Province received rainfall in excess of 50 mm on the 14th (Figure 6.19), while only moderate falls were reported over the Northwest.

Drier air moved in over the western parts of the country on the 15th (Figure 6.20), but light falls still occurred in the east. Moderate to heavy falls were reported in Northwest, the Northern Province and Mpumalanga.

On the 16th (Figure 6.21) light falls (not exceeding 25mm) were recorded over the eastern parts.

On the 17th (Figure 6.22) light falls were still occurring but only a small area reported more than 25 mm.

6.7 Eta model evaluation

In general the surface (mean sea level pressure or MSLP) and upper-air (500 hPa) analyses patterns of the period were handled well by the Eta model, but the tropical low

pressure system which was present over Botswana in the upper air, was not shown on the Eta analyses maps. The west wind trough building west of the country and crossing eastwards was, however, depicted very well on the 500 hPa analysis. When the upper-air low pressure system (COL) formed on the 15th, it was handled well by the Eta model. The weakening and southward movement was also shown clearly as well as the upper trough remaining on 29E.

The surface patterns were also represented quite well by the model. Even the tropical low pressure system which was present over the northern interior on the 14th, was shown clearly. The ridging of the high pressure system and the troughs forming on the east and west coasts were also represented well on the Eta model analyses.

All in all the model handled the westerly upper-air system as well as the passing of the cold front and the surface high pressure system very well.

6.8 Isentropic analysis results

6.8.1 ETA analysis date : 96021200 with a 12-hour forecast for 96021212

The vertical cross-sections show a relatively thick layer of moisture over the northern parts (25S) where the tropical low was present (Figure 6.23), in comparison to much less moisture in the south (28S,30S). On 315K warm (720 hPa), nearly saturated (50 -100 hPa) air was in circulation over the north-eastern parts of the country (Figure 6.24) and falls of up to 40 mm were recorded here. On 325K (Figure 6.25) condensation pressure differences indicated that the air was close to saturation in the northeast as well as over the Cape Peninsula where falls in excess of 20 mm were recorded. Over the eastern and north-eastern parts of the country 0.5 g kg^{-1} $hour^{-1}$ moisture was advected and this area was also favoured by the moisture flux convergence on 315K (Figure 6.26). Positive moisture advection was evident over the southern and south-eastern parts of the country where moisture moved in ahead of the cold front and behind the coastal low pressure system on the south-east coast. Upward adiabatic motion on 315K was present over most of the country (excluding the far northern Cape) with preference to the south-eastern Cape and KwaZulu/Natal. On 325K (Figure 6.27) upward adiabatic motion was evident over the southern parts of the

country (east of the westerly upper-air trough) as well as north and north-east of Lesotho (south-east of the upper-air low pressure system). Static instability was indicated along 25E with values ranging between 120 hPa and 160 hPa.

6.8.2 *ETA analysis date : 96021300 with a 12-hour forecast for 96021312*

The vertical cross-sections show an increase in moisture from the west on 30S (Figure 6.28) where the cold front had moved in. More or less the same amount of moisture was available on 28S and 25S as the previous day and a westerly flow still dominated the cross-sections.

Warmer air was still evident over the north-eastern half of the country (values around 720 hPa) on 315K (Figure 6.29) , but the influx of colder air from the west could clearly be seen on the pressure field. In this case a limiting streamline is visible over the central/eastern parts of the country and this coincides with the cloud band on the satellite image, low stability and warm, moist air. Little precipitation occurred west of this separation zone, while moderate to heavy falls were reported to the east of it. Moderate (5 microbar s^{-1}) vertical adiabatic motion was evident on 315K (Figure 6.30) over the north-eastern parts where most of the heavy precipitation occurred. On 325K (Figure 6.31) values as high as 8 microbar s^{-1} were evident over the southern and south-western interior; this came as no surprise since the developing westerly upper-air trough was lying to the west of that on the 13th. Moist, nearly saturated air was present over the north-eastern parts of the country on 315 and 325K and the area covered by condensation difference values less than 90 hPa (Figure 6.32) was in close correlation to the area where heavier falls occurred. This warm, moist airmass (also visible on the satellite image of the 13th) stretching from the south-east north-westwards was mirrored in the static stability chart (Figure 6.33) where values of more than 160 hPa occurred. Nearly saturated air could also be seen in the south-west (on 315 and 325K), where moisture was advected behind the cold front. Moisture advection and flux convergence patterns on 315K (Figure 6.34) favoured the areas south and south-east of Lesotho (where moisture flux convergence was 1.2 g kg^{-1} $hour^{-1}$ and moisture advection was in excess of 1.2 g kg^{-1} $hour^{-1}$) and the northern and north-eastern parts of the country (where moisture flux convergence was 0.6 to 0.9 g kg^{-1} $hour^{-1}$). An area favourable for precipitation was also indicated on the advection and flux convergence

charts stretching north-westwards from the south coast. All of these areas reported falls of more than 20 mm. The tongue of drier air between the moist air in the south-west and the moist, tropical air in the north-east evident on the satellite picture could clearly be seen on the condensation difference charts.

6.8.3 *Eta analysis date : 96021400 with a 12-hour forecast for 96021412*

Moisture increased in the south (30S and 28S) spreading in the vertical to a thicker layer due to the high pressure stem ridging on the south-east coast. Strong updraughts (16 cm s^{-1} on 28S) occurred east of 28E extending beyond 500 hPa (Figure 6.35). This clearly illustrates the ridging of the high pressure system on the east coast. On 25S and 23S a westerly flow was still predominant.

The influx of the cold air behind the cold front over the southern half of the country could clearly be seen on the pressure chart (Figure 6.36), where values as low as 480 hPa were present. Warmer air was still present over the northern parts but the 720 hPa isobar withdrew to the far north showing that the tropical air mass was gradually being modified by the cooler, maritime air. A limiting streamline was located over the eastern parts of the country. This airstream from the west has gone beyond the thermal ridge and is rising over the cool dome over the eastern parts. The heavier falls were reported east of the limiting streamline. Vertical adiabatic motion (VAM) on 315K (Figure 6.37) was the strongest (10-15 microbar s^{-1}) over the south-eastern interior which coincided with the cold, maritime air (behind the cold front) meeting the warmer, tropical continental air (frontal uplift and undercutting). The strongest (8 microbar s^{-1}) vertical adiabatic motion on the 325K level (Figure 6.38) was evident over the south-eastern parts east of the upper-air trough which was lying along the 25S longitude. Very moist, nearly saturated (50-100 hPa) air was still in circulation on 315K (Figure 6.39) and 325K (Figure 6.40), with preference to the area east and north-east of Lesotho where the heaviest falls occurred. Strong (0.4 g kg^{-1} $hour^{-1}$) moisture advection (Figure 6.41) in the south-east and flux convergence in the north-east were still evident which coincided with the areas where heavier falls occurred. Static stability values of 120-160 hPa occurred north of Lesotho where thundershower activity was likely according to the satellite picture.

6.8.4 *Eta analysis date : 96021500 with a 12-hour forecast for 96021512*

Inflow of moisture from the east was more pronounced on all of the vertical cross-sections due to a high pressure system ridging on the east coast behind the cold front (Figure 6.42 shows 28S). Strong (8 cm s^{-1}) up to and beyond 500 hPa updraughts were present east of 30E (orographic uplift) on all the cross-sections (Figure 6.43 shows 25S).

Colder air was still evident over the south-eastern part of the country behind the passing cold front, while warm, tropical air was again invading the northern and western parts of the country (Figure 6.44). The area where falls in excess of 50 mm were recorded was over the western parts of Gauteng and in the Northwest Province, and this area coincided with the warmest air (760 hPa), with strong vertical adiabatic motion on 310K (Figure 6.45) of up to 7 microbar s^{-1}, condensation difference of less than 100 hPa on 310K (Figure 6.46), maximum (1.0 g kg^{-1} $hour^{-1}$) moisture advection (Figure 6.47), maximum (1.2 g kg^{-1} $hour^{-1}$) flux convergence (Figure 6.48) and maximum instability (up to 160 hPa). VAM on 325K scaled down from the previous day to 2 microbar s^{-1} over the eastern parts and larger areas of sinking motion in the west as the westerly upper-air system weakened and moved eastwards. Condensation difference values on 310K still favoured the entire eastern half of the country, but on 325K it was clear that the upper-air systems was on its way out because the most saturated air lay only over the extreme eastern parts.

6.8.5 *Eta analysis date: 96021600 with a 12-hour forecast for 96021612*

Inflow of moisture from the east was still evident on all cross-sections due to the high pressure system east of the country still advecting moisture westwards. The area of higher humidity extended to the west on 25 and 23S but was only a shallow layer of moisture. The strongest rising occurred east of the escarpment (Figure 6.49 shows 25S) showing the important role orographic uplift played in the rainfall over the eastern parts. Warmer air extended from the north southwards to Lesotho (720 hPa) while warmer air was also evident in the south-west where an off-shore flow prevailed. Moderate (3 microbar s^{-1}) vertical adiabatic motion on 310K (Figure 6.50) was present in a band stretching from the south-east to the north-west. This pattern was echoed by

the moisture advection and flux convergence as well as the static stability charts with reference to 310K. Rainfall reports in this area were up to 24 mm. Condensation difference values (Figure 6.51 shows 310K) still favoured the eastern half of the country showing that a great deal of moisture was still available as seen on the satellite picture. VAM on 325K was much less than the previous day, which coincided with the weakening of the upper-air low pressure system, and values were generally below 2 microbars s^{-1} over the eastern parts of the country.

6.9 Conclusions

A general idea of the precipitation area was nearly always given by the condensation pressure pattern where values of more than 600 hPa occurred and where condensation differences were less than 100 hPa. Anderson (1984) states that precipitation of some sort is guaranteed when moisture is increasing, the air mass is nearly saturated and there is upslope motion (vertical adiabatic motion). Although this was evident in certain cases, South Africa's topography also plays a major role and often supplied enough orographic uplift to produce heavy falls over the eastern parts of the country even with little VAM. A combination of low condensation difference values, positive moisture flux convergence and vertical movement of some sort (orographic uplift or adiabatic vertical motion) proved to be a clear indicator of the area of heavy rainfall.

In this tropical summer case study it was clear that the temperature of the air column below the isentrope over the northern parts of the country was relatively high. The air over the eastern parts of the country was close to saturation in the lower as well as the higher levels during the entire period. The upper-air disturbance's influence could clearly be seen on the VAM charts (rising motion east of the upper-air trough/COL). Although warm moist air was still in circulation over the eastern parts of the country after the cut-off low had passed, no further significant rain occurred due to the lack of a trigger mechanism in the upper air.

Looking at Figures 6.35, 6.42, 6.43 and 6.49 (the vertical cross-sections) the riding of the high pressure system on the east coast and the extending of the ridge to the west (over the interior) could clearly be seen. This is another advantage of the vertical cross-sections, namely that the intensity and the displacement of weather phenomena is

evident looking at the vertical motion indicated by the wind arrows.

The Eta model handled this case much better than the January case studied; the reason could probably be that it was more of a baroclinic situation, with only the remnants of a tropical circulation still present.

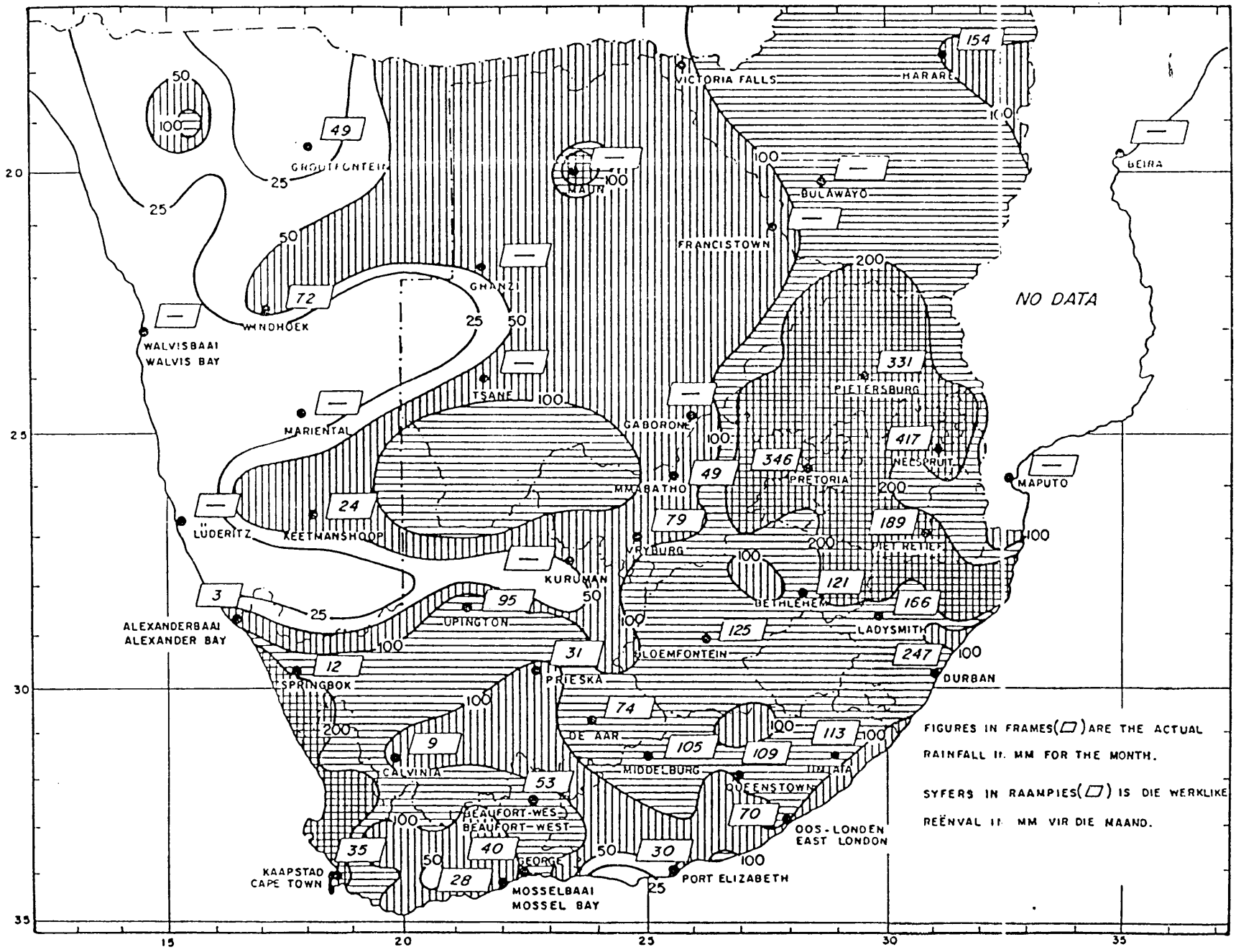

Fig. 6.1 Percentage of the normal rainfall in February 1996 over South Africa

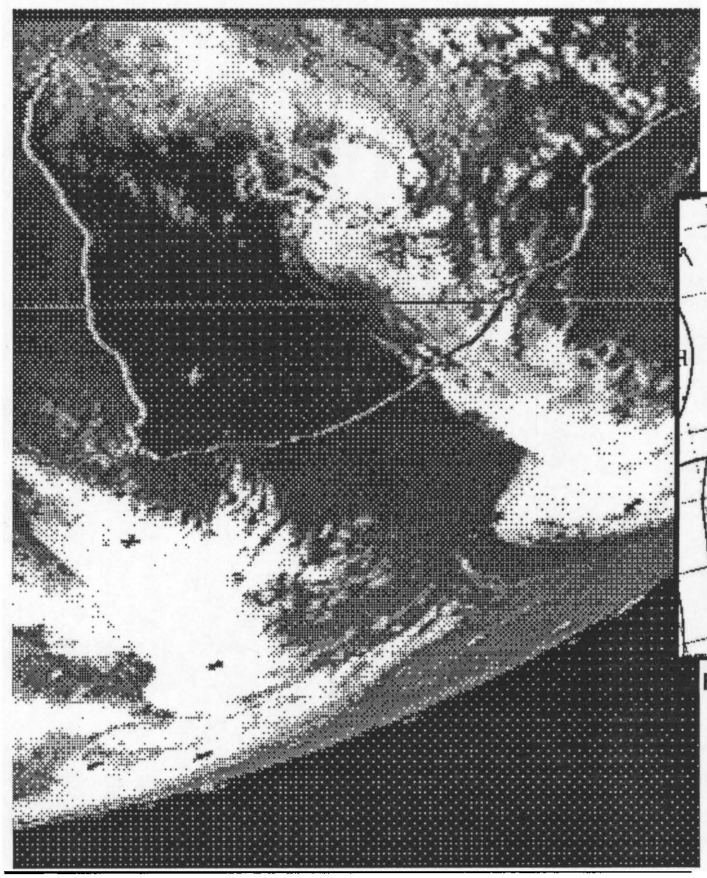

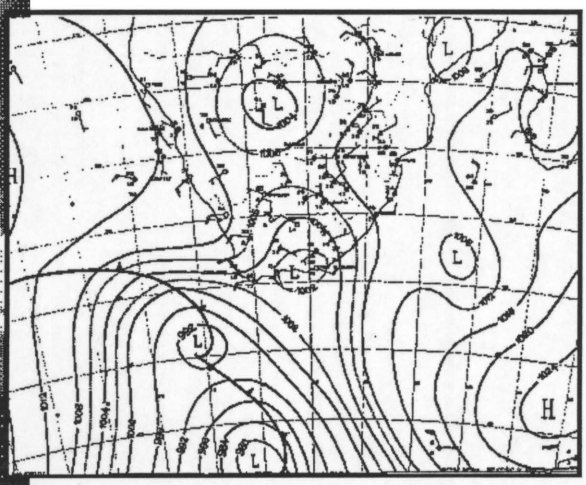

Figure 6.3 Surface pressure chart for 12:00 UT on 12 February 1996. Isobars are in hPa and spaced every 4 hPa. Over the interior the pressures were hydrostatically converted to sea level.

Figure 6.2 Meteosat IR image at 12:00 UT on 12 February 1996

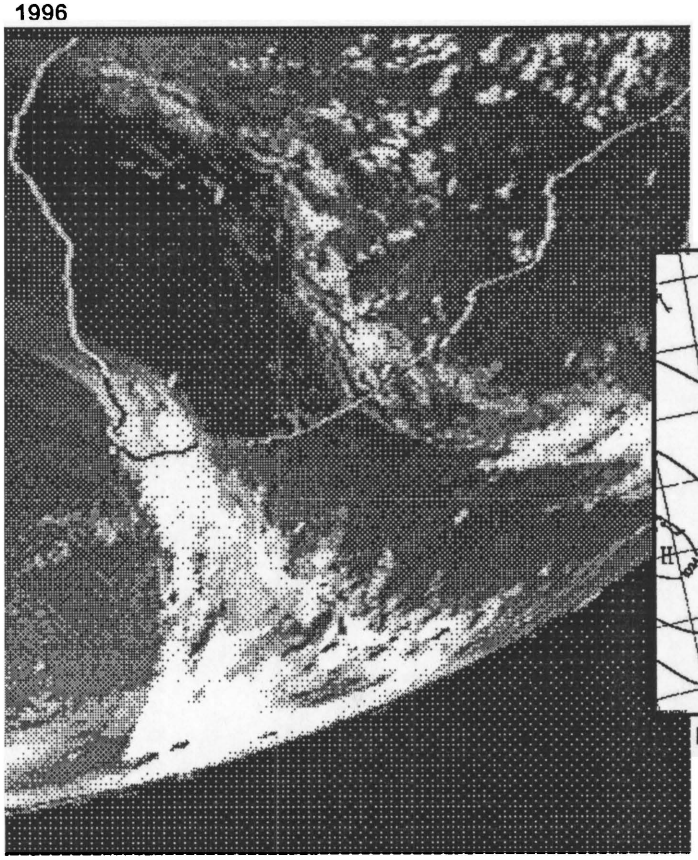

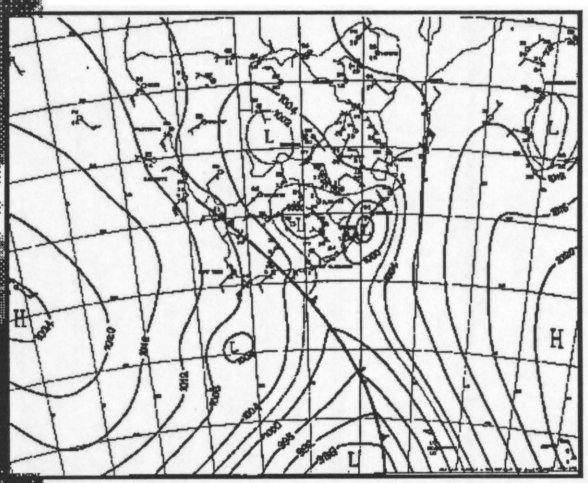

Figure 6.5 As Fig. 6.3 but on 13 February 1996

Figure 6.4 As Fig. 6.2 but on 13 February 1996

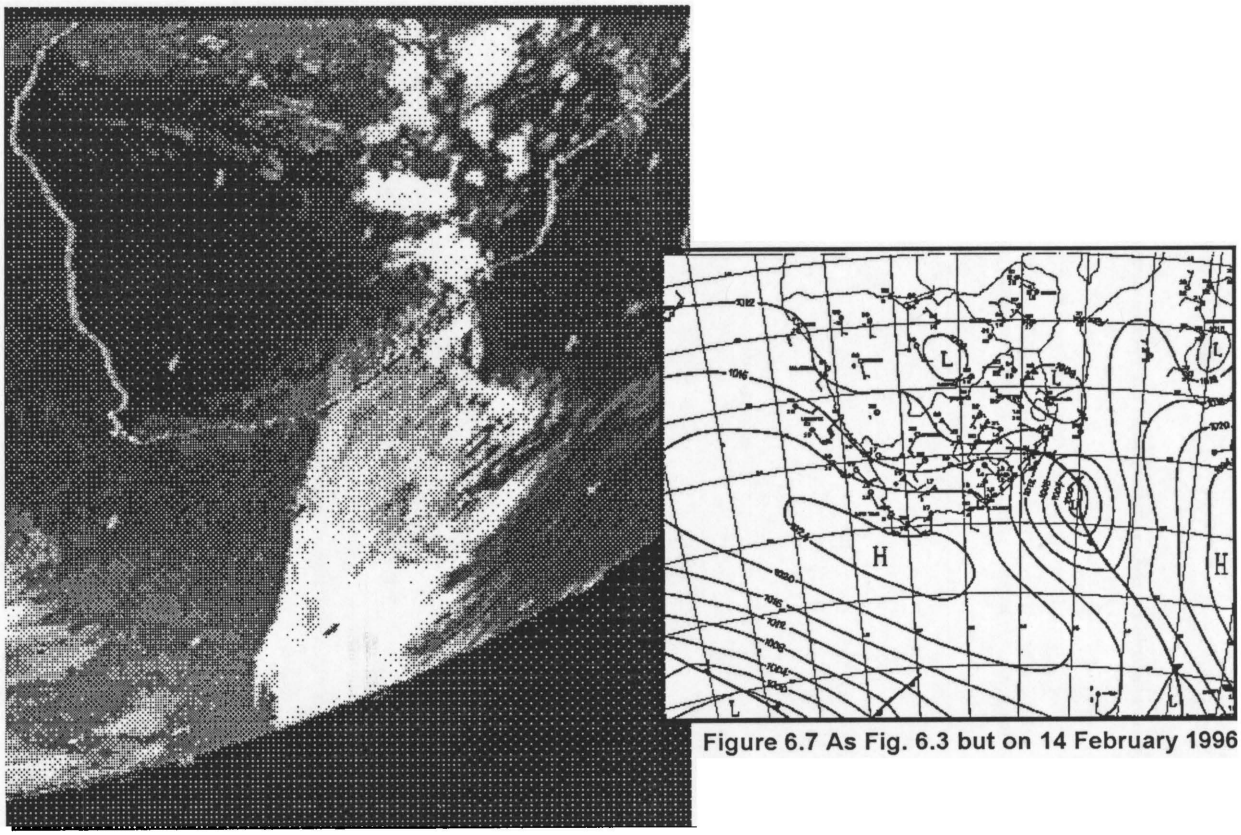

Figure 6.7 As Fig. 6.3 but on 14 February 1996

Figure 6.6 As Fig. 6.2 but on 14 February 1996

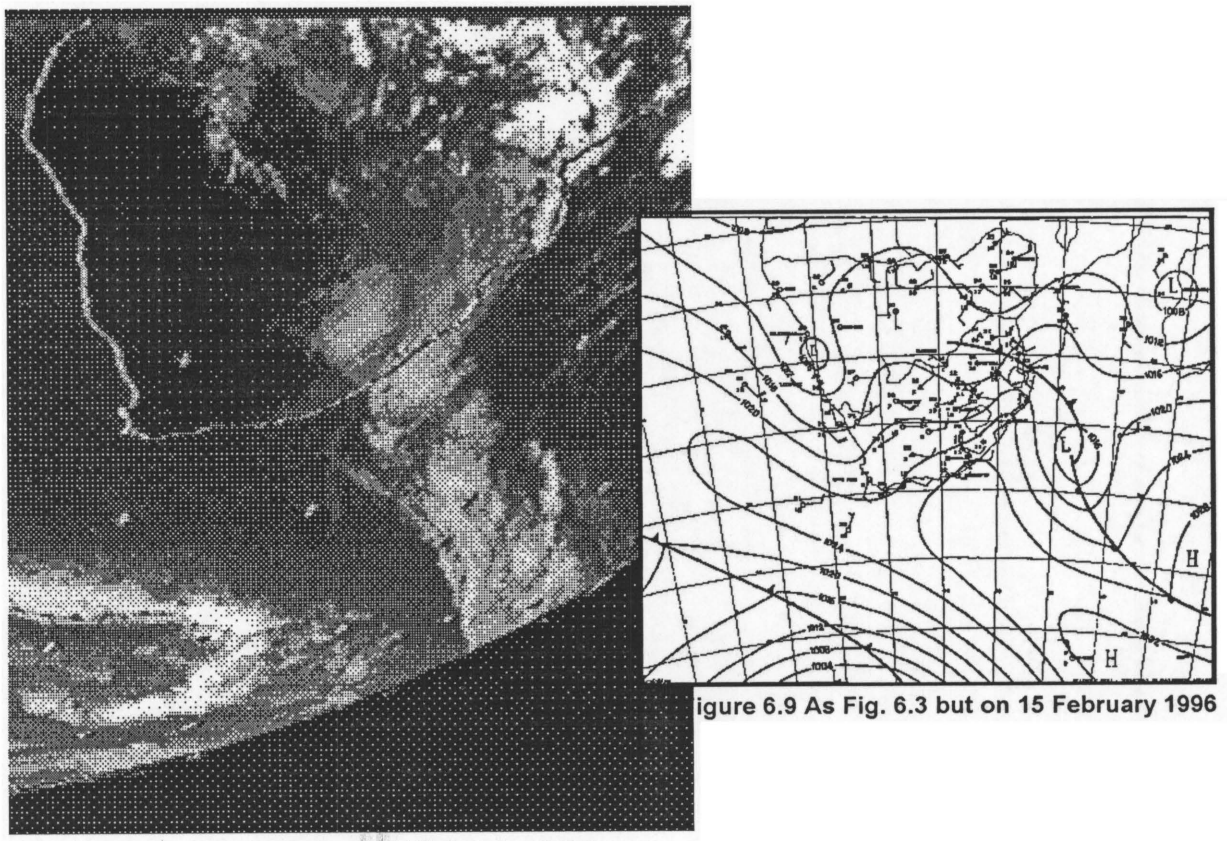

igure 6.9 As Fig. 6.3 but on 15 February 1996

Figure 6.8 As Fig. 6.2 but on 15 February 1996

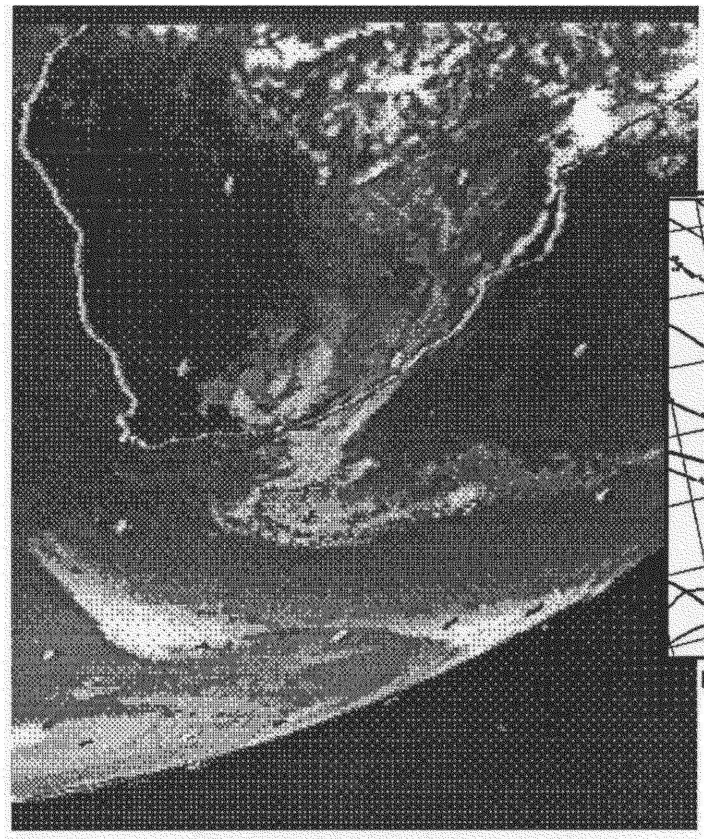

Figure 6.10 As Fig.6.2 but on 16 February 1996

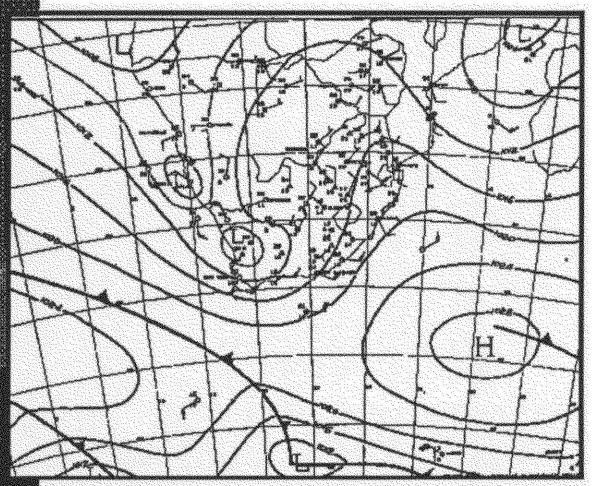

Figure 6.11 As Fig.6.3 but on 16 February 1996

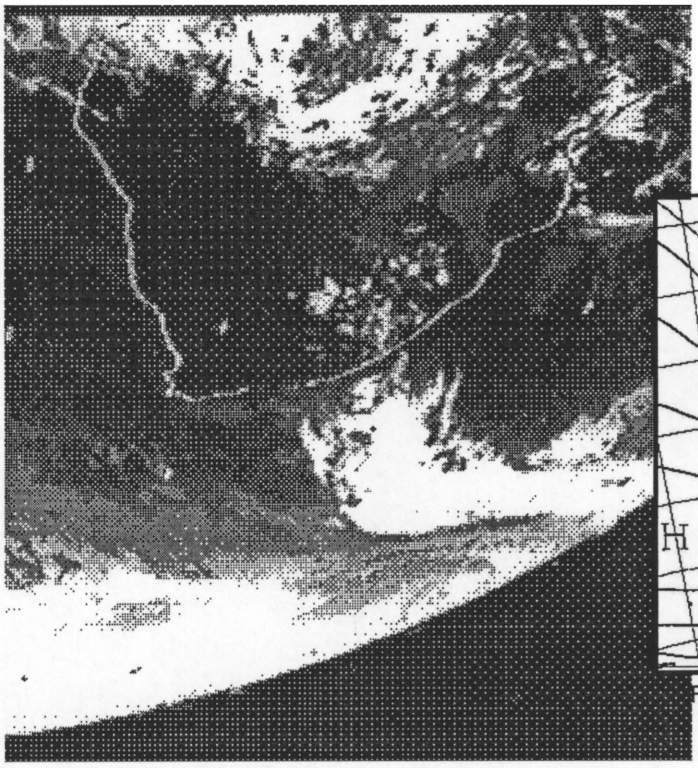

Figure 6.12 As Fig.6.2 but on 17 February 1996

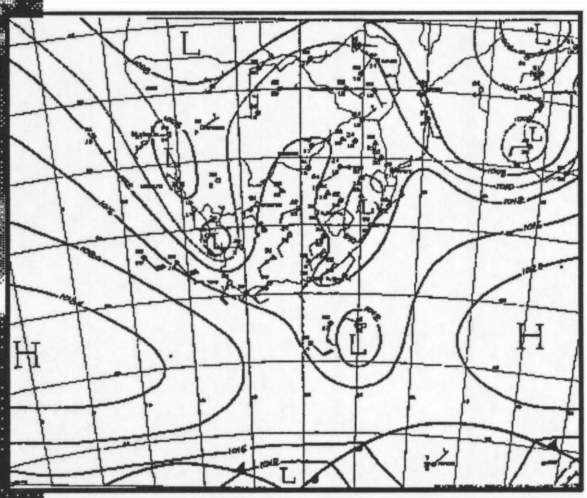

Figure 6.13 As Fig.6.3 but on 17 February 1996

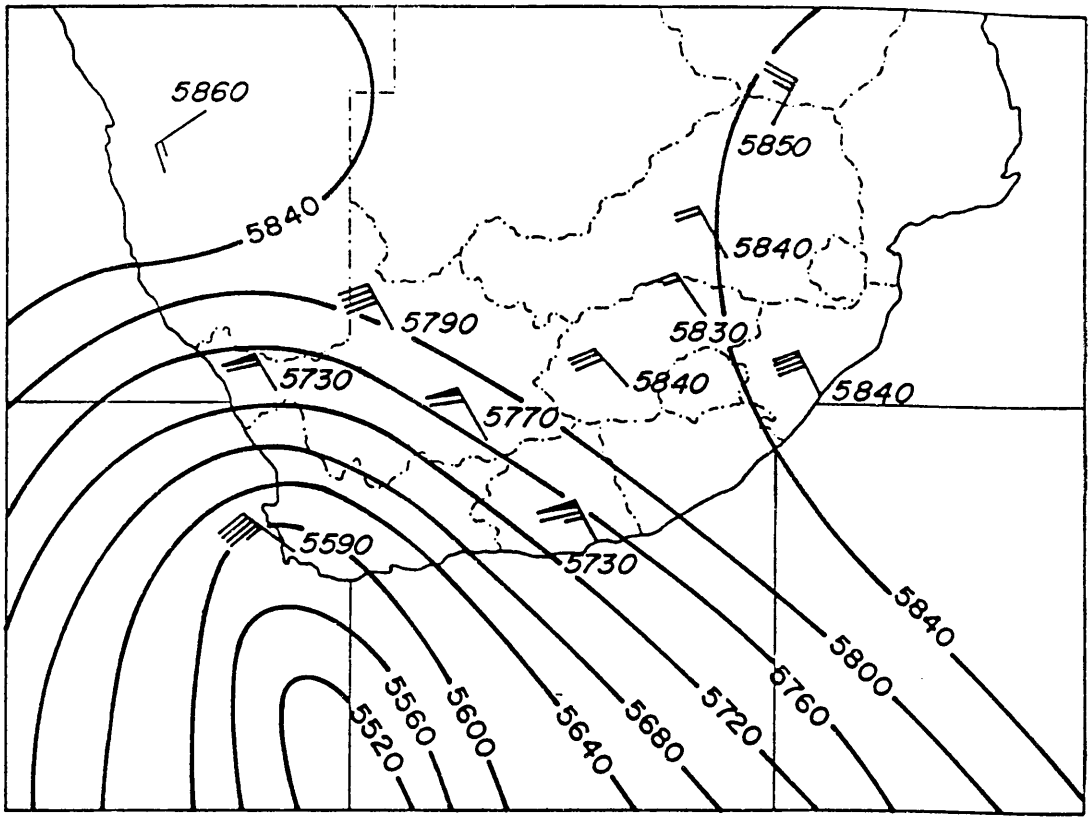

Fig. 6.14 500 hPa constant pressure map for 13 February 1996. Contours are in geopotential meters (gpm). Contour spacing is 40 gpm.

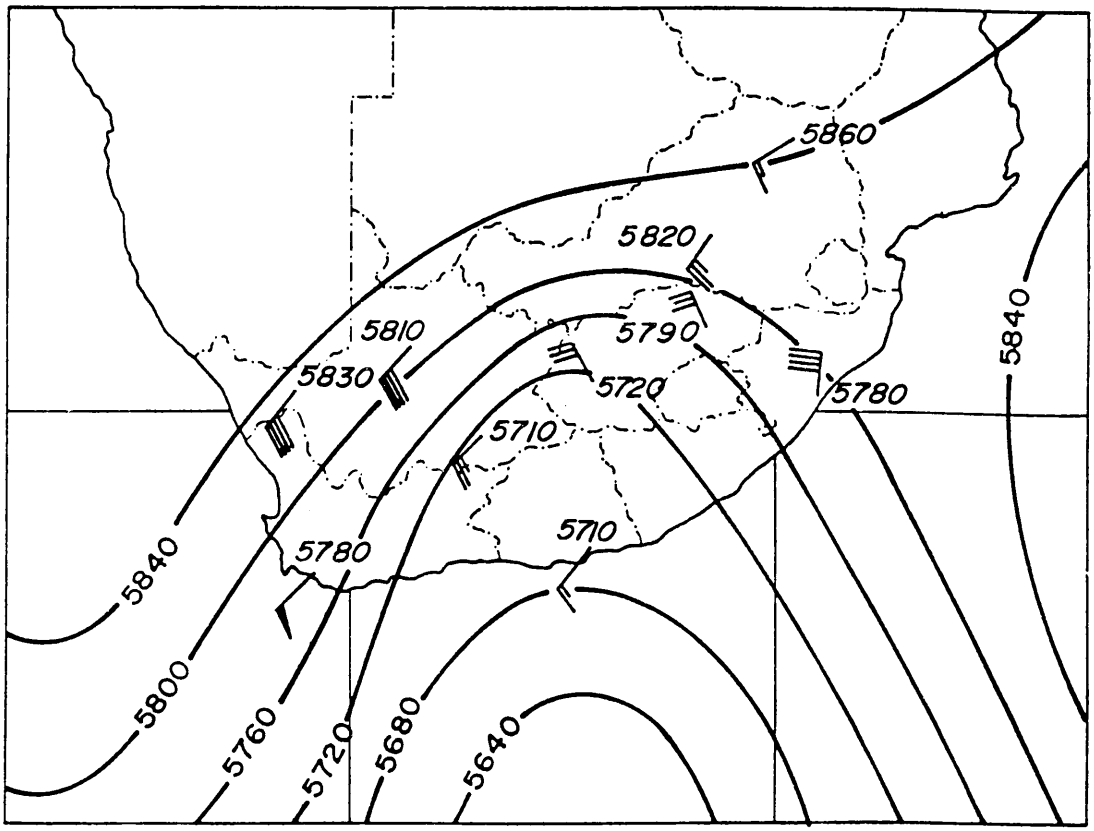

Fig. 6.15 As Fig. 6.14 but on 14 February 1996

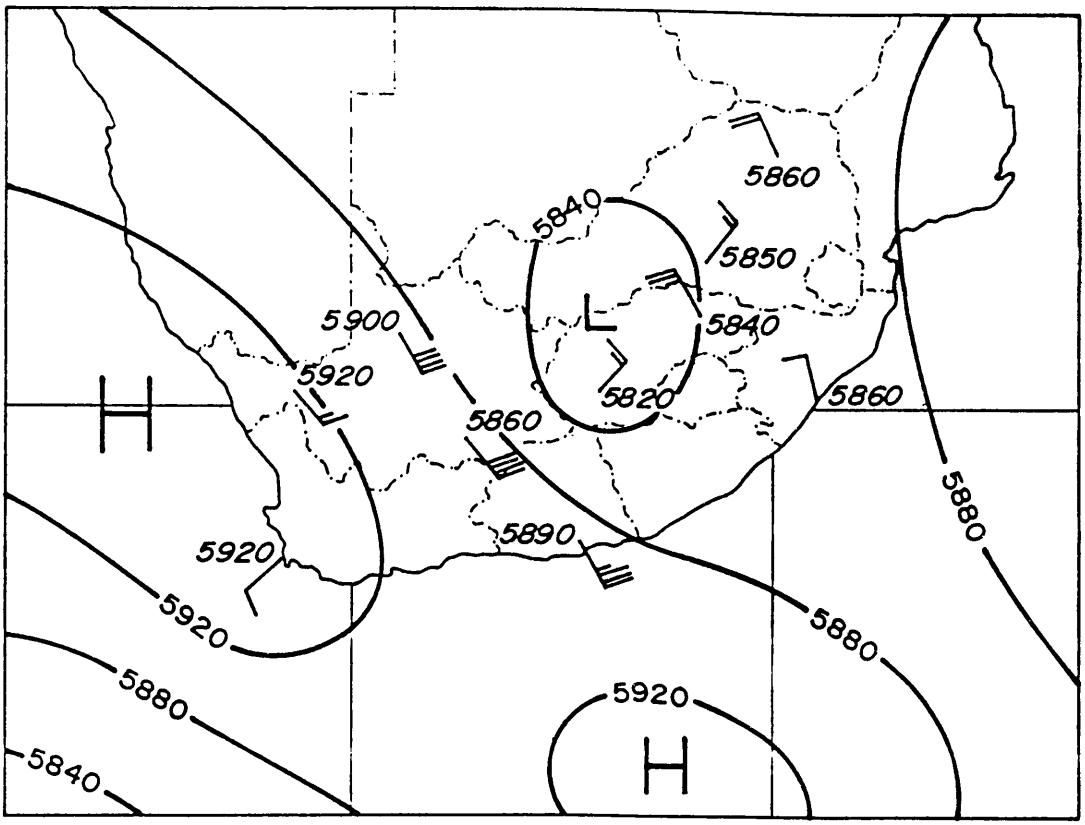

Fig. 6.16 As Fig. 6.14 but on 15 February 1996

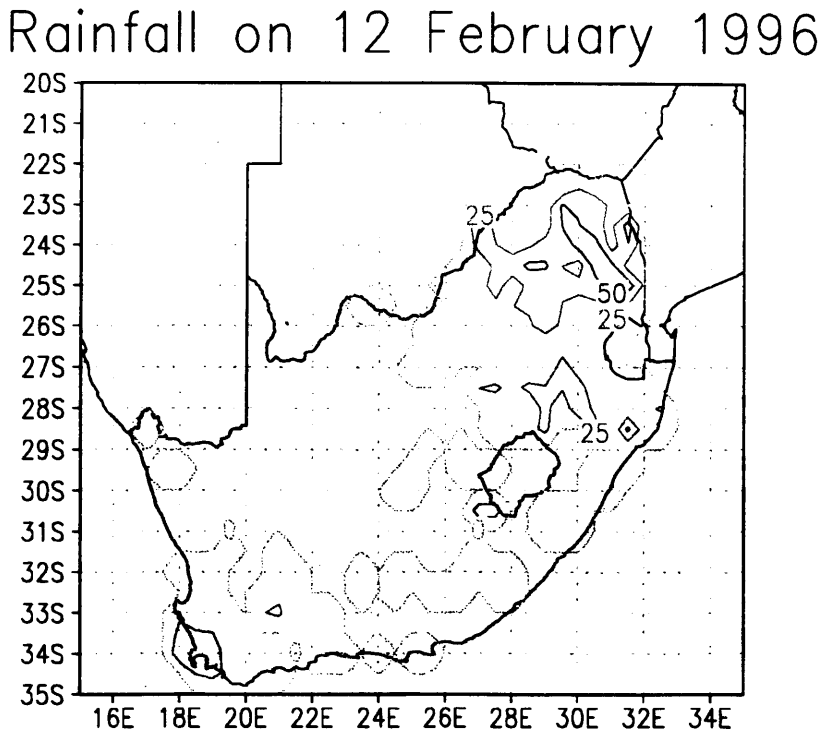

Fig. 6.17 Rainfall on 12 February 1996 in millimeters. Spacing is 25 mm.

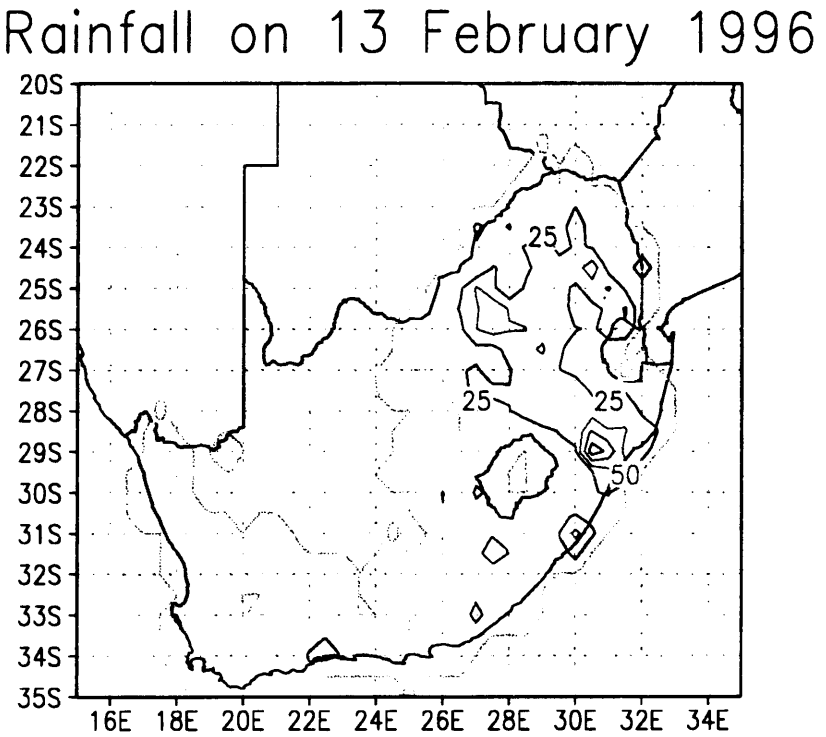

Fig. 6.18 As Fig. 6.17 but on 13 February 1996

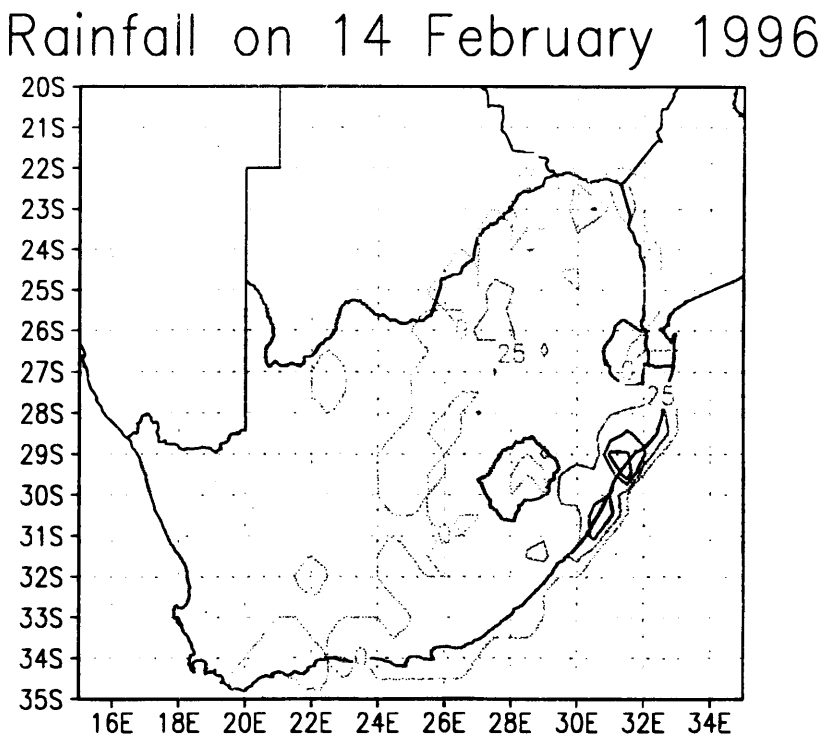

Fig. 6.19 As Fig. 6.17 but on 14 February 1996

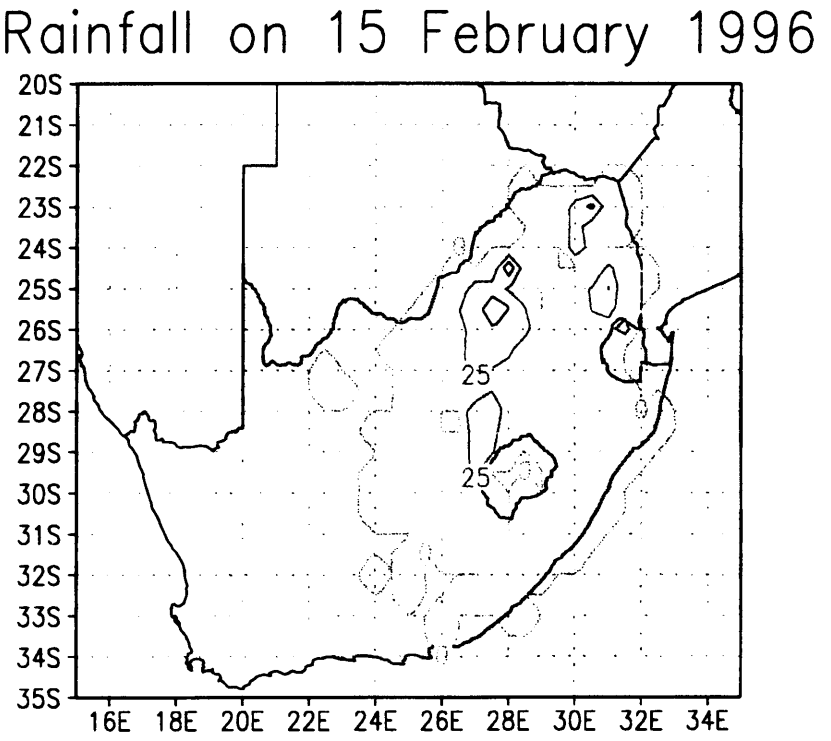

Fig. 6.20 As Fig. 6.17 but on 15 February 1996

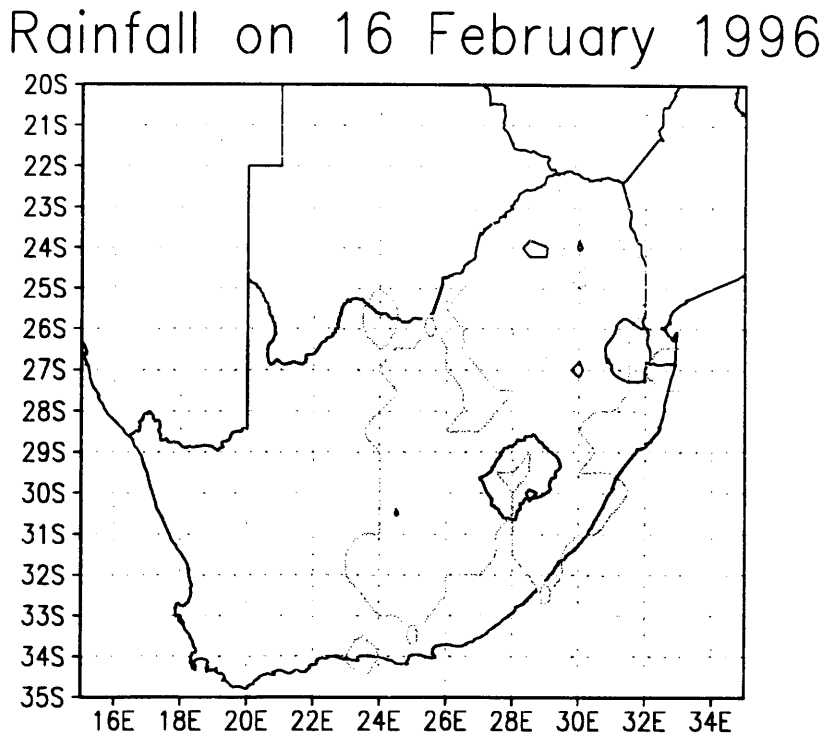

Fig. 6.21 As Fig. 6.17 but on 16 February 1996

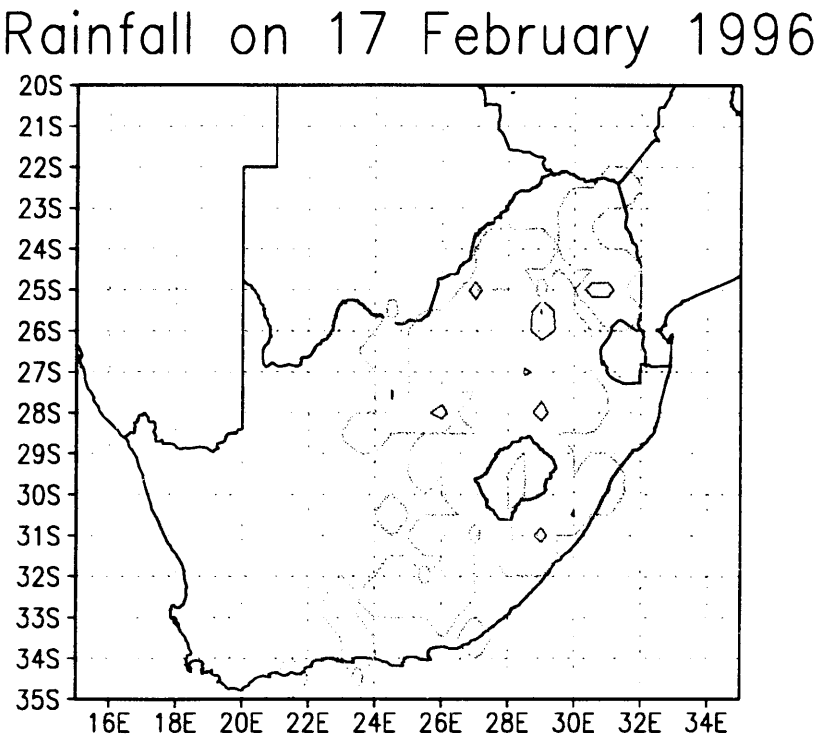

Fig. 6.22 As Fig. 6.17 but on 17 February 1996

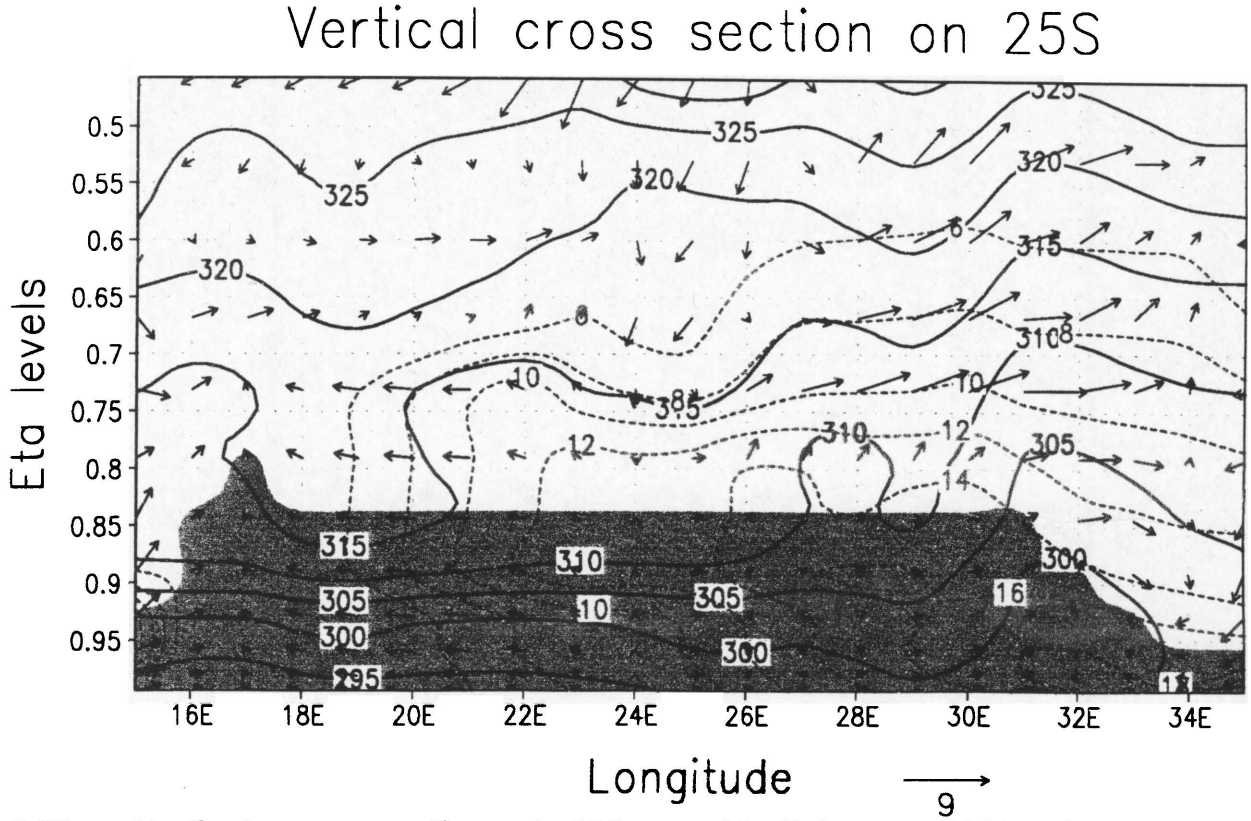

Fig. 6.23 **Vertical cross-section at 25S on 12 February 1996 of potential temperature in Kelvin (solid line), horizontal component of the wind in m s^{-1}, vertical component of the wind in cm s^{-1}, and specific humidity in g kg^{-1}(dotted line). Topography is indicated by the shaded area.**

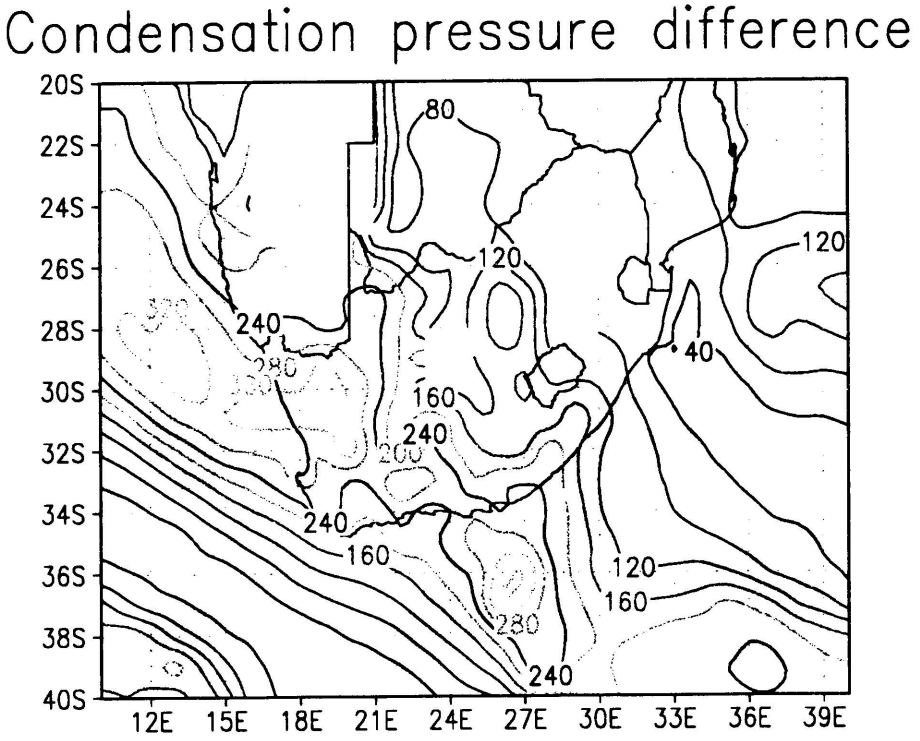

Fig. 6.24 **Condensation pressure difference (hPa) on 315K on 12 February 1996**

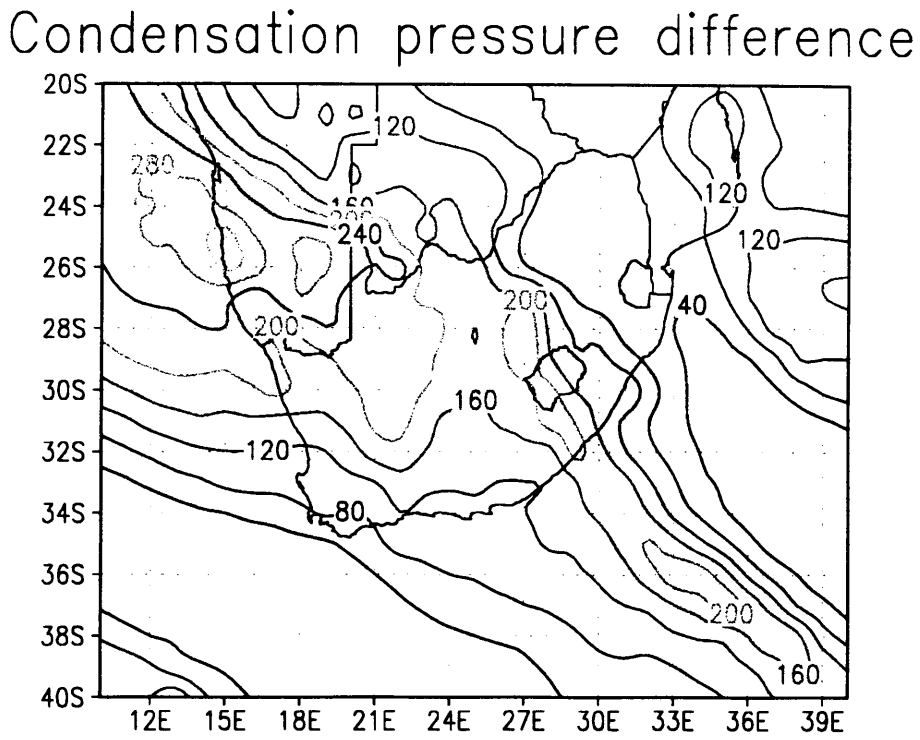

Fig. 6.25 Condensation pressure difference (hPa) on 325K on 12 February 1996

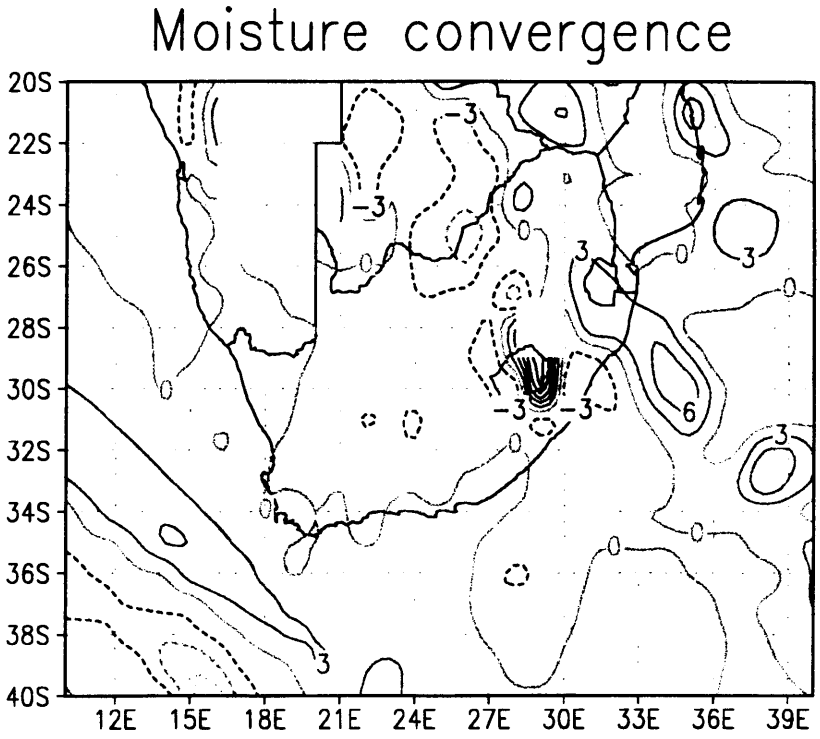

Fig. 6.26 Moisture convergence (g kg^{-1} h^{-1} X10) on 315K on 12 February 1996

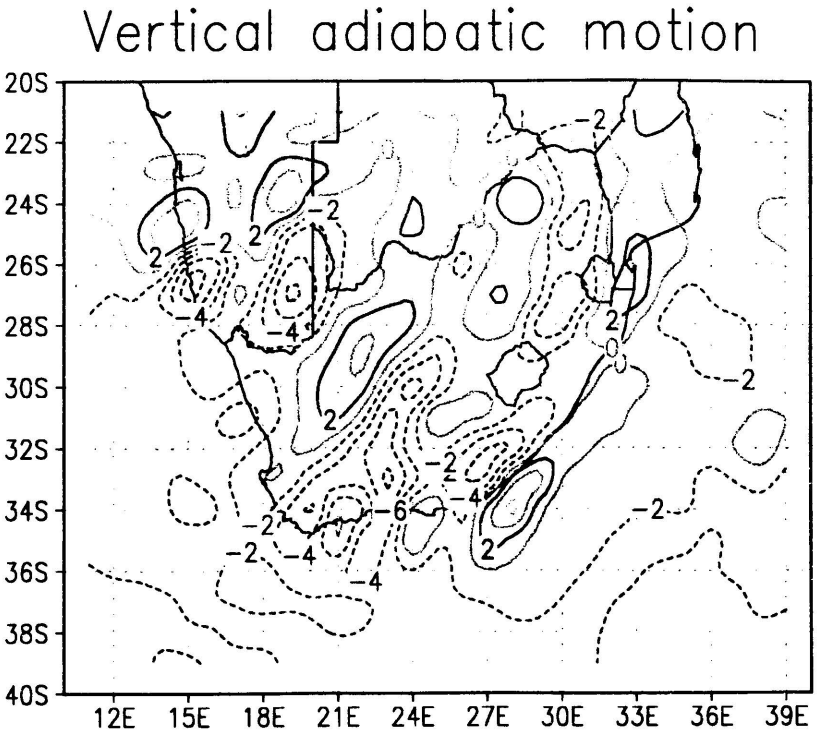

Fig. 6.27 Vertical adiabatic motion (microbar s^{-1}) on 325K on 12 February 1996

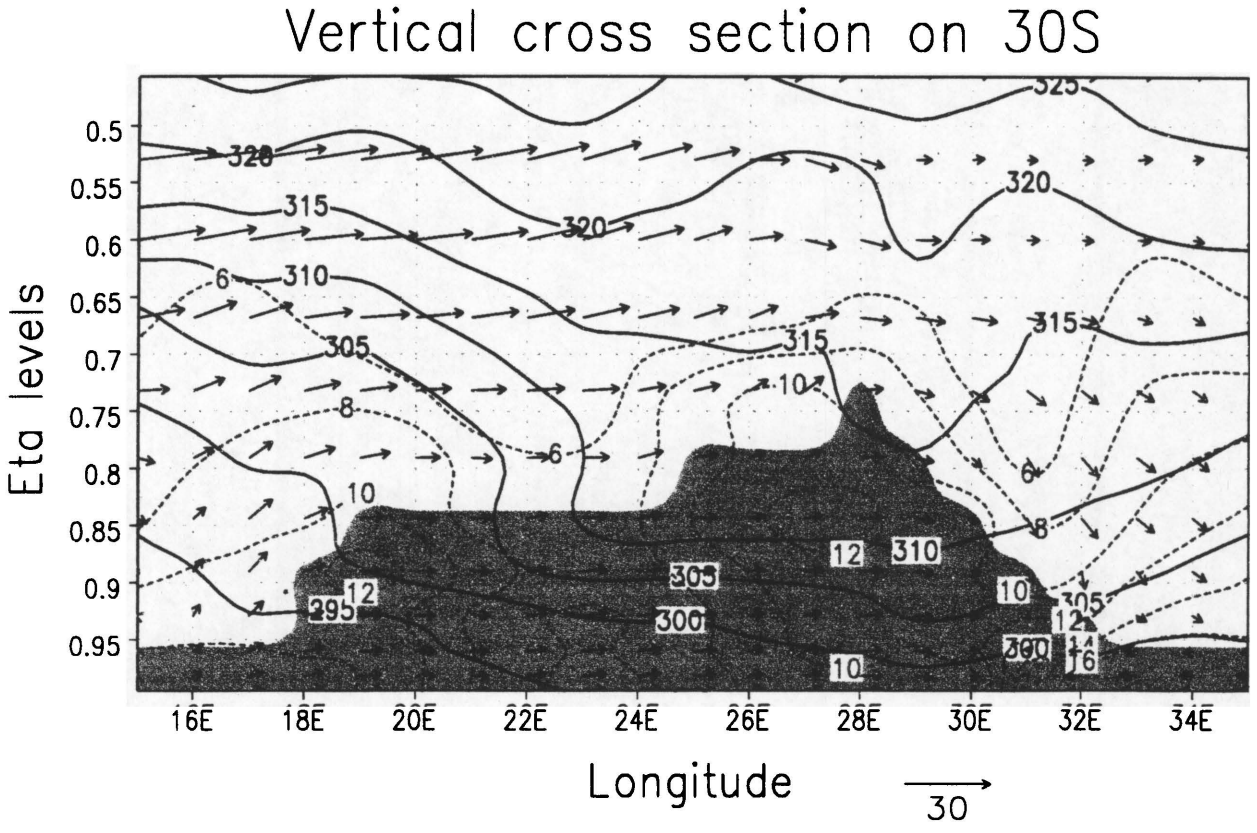

Fig. 6.28 As Fig. 6.23 but at 30S on 13 February 1996

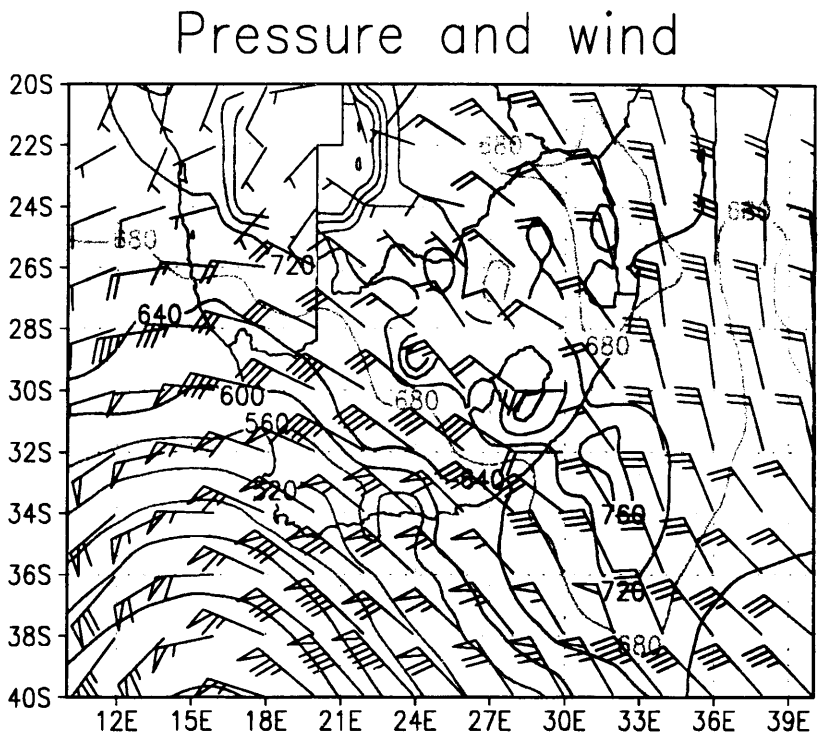

Fig. 6.29 **Pressure (hPa) on 315K on 13 February 1996 where pressure is in hPa and windspeed (knots).**

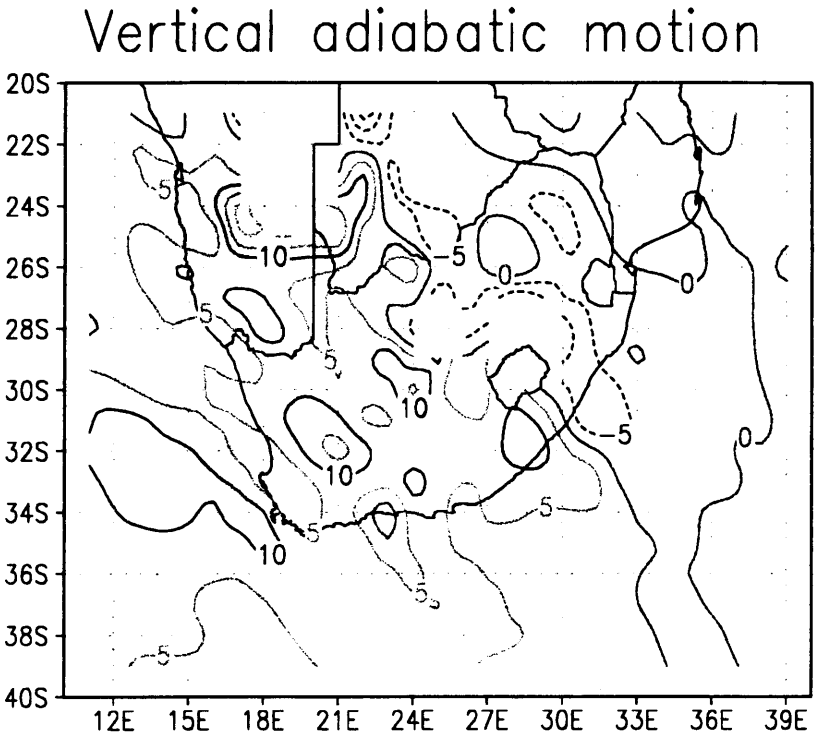

Fig. 6.30 **Vertical adiabatic motion (microbar s^{-1}) on 315K on 13 February 1996**

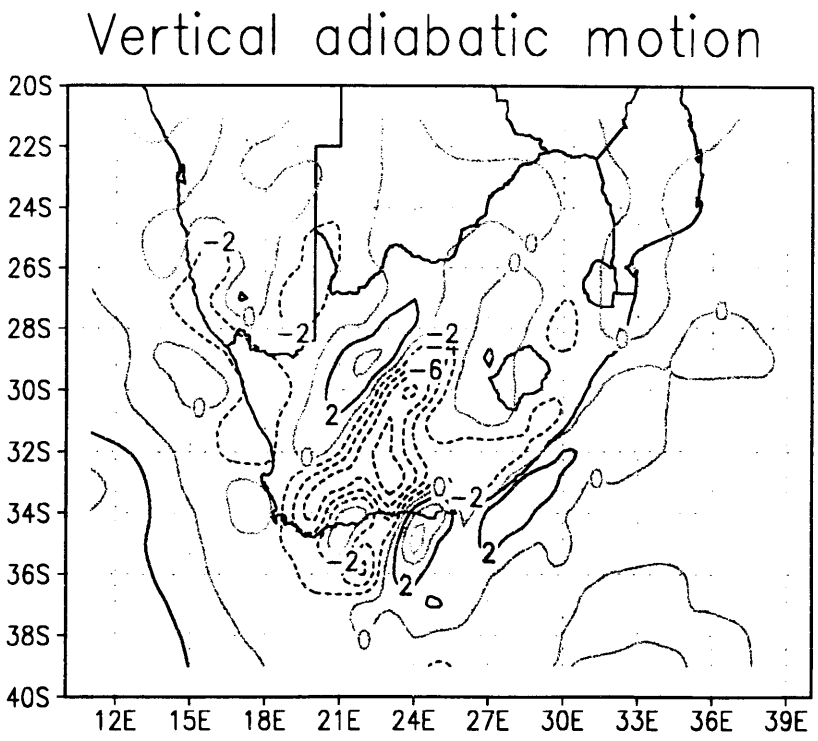

Fig. 6.31 Vertical adiabatic motion (microbar s^{-1}) on 325K on 13 February 1996

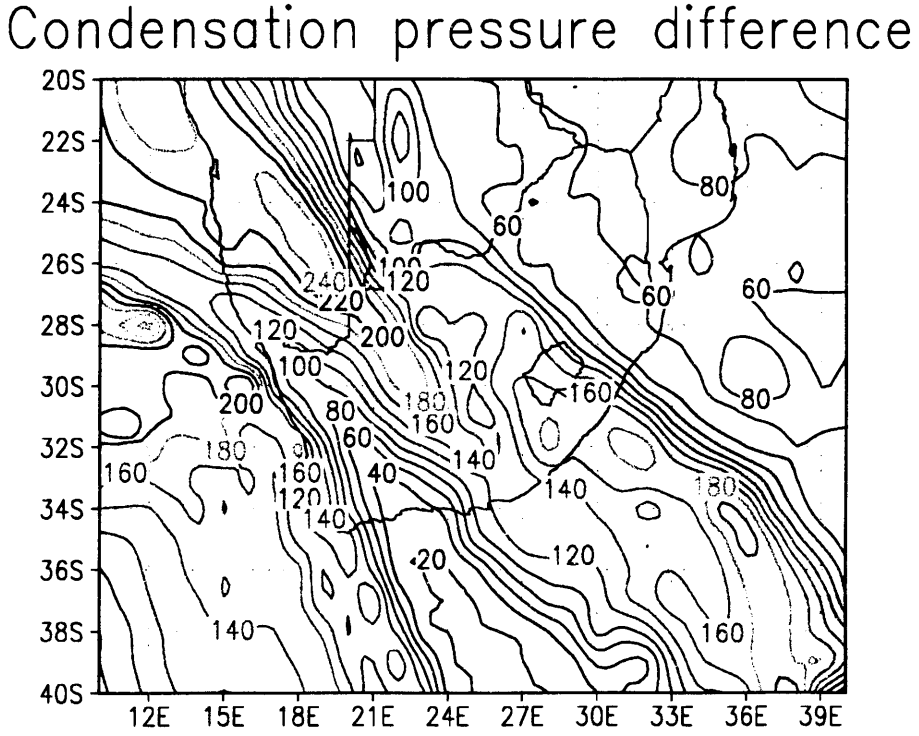

Fig. 6.32 Condensation pressure difference (hPa) on 325K on 13 February 1996

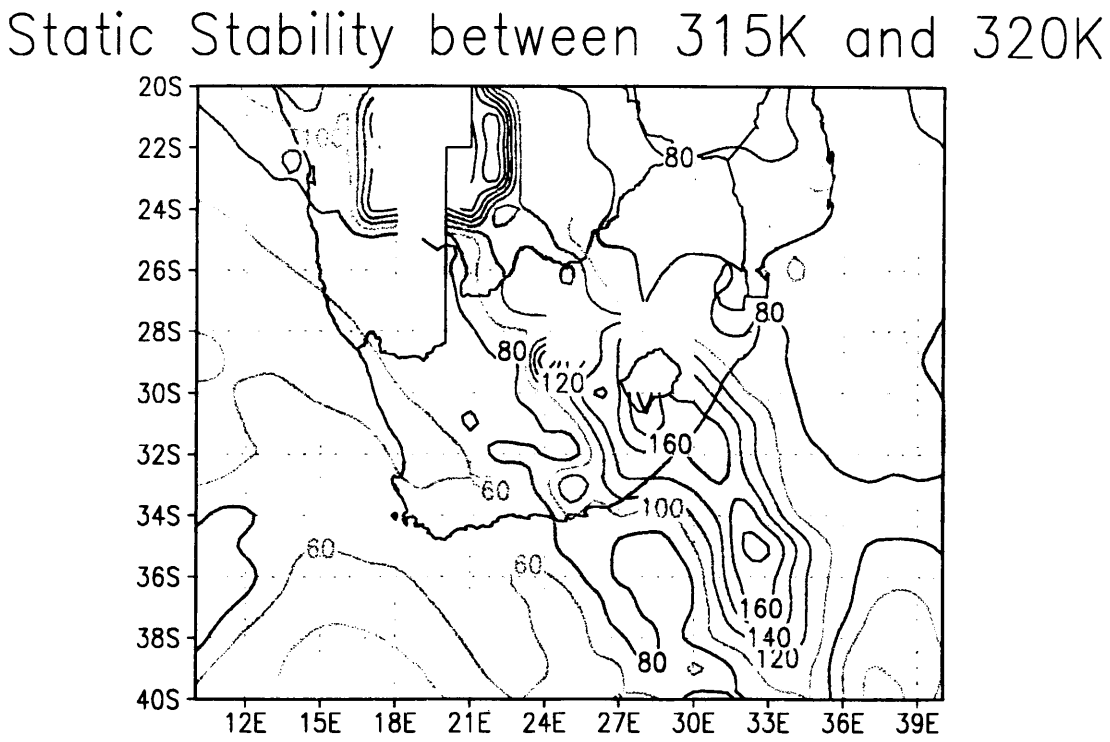

Fig. 6.33 Static stability (hPa) between 315 and 320K on 13 February 1996

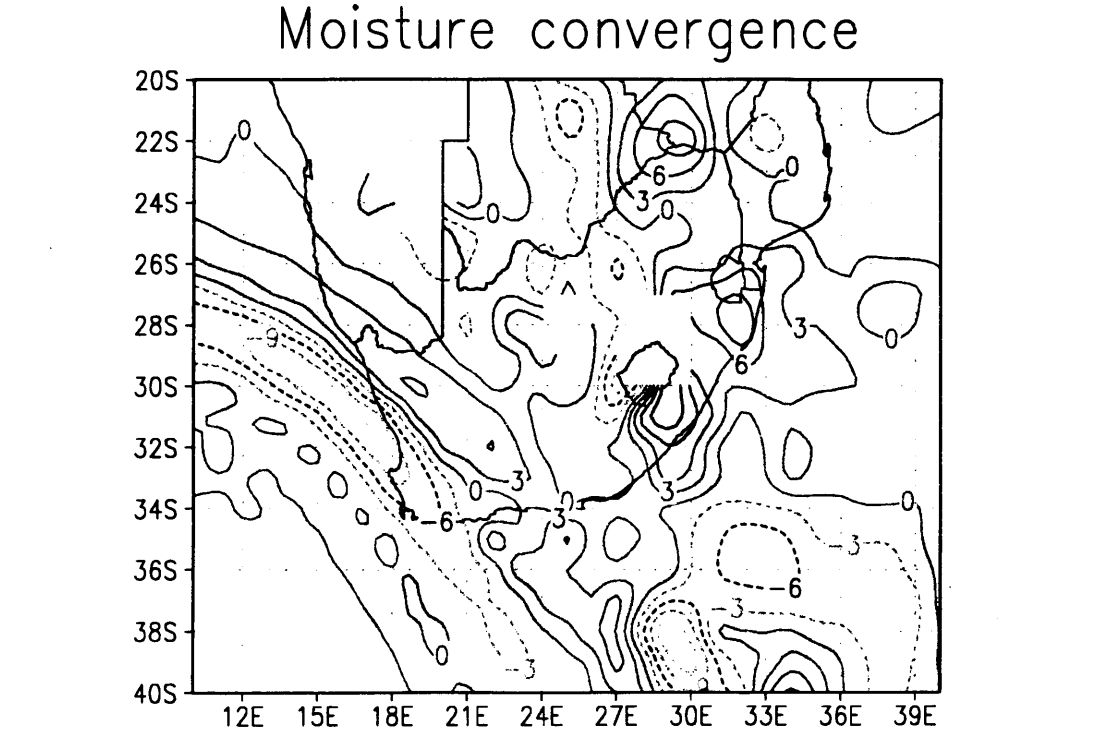

Fig. 6.34 Moisture convergence (g kg^{-1} h^{-1} X10) on 315K on 13 February 1996

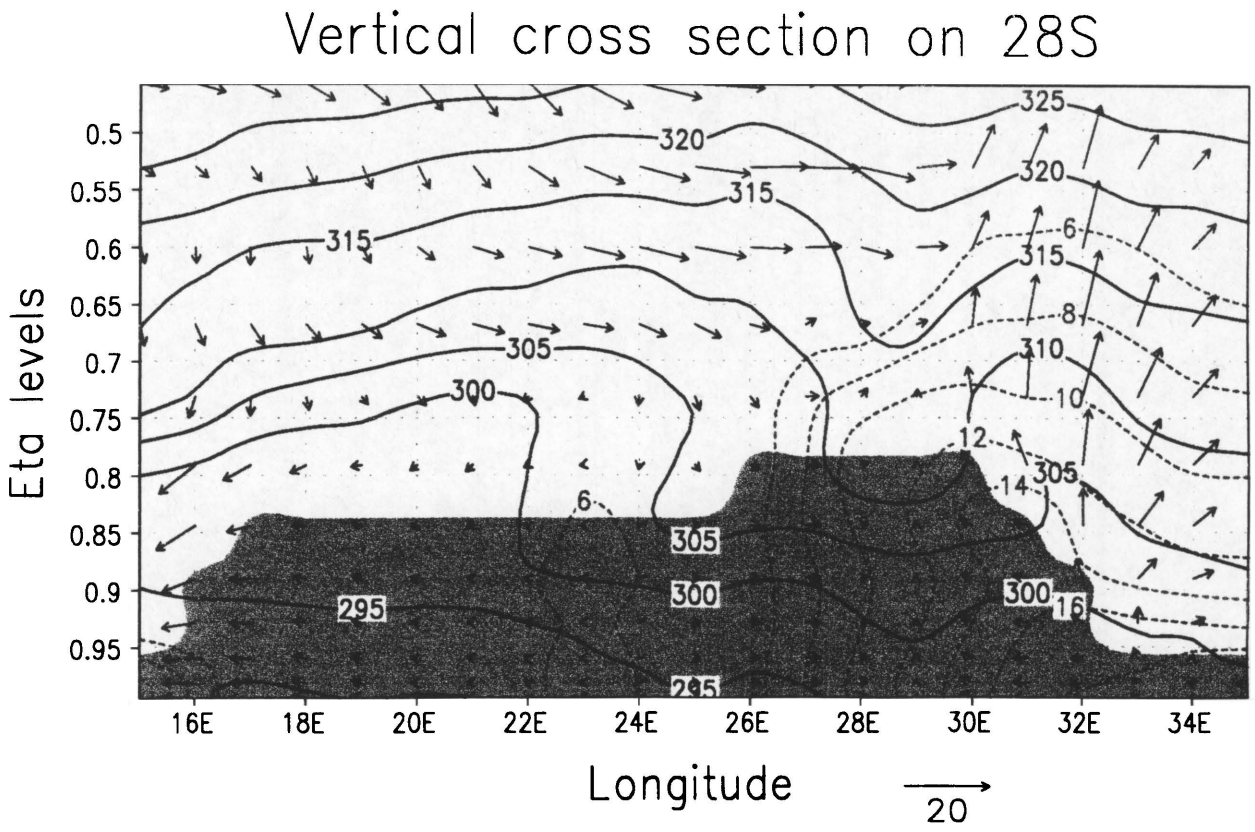

Fig. 6.35 As Fig. 6.23 but at 28S on 14 February 1996

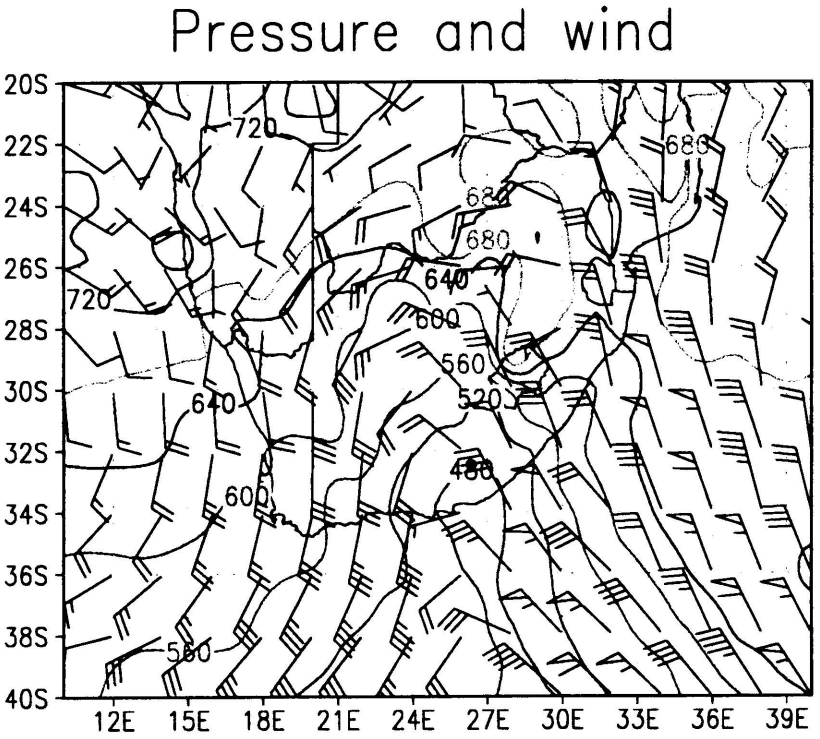

Fig. 6.36 As Fig. 6.29 but on 315K on 14 February 1996

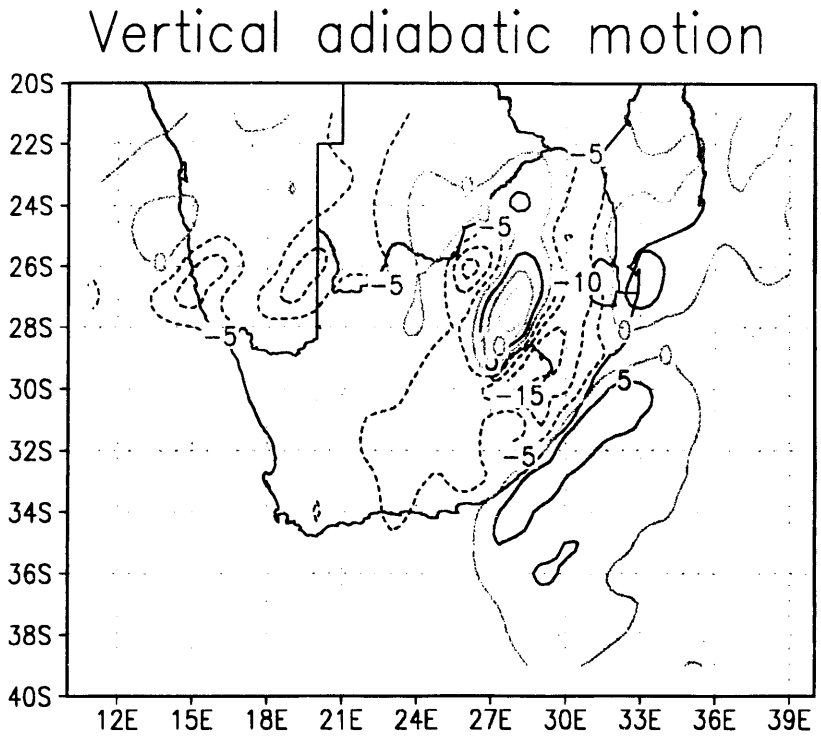

Fig. 6.37 Vertical adiabatic motion (microbar s^{-1}) on 315K on 14 February 1996

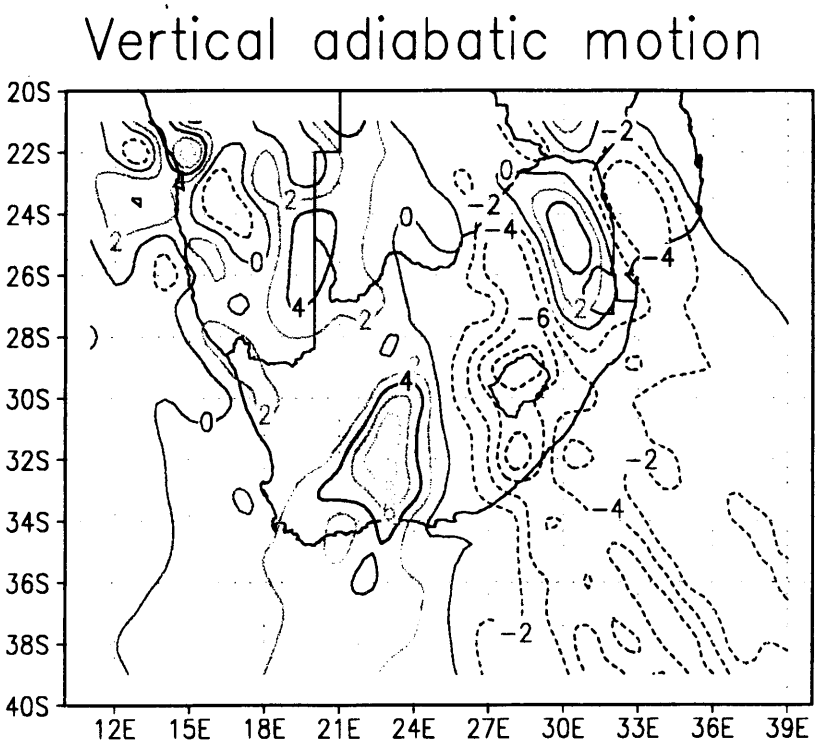

Fig. 6.38 Vertical adiabatic motion (microbar s^{-1}) on 325K on 14 February 1996

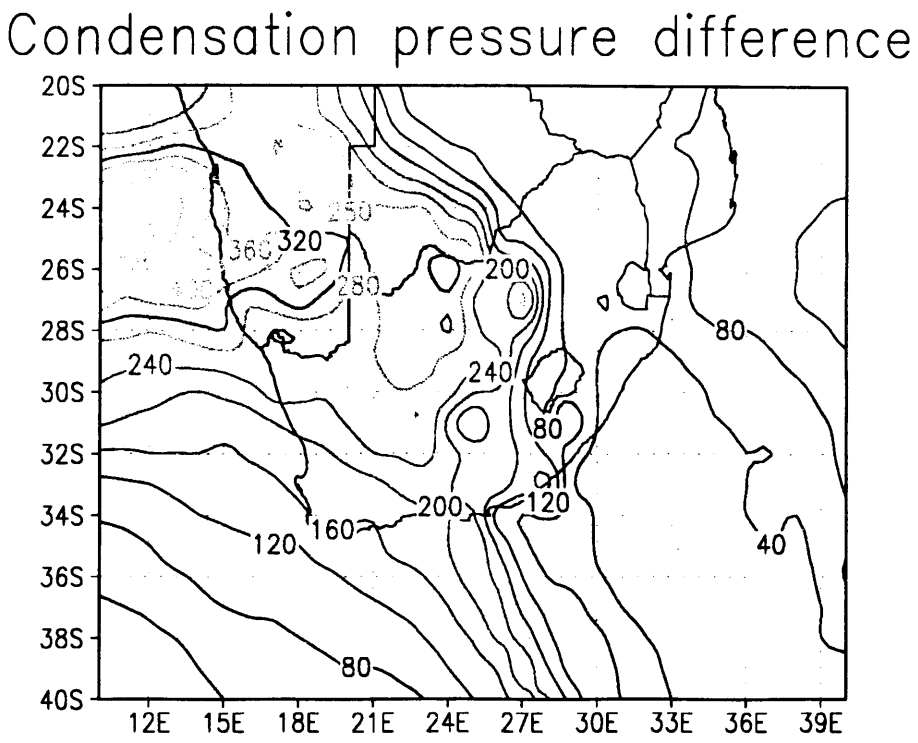

Fig. 6.39 Condensation pressure difference (hPa) on 315K on 14 February 1996

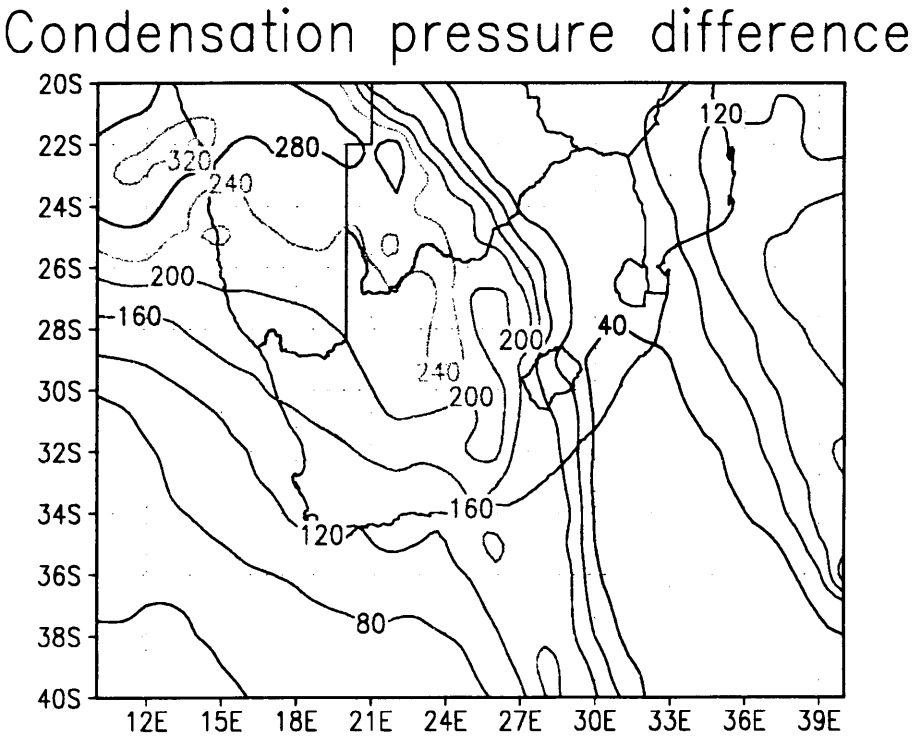

Fig. 6.40 Condensation pressure difference (hPa) on 325K on 14 February 1996

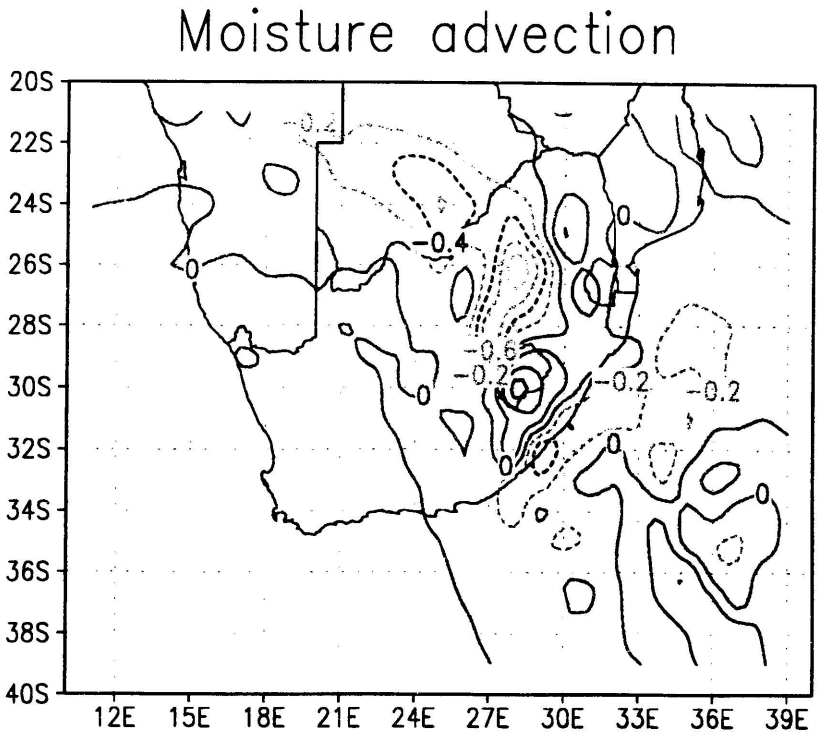

Fig. 6.41 **Moisture advection (g kg^{-1} h^{-1}) on 315K on 14 February 1996**

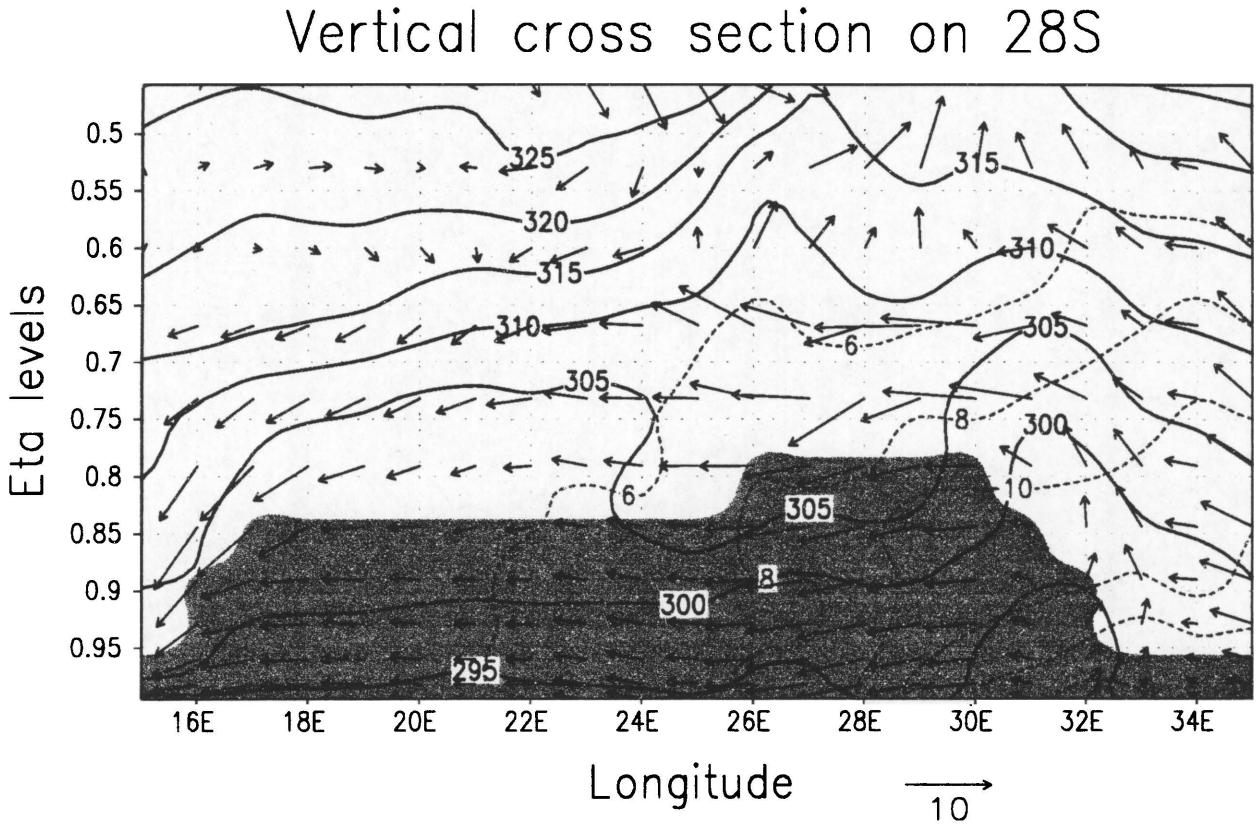

Fig. 6.42 **As Fig. 6.23 but at 28S on 15 February 1996**

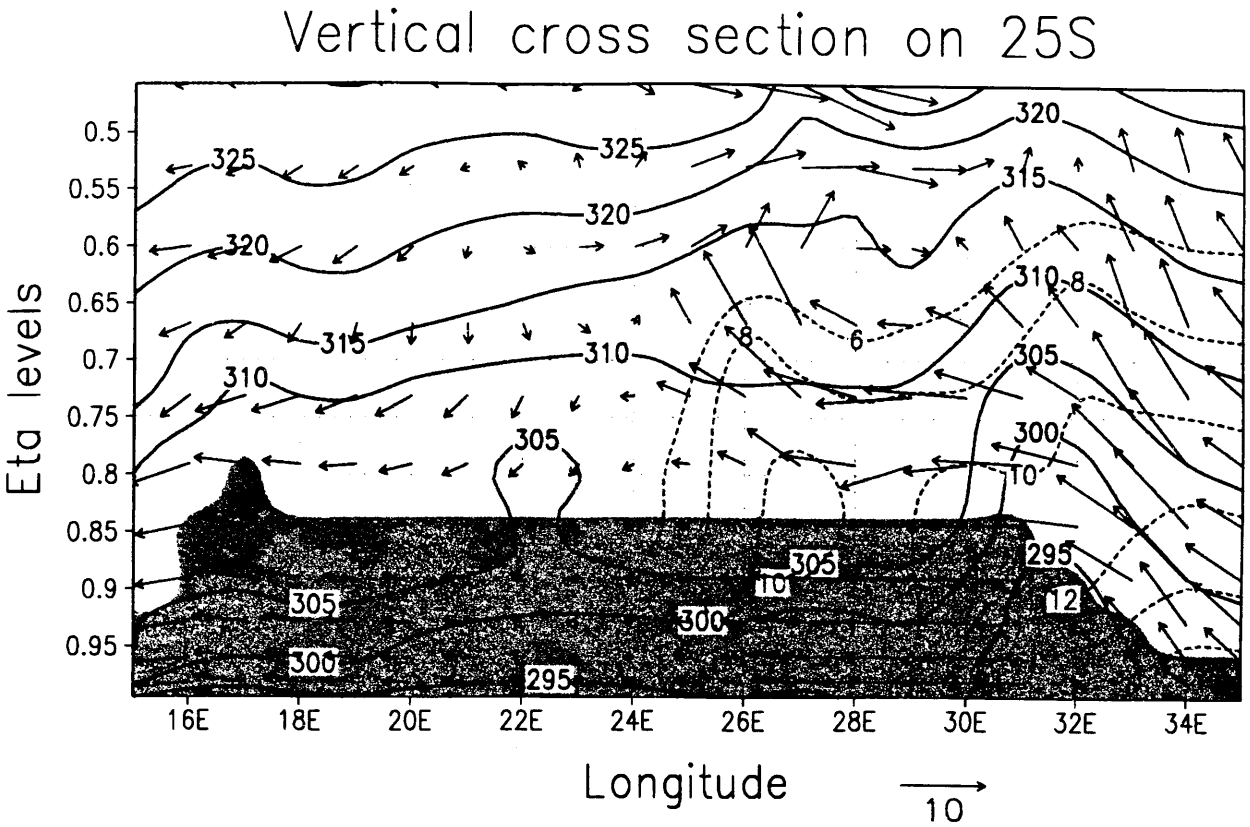

Fig. 6.43 As Fig. 6.23 but at 25S on 15 February 1996

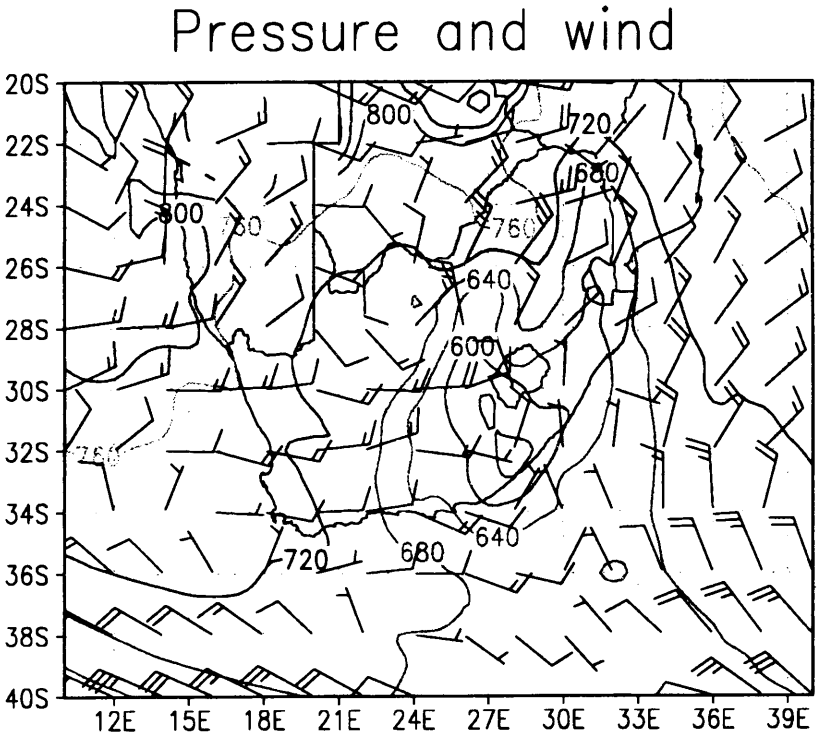

Fig. 6.44 As Fig. 6.29 but for 310K on 15 February 1996

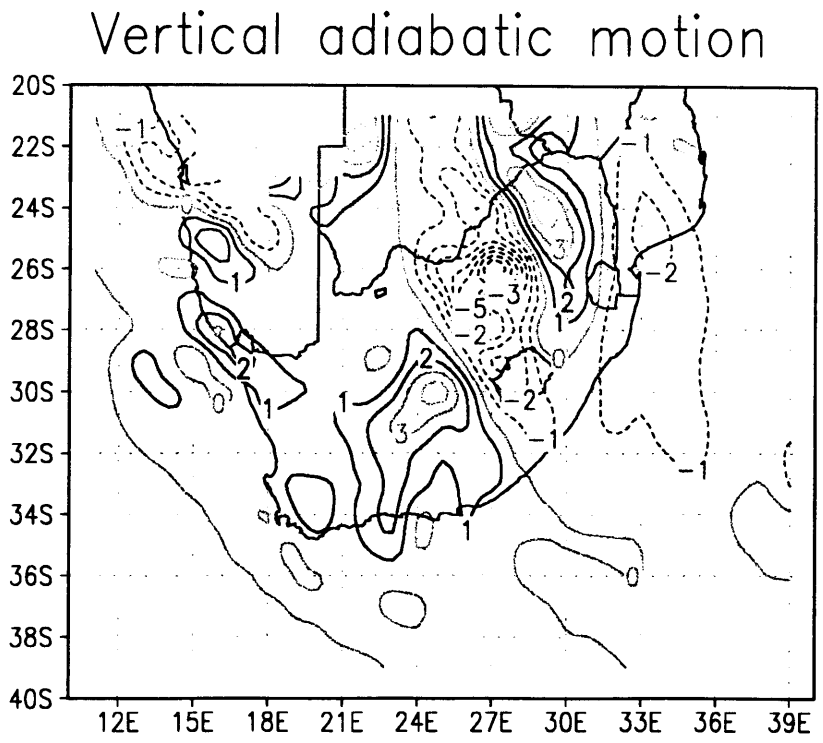

Fig. 6.45 Vertical adiabatic motion (microbar s^{-1}) on 310K on 15 February 1996

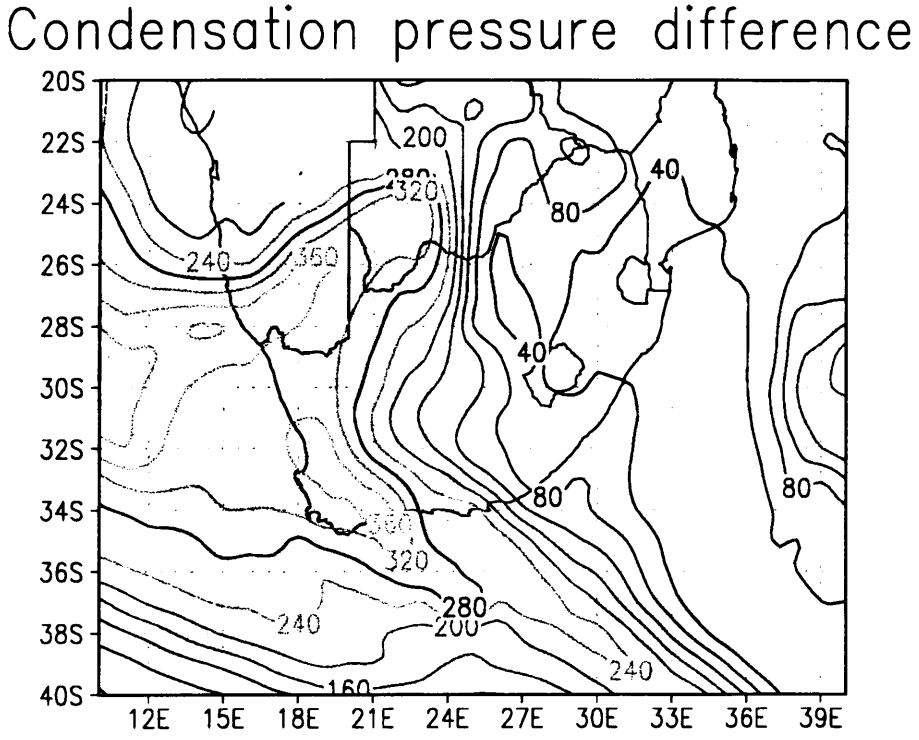

Fig. 6.46 Condensation pressure difference (hPa) on 310K on 15 February 1996

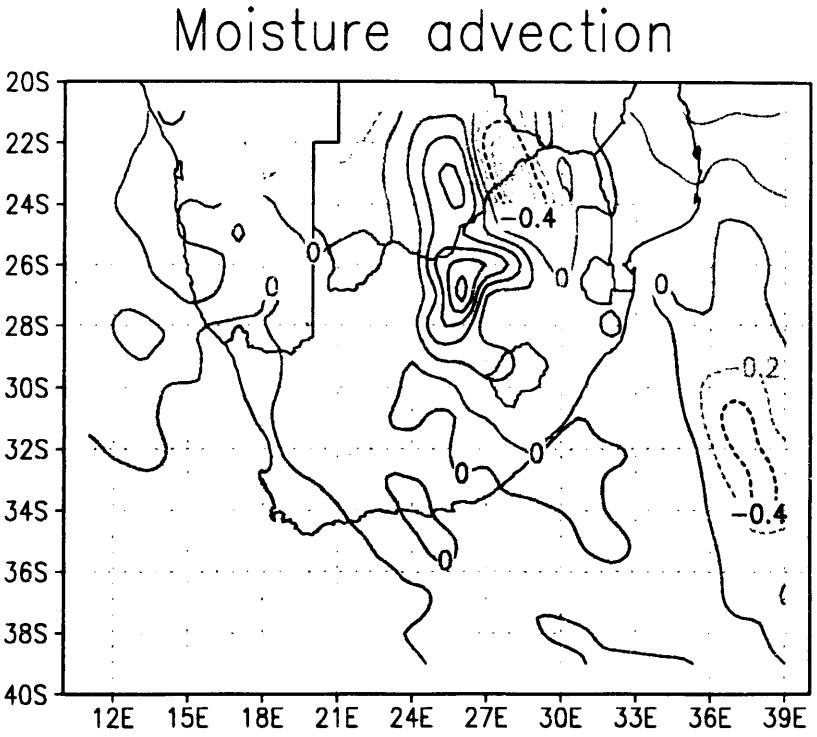

Fig. 6.47 Moisture advection (g kg^{-1} h^{-1}) on 310K on 15 February 1996

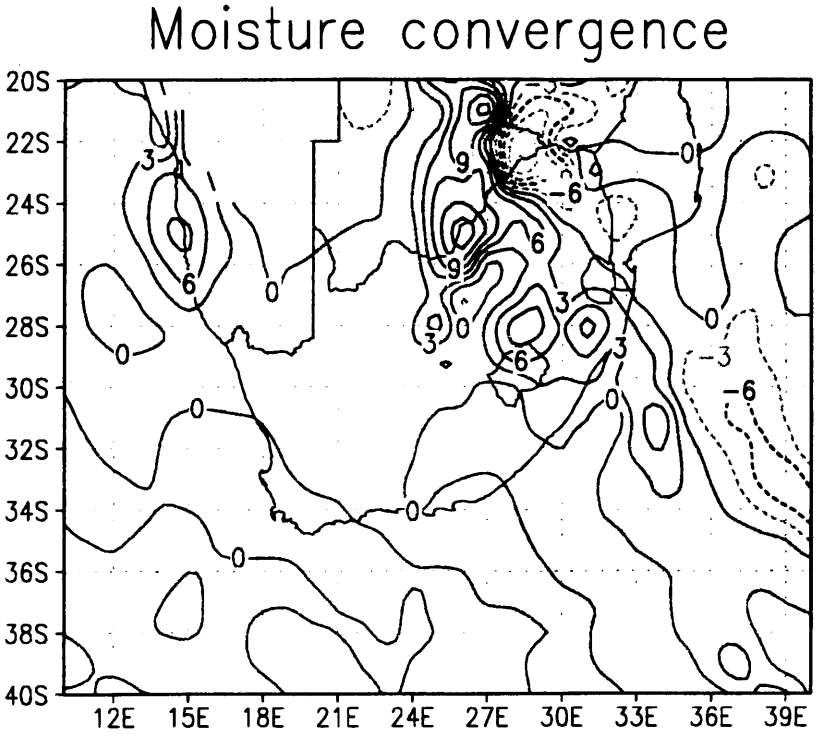

Fig. 6.48 Moisture convergence (g kg^{-1} h^{-1} X10) on 310K on 15 February 1996

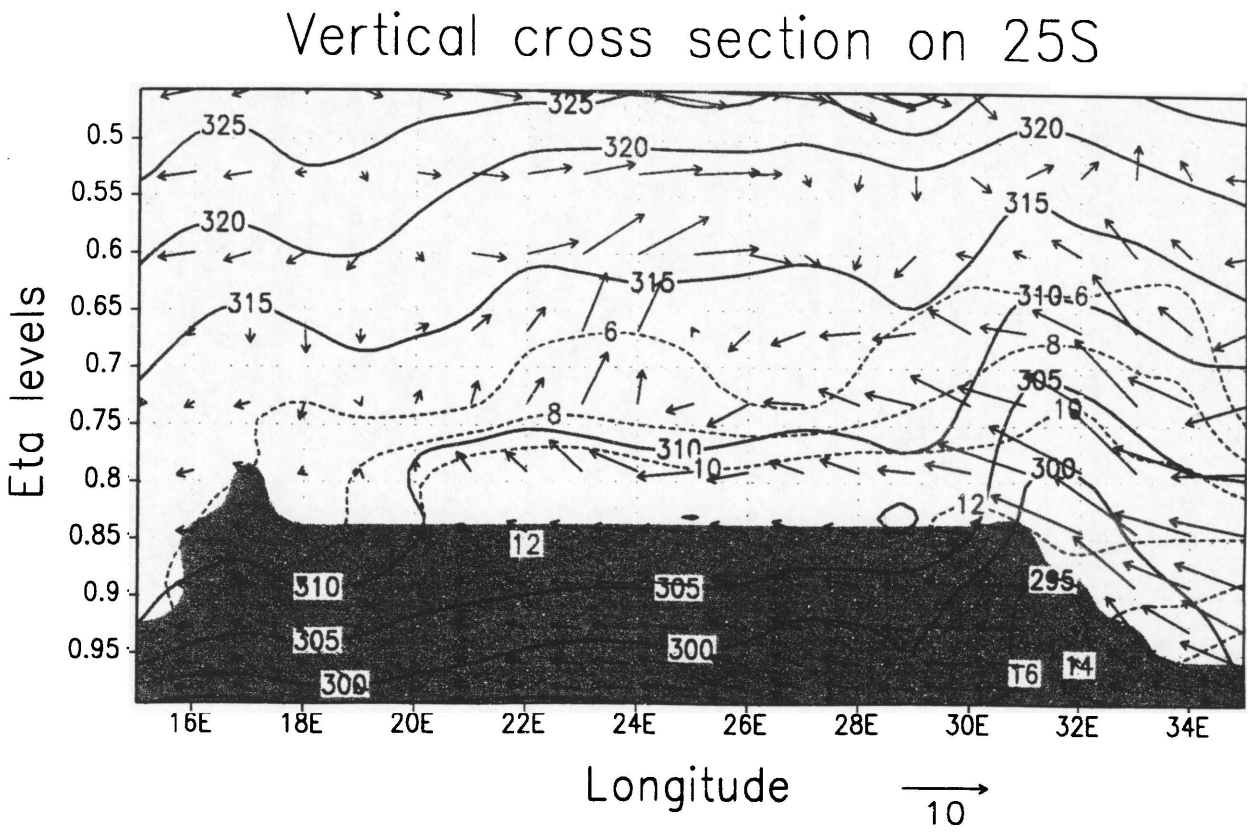

Fig. 6.49 As Fig. 6.23 but at 25S on 16 February 1996

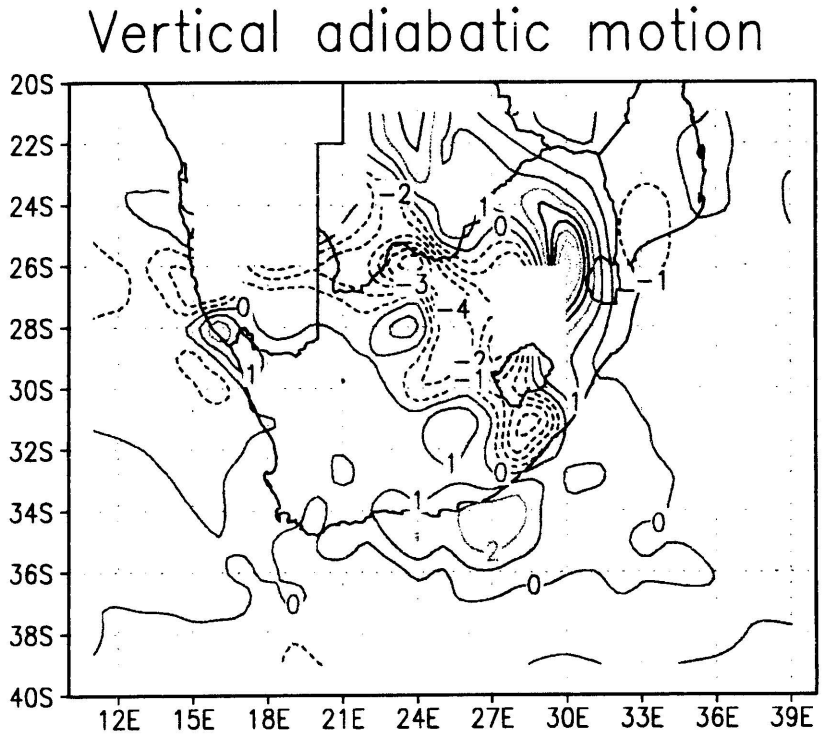

Fig. 6.50 Vertical adiabatic motion (microbar s^{-1}) on 310K on 16 February 1996

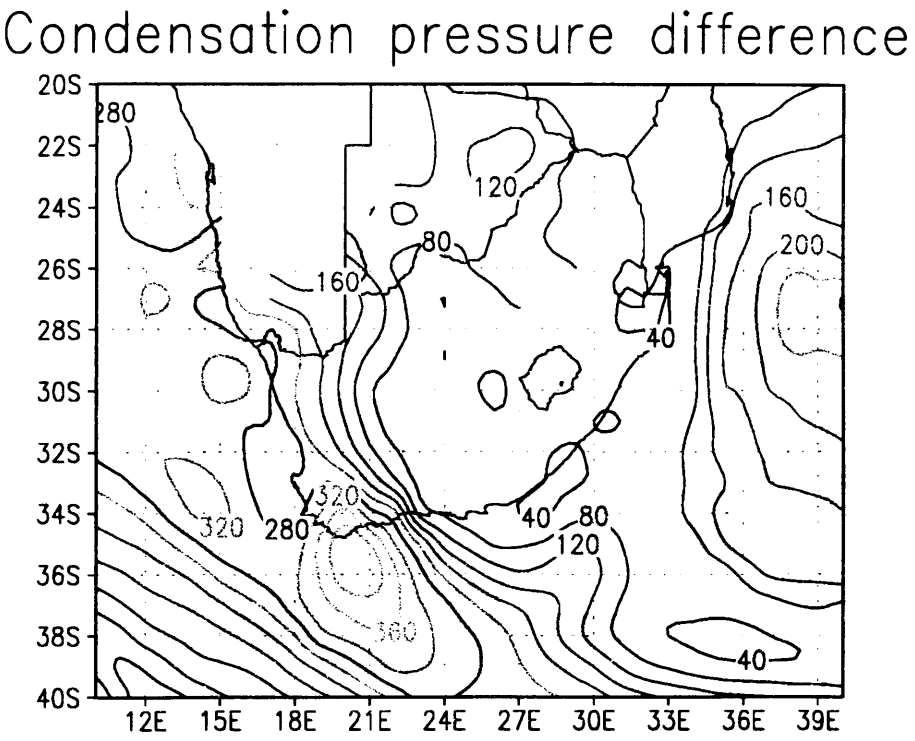

Fig. 6.51 Condensation pressure difference (hPa) on 310K on 16 February 1996

CHAPTER 7

CASE STUDY IN MAY 1996

7.1 Introduction

The month of May is traditionally the last month of autumn in the Southern Hemisphere and this is also the time of the year when more baroclinic weather systems occur. According to Taljaard (1982) it is also a month with peak occurrence in cut-off low pressure systems. During the latter part of May such a cut-off low pressure system developed over South Africa and produced widespread rain over the central and eastern parts of the country.

7.2 Aims of the case study

The January and February heavy rainfall events were characterized by not only heavy rainfall but also tropical weather systems. It was decided to investigate a typical baroclinic winter weather system to see the differences in the isentropic analyses. The specific time period which was studied was 24-29 May 1996.

7.3 Data used

Daily synoptic charts were used to obtain the synoptic sequence of events for the week. The Climate Section of the SAWB supplied daily rainfall figures. Satellite images taken at 12:00 UT were also used to get an indication of the cloud cover and the movement of the cold front and upper-air system. Data for the isentropic analysis were derived by the methods described in Chapter 3 using the 12-hour forecast fields of the Eta model.

7.4 Synoptic sequence of events for 24-29 May 1996

Surface at 12:00 UT:

A cold front was situated over the south-eastern parts of the country on the 24th

(Figure 7.2). The Atlantic Ocean high pressure system lay south of the country and advected colder, moist air onto the south-east coast behind the cold front. It was partly cloudy and cold over the southern and south-eastern parts of the country, but fine and mild over the northern parts.

By the 25th the cold front was situated over the eastern parts and in its rear a strong high pressure system south of the country caused cold and rainy conditions over the south-eastern and eastern areas (Figure 7.4).

The cold front had advanced into Zimbabwe by the 26th (Figure 7.6) and cloudy, cold conditions with showers occurred over the eastern half of the country. Over the highveld it was very cold. Showers were falling over Botswana and the Northwest Province, while fine conditions prevailed over the Western Cape due to an off-shore flow.

The strong high pressure system south-east of the country on the 27th (Figure 7.8) caused an on-shore flow over the eastern part of the country with drizzle along the coast and escarpment. Showers and thundershowers occurred over the eastern interior, while fine and mild conditions prevailed over the western part of the country.

A weak cold front lay to the immediate west of the Western Cape on the 28th (Figure 7.10) preceded by dry, windy weather over the western interior and hot off-shore winds on the west coast. Cloudy conditions with light rain were still being experienced over the Lowveld and Mozambique.

With a coastal low along the south coast and a high pressure system to the east of the country on the 29th (Figure 7.12), fine and warm conditions were reported over most of the country.

Upper air at 12:00 UT:

On the 24th (not shown) a trough of low pressure was lying north-westwards of Port Elizabeth with a low pressure system situated on 25E and 35S. Strong westerly winds dominated over the entire country.

The main westerly trough moved eastwards towards the east coast on the 25th (Figure 7.13). Another trough developed over the western parts of the country. At this time a cut-off low (COL) pressure system developed over the south-western coast of Namibia. On the 26th (Figure 7.14) this COL was lying over the southern parts of Namibia with a trough of low pressure stretching south-eastwards. An upper ridge developed south of the country.

On the 27th (Figure 7.15) the COL was situated on 25E and 25S with a trough stretching south-eastwards to an area of lower pressure south the country.

The COL was lying east of the country on the 28th (not shown) and a high pressure system was situated over the western and central parts. An upper-air trough started to develop on the south-west coast where north-westerly winds prevailed.

The development of the COL was typical of winter time upper air systems as described by Taljaard (1995).

7.5 Satellite images on 12:00 UT:

Only a little moisture is visible on the satellite image for 24 May (Figure 7.1) and it is restricted to the south-eastern parts of the country (behind the cold front and ahead of the ridging high pressure system.

On the 25th (Figure 7.3) cloud development is seen over Namibia east of the upper air low pressure system or cut-off low (COL) which was situated over the southern part of Namibia. Moisture is also visible over the eastern parts where the high pressure system was advecting moisture behind the cold front.

On the 26th (Figure 7.5) the upper air COL was still present in the west with associated clouds over the northern and central parts of the country.

Figure 7.7 shows that there was a great deal of moisture in circulation over the north-eastern parts of the country on the 27th. By this time the cut-off low was situated on 25S and 25E (with an accompanying trough extending south-eastwards) and a surface

high pressure system was feeding in moisture from the east - both these systems thus contributed to the large amount of cloud visible on the satellite image.

On the 28th (Figure 7.9) the next approaching cold front could be seen on the south-western coast of South Africa and low level moisture was still evident in the east.

On the 29th (Figure 7.11) skies were clear over South Africa.

7.6 Rainfall distribution and intensity

On the 24th (Figure 7.16) showers occurred over the north-eastern parts of the country with falls of up to 20 mm over the southern parts of KwaZulu/Natal. Light falls were also reported over parts of Mpumalanga, Gauteng and the Northwest Province.

Heavier falls were reported on the 25th (Figure 7.17) with preference to the south-east coast (up to 40 mm) and parts of the Northwest Province (up to 30 mm).

Widespread falls occurred on the 26th (Figure 7.18) over large parts of the Northwest Province and Gauteng (up to 40 mm), KwaZulu/Natal (up to 40 mm) and along the southern and south-eastern coastal belts.

On the 27th (Figure 7.19) heavier falls were reported over the Northwest Province (up to 40 mm) and light showers occurred in the east as well as in the south-west.

Falls of below 10 mm were recorded over the eastern parts of the country on the 28th (Figure 7.20).

7.7 Eta model evaluation

The 0-hour analyses of the Eta model were evaluated against observations. The overall impression was that the surface (mean sea level pressure or MSLP) and upper air (500 hPa gpm) patterns of the period were handled well by the Eta model. The upper air westerly trough and cut-off low system was depicted very close to observations on all

the Eta analyses.

7.8 Isentropic analysis results

7.8.1 ETA analysis date: 96052500 with a 12-hour forecast for 96052512

On 30S (Figure 7.21) inflow of moisture was evident east of the escarpment, but specific humidity values were only in the order of 6 g kg^{-1}. No significant vertical motion occurred. A westerly flow dominated on 28S (not shown).

On 305K cooler air was in circulation over the south-eastern parts behind the cold front where pressure values were less than 640 hPa. Warmer air was in circulation over the northern interior ahead of the cold front which was lying along 26S (Figure 7.22). Low level (305K) upward adiabatic motion (although slight) was evident over most of the country with preference to the eastern parts (along 30E) and between 24E and 27E which coincided with heavier falls in the Northwest Province. In the upper air (315K) values of 12 microbar s^{-1} appeared over the south-western interior ahead of the upper air trough. Condensation difference values were less than 90 hPa on 305K (Figure 7.23) over the north-eastern and south-eastern parts of the country, while values of below 60 hPa occurred over the northern parts of the country on 315K (Figure 7.24). Positive moisture advection on 305K (Figure 7.23) was evident over the north-eastern parts favouring the area west of Swaziland where values of 0.2 g kg^{-1} $hour^{-1}$ could be seen and rainfall figure were more than 10 mm. Static stability values between 305 and 310K (Figure 7.26) were more than 200 hPa over parts of the Northwest Province and Northern Cape , which coincided with the area of heavier precipitation.

7.8.2 Eta analysis date : 96052600 with a 12-hour forecast for 96052612

Strong (12 cm s^{-1}) updraughts could be seen on 30S (Figure 7.27) along the escarpment together with a low level inflow of moisture from the east. On 28S (not shown) 8cm s^{-1} updraughts occurred along the escarpment and the flow changed to easterly. On 25S (Figure 7.28) a shallow layer of moisture (6 g kg^{-1}) stretched from east to west with strong rising along 26E.

The entire country was under the influence of cooler air with pressure values on 305K (Figure 7.29) nearly all below 640 hPa except for the extreme western parts. Vertical adiabatic motion was upward over most of the country with higher values over the Northwest Province as well as the Northern Cape where widespread moderate falls occurred. On 315K (Figure 7.30) negative values for VAM were evident over the southern and eastern parts of the country which coincided with the upper air trough lying in the west. The strongest upward motion was over the southern and eastern Cape, KwaZulu-Natal, the eastern Free State, Mpumalanga and parts of the Northwest Province which tied in with the areas of precipitation. Condensation difference values on 305K (Figure 7.31) were less than 100 hPa over the Northern Province, the Northwest Province and the coast of KwaZulu-Natal. This pattern was similar to the one on 315K (Figure 7.32) where condensation pressure differences were below 100 hPa over the northern parts of the country as well as along the east and south coasts. These patterns highlighted the areas where widespread falls occurred. Moisture on 305K (Figure 7.33) was being advected to the eastern half of the country, with preference to the Northern Cape and Mpumalanga. Moisture flux convergence patterns were similar with preference to the Northern Province and parts of Northwest. Static stability values were no more than 120 hPa.

7.8.3 Eta analysis date : 96052700 with a 12-hour forecast for 96052712

Little moisture was available on 30S, but the moisture increased on 28S and the layer of moisture was relatively thick on 23S (Figure 7.34), where strong upward motion was visible. Strong descent was visible east of 24E which was just west of the upper-air low pressure system.

On 300K relatively warm air was in circulation over the entire country with values of up to 880 hPa over the western parts where an off-shore flow was present (Figure 7.35). A limiting streamline is visible stretching from the northeast to the southwest; it was a difficult to recognize as the flow changes direction around the high pressure system and heads back south in the west where the air sinks down and dries out. Weak VAM was evident on 300K, but on 315K one could see upward VAM over the eastern half of the country, with the highest values over the southern and eastern Cape interior, parts of the Northwest Province as well as Mpumalanga (Figure 7.36). All of these

areas were east of the upper-air trough line which stretched north-westwards from the Port Elizabeth area. Condensation differences of less than 100 hPa were similar to the rainfall patterns and were evident on 300K over the north-eastern part of the country (Figure 7.37) and over the northern half of the country and the south coast on 315K (Figure 7.38). Moisture advection on 300K (Figure 7.39) favoured the Northern Cape as well as the Northwest Province and the southern Cape interior, while moisture flux convergence values were not very high. Static instability values of more than 120 hPa occurred over the north-eastern Free State and the Northern Cape and the Northwest Province.

7.8.4 Eta analysis date : 96052800 with a 12-hour forecast for 96052812

Low level inflow of moisture was still evident on 30S, but the moisture did not cross the Drakensberg. A little less moisture was available on 28S than the previous day and a westerly flow dominated. On 25S (Figure 7.40) strong inflow of moisture was visible from the east with strong rising along the escarpment where light falls still occurred.

By the 27th the country had recovered from the influence of the cold front and pressure values on 300K were relatively high. VAM on 300K indicated weak rising over the central parts of the country, while stronger rising was still evident on 315K (Figure 7.41) over the eastern parts. Strong upward motion also occurred on the west coast along with another approaching upper air trough. Condensation pressure differences were less than 60 hPa over the north-eastern parts of the country on 300K and less than 100 hPa over the extreme eastern parts on 315K (Figure 7.42) which tied in with the precipitation areas. The inflow of moist air together with the approaching upper air system was also evident on the south-west coast on 315K. Moisture advection and flux convergence patterns on 300K (Figure 7.43) were similar and favoured the western and southern parts of the country in close correlation to the cloud pattern on the satellite image of the approaching cold front and upper air system. Static stability values were generally less than 120 hPa.

7.9 Conclusions

The main difference between this case study and the previous two is that it was a

winter situation. This was clearly seen in the colder temperature indicated by the pressure charts with the passing of the cold front as well as the recovery afterwards when an off-shore flow developed.

The large amount of moisture which was nearly always visible on the cross-sections in January and February was not at all indicated by the cross-sections in May.

The isentropic levels to work with also differed from the previous cases; 300 or 305K was suitable for analysis of the lower levels and 315K (close to 500 hPa) was chosen as the mid-level analysis level.

Although the passing of the upper-air cut-off low did not cause widespread, heavy rain, heavy falls were nevertheless reported over small areas. The influx of moisture from the north seen in the previous two cases was noticeably absent but would not be expected in May.

The areas where heavy precipitation occurred could be identified by looking at the VAM on 315K (nearly 500 hPa) and the condensation differences on 300 and 315K as well as the moisture flux convergence and advection patterns on 300 or 305K.

These results prove that isentropic analysis could have aided the forecaster in a positive way to identify rainfall areas, temperature differences and areas favourable for heavier precipitation.

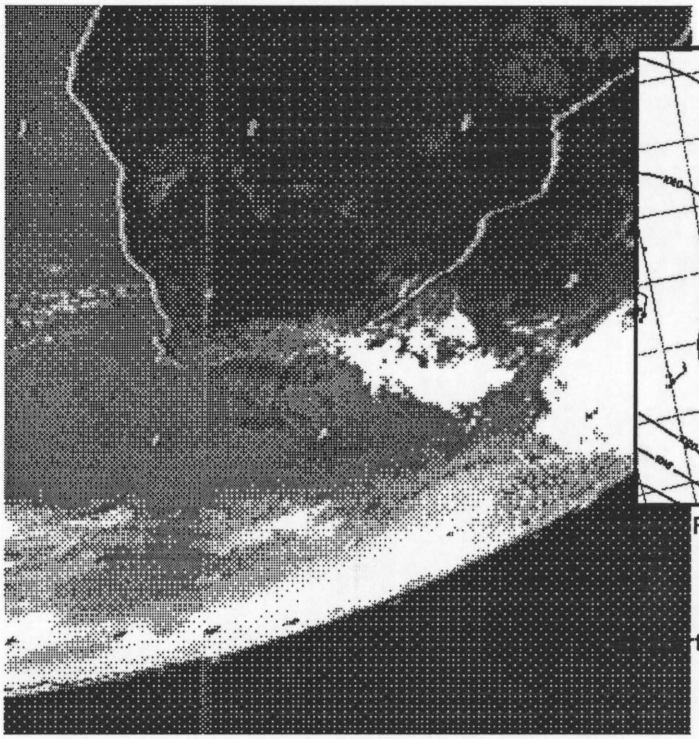

Figure 7.1 Meteosat IR image for 12:00 UT on 24 May 1996

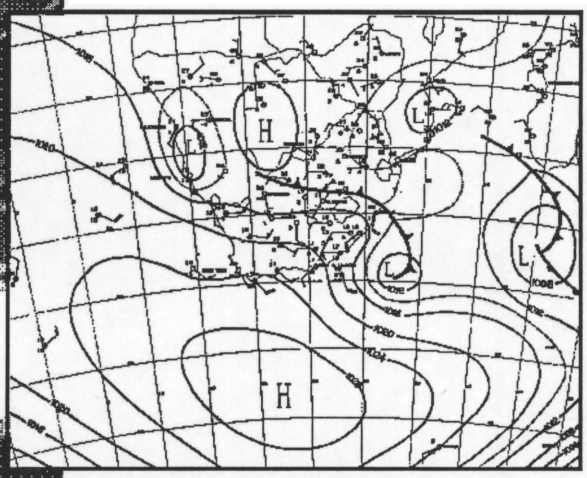

Figure 7.2 Surface pressure chart for 12:00 UT on 24 May 1996. Isobars are in hPa and spaced every 4 hPa. Over the interior pressures were hydrostatically ted to sea level.

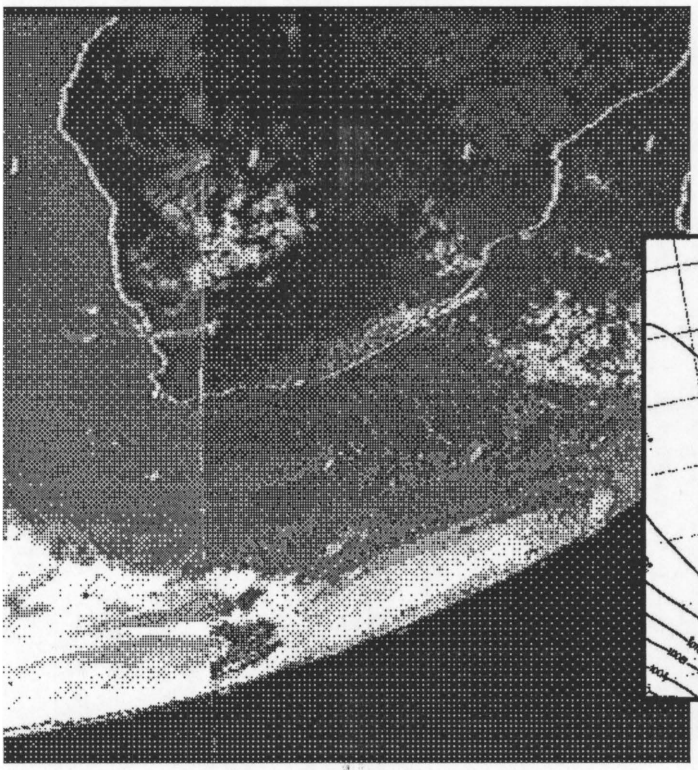

Figure 7.3 As Fig.7.1 but on 25 May 1996

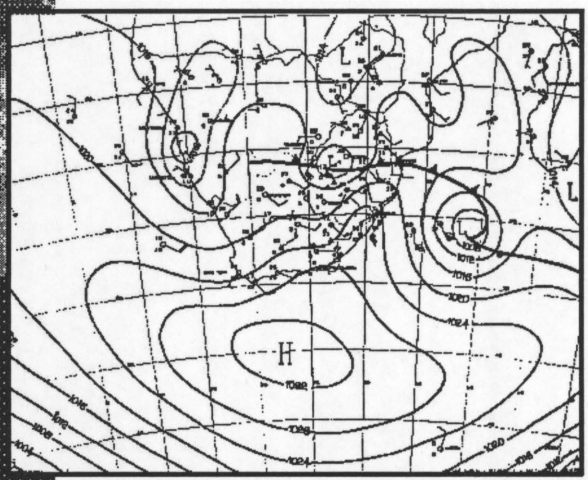

Figure 7.4 As Fig.7.2 but on 25 May 1996

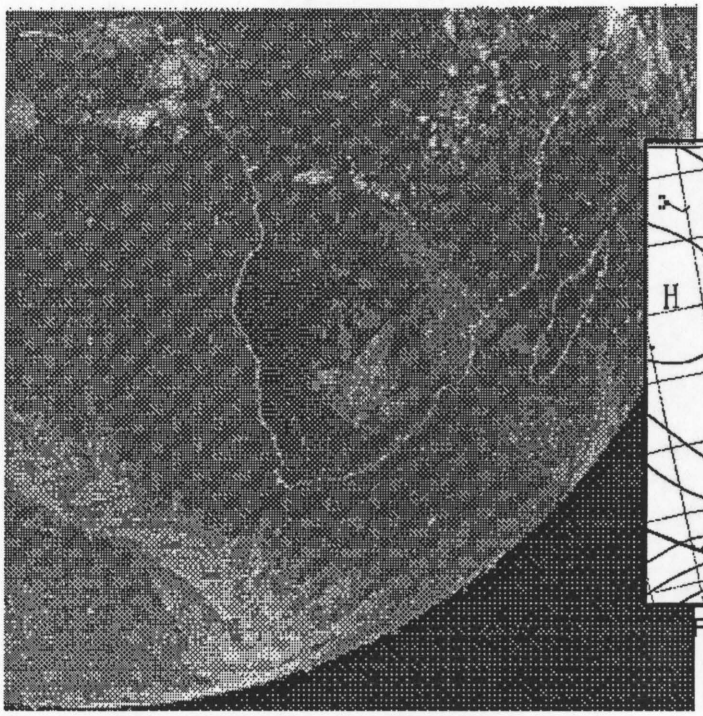

Figure 7.5 As Fig.7.1 but on 26 May 1996

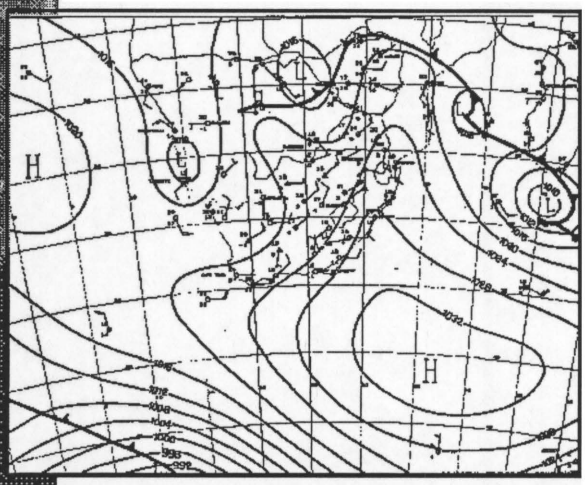

Figure 7.6 As Fig. 7.2 but on 26 May 1996

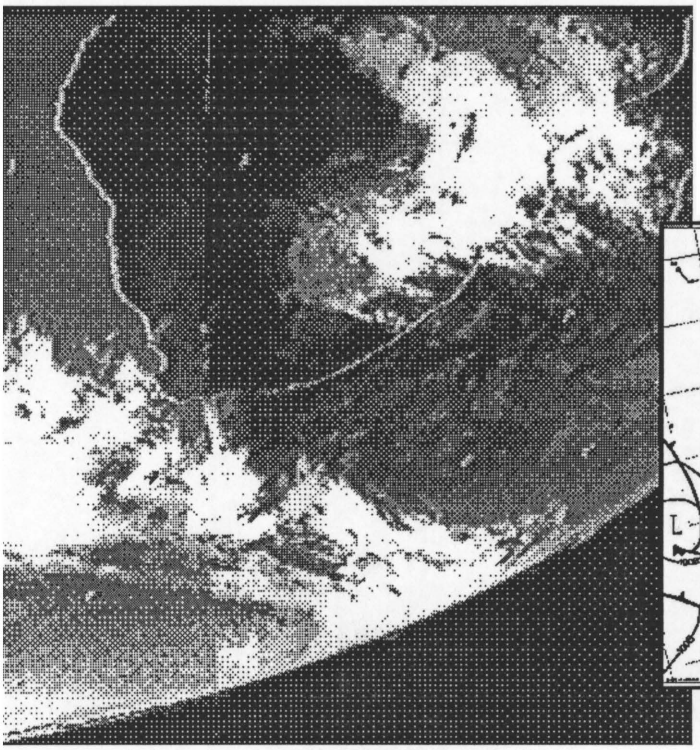

Figure 7.7 As Fig.7.1 but on 27 May 1996

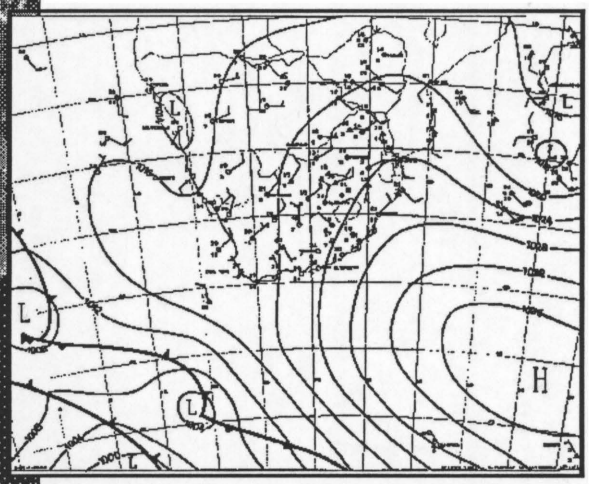

Figure 7.8 As Fig.7.2 but on 27 May 1996

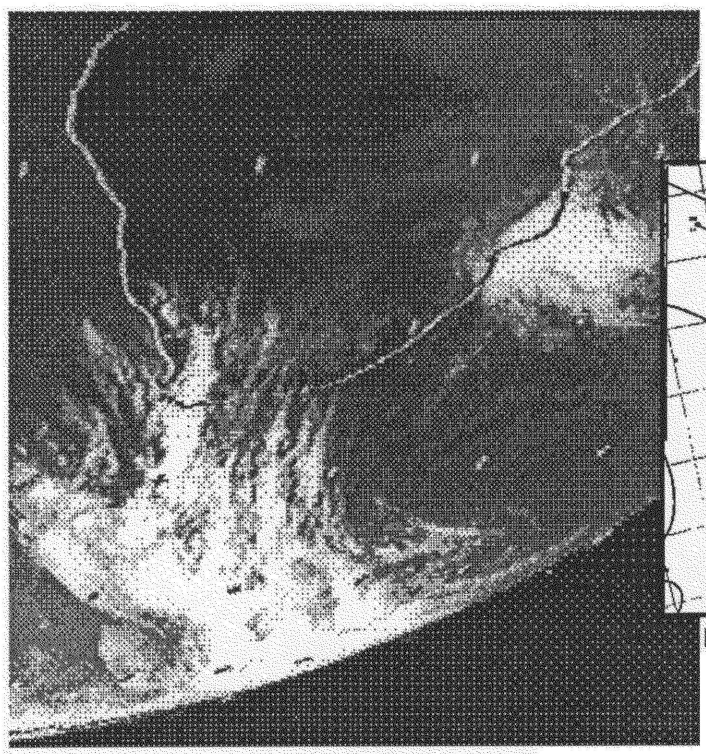

Figure 7.9 As Fig.7.1 but on 28 May 1996

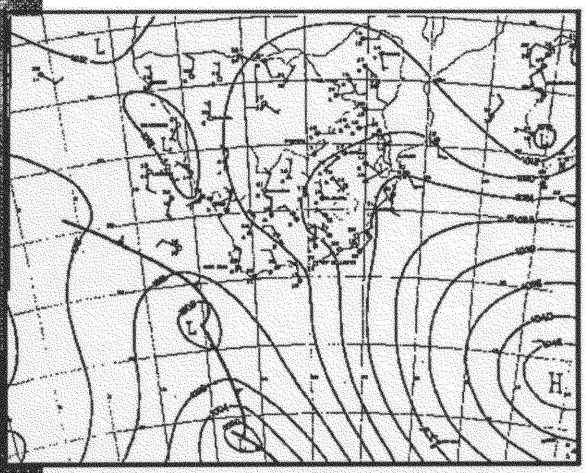

Figure 7.10 As Fig.7.2 but on 28 May 1996

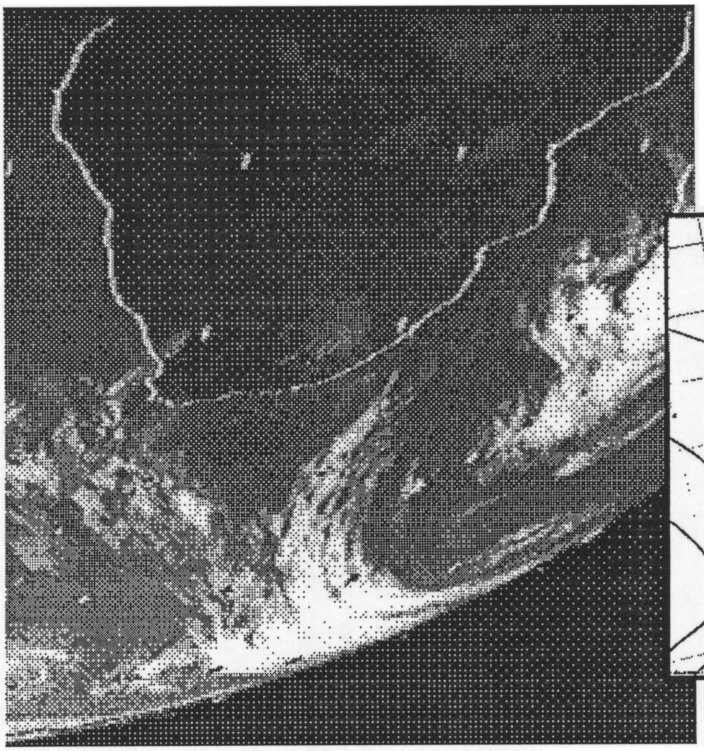

Figure 7.11 As Fig.7.1 but on 29 May 1996

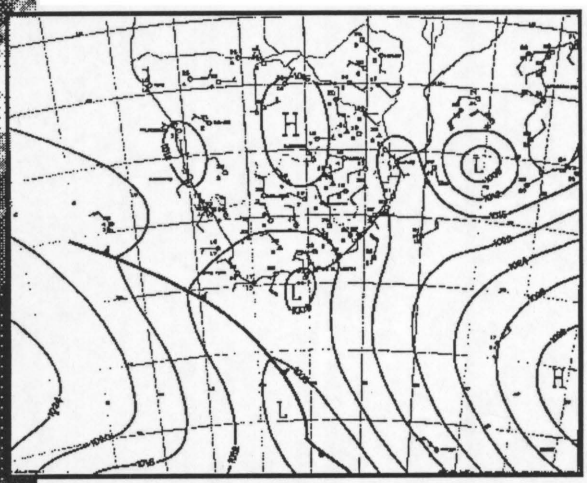

Figure 7.12 As Fig.7.2 but on 29 May 1996

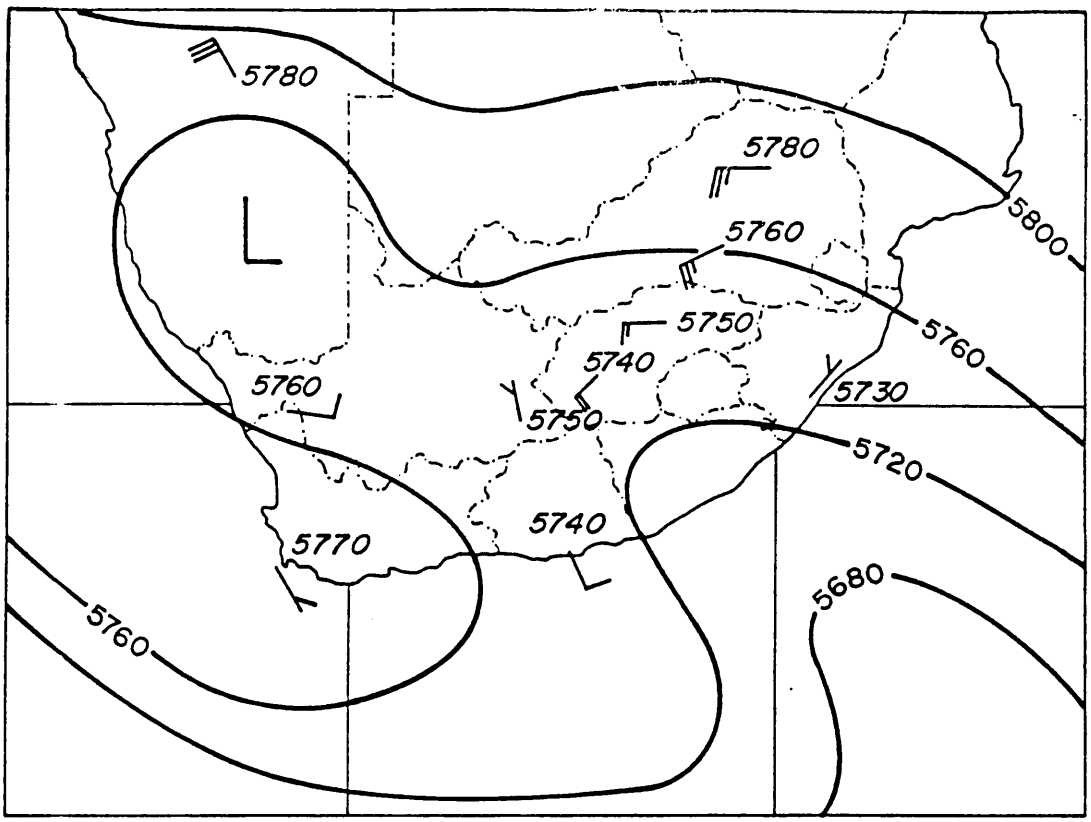

Fig. 7.13 500 hPa constant pressure map for 25 May 1996. Contours are in geopotential meters (gpm) and spacing in every 40 gpm.

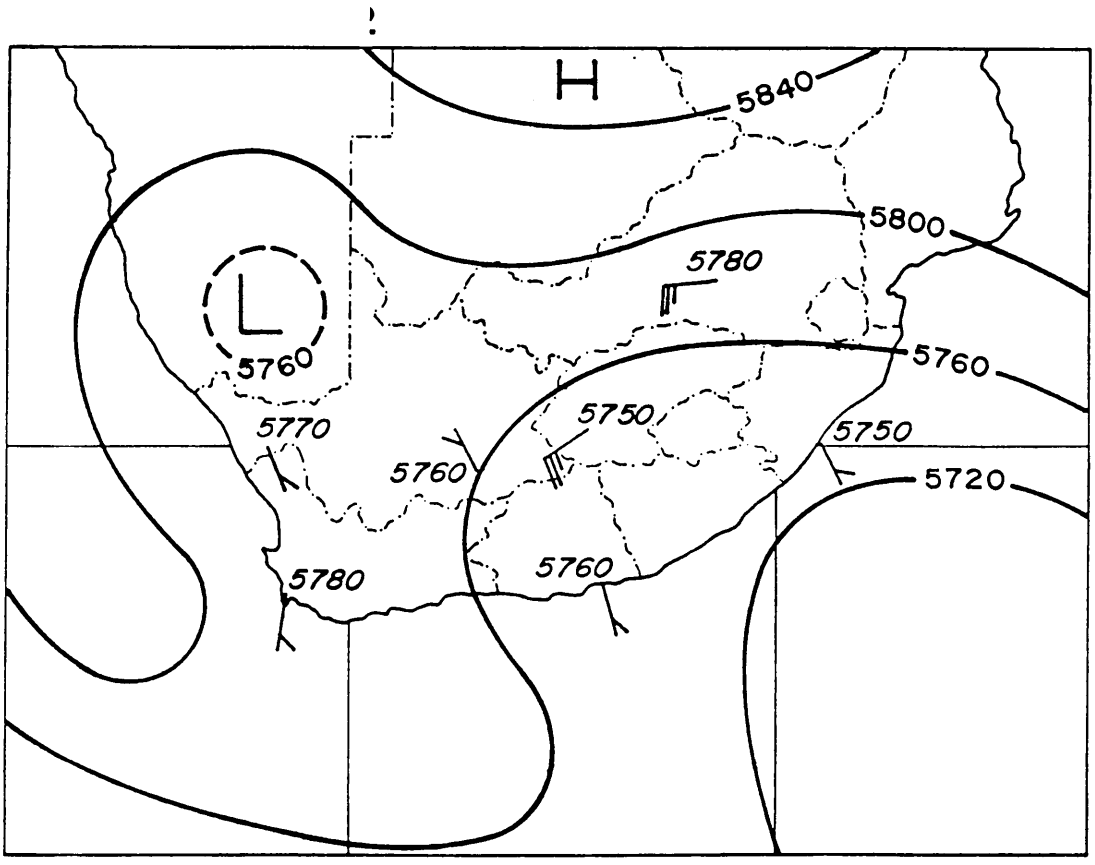

Fig. 7.14 As Fig. 7.13 but on 26 May 1996

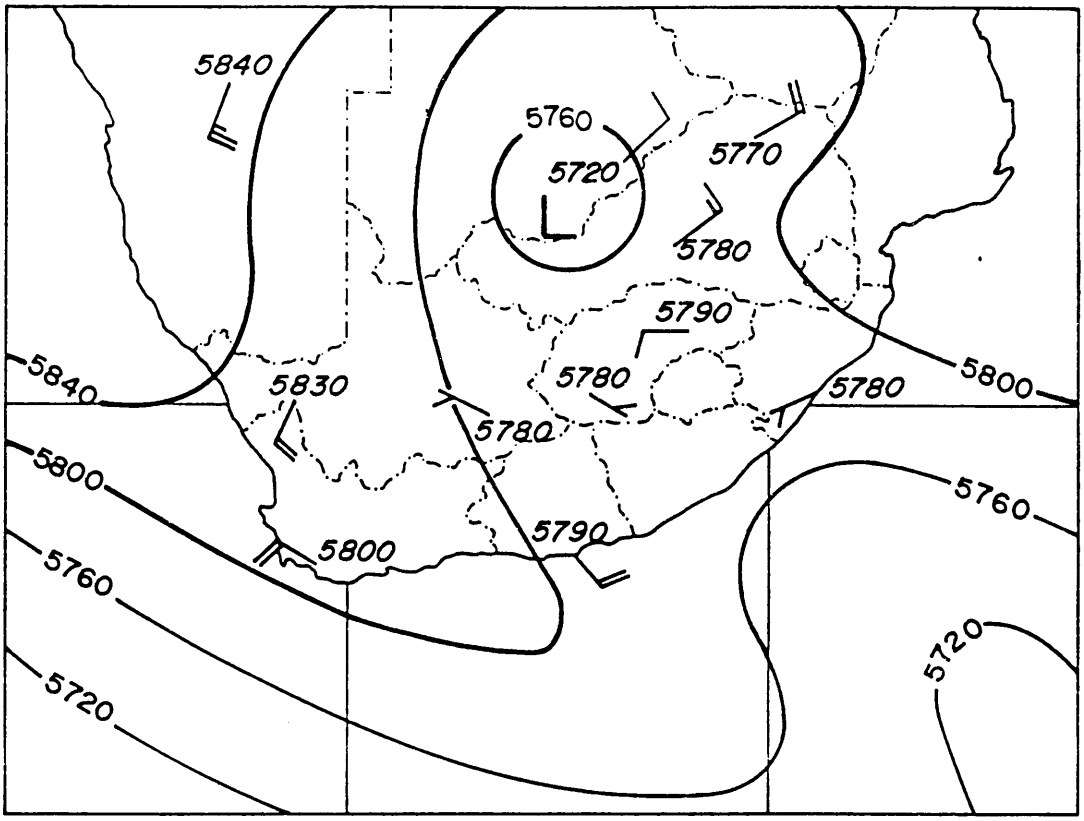

Fig. 7.15 As Fig. 7.13 but on 27 May 1996

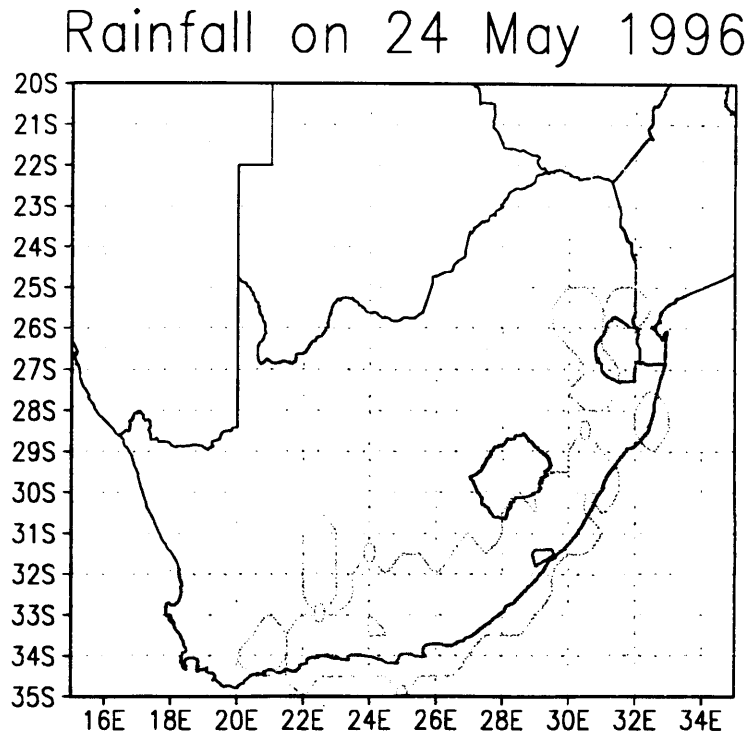

Fig. 7.16 **Rainfall on 24 May 1996 in millimeters. Spacing is 20 mm.**

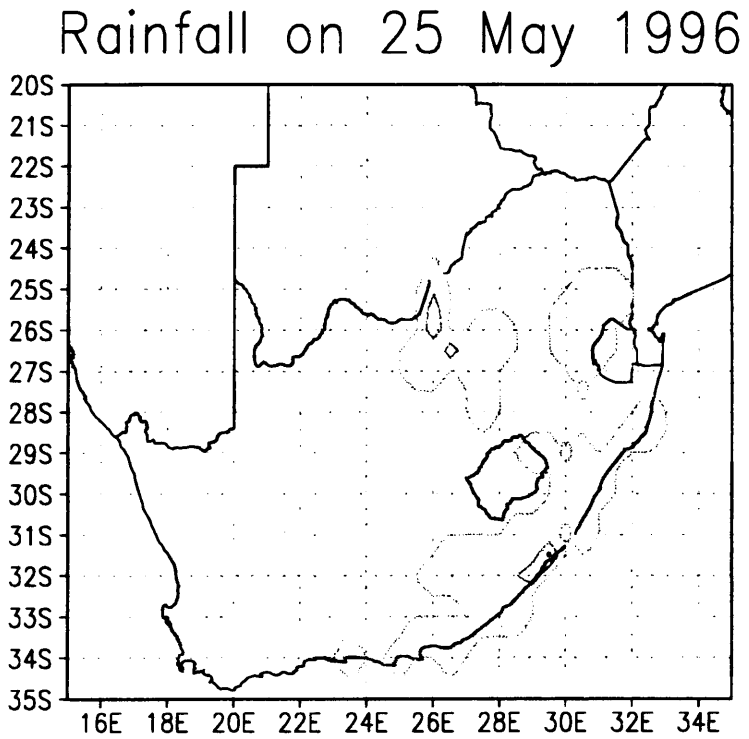

Fig. 7.17 **As Fig. 7.16 but on 25 May 1996**

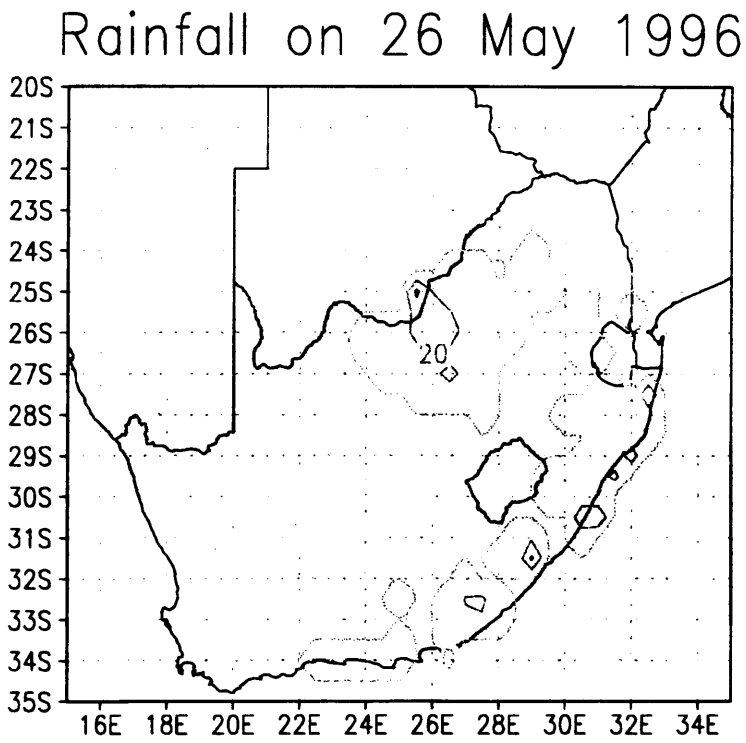

Fig. 7.18 As Fig. 7.16 but on 26 May 1996

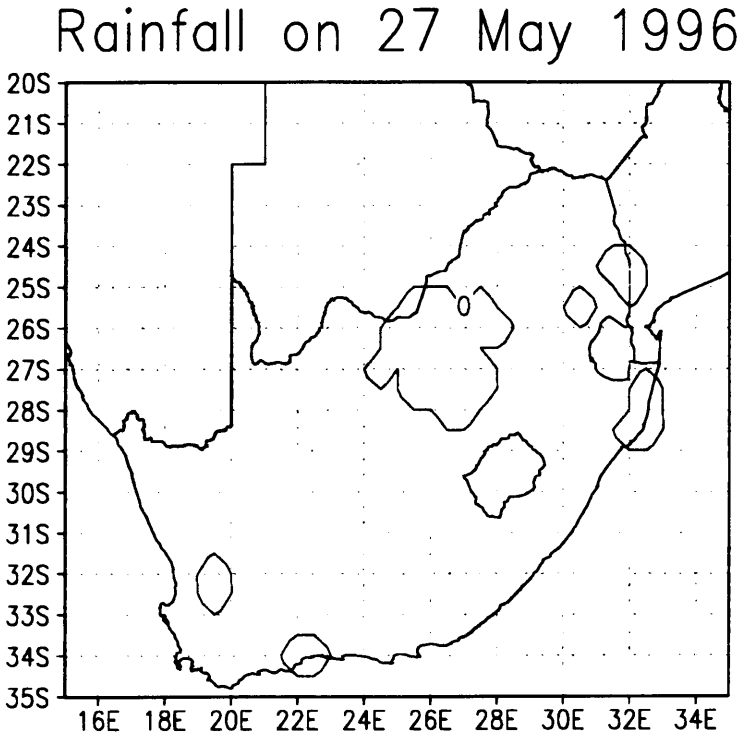

Fig. 7.19 As Fig. 7.16 but on 27 May 1996

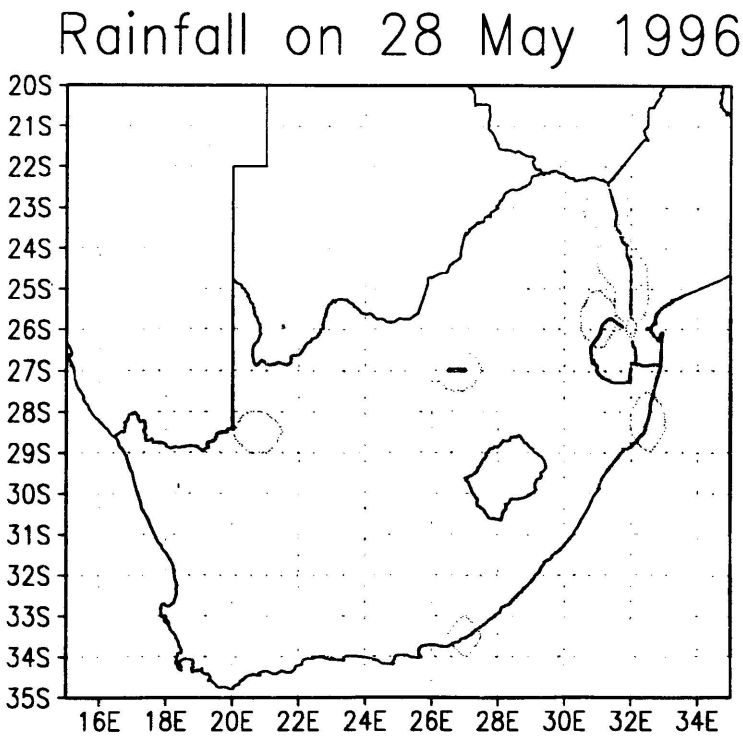

Fig. 7.20 **As Fig. 7.16 but on 28 May 1996**

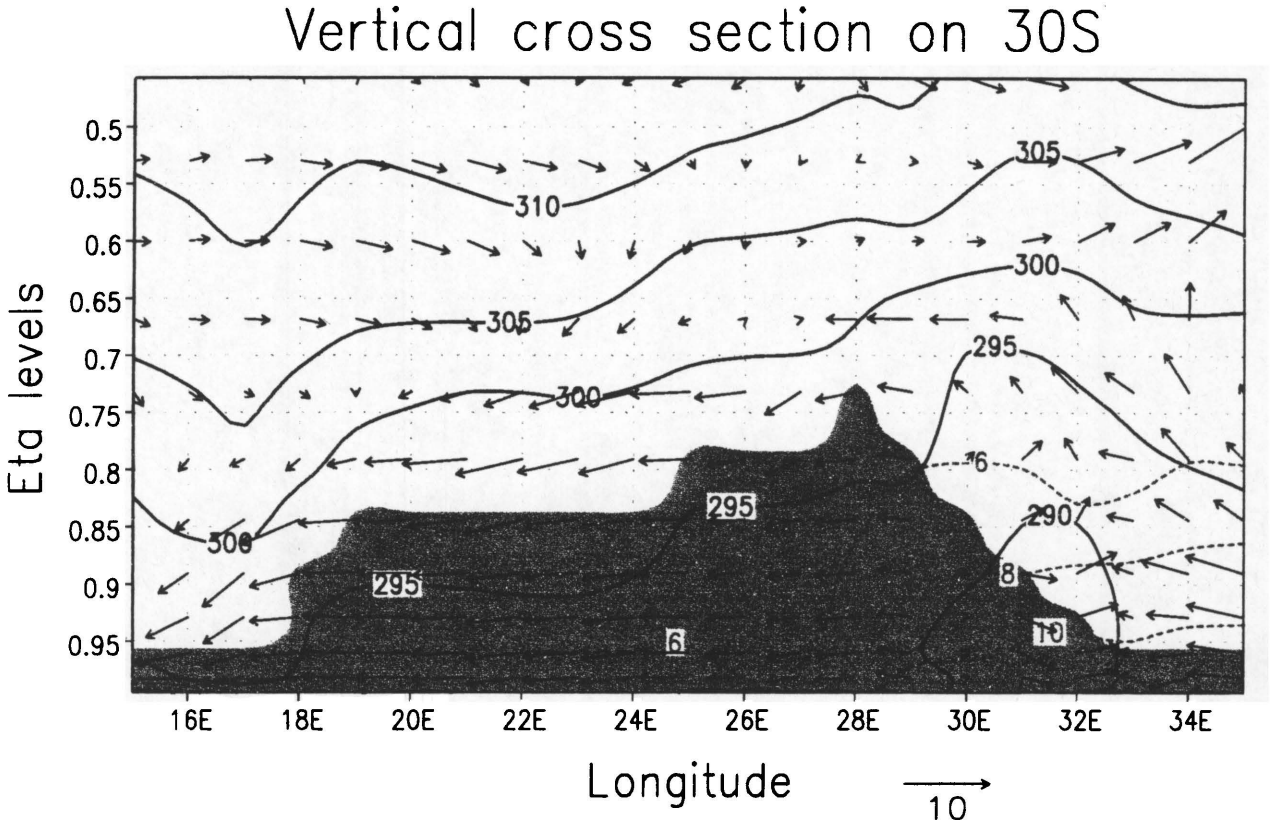

Fig. 7.21 **Vertical cross section at 30S on 25 May 1996 of potential temperature in Kelvin (solid line), horizontal component of the wind in m s^{-1}, vertical component of the wind in cm s^{-1}, and specific humidity in g kg^{-1}(dotted line). Topography is indicated by the shaded area.**

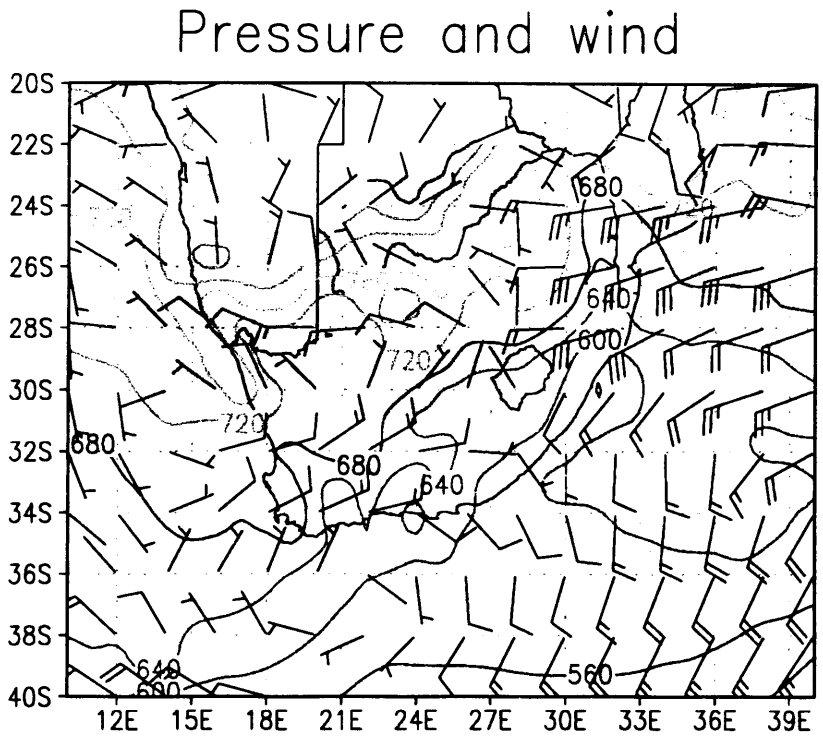

Fig. 7.22 Pressure on 305K on 25 May 1996 where pressure is in hPa and windspeed in knots.

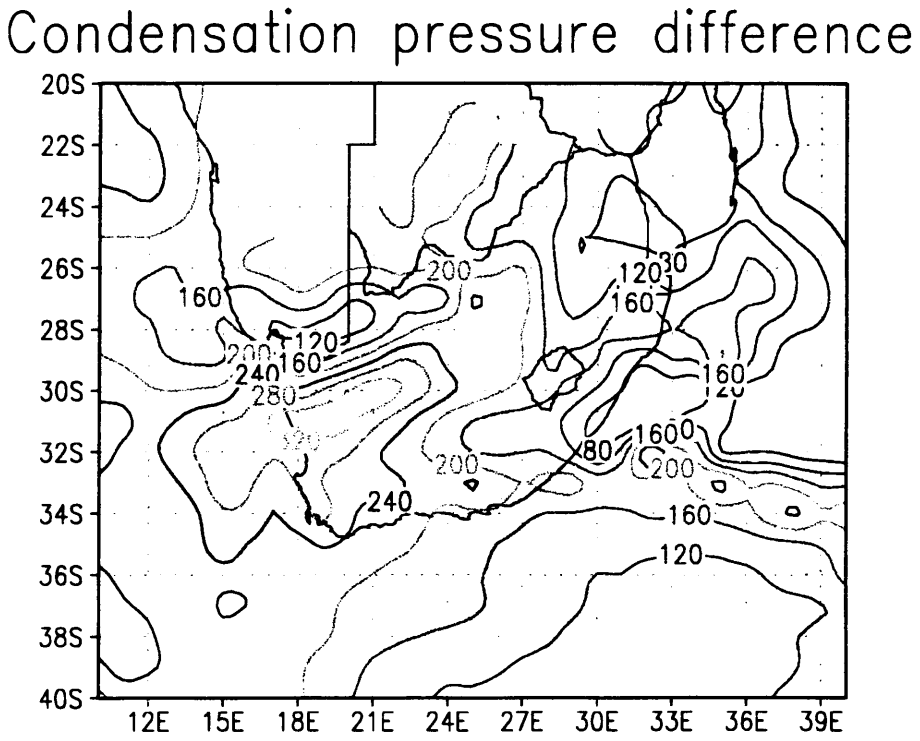

Fig. 7.23 Condensation pressure difference (hPa) on 305K on 25 May 1996

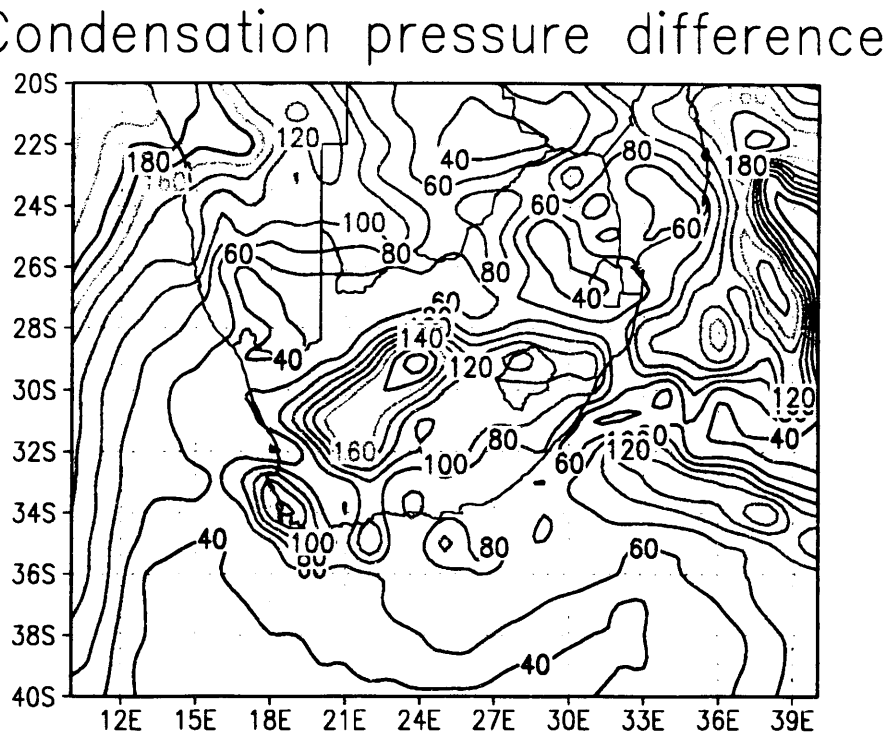

Fig. 7.24 Condensation pressure difference (hPa) on 315K on 25 May 1996

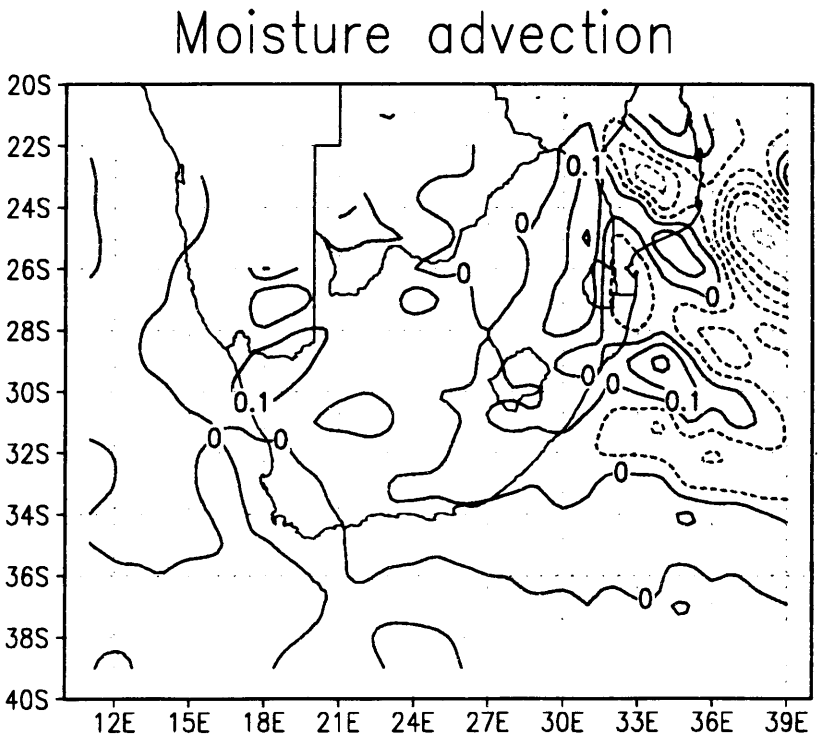

Fig. 7.25 Moisture advection (g kg^{-1} h^{-1}) on 305K on 25 May 1996

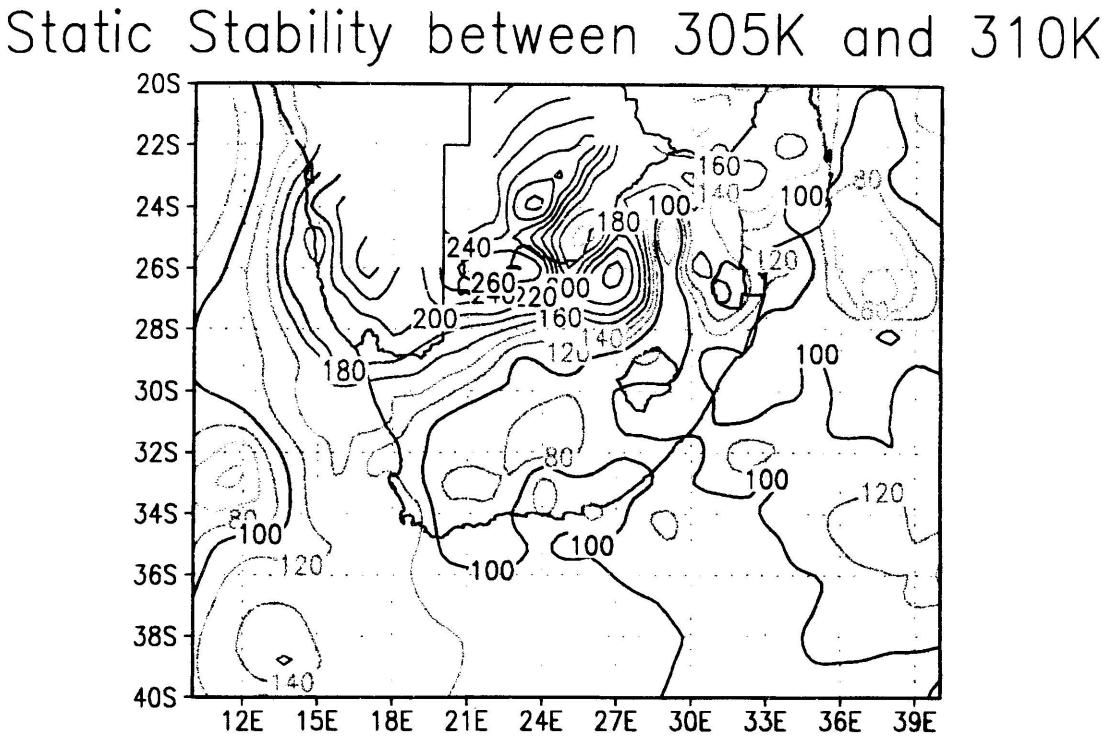

Fig. 7.26 Static Stability (hPa) between 305 and 310K on 25 May 1996

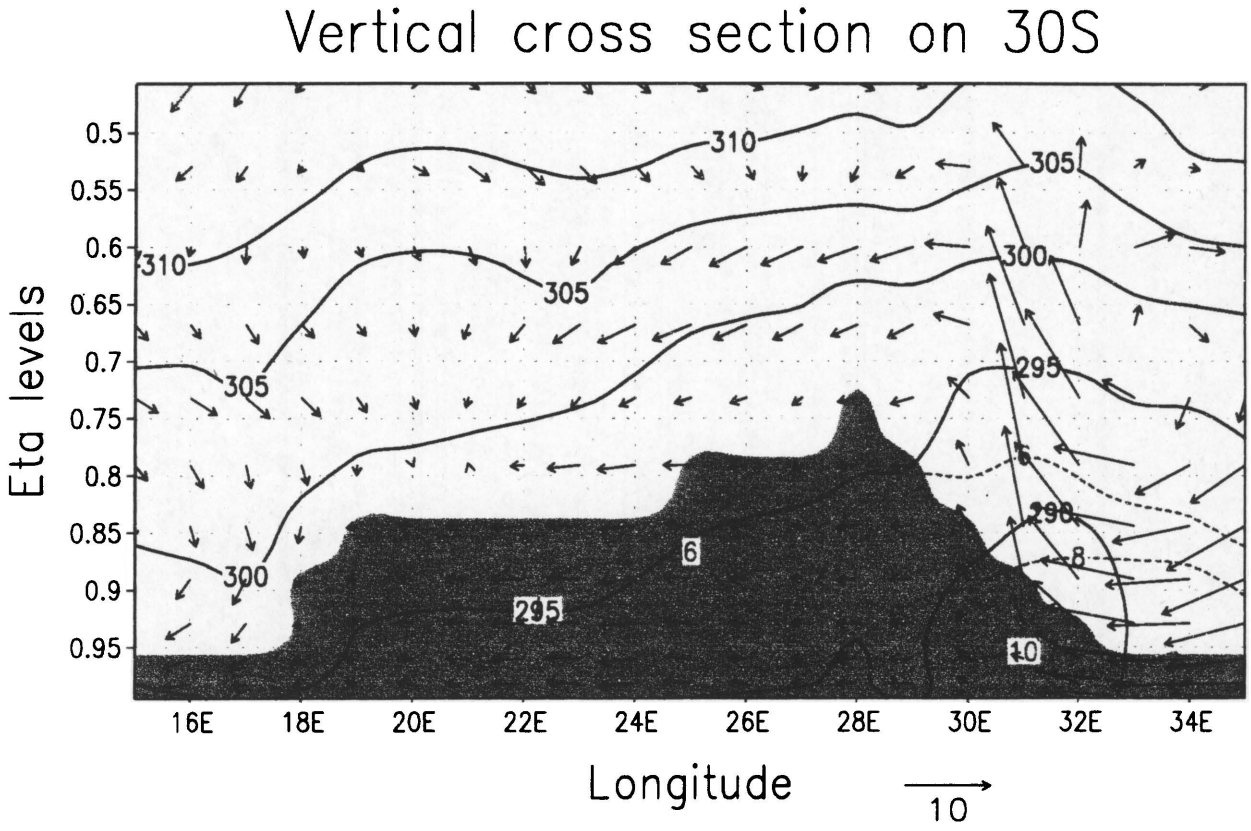

Fig. 7.27 As Fig. 7.21 but at 30S on 26 May 1996

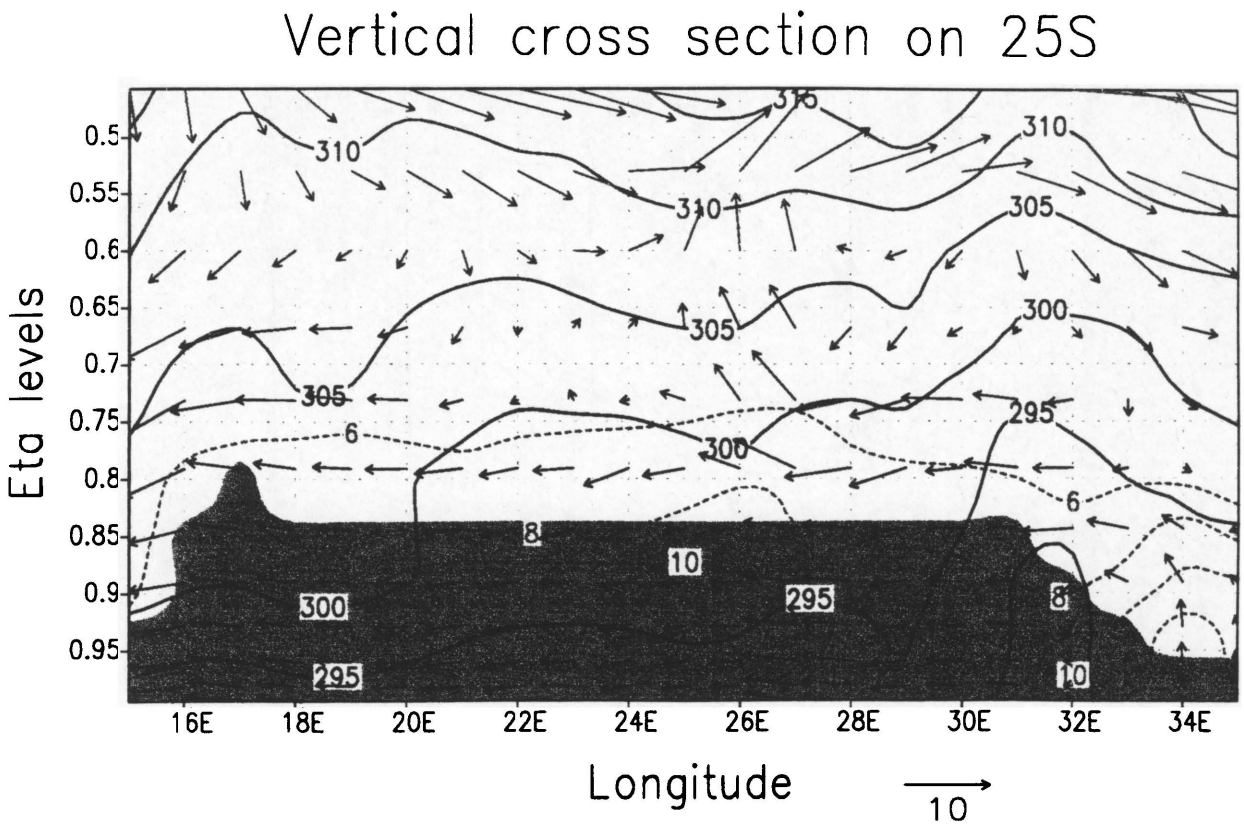

Fig. 7.28 **As Fig. 7.21 but at 25S on 26 May 1996**

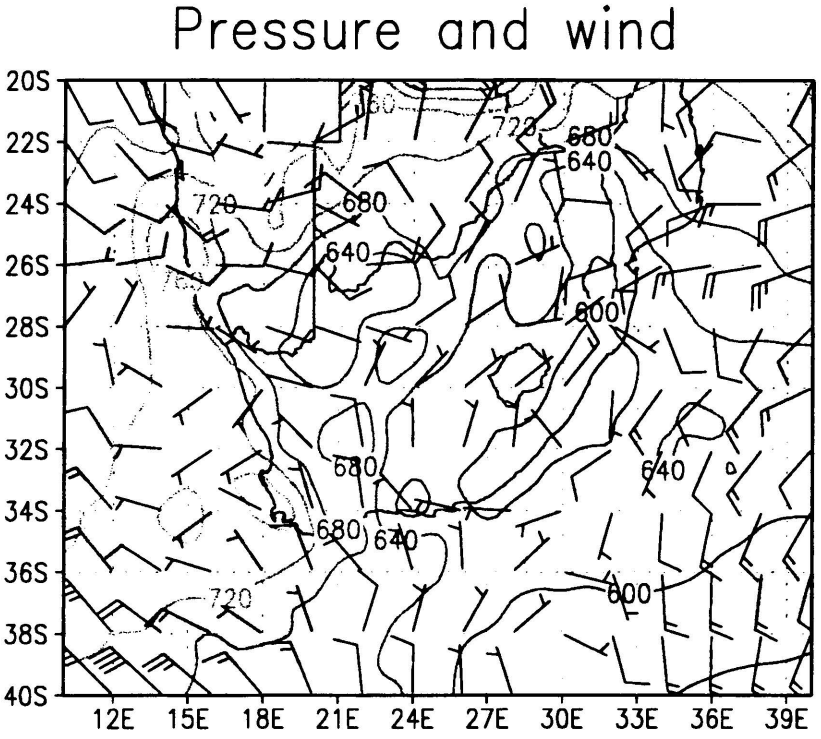

Fig. 7.29 **As Fig. 7.22 but on 26 May 1996**

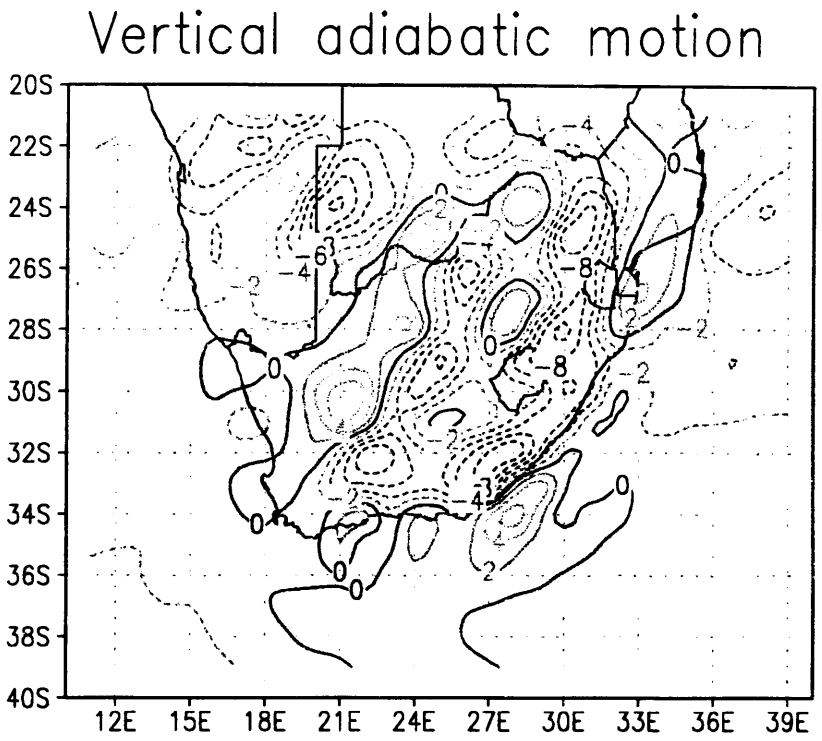

Fig. 7.30 Vertical adiabatic motion (microbar s^{-1}) on 315K on 26 May 1996

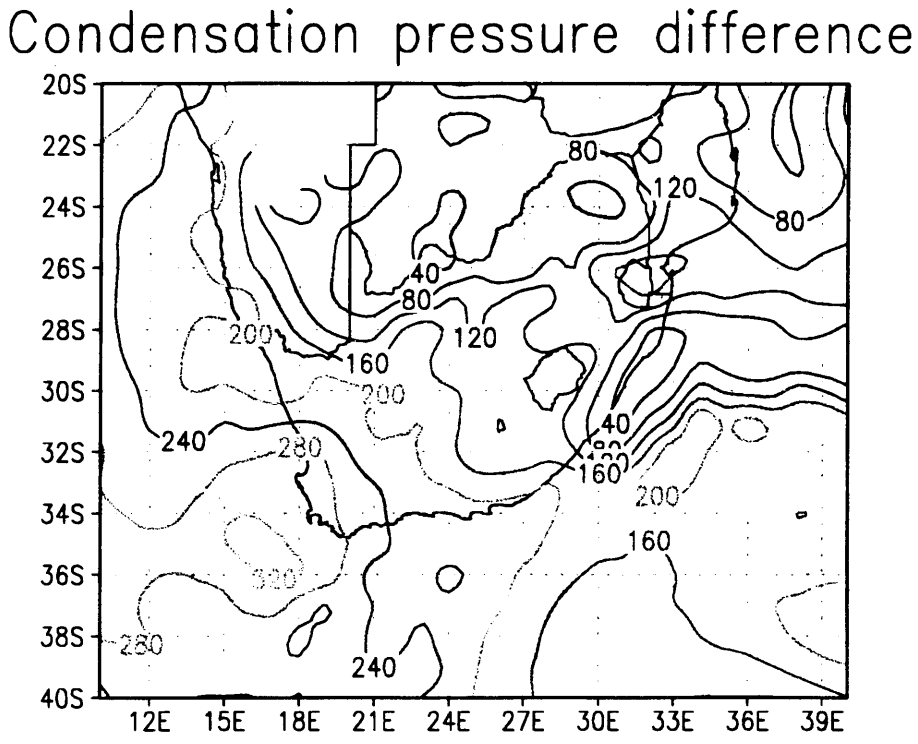

Fig. 7.31 Condensation pressure difference (hPa) on 305K on 26 May 1996

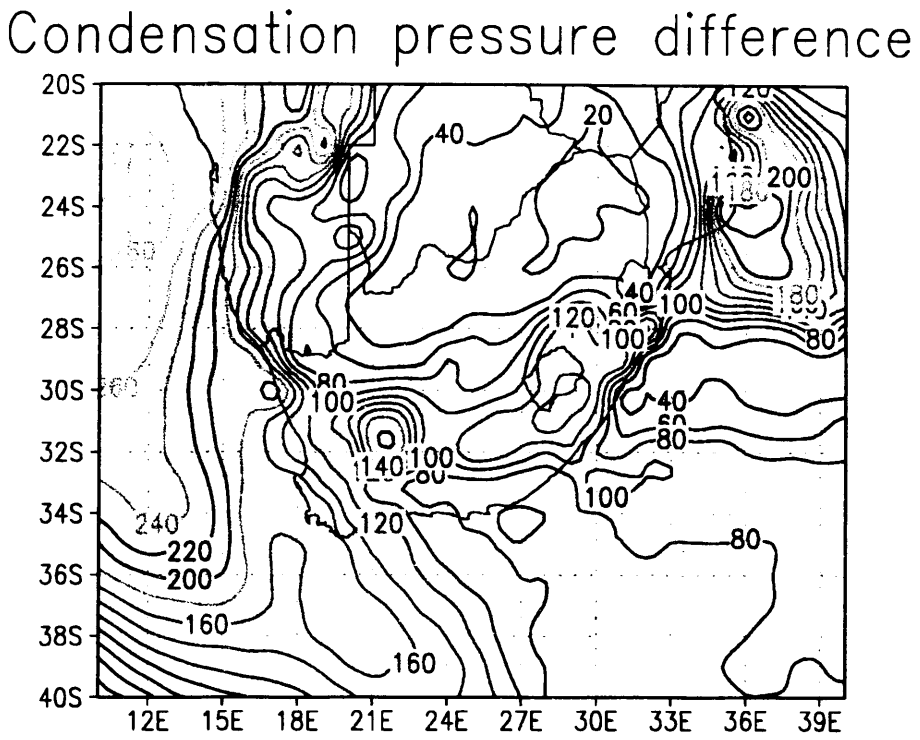

Fig. 7.32 Condensation pressure difference (hPa) on 315K on 26 May 1996

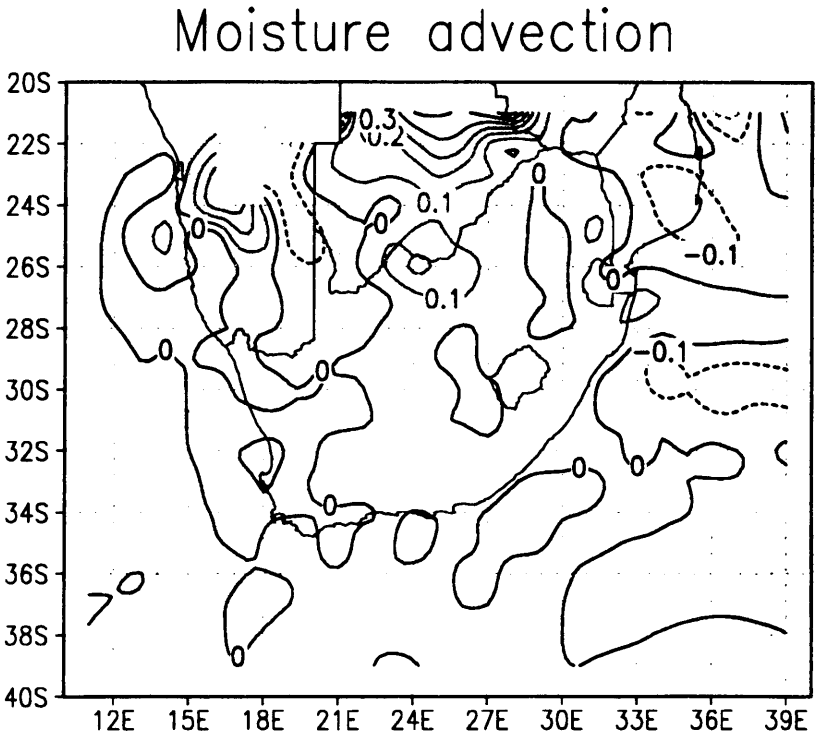

Fig. 7.33 Moisture advection (g kg^{-1} h^{-1}) on 305K on 26 May 1996

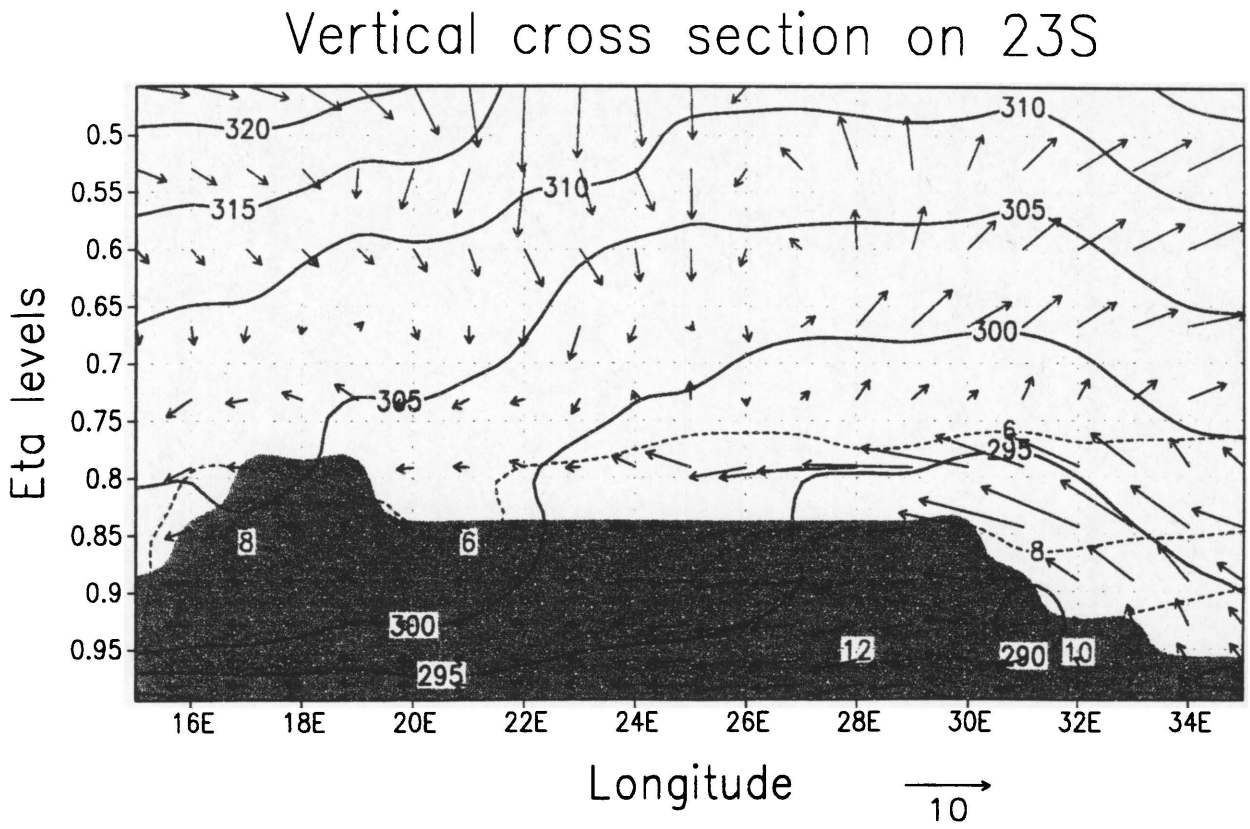

Fig. 7.34 As Fig. 7.21 but at 23S on 27 May 1996

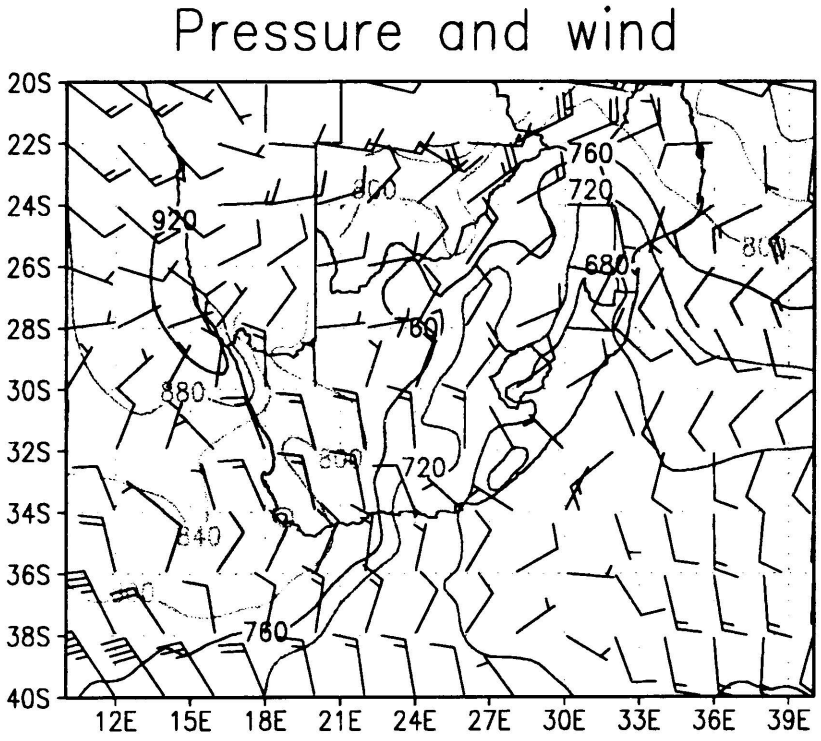

Fig. 7.35 As Fig. 7.22 but at 300K on 27 May 1996

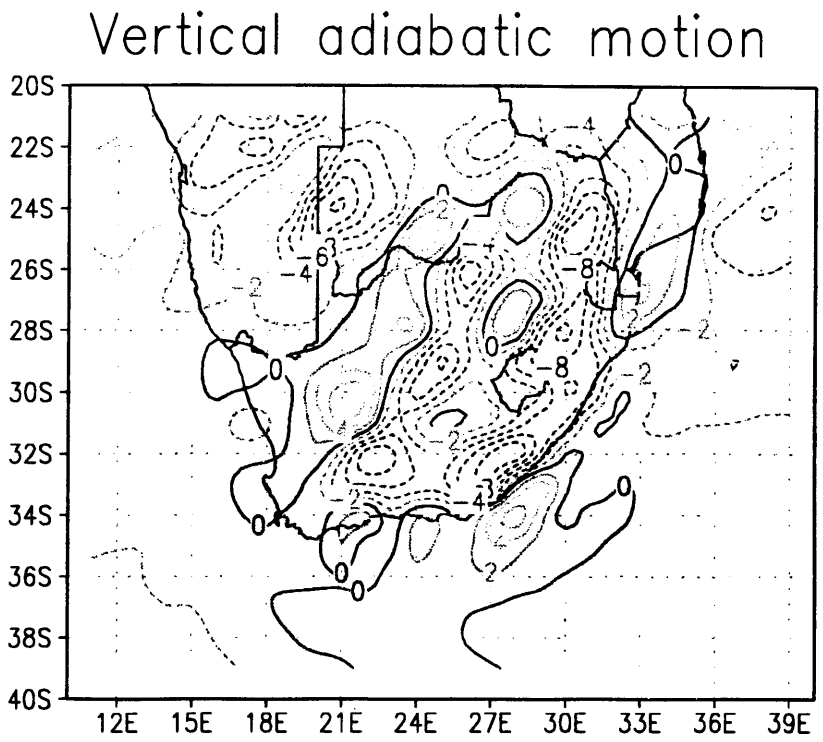

Fig. 7.36 Vertical adiabatic motion (microbar s^{-1}) on 315K on 27 May 1996

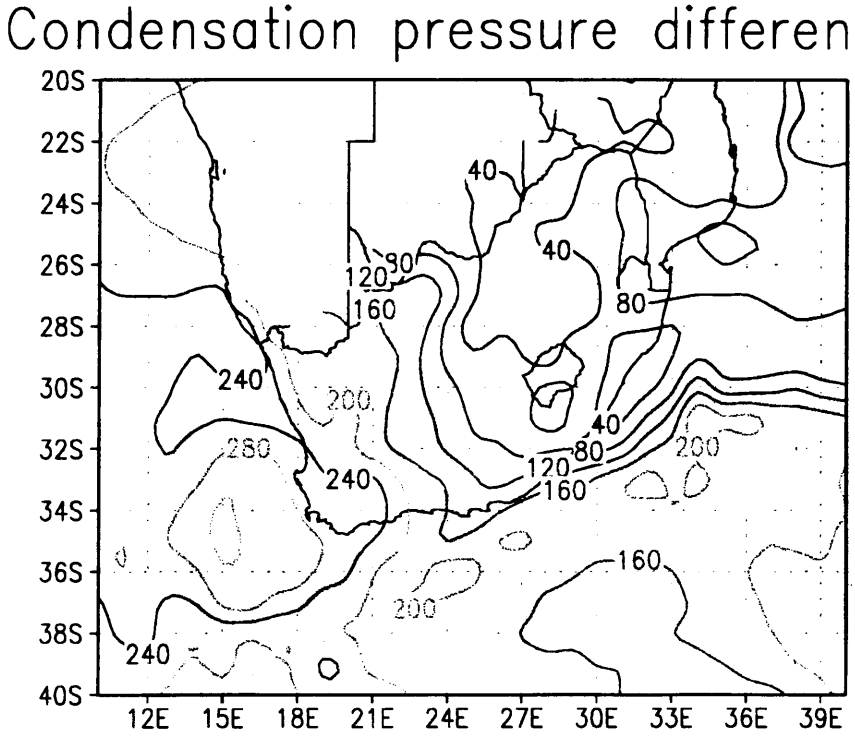

Fig. 7.37 Condensation pressure difference (hPa) on 300K on 27 May 1996

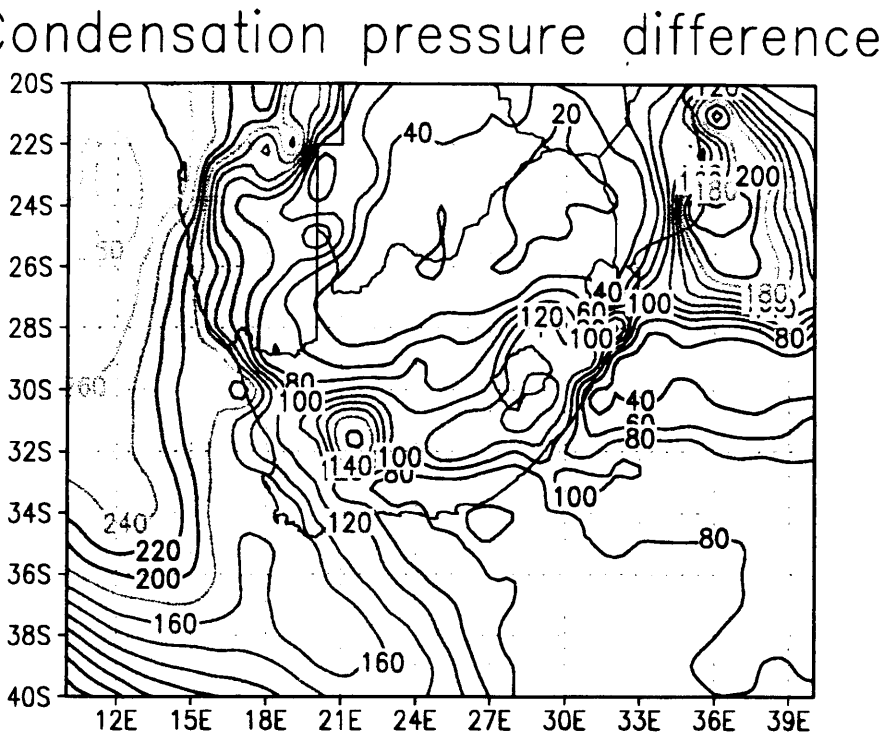

Fig. 7.38 Condensation pressure difference (hPa) on 315K on 27 May 1996

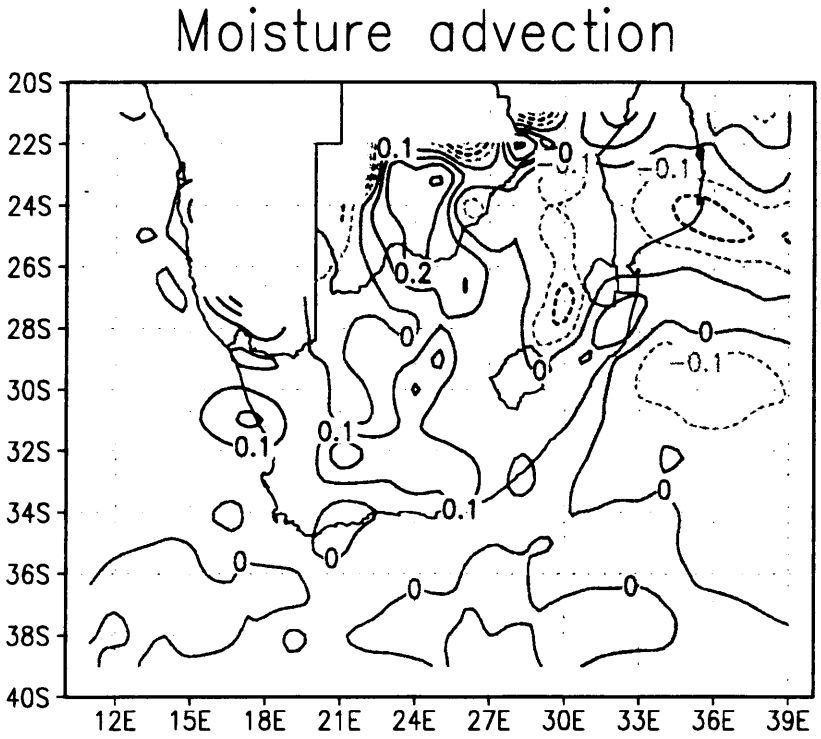

Fig. 7.39 Moisture advection (g kg^{-1} h^{-1}) on 300K on 27 May 1996

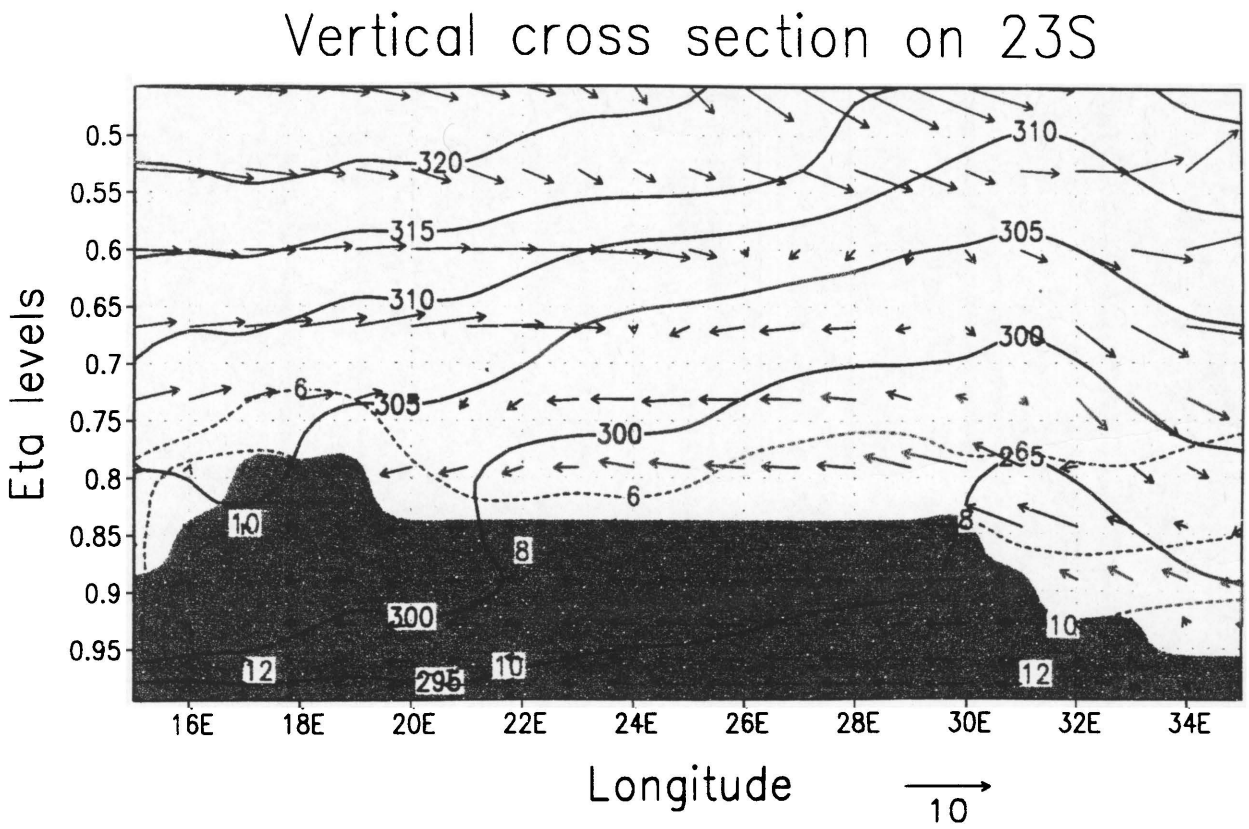

Fig. 7.40 **As Fig. 7.21 but at 23S on 28 May 1996**

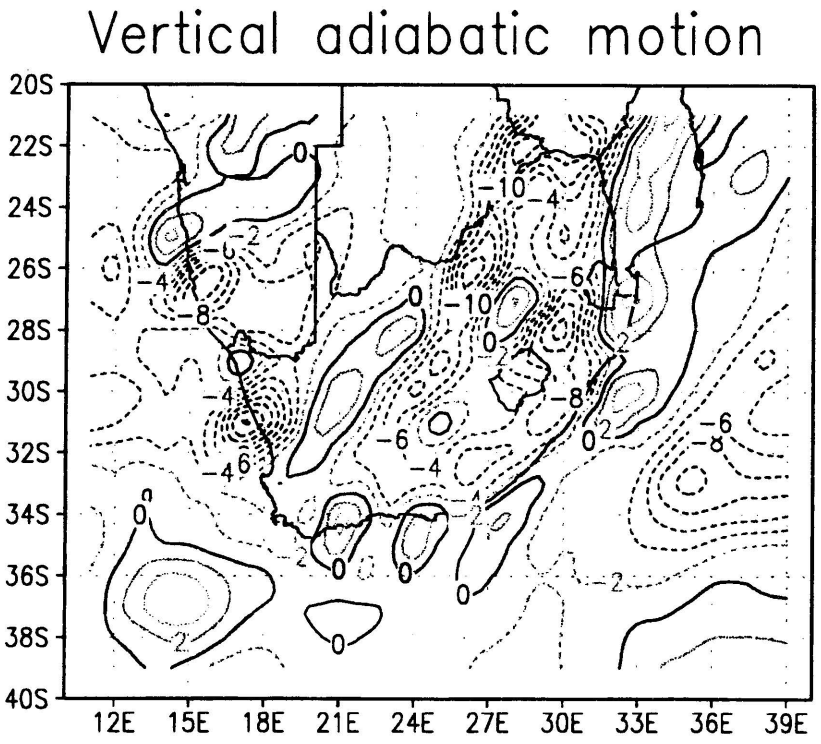

Fig. 7.41 **Vertical adiabatic motion (microbar s^{-1}) on 315K on 28 May 1996**

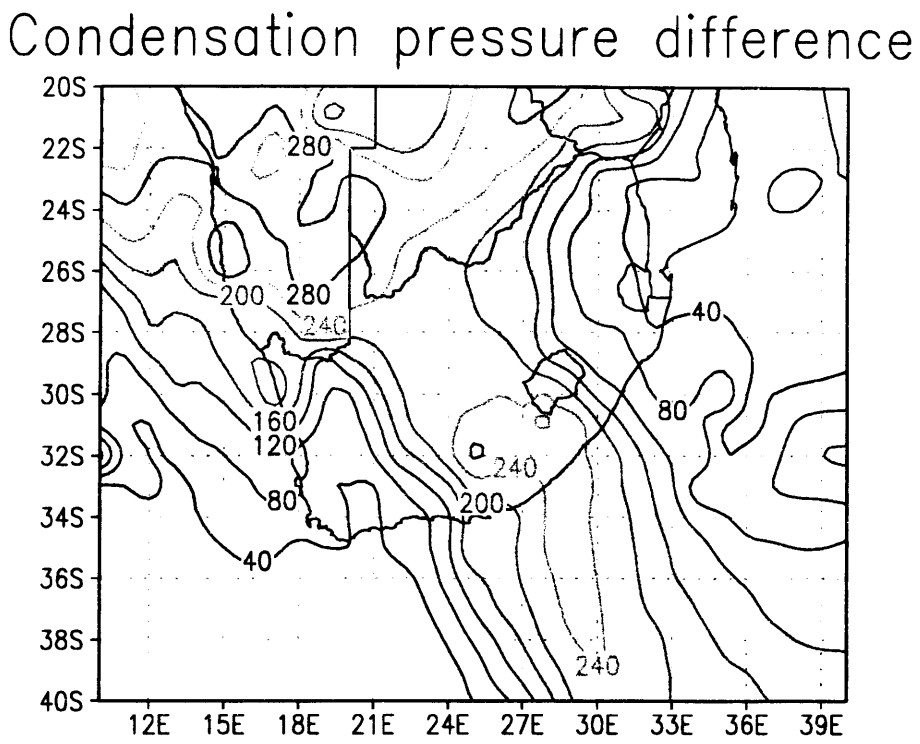

Fig. 7.42 Condensation pressure difference (hPa) on 315K on 28 May 1996

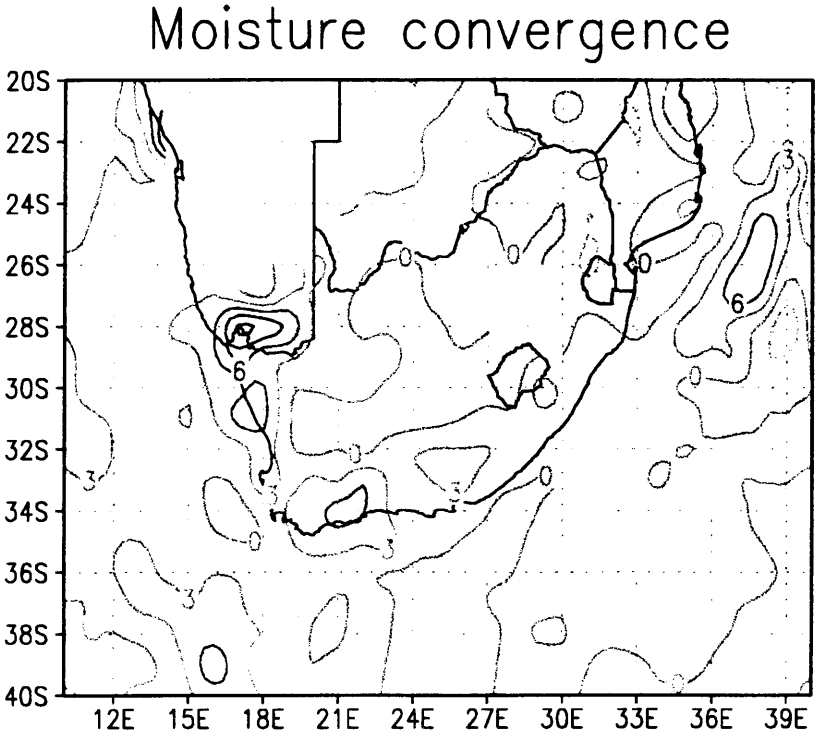

Fig. 7.43 Moisture convergence (g kg^{-1} h^{-1} X10) on 300K on 28 May 1996

CHAPTER 8

SUMMARY, CONCLUSIONS AND RECOMMENDATIONS

8.1 General summary

In this study isentropic analysis techniques were studied and implemented using the output of the Eta model. Using a model's output as input to isentropic analysis does have disadvantages, among these is a model's inability to have a completely realistic topography. The Eta model certainly is, however, one of the best numerical weather prediction models available with regard to modelling topography, and the excellent vertical and horizontal resolution of the model makes it worth the while.

The methods to calculate the different variables used on isentropic levels were described and a brief overview was given on the interpretation of these variables. Three case studies were undertaken of which two were in the heavy rainfall period in mid-summer (January and February 1996) and the last at the end of autumn (May 1996). In these cases different weather systems played key roles and the purpose was to determine whether isentropic analysis could have aided the weather forecaster in making the short term forecast.

8.2 Summary of results

A detailed summary of each case has been presented at the end of chapters 5, 6 and 7. Brief summaries are compiled here in order to intercompare cases and to show how various isentropic analysis display products can be used in different weather situations.

8.2.1 The January case study

Orographic uplift and subsequent moisture flux convergence along the escarpment played key roles in the rain production for the areas closest to the escarpment and this upward motion could clearly be seen on the vertical cross-sections.

The areas where heavier precipitation occurred generally coincided with the area where the condensation pressure values were the highest, the condensation difference values were less than 100 hPa (and even as low as 30 hPa) and where moisture accumulation (convergence) took place.

The presence of the summer time, warm, tropical air over the interior, as well as the passage of the cold front, when the colder maritime air replaced the warmer air, could clearly be seen on the pressure charts.

The Eta model did not handle the surface and upper air troughs/low pressure systems very well on the 25th, but a good indication of the rainfall area could nevertheless be obtained. Once the Eta model forecasts became more accurate throughout the remainder of the event, the isentropic analysis products again had value for operational forecasting.

8.2.2 The February case study

A general idea of the precipitation area was nearly always given by a combined interpretation of condensation pressure pattern (values of more than 600 hPa) and condensation differences (values less than 100 hPa). South Africa's topography played a major role in the rain production over the eastern parts and supplied enough orographic uplift to produce heavy falls.

A clear indicator of the area(s) where heavier falls would occur was given by low condensation difference values, positive moisture flux convergence and upward vertical motion.

The Eta model handled this case better than the January case (probably due to the fact that there were less tropical influences) and this contributed to more meaningful isentropic analysis results.

8.2.3 The May case study

The important difference between this case study and the previous two was that it was

a late autumn or winter situation. The colder temperatures were clearly indicated by the pressure charts with the passing of the cold front as well as the recovery afterwards when an off-shore flow developed.

The isentropic levels which were suitable for analysis of the lower levels were 300 or 305K, and 315K was chosen as the mid-level (close to 500 hPa) analysis level. Isentropic surfaces at lower potential temperature values were used in this cool season case.

The areas where heavier falls were reported could be identified by combining the vertical adiabatic motion patterns with the areas where the air was closest to saturation and where positive moisture flux convergence and advection took place.

8.3 Conclusions and recommendations

In the light of the positive results obtained in these three case studies and the results of other researchers, it seems inevitable that isentropic analysis should be part of the short term forecasting process in the South African Weather Bureau. Although isentropic analysis does not solve every forecasting problem and will only be a tool additional to isobaric analysis, it can certainly be used to the advantage of the forecasting process.

New display products as output of the Eta model can be made available to the forecaster. These include:

a) vertical cross-sections,
b) two-dimensional winds and pressure,
c) adiabatic vertical motion,
d) condensation pressure difference,
d) moisture advection,
e) moisture flux convergence and
f) static stability

for the chosen isentropic level. Not every product is equally revealing in every situation.

Different factors and processes are dominant from one case to the next. Thus, a very good way for the forecaster to use the products is to intercompare the isentropic analyses to cloud patterns from satellite images. The charts which correlate well can then be used to better understand the nature of the forcing of that day's weather.

One of the most important advantages of isentropic analysis is that a "third" or vertical dimension is built into the parameters due to the fact that isentropic surfaces vary with height or pressure. Because air tends to follow these sloping isentropic surfaces, isentropic analysis can be extremely useful in the identification of the movement of dry or moist and cold or warm tongues of air.

Another important advantage is that limiting streamlines can be used to distinguish between air masses of different origin. This can make the distinction between maritime or continental and tropical or polar air masses easier. If such a limiting streamline coincides with the cloud band and moisture flux convergence and/or low stability, it might be indicative of the area where development might take place.

Isentropic analysis can give a forecaster additional information about the weather situation which is not available on isobaric surfaces and therefore short term forecasting of the weather will definitely benefit.

Uccellini (1976) stated that: "*The increasing number of meteorologists who are becoming acquainted with isentropic analysis recognize it as a valuable tool and they desire the transmission of detailed isentropic charts to supplement the current standard pressure analysis.*" If this was the case in America in 1976, isentropical analysis can surely also come to mean a great deal to South African weather forecasters.

Even though the isentropic way of thinking is totally different from what a forecaster is accustomed to, it is not impossible either to train the forecasters in this "new" way of thinking, or to present the output of isentropic analysis charts in a way that is user friendly and easy to interpret.

REFERENCES

Anderson, J.L.1984. *The use and interpretation of isentropic analyses.* Scientific Services Division, National Weather Service Western Region, Salt Lake City, Utah. (NOAA Technical memorandum NWS WR-188).

Bleck, R. 1973. Numerical Forecasting Experiments Based on the Conservation of Potential Vorticity on Isentropic Surfaces. *J. Appl. Meteor.*, 12:737-752.

Byers, H.R. 1938. On the thermodynamic interpretation of isentropic charts. *Monthly Weather Review*, 66:3:63-69.

Carlson, T.N. 1991. Airflow through mid-latitude synoptic scale disturbances . *In: Mid-latitude Weather Systems.* NY: Harper-Collins Academic. p. 284-341.

Danielsen, E. F.1959. The Laminar Structure of the Atmosphere and its relation to the Concept of the Tropopause. *Arch. Meteor. Geophys., BioKlim, Atol., Ser. A*, 11:232-293.

Danielsen, E.F. 1961. Trajectories: Isobaric and Actual. *J. Meteor.* 18:479-486.

Gerard, A. 1995. Ground-relative and System-relative vertical motion fields on isentropic surface. *Proceedings of the Conference on Isentropic Analysis and forecasting.* Lancaster, Pennsylvania, March 31 - April 2, 1995. p.14-16.

Harrison, M.S.J. 1986. *A synoptic climatology of South African rainfall variations.* Johannesburg: University of the Witwatersrand. (Ph.D. thesis)

Hess, S. L. 1959. *Introduction to Theoretical Meteorology.* New York. Holt, Rinehart and Winston.

Holton, J.R. 1979. The Basic Conservation Laws. *In: An introduction to Dynamic Meteorology Second Edition.* Orlando, Florida: Academic Press Inc. p. 26-53.

Kirkpatrick, J.D. 1992. The February 1989 Flood in Kentucky. *National Weather Digest.* 17:3:2-18.

Kurz, M. 1994. The role of diagnostic tools in modern weather forecasting, *Met Apps.* 1: 45-67

Leroux, M. 1983. *The Climate of tropical Africa*. Paris: Champion.

Market, P.S. & Moore, J.T. 1995. An isentropic perspective on elevated thunderstorms with heavy rainfall. *Proceedings of the Conference on Isentropic Analysis and forecasting.* Lancaster, Pennsylvania, March 31 - April 2, 1995. p.37-29.

Mesinger, F. 1984. A blocking technique for representation of mountains in atmospheric models. *Riv. Meteor. Aeronautica*, 44:195-202

Mesinger, F. , Janjić, Z., Ničković, S., Gavrilov, D. & Deaven, D. 1988. The Step-Mountain Coordinate: Model description and preformance for cases of Alpine lee cyclogenesis and for a case of an Appalacian redevelopment. *Monthly Weather Review,* 116:1493-1518.

Mills, G.A. & Bao-Jun, W. 1995: The Cuddle Creek Flash flood - an example of synpotic scale forcing of a mesoscale event. *Australian Met. Magazine*, 44:201-218.

Montgomery, R. B. 1937. A suggested method for respresenting gradient flow in isentropic surfaces. *Bull. Amer. Meteor. Soc.* 18:210-212.

Moore, J.T. 1992. *Isentropic Analysis and interpretation: Operational applications to synoptic and mesoscale forecast problems.* Department of Earth and Atmospheric Sciences, Saint Louis University.

Namias, J. 1940. Isentropic Analysis. *In:* Robert G. Stone. *An Introduction to the study of Air Mass and Isentropic Analysis*, Boston, MA: Amer. Met. Soc. 136-175

Nolan, M. & Moore, J.T. 1995. An isentropic analysis of a heavy snow event associated

with weak cyclogenesis. *Proceedings of the Conference on Isentropic analysis and Forecasting.* Lancaster, Pennsylvania, March 31 - April 2, 1995. p. 5 - 7.

Oliver, V.J. & M.B. Oliver. 1951. Meteorological Analysis in the middle latitudes. Compendium of Meteorology, Boston, MA: Amer. Meteor. Soc., 715-727.

Philips, N.A. 1957. A coordinate system having some special advantages for numerical forecasting. *J. Meteor.*.14:297-300.

Presston-Whyte R.A. & Tyson P.D. 1988. Modelling in meteorology and climatology. *In: The Atmosphere and weather of Southern Africa.* Cape Town: Oxford University Press. p. 319-338.

Rogers, R.R. & Yau, M.K. 1989. *A short course in cloud physics. Third Edition*, Great Brittan: Pergamon Press.

Rossby, C.G. and collaborators. 1937. Isentropic Analysis, *Bull. Amer. Meteor.* 18:201-209.

Schulze, B.R. 1984.: *Climate of South Africa, Part 8, General Survey*, Pretoia: Weather Bureau, Department of Transport. (WB28)

Spaete, P., Johnson D.R. & Schaak, T.K. 1993. Stratospheric-tropospheric mass exchange during the President's Day Storm. *Monthly Weather Review.* 122:424-439.

Taljaard, J.J. 1982. Cut-off lows and heavy rain over the Republic. *South African Bureau Newsletter.* 403:155-156.

Taljaard, J.J. 1995. *Atmospheric Circulations systems in the South African region Part 2 : Atmospheric Circulation Systems, synoptic Climatology and weather phenomena of South Africa.* Pretoria: Goverment Printer. (Technical paper 28)

Treadon, R. 1993. *The NMC ETA model post processor : a Documentation.* NWS. (Office Note 394).

Uccellini, L.W. 1976. Operational Diagnostic Applications of Isentropic Analysis. *Nat. Wea. Dig.* 1:4-12.

Uccellini, L.W. 1995. Conference on isentropic Analysis. *In: Proceedings of the Conference on Isentropic Analysis and Forecasting.* Lancaster, Pennsylvania, March 31 - April 2, 1995. p. 11-13.

Van Heerden J. & Hurry, L., (1987) : *Southern Africa's weather patterns : an introductory guide, 2nd edition.* Pretoria: Acacia.

Wallace, J.M. & Hobbs, P.V. 1977. Atmospheric thermodynamics. *In: Atmospheric Science - An introductory survey.* Orlando, Florida: Academic Press Inc. p. 47-107.

Wilson, L.J. 1985. Isentropic Analysis - Operational Applications and Interpretation, third edition. Edited for Training Branch by James Percy. Atmospheric Environment Service, Canada, 35p.

Wilson, L.J., Siok S. & Marios, B. 1980. Operational application of isentropic analysis to the diagnoses of severe convective weather threat areas. *Proceedings of the Eighth Conference on Weather Forecasting and Analysis.* Denver, CO. Jun 10 -13, 1980. Amer. Meteor. Soc., 166-173.

APPENDIX A: Software code

```
# QSUB -s /bin/ksh
# QSUB -eo
# QSUB -lM 8Mw -lm 8Mw
# QSUB -lT 300 -lt 200
# QSUB -u eugene
# QSUB -q research

set -x

######################## isentrop5.p ########################
### Creates fileds for isentropic analysis for case studies
#############################################################
algdir=/home/short/eugene/estelle
locdir=/home/short/eugene/estelle/isen
export locdir
cd $TMPDIR
### horisontale deursnitte
$locdir/horgeval 00 /home/short/eugene/estelle/isen/dat/96012500/

rm -f $locdir/dat/96012500/isen*00.dat

$locdir/horgeval 12 /home/short/eugene/estelle/isen/dat/96012500/
rcp $locdir/dat/96012500/isenp12.dat estelle@navors1:dat/96012500/
rcp $locdir/dat/96012500/isenu12.dat estelle@navors1:dat/96012500/
rcp $locdir/dat/96012500/isenv12.dat estelle@navors1:dat/96012500/
rcp $locdir/dat/96012500/isenr12.dat estelle@navors1:dat/96012500/
rcp $locdir/dat/96012500/isenq12.dat estelle@navors1:dat/96012500/
rcp $locdir/dat/96012500/isenm12.dat estelle@navors1:dat/96012500/
rcp $locdir/dat/96012500/isenpc12.dat estelle@navors1:dat/96012500/
rcp $locdir/dat/96012500/isentp12.dat estelle@navors1:dat/96012500/
rcp $locdir/dat/96012500/isenav12.dat estelle@navors1:dat/96012500/
rcp $locdir/dat/96012500/isenw12.dat estelle@navors1:dat/96012500/

rm -f $locdir/dat/96012500/isen*12.dat

#### bereken c
$locdir/berekc2 12 /home/short/eugene/estelle/isen/dat/96012500/
rcp $locdir/dat/96012500/isencu12.dat estelle@navors1:dat/96012500/
rcp $locdir/dat/96012500/isencv12.dat estelle@navors1:dat/96012500/

rm -f $locdir/dat/96012500/isenc*.dat

################################
### vertikale deursnitte
$locdir/vergeval 12 /home/short/eugene/estelle/isen/dat/96012500/
rcp $locdir/dat/96012500/isenvu12.dat estelle@navors1:dat/96012500/
rcp $locdir/dat/96012500/isenvv12.dat estelle@navors1:dat/96012500/
rcp $locdir/dat/96012500/isenvw12.dat estelle@navors1:dat/96012500/
rcp $locdir/dat/96012500/isenvq12.dat estelle@navors1:dat/96012500/
rcp $locdir/dat/96012500/isenvth12.dat estelle@navors1:dat/96012500/
rcp $locdir/dat/96012500/isenvrf12.dat estelle@navors1:dat/96012500/

rm -f $locdir/dat/96012500/isenv*12.dat

set +x
```

```
      Program horgeval
*** This programme prepares data for horizontal isentropic surfaces
*** for case studies.
      dimension grid(19,10,8646),ref(8646)
      dimension jpos(9),kpos(9)
      character*20 field(60)
      character proj*6,arg1*2,outfn*80,datain*80,dataout*80
      logical north
      REAL eta(19),SFC(19),Ps(8646),Zs(8646),Zsgr(66,131)
      REAL Ua(8646),Va(8646)
      REAL T1(19,8646),P1(19,8646),U1(19,8646),V1(19,8646)
      REAL W1(19,8646),Q1(19,8646),R1(19,8646),Z1(19,8646)
      REAL M1(19,8646),A1(19,8646)
      REAL Te(19,8646),Ue(19,8646),Ve(19,8646),We(19,8646)
      REAL RHe(19,8646),Ze(19,8646),Pe(19,8646),Qe(19,8646)
      REAL Me(19,8646),AVe(19,8646)
      REAL THO(9)
      REAL Ti(9,8646),Ui(9,8646),Vi(9,8646),Wi(9,8646)
      REAL RHi(9,8646),Zi(9,8646),Pi(9,8646),Qi(9,8646)
      REAL Mi(9,8646),AVi(9,8646),Tci(9,8646),Pci(9,8646)
      REAL Tgr(9,66,131),Ugr(9,66,131),Vgr(9,66,131),Wgr(9,66,131)
      REAL RHgr(9,66,131),Zgr(9,66,131),Pgr(9,66,131),Qgr(9,66,131)
      REAL AVgr(9,66,131),Mgr(9,66,131),PCgr(9,66,131)
      REAL Uagr(66,131),Vagr(66,131)
      REAL AVmax(9)
      REAL teken(9,66,131),verskil(9,66,131)
*** work on 19 eta levels
      PARAMETER(km= 19 )
*** work on 9 isentropic levels
      PARAMETER(KO= 9 )
*** work from bottom to top
      data THO/290.,295.,300.,305.,310.,315.,320.,325.,330./
*** read hour
      call getarg(1,arg1)
      read(arg1,'(i2)')iuur
c     print*,'Lopie is vir ',iuur,' uur data'
*** read output of postprocessor
      write(outfn,'("/tmp/pcst"
     *,i2.2,".tm00")')iuur
      open(1,file=outfn)
      open(2,file='/home00/estelle/isen/dat/ref.dat')
            READ(1,'(30x,5(I5,1X))')IHRST,IMM,IDD,IYY,IHH
            READ(1,'(30x,I5,1X,A6,1X,L1,1X,I5,1X,I5)')
     2                      KGTYP,PROJ,NORTH,IMOUT,JMOUT
            READ(1,'(30x,4(G12.6,1X))')
     2                      POLEI,POLEJ,ALONVT,XMESHL
      ijout=imout*jmout
*** loop for 19 eta-levels
      do 20 i=1,19
*** loop for amount of eta-parameters
      do 15 j=1,10
      READ(1,'(30x,I3,1X,A20,1X,G12.6)')
     2                IFLD,FIELD(IFLD),SFC(i)
      READ(1,'(10E12.5)') (GRID(i,j,k),K=1,IJOUT)
      if(field(ifld)(1:5).eq.'PRESS')then
        do k=1,ijout
        P1(i,k)=grid(i,j,k)
        enddo
      endif
      if(field(ifld)(1:5).eq.'HEIGH')then
        do k=1,ijout
        Z1(i,k)=grid(i,j,k)
        enddo
      endif
      if(field(ifld)(1:5).eq.'TEMP ')then
        do k=1,ijout
        T1(i,k)=grid(i,j,k)
        enddo
      endif
      if(field(ifld)(1:5).eq.'REL H')then
        do k=1,ijout
        R1(i,k)=grid(i,j,k)
        enddo
      endif
      if(field(ifld)(1:5).eq.'SPEC ')then
        do k=1,ijout
        Q1(i,k)=grid(i,j,k)
        enddo
      endif
      if(field(ifld)(1:5).eq.'MST C')then
        do k=1,ijout
        M1(i,k)=grid(i,j,k)
        enddo
      endif
      if(field(ifld)(1:5).eq.'U WIN')then
```

```
        do k=1,ijout
        U1(i,k)=grid(i,j,k)
        enddo
       endif
       if(field(ifld)(1:5).eq.'V WIN')then
        do k=1,ijout
        V1(i,k)=grid(i,j,k)
        enddo
       endif
       if(field(ifld)(1:5).eq.'OMEGA')then
        do k=1,ijout
        W1(i,k)=grid(i,j,k)
        enddo
c      print*,'horgeval W1= ',W1(i,4),' ',W1(i,6),' ',W1(i,3346)
       endif
       if(field(ifld)(1:5).eq.'ABS V')then
        do k=1,ijout
        A1(i,k)=grid(i,j,k)
        enddo
       endif
15     enddo
20     enddo
***    read surface pressure at the end of the file
       READ(1,'(30x,I3,1X,A20,1X,G12.6)')
      2                IFLD,FIELD(IFLD),SFC(i)
       READ(1,'(10E12.5)') (Ps(k),K=1,IJOUT)
***    read surface height at the end of the file
       READ(1,'(30x,I3,1X,A20,1X,G12.6)')
      2                IFLD,FIELD(IFLD),SFC(i)
       READ(1,'(10E12.5)') (Zs(k),K=1,IJOUT)
*** read etaref
       do i=1,8646
       read(2,'(E14.7)')ref(i)
       enddo
*** finished reading ***
*** INTERPOLATE from ETA TO ISENTROPIC LEVELS
       call eta2i(ijout,km,SFC,T1,U1,V1,W1,Z1,R1,P1,Q1,M1,A1,
      *ref,Ps,KO,tho,Ti,Ui,Vi,Zi,Wi,RHi,Pi,Qi,Mi,AVi)
       call conP(Ti,Pi,Qi,RHi,w,Tci,Pci)
*** Convert from 9,8646 to 9,66,131 matrix
       do i=1,9
       ii=1
       do j=1,66
       do k=1,131
       Pgr(i,j,k)=Pi(i,ii)
       Tgr(i,j,k)=Ti(i,ii)
       Ugr(i,j,k)=Ui(i,ii)
       Vgr(i,j,k)=Vi(i,ii)
       Zgr(i,j,k)=Zi(i,ii)
       Wgr(i,j,k)=Wi(i,ii)
       RHgr(i,j,k)=RHi(i,ii)
       Qgr(i,j,k)=Qi(i,ii)
       Mgr(i,j,k)=Mi(i,ii)
       AVgr(i,j,k)=AVi(i,ii)
       PCgr(i,j,k)=Pci(i,ii)
       if(ii.lt.8647)ii=ii+1
       enddo
       enddo
       enddo
       ii=1
       do j=1,66
       do k=1,131
       Zsgr(j,k)=Zs(ii)
       if(ii.lt.8647)ii=ii+1
       enddo
       enddo
*** get maxsimum AV position
       do i=1,9
       AVmax(i)=AVgr(i,21,56)
*** search for maxs AV in window 20s-40s and 10e-40e
        do j=26,46
         do k=51,81
         if(AVgr(i,j,k).gt.AVmax(i))then
           AVmax(i)=AVgr(i,j,k)
           jpos(i)=j
           kpos(i)=k
           print*,'AVmx natoets =',AVmax(i),'j=',jpos(i),' k=',kpos(i)
         endif
         enddo
        enddo
       enddo
       print*,'AVmax=',(AVmax(i),i=1,9)
       print*,'jpos=',(jpos(i),i=1,9)
       print*,'kpos=',(kpos(i),i=1,9)
       write(outfn,'("avmax",i2.2,".dat")')iuur
```

```
      call pathfnm(dataout,2,outfn)
      print*,'dataout (50)',dataout
      open(50,file=dataout)
      do i=1,9
       write(50,'(i2,2x,i2,1x,f13.8)')jpos(i),kpos(i),AVmax(i)
      enddo
*** Calculate the areas where isentropic level is underneath the surface
      do i=1,9
        do j=1,66
        do k=1,131
        verskil(i,j,k)=Zgr(i,j,k)-Zsgr(j,k)
        if(verskil(i,j,k).gt.0)teken(i,j,k)=1.
        if(verskil(i,j,k).le.0)teken(i,j,k)=-1.
        enddo
        enddo
      enddo
*****Write out
      write(outfn,'("isentp",i2.2,".dat")')iuur
      call pathfnm(dataout,2,outfn)
      open(12,file=dataout)
      write(outfn,'("isenp",i2.2,".dat")')iuur
      call pathfnm(dataout,2,outfn)
      open(13,file=dataout)
      write(outfn,'("isent",i2.2,".dat")')iuur
      call pathfnm(dataout,2,outfn)
      open(14,file=dataout)
      write(outfn,'("isenu",i2.2,".dat")')iuur
      call pathfnm(dataout,2,outfn)
      open(15,file=dataout)
      write(outfn,'("isenv",i2.2,".dat")')iuur
      call pathfnm(dataout,2,outfn)
      open(16,file=dataout)
      write(outfn,'("isenz",i2.2,".dat")')iuur
      call pathfnm(dataout,2,outfn)
      open(17,file=dataout)
      write(outfn,'("isenw",i2.2,".dat")')iuur
      call pathfnm(dataout,2,outfn)
      open(18,file=dataout)
      write(outfn,'("isenr",i2.2,".dat")')iuur
      call pathfnm(dataout,2,outfn)
      open(19,file=dataout)
      write(outfn,'("isenq",i2.2,".dat")')iuur
      call pathfnm(dataout,2,outfn)
      open(20,file=dataout)
      write(outfn,'("isenm",i2.2,".dat")')iuur
      call pathfnm(dataout,2,outfn)
      open(21,file=dataout)
      write(outfn,'("isenav",i2.2,".dat")')iuur
      call pathfnm(dataout,2,outfn)
      open(22,file=dataout)
      write(outfn,'("isenpc",i2.2,".dat")')iuur
      call pathfnm(dataout,2,outfn)
      open(23,file=dataout)
      do i=1,9
        do j=1,66
*** Multiply pressure with 10 to go to hPa
         write(12,'(E12.5)')(teken(i,j,k),k=1,131)
         write(13,'(E12.5)')(Pgr(i,j,k)*10.,k=1,131)
         write(14,'(E12.5)')(Tgr(i,j,k),k=1,131)
         write(15,'(E12.5)')(Ugr(i,j,k),k=1,131)
         write(16,'(E12.5)')(Vgr(i,j,k),k=1,131)
         write(17,'(E12.5)')(Zgr(i,j,k),k=1,131)
         write(18,'(E12.5)')(Wgr(i,j,k),k=1,131)
         write(19,'(E12.5)')(RHgr(i,j,k),k=1,131)
*** Multiply by 1000 to get  g/kg
         write(20,'(E12.5)')(Qgr(i,j,k)*1000.,k=1,131)
*** Multiply by 36000000 to go from s-1 to g/kg-hour (*10 to look better)
         write(21,'(E12.5)')(Mgr(i,j,k)*36000000.,k=1,131)
*** Multiply by 100000  to look better
         write(22,'(E12.5)')(AVgr(i,j,k)*100000.,k=1,131)
         write(23,'(E12.5)')(PCgr(i,j,k),k=1,131)
        enddo
      enddo
      close(1)
      close(2)
      close(12)
      close(13)
      close(14)
      close(15)
      close(16)
      close(17)
      close(18)
      close(19)
      close(20)
      close(21)
```

```
      close(22)
      close(23)
      close(24)
      close(50)
c     close(51)
c     close(52)
      end
      SUBROUTINE eta2i(ijout,KM,SFC,T1,U1,V1,W1,Z1,R1,P1,Q1,M1,A1
     *,ref,Ps,KO,THO,Ti,Ui,Vi,Zi,Wi,RHi,Pi,Qi,Mi,AVi)
C$$$  SUBPROGRAM DOCUMENTATION BLOCK
C
C  SUBPROGRAM:    ETA2I       ETA TO ISENTROPIC INTERPOLATION
C   PRGMMR: E de Coning          ORG: Weerburo    DATE: 95-09-29
C
C ABSTRACT: INTERPOLATES TEMPERATURE, WINDS, HEIGHT, HUMIDITY  ETC
C   FROM THE ETA COORDINATE SYSTEM TO ISENTROPIC SURFACES.
C
C PROGRAM HISTORY LOG:
C   95-09-29  Estelle
C
C   INPUT ARGUMENT LIST:
C     ijout       - INTEGER NUMBER OF POINTS (131*66)
C     KM       - INTEGER NUMBER OF ETA LEVELS
C     SFC       - REAL(KM) ETA VALUES
C     Ps     - REAL SURFACE PRESSURE IN KPA
C     grid(i,1,ijout)  Pe     - REAL Pressure IN Kpa
C     grid(i,2,ijout)  Ze     - REAL HEIGHTS IN M
C     grid(i,3,ijout)  Te     - REAL TEMPERATURE IN K
C     grid(i,4,ijout)  RHe    - REAL RELATIVE HUMIDITY IN PERCENT
C     grid(i,5,ijout)  Qe     - REAL Spesific HUMIDITY IN g/ g
C     grid(i,6,ijout)  Me     - REAL Moisture convergence
C     grid(i,7,ijout)  Ue     - REAL ZONAL WIND IN M/S
C     grid(i,8,ijout)  Ve     - REAL Merid wind in m/s
C     grid(i,9,ijout)  We     - REAL Vertical velocity mikrobar/sec
C     grid(i,10,ijout) AVe    - REAL Absolute Vorticity
C     KO       - INTEGER NUMBER OF ISENTROPIC LEVELS
C     THO      - REAL (KO) POTENTIAL TEMPERATURE IN K
C
C   OUTPUT ARGUMENT LIST:
C     Pi      - REAL (ijout,KO) Pressure IN Kpa
C     Ti      - REAL (ijout,KO) TEMPERATURE IN K
C     Ui      - REAL (ijout,KO) ZONAL WIND IN M/S
C     Vi      - REAL (ijout,KO) MERID WIND IN M/S
C     Wi      - REAL (ijout,KO) VERTICAL VELOCITY IN PA/S
C     RHi     - REAL (ijout,KO) RELATIVE HUMIDITY IN PERCENT
C     Qi      - REAL (ijout,KO) Spesific HUMIDITY IN g/g
C     Zi      - REAL (ijout,KO) HEIGHTS IN M
C     Mi      - REAL (ijout,KO) Moisture Convergence
C     AVi     - REAL (ijout,KO) Absolute vorticity
C
C SUBPROGRAMS CALLED:
C   ISRCHFGT - FIND FIRST VALUE IN AN ARRAY GREATER THAN TARGET VALUE
C
C ATTRIBUTES:
C   LANGUAGE: CRAY FORTRAN
C
C$$$
      REAL ref(8646)
      REAL eta(19),SFC(KM),Ps(ijout)
      REAL T1(KM,ijout),P1(KM,ijout),U1(km,ijout),V1(km,ijout)
      REAL W1(KM,ijout),Q1(KM,ijout),R1(km,ijout),Z1(km,ijout)
      REAL M1(KM,ijout),A1(KM,ijout)
      REAL Te(KM,ijout),Ue(KM,ijout),Ve(KM,ijout),We(KM,ijout)
      REAL RHe(KM,ijout),Ze(KM,ijout),Pe(KM,ijout),Qe(KM,ijout)
      REAL Me(KM,ijout),AVe(KM,ijout)
      REAL THO(KO)
      REAL Ti(KO,ijout),Ui(KO,ijout),Vi(KO,ijout),Wi(KO,ijout)
      REAL RHi(KO,ijout),Zi(KO,ijout),Pi(KO,ijout),Qi(KO,ijout)
      REAL Mi(KO,ijout),AVi(KO,ijout)
      REAL Aeta(KM),ATHO(KO),ATH(KM,ijout),ATHMIN(KM),
     *ATHMAX(KM)
      PARAMETER(G= 9.8000E+0 ,CP= 1.0046E+3 )
      PARAMETER(RD= 2.8705E+2 )
******PO=100 KPA or 1000 hPa and Ptop=50hPa or 5 KPA
      PARAMETER(PO=1000.E-1,ROCP=RD/CP,ROG=RD/G,PT=5.)
C - - - - - - - - - - - - - - - - - - - - - - - - - - - - - - - -
***   Tkes grid to different parameters
      do i=1,KM
*** swop eta-levels to go from bottom to top
        kmm=km+1
        eta(i)=SFC(kmm-i)
        do k=1,ijout
*** Pe is in hPa - divide by 10 to get KPA
        Pe(i,k)=P1(kmm-i,k)/10.
*** Ze is in meters
```

```
        Ze(i,k)=Z1(kmm-i,k)
*** Te is in Kelvin
        Te(i,k)=T1(kmm-i,k)
*** RH is in percentage
        RHe(i,k)=R1(kmm-i,k)
*** Qe is in g/g
        Qe(i,k)=Q1(kmm-i,k)
*** MOISTURE CONVERGENCE
        Me(i,k)=M1(kmm-i,k)
*** Ue is in m/s
        Ue(i,k)=U1(kmm-i,k)
*** Ve is in m/s
        Ve(i,k)=V1(kmm-i,k)
*** We is in Pa / sek
        We(i,k)=W1(kmm-i,k)
*** Absolute vorticity
        AVe(i,k)=A1(kmm-i,k)
        enddo
      enddo
*** calculate theta on each eta level
C  COMPUTE LOGS FOR INTERPOLATION
      APO=LOG(PO)
      Aeta=LOG(eta)
      ATHO=LOG(THO)
      DO K=1,KM
*** Ps is in HektoPascal, want it in KPA- divide by 10
        ATH(k,1)=LOG(Te(k,1))+ROCP*(APO-LOG((eta(k)/ref(1))*
     *(Ps(1)/10.-PT)+PT))
        ATHMIN(K)=ATH(k,1)
        ATHMAX(K)=ATH(k,1)
        DO I=2,ijout
*** Ps is in HektoPascal, want it in KPA- divide by 10
        ATH(k,i)=LOG(Te(k,i))+ROCP*(APO-LOG((eta(k)/ref(i))*
     *(Ps(i)/10.-PT)+PT))
          ATHMIN(K)=MIN(ATHMIN(K),ATH(k,i))
          ATHMAX(K)=MAX(ATHMAX(K),ATH(k,i))
        ENDDO
      ENDDO
C - - - - - - - - - - - - - - - - - - - - - - - - - - - - - - - - - -
C  DETERMINE ETA LAYERS BRACKETING ISENTROPIC LAYER.
C  WITHIN ETA STRUCTURE, INTERPOLATE FIELDS LINEARLY IN LOG THETA
C  BETWEEN BRACKETING FULL ETA LAYERS.
      KD1=1
      DO K=1,KO
        KD1=KD1+ISRCHFGT(KM-KD1-1,ATHMAX(KD1+1),1,ATHO(K))-1
        KD2=KD1+ISRCHFGT(KM-KD1-1,ATHMIN(KD1+1),1,ATHO(K))-1
        DO 15 KD=KD1,KD2
          KU=KD+1
          DO 10 I=1,ijout
            IF((ATHO(K).ge.ATH(kd,i)).AND.(ATHO(K).lt.ATH(ku,i))) THEN
              WU=(ATHO(K)-ATH(kd,i))/(ATH(ku,i)-ATH(kd,i))
              Pi(k,i)=Pe(kd,i)+WU*(Pe(ku,i)-Pe(kd,i))
              Ti(k,i)=Te(kd,i)+WU*(Te(ku,i)-Te(kd,i))
              Ui(k,i)=Ue(kd,i)+WU*(Ue(ku,i)-Ue(kd,i))
              Vi(k,i)=Ve(kd,i)+WU*(Ve(ku,i)-Ve(kd,i))
              Wi(k,i)=We(kd,i)+WU*(We(ku,i)-We(kd,i))
              RHi(k,i)=RHe(kd,i)+WU*(RHe(ku,i)-RHe(kd,i))
              Qi(k,i)=Qe(kd,i)+WU*(Qe(ku,i)-Qe(kd,i))
              Zi(k,i)=Ze(kd,i)+WU*(Ze(ku,i)-Ze(kd,i))
              Mi(k,i)=Me(kd,i)+WU*(Me(ku,i)-Me(kd,i))
              AVi(k,i)=AVe(kd,i)+WU*(AVe(ku,i)-AVe(kd,i))
            ENDIF
10        continue
15      continue
C - - - - - - - - - - - - - - - - - - - - - - - - - - - - - - - - - -
C  INTERPOLATE ETA TO ISENTROPIC OUTSIDE MODEL DOMAIN
C  KEEP FIELDS CONSTANT BUT EXTRAPOLATE HEIGHT
        DO 20 I=1,ijout
          IF(ATHO(K).lt.ATH(1,i)) THEN
            Pi(k,i)=Pe(1,i)
            Ti(k,i)=Te(1,i)
            Ui(k,i)=Ue(1,i)
            Vi(k,i)=Ve(1,i)
            Wi(k,i)=We(1,i)
            RHi(k,i)=RHe(1,i)
            Qi(k,i)=Qe(1,i)
            Zi(k,i)=Ze(1,i)
            Mi(k,i)=Me(1,i)
            AVi(k,i)=AVe(1,i)
          ELSEIF(ATHO(K).ge.ATH(km,i)) THEN
            Pi(k,i)=Pe(km,i)
            Ti(k,i)=Te(km,i)
            Ui(k,i)=Ue(km,i)
            Vi(k,i)=Ve(km,i)
            Wi(k,i)=We(km,i)
```

```
            RHi(k,i)=RHe(km,i)
            Qi(k,i)=Qe(km,i)
            Zi(k,i)=Ze(km,i)
            Mi(k,i)=Me(km,i)
            AVi(k,i)=AVe(km,i)
          ENDIF
 20      continue
       ENDDO
       RETURN
       END
       subroutine conP(T,p,q,RH,w,Tc,Pci)
************************************************************
*** Calculte RH on pressure level:
***  RH= r/rw met r=q/(1-q)  that means
***  RH= q/(rw*(1-q))   with
***  rw= eps*ew/p    with ew from clausius clapeyron:
***  ew= 6.11*exp(L/Rv*(1/273.16 - 1/T))
*** Units for 6.11 is mbar or hPa
*** (No need to convert to SI units)
*** Units for q,qs are g/kg
*** Dewpoint calculated according to an eq. from Bracknell:
***  Td= 2720*T / (T*ln(100/RH)/2 + 2720)
************************************************************
       dimension T(9,8646),q(9,8646),w(9,8646),RH(9,8646),Td(9,8646)
       dimension P(9,8646),Tc(9,8646),Tc1(9,8646),Pci(9,8646)
       data hL/2464759.0/,Rd/287.04/,eps/0.622/,dp/500./
       data Rv/461.48/,A/2.53E9/,zappa/0.286/,cp/1004.64/
       do k=1,9
       do i=1,8646
         Td(k,i)=2720.0*T(k,i) /
     *          ((T(k,i)*log(100.0/RH(k,i)))/2.0 + 2720.0)
         t1=T(k,i)
         TD1=Td(k,i)
*** go from kPa to Pa
         druk=P(k,i)*1000.
         hL=(-0.566*(TD1-273.16)+597.3)*4186.0
*** 611. is for Pa
         e=611.*exp(hL/Rv*(1/273.16 - 1/TD1))
         r=eps*e/druk
         do j=1,100
           hL=(-0.566*(t1-273.16)+597.3)*4186.0
           es=611.0*exp(hL/Rv*(1/273.16 - 1/t1))
           rs=eps*es/druk
           if(rs.le.r)goto 10
           t2=t1-Rd*t1/(cp*druk)*dp
           t1=t2
           druk=druk-dp
         enddo
10       Pci(k,i)=P(k,i)*10.*((t1/T(k,i))**(1./zappa))
       enddo
       enddo
       return
       end
```

```
      Program vergeval
*** This programme prepares data for vertical corss-sections for case studies
      dimension grid(19,10,8646),ref(8646)
      character*20 field(60)
      character proj*6,arg1*2,outfn*80,datain*80,dataout*80
      logical north
      REAL etamin(19),etamax(19)
      REAL eta(19),SFC(19),Ps(8646)
      REAL T1(19,8646),P1(19,8646),U1(19,8646),V1(19,8646)
      REAL W1(19,8646),Q1(19,8646),R1(19,8646),Z1(19,8646)
      REAL M1(19,8646),A1(19,8646)
      REAL Te(19,8646),Ue(19,8646),Ve(19,8646),We(19,8646)
      REAL RHe(19,8646),Ze(19,8646),Pe(19,8646),Qe(19,8646)
      REAL Me(19,8646),AVe(19,8646)
      REAL the(19,8646),top(19,8646),wom(19,8646)
      REAL thegr(19,66,131),Ugr(19,66,131),Vgr(19,66,131),Wgr(19,66,131)
      REAL RHgr(19,66,131),Zgr(19,66,131),Pgr(19,66,131),Qgr(19,66,131)
      REAL Mgr(19,66,131),AVgr(19,66,131)
      REAL Tgr(19,66,131),refgr(19,66,131)
*** work on 19 eta levels
      PARAMETER(km= 19 )
*** read hour
      call getarg(1,arg1)
      read(arg1,'(i2)')iuur
*** read output from postprocessor
      write(outfn,'("/tmp/pcst"
     *,i2.2,".tm00")')iuur
      open(1,file=outfn)
      open(2,file='/home00/estelle/isen/dat/ref.dat')
            READ(1,'(30x,5(I5,1X))')IHRST,IMM,IDD,IYY,IHH
            READ(1,'(30x,I5,1X,A6,1X,L1,1X,I5,1X,I5)')
     2                      KGTYP,PROJ,NORTH,IMOUT,JMOUT
            READ(1,'(30x,4(G12.6,1X))')
     2                      POLEI,POLEJ,ALONVT,XMESHL
      open(50,file='/home00/estelle/isen/dat/test')
      ijout=imout*jmout
*** loop for 19 eta-levels
      do 20 i=1,19
*** loop for eta-parameters
      do 15 j=1,10
      READ(1,'(30x,I3,1X,A20,1X,G12.6)')
     2                IFLD,FIELD(IFLD),SFC(i)
      READ(1,'(10E12.5)') (GRID(i,j,k),K=1,IJOUT)
      if(field(ifld)(1:5).eq.'PRESS')then
        do k=1,ijout
        P1(i,k)=grid(i,j,k)
        enddo
      endif
      if(field(ifld)(1:5).eq.'HEIGH')then
        do k=1,ijout
        Z1(i,k)=grid(i,j,k)
        enddo
      endif
      if(field(ifld)(1:5).eq.'TEMP ')then
        do k=1,ijout
        T1(i,k)=grid(i,j,k)
        enddo
      endif
      if(field(ifld)(1:5).eq.'REL H')then
        do k=1,ijout
        R1(i,k)=grid(i,j,k)
        enddo
      endif
      if(field(ifld)(1:5).eq.'SPEC ')then
        do k=1,ijout
        Q1(i,k)=grid(i,j,k)
        enddo
      endif
      if(field(ifld)(1:5).eq.'MST C')then
        do k=1,ijout
        M1(i,k)=grid(i,j,k)
        enddo
      endif
      if(field(ifld)(1:5).eq.'U WIN')then
        do k=1,ijout
        U1(i,k)=grid(i,j,k)
        enddo
      endif
      if(field(ifld)(1:5).eq.'V WIN')then
        do k=1,ijout
        V1(i,k)=grid(i,j,k)
        enddo
      endif
      if(field(ifld)(1:5).eq.'OMEGA')then
        do k=1,ijout
```

```
        W1(i,k)=grid(i,j,k)
        enddo
       endif
       if(field(ifld)(1:5).eq.'ABS V')then
        do k=1,ijout
        A1(i,k)=grid(i,j,k)
        enddo
       endif
15     enddo
20     enddo
***    reads surface pressure
       READ(1,'(30x,I3,1X,A20,1X,G12.6)')
      2                IFLD,FIELD(IFLD),SFC(i)
       READ(1,'(10E12.5)') (Ps(k),K=1,IJOUT)
*** reads etaref
       do i=1,8646
       read(2,'(E14.7)')ref(i)
       enddo
*** finished reading ***
       call thoneta(ijout,km,SFC,T1,Z1,R1,Q1,U1,V1,W1,P1,M1,A1,ref,
      *Ps,the,Te,Ze,RHe,Qe,Ue,Ve,We,Pe,Me,AVe,eta)
*** theta calculated
       call omegaom(Pe,Te,We,wom)
*** creates topography vector ***
       do i=1,19
        do j=1,8646
        top(i,j)=0.
       enddo
       enddo
       do i=1,19
       etamax(i)=eta(i)+0.05
         do j=1,8646
         if((ref(j).le.etamax(i)))then
         top(i,j)=1.
         endif
         enddo
       enddo
*** creates 66*131 matrixes from 8646 vectors ***
       do i=1,19
       ii=1
       do j=1,66
       do k=1,131
       refgr(i,j,k)=top(i,ii)
       Pgr(i,j,k)=Pe(i,ii)
       Tgr(i,j,k)=Te(i,ii)
       Ugr(i,j,k)=Ue(i,ii)
       Vgr(i,j,k)=Ve(i,ii)
       Zgr(i,j,k)=Ze(i,ii)
       Wgr(i,j,k)=wom(i,ii)
       RHgr(i,j,k)=RHe(i,ii)
       Qgr(i,j,k)=Qe(i,ii)
       thegr(i,j,k)=the(i,ii)
       Mgr(i,j,k)=Me(i,ii)
       AVgr(i,j,k)=AVe(i,ii)
       if(ii.lt.8647)ii=ii+1
       enddo
       enddo
       enddo
       do i=1,19
          write(50,'(41(f5.3))')(refgr(i,30,k),k=50,90)
       enddo
       write(outfn,'("isenvp",i2.2,".dat")')iuur
       call pathfnm(dataout,2,outfn)
       open(13,file=dataout)
       write(outfn,'("isenvt",i2.2,".dat")')iuur
       call pathfnm(dataout,2,outfn)
       open(14,file=dataout)
       write(outfn,'("isenvu",i2.2,".dat")')iuur
       call pathfnm(dataout,2,outfn)
       open(15,file=dataout)
       write(outfn,'("isenvv",i2.2,".dat")')iuur
       call pathfnm(dataout,2,outfn)
       open(16,file=dataout)
       write(outfn,'("isenvz",i2.2,".dat")')iuur
       call pathfnm(dataout,2,outfn)
       open(17,file=dataout)
       write(outfn,'("isenvw",i2.2,".dat")')iuur
       call pathfnm(dataout,2,outfn)
       open(18,file=dataout)
       write(outfn,'("isenvr",i2.2,".dat")')iuur
       call pathfnm(dataout,2,outfn)
       open(19,file=dataout)
       write(outfn,'("isenvq",i2.2,".dat")')iuur
       call pathfnm(dataout,2,outfn)
       open(20,file=dataout)
```

```
      write(outfn,'("isenvth",i2.2,".dat")')iuur
      call pathfnm(dataout,2,outfn)
      open(21,file=dataout)
      write(outfn,'("isenvrf",i2.2,".dat")')iuur
      call pathfnm(dataout,2,outfn)
      open(22,file=dataout)
      write(outfn,'("isenvm",i2.2,".dat")')iuur
      call pathfnm(dataout,2,outfn)
      open(23,file=dataout)
      write(outfn,'("isenvav",i2.2,".dat")')iuur
      call pathfnm(dataout,2,outfn)
      open(24,file=dataout)
      do i=1,19
        do j=1,66
*** multiply by 10 to go from kPa to hPa
         write(13,'(E12.5)')(Pgr(i,j,k)*10.,k=1,131)
         write(14,'(E12.5)')(Tgr(i,j,k),k=1,131)
         write(15,'(E12.5)')(Ugr(i,j,k),k=1,131)
         write(16,'(E12.5)')(Vgr(i,j,k),k=1,131)
         write(17,'(E12.5)')(Zgr(i,j,k),k=1,131)
*** multiply by 100 to go m/s to cm/sec
         write(18,'(E12.5)')(Wgr(i,j,k)*100.,k=1,131)
         write(19,'(E12.5)')(RHgr(i,j,k),k=1,131)
*** multiply by 1000 to go g/g to g/kg
         write(20,'(E12.5)')(Qgr(i,j,k)*1000.,k=1,131)
         write(21,'(E12.5)')(thegr(i,j,k),k=1,131)
         write(22,'(E12.5)')(refgr(i,j,k),k=1,131)
         write(23,'(E12.5)')(Mgr(i,j,k),k=1,131)
         write(24,'(E12.5)')(AVgr(i,j,k),k=1,131)
        enddo
      enddo
      close(1)
      close(2)
      close(13)
      close(14)
      close(15)
      close(16)
      close(17)
      close(18)
      close(19)
      close(20)
      close(21)
      close(22)
      close(23)
      close(24)
      close(50)
      end
      SUBROUTINE thoneta(ijout,KM,SFC,T1,Z1,R1,Q1,U1,V1,W1,P1,M1,A1,
     *ref,Ps,the,Te,Ze,RHe,Qe,Ue,Ve,We,Pe,Me,AVe,eta)
C$$$  SUBPROGRAM DOCUMENTATION BLOCK
C
C  SUBPROGRAM:    thoneta
C   PRGMMR: E de Coning
C
C ABSTRACT: Calculates theta on each eta-level
C
C PROGRAM HISTORY LOG:
C   95-11-09  Estelle
C
C   INPUT ARGUMENT LIST:
C     ijout       - INTEGER NUMBER OF POINTS (131*66)
C     KM       - INTEGER NUMBER OF ETA LEVELS
C     SFC       - REAL(KM) ETA VALUES
C     Ps     - REAL SURFACE PRESSURE IN KPA
C     grid(i,1,ijout)  Pe     - REAL Pressure IN Kpa
C     grid(i,2,ijout)  Ze     - REAL height in meters
C     grid(i,3,ijout)  Te     - REAL TEMPERATURE IN K
C     grid(i,4,ijout)  Rhe    - REAL Rel hum in percent
C     grid(i,5,ijout)  Qe     - REAL  Spec hum in g/g
C     grid(i,6,ijout)  Me     - REAL Moisture convergence
C     grid(i,7,ijout)  Ue     - REAL  u wind in m/s
C     grid(i,8,ijout)  Ve     - REAL u wind in m/s
C     grid(i,9,ijout)  We     - REAL vertical movement in pa/sec
C     grid(i,10,ijout) AVe    - REAL ABS VORTICITY
C
C   OUTPUT ARGUMENT LIST:
C   the(19,8646)    -    theta op elke eta vlak
C
C ATTRIBUTES:
C   LANGUAGE: CRAY FORTRAN
C
C$$$
      REAL ref(8646)
      REAL eta(19),SFC(KM),Ps(ijout)
      REAL T1(KM,ijout),P1(KM,ijout),U1(km,ijout),V1(km,ijout)
```

```
      REAL W1(KM,ijout),Q1(KM,ijout),R1(km,ijout),Z1(km,ijout)
      REAL M1(KM,ijout),A1(KM,ijout)
      REAL Te(KM,ijout),Pe(KM,ijout),Ue(km,ijout),Ve(km,ijout)
      REAL We(KM,ijout),Qe(KM,ijout),RHe(km,ijout),Ze(km,ijout)
      REAL Me(KM,ijout),AVe(KM,ijout)
      REAL Aeta(KM),ATH(KM,ijout),the(km,ijout)
      PARAMETER(G= 9.8000E+0 ,CP= 1.0046E+3 )
      PARAMETER(RD= 2.8705E+2 )
******PO=100 KPA or 1000 hPa en Ptop=50hPa or 5 KPA
      PARAMETER(PO=1000.E-1,ROCP=RD/CP,ROG=RD/G,PT=5.)
C - - - - - - - - - - - - - - - - - - - - - - - - - - - - - - - - - -
***   Converts grid in different parameters
      do i=1,KM
*** swop eta levels to work from ottom to top
        kmm=km+1
        eta(i)=SFC(kmm-i)
        do k=1,ijout
*** Pe is in hPa - divide by 10 to get KPA
        Pe(i,k)=P1(kmm-i,k)/10.
        Ze(i,k)=Z1(kmm-i,k)
*** Te is in Kelvin
        Te(i,k)=T1(kmm-i,k)
        RHe(i,k)=R1(kmm-4,k)
        Qe(i,k)=Q1(kmm-i,k)
        Me(i,k)=M1(kmm-i,k)
        Ue(i,k)=U1(kmm-i,k)
        Ve(i,k)=V1(kmm-i,k)
        We(i,k)=W1(kmm-i,k)
        AVe(i,k)=A1(kmm-i,k)
        enddo
      enddo
*** Calculates thetae on each eta level
      APO=LOG(PO)
      Aeta=LOG(eta)
      ATHO=LOG(THO)
      DO K=1,KM
        DO I=2,ijout
*** Ps is in HektoPascal, divide by 10 to get KPA
        ATH(k,i)=LOG(Te(k,i))+ROCP*(APO-LOG((eta(k)/ref(i))*
     *(Ps(i)/10.-PT)+PT))
        the(k,i)=exp(ath(k,i))
        ENDDO
      ENDDO
      RETURN
      END
      SUBROUTINE omegaom(Pe,Te,We,wom)
      real Pe(19,8646),We(19,8646),wom(19,8646),Te(19,8646)
      real p(22),t(22,5),gpm(22,5)
      open(11,file='/home00/estelle/isen/dat/ptgpm2.dat')
*** read standard gpm rise per millibar (Table in Smithsonian)
      do i=1,22
        do j=1,5
        read(11,'(f4.0,1x,f3.0,1x,f6.2)')p(i),t(i,j),gpm(i,j)
        enddo
      enddo
      do 6 i=1,19
        do 5 j=1,8646
*** multiply by 10 to go from kPa to hPa
        do 4 l=1,22
        if(Pe(i,j)*10..lt.p(l).and.Pe(i,j)*10..ge.p(l+1))then
          do k=1,5
*** temperature from Smith.table is in celsius
          if((Te(i,j).ge.t(l,k)+273.16).and.(Te(i,j).lt.
     *t(l,k+1)+273.16))then
          a1=(Te(i,j)-(t(l,k)+273.16))/((t(l,k)+273.16)-
     *(t(l,k+1)+273.16))
          a2=gpm(l,k)-gpm(l,k+1)
          a3=gpm(l,k)+a1*a2
*** a3 is gpm rise per millibar
*** We is in microbar/sec (=10**-3 hPa/sec of 10**-3mbar/sec)
          wom(i,j)=a3*(We(i,j)*10.**-3)
          if(j.lt.8646)then
            goto 5
          else
            goto 6
          endif
          endif
          enddo
        endif
4       continue
5       continue
6     continue
      close(11)
      return
      end
```